AD-A239 310

CUMENTATION PAGE

Form Approved
OMB No. 0704-0188

nation is estimated to average 1 hour per response, including the time for reviewing instructions, searching existing data sources, mpleting and reviewing the collection of information. Send comments regarding this burden estimate or any other aspect of this reducing this burden, to Washington Headquarters Services, Directorate for Information Operations and Reports, 1215 Jefferson 02, and to the Office of Management and Budget, Paperwork Reduction Project (0704-0188), Washington, DC 20503

1. AGENCY USE ONLY (Leave blank)	2. REPORT DATE	3. REPORT TYPE AND DATES COVERED
	28 May 91	THESIS/DISSERTATION

4. TITLE AND SUBTITLE
A Field-Portable, Fiber-Optic Based Near-Infrared Spectrometer and it Applications to Fuels Analysis

5. FUNDING NUMBERS

6. AUTHOR(S)
Michael J. Lysaght, Captain

7. PERFORMING ORGANIZATION NAME(S) AND ADDRESS(ES)
AFIT Student Attending: University of Washington

8. PERFORMING ORGANIZATION REPORT NUMBER
AFIT/CI/CIA-91-013d

9. SPONSORING/MONITORING AGENCY NAME(S) AND ADDRESS(ES)
AFIT/CI
Wright-Patterson AFB OH 45433-6583

10. SPONSORING/MONITORING AGENCY REPORT NUMBER

11. SUPPLEMENTARY NOTES

12a. DISTRIBUTION/AVAILABILITY STATEMENT
Approved for Public Release IAW 190-1
Distributed Unlimited
ERNEST A. HAYGOOD, 1st Lt, USAF
Executive Officer

12b. DISTRIBUTION CODE

13. ABSTRACT *(Maximum 200 words)*

DTIC
ELECTE
AUG 09 1991
S D
D

41 91-07360

14. SUBJECT TERMS	15. NUMBER OF PAGES
	16. PRICE CODE

17. SECURITY CLASSIFICATION OF REPORT	18. SECURITY CLASSIFICATION OF THIS PAGE	19. SECURITY CLASSIFICATION OF ABSTRACT	20. LIMITATION OF ABSTRACT

NSN 7540-01-280-5500

Standard Form 298 (Rev. 2-89)
Prescribed by ANSI Std. Z39-18

91 8 08 041

A Field-Portable, Fiber-Optic Based Near-Infrared Spectrometer

and its Applications to Fuels Analysis

by

Michael J. Lysaght

A dissertation submitted in partial fulfillment
of the requirements for the degree of

Doctor of Philosophy

University of Washington

1991

Accesion For
NTIS CRA&I
DTIC TAB
Unannounced
Justification
By
Distribution
Dist
A-1

Approved by James B. Callis
(Chairperson of Supervisory Committee)

Program Authorized
to Offer Degree Chemistry

Date May 28, 1991

© Copyright 1991

Michael J. Lysaght

Doctoral Dissertation

In presenting this dissertation in partial fulfillment of the requirements for the Doctoral degree at the University of Washington, I agree that the Library shall make its copies freely available for inspection. I further agree that extensive copying of this dissertation is allowable only for scholarly purposes, consistent with "fair use" as prescribed in the U.S. Copyright Law. Requests for copying or reproduction of this dissertation may be referred to University Microfilms, 300 North Zeeb Road, Ann Arbor, Michigan 48106, to whom the author has granted "the right to reproduce and sell (a) copies of the manuscript in microform and/or (b) printed copies of the manuscript made from microform."

Signature Michael J. Tyzenhoff

Date 29 May 1991

University of Washington

Abstract

A Field-Portable, Fiber-Optic Based Near-Infrared Spectrometer and its Applications to Fuels Analysis

by

Michael J. Lysaght

Chairperson of Supervisory Committee: Professor James B. Callis
Department of Chemistry

A field-portable, fiber-optic spectrometer for measurement in the short wavelength near-infrared (SW-NIR) region (700-1100 nm) of the spectrum is presented. Slightly larger than a briefcase and weighing only 23 pounds, the instrument is controlled by a 12 MHz laptop computer. The optical scheme of the instrument employs a concave holographic grating for wavelength dispersion, and a thermoelectrically temperature-stabilized 1024-element silicon photodiode array (PDA) for detection. A computer-controlled 5.5 watt tungsten lamp, with optical feedback, is used as the light source. The spectral signal is digitized at a data rate of 22 Khz to 16 bits resolution. Sample measurements are made in either transmission or transflectance mode, using fiber-optic bundles as light pipes. The portable spectrometer has a resolution of 3 nm, a stray light intensity level of 0.05%, a baseline noise level of 25.5 micro-absorbance units, and a dynamic range

of three orders of magnitude. Instrument performance is compared with two, commercially available, near-infrared spectophotometers.

The performance of the portable spectrometer is evaluated in two application studies. First, NIR spectroscopy is developed as a rapid method for the simultaneous estimation of the freezing point and volume percentages of aromatics and saturates in JP-4 jet aviation fuel. Both multiple linear regression and partial least squares analysis methods are employed to predict the physical parameters mentioned above. The NIR spectral analysis predictions are within published ASTM reproducibility criteria, with the prediction of percent aromatics and percent saturates less than 1 percent, and freezing point less than 2.5°C. Second, the quantitative analysis of xylene mixtures is presented. Classical least squares, multiple linear regression and partial least squares analysis techniques are used to predict the volume percent of *ortho*-, *meta*-, and *para*-xylene in a series of xylene mixtures. Prediction results are accurate to within 0.50% for each of the statistical analysis methods.

Table of Contents

page

List of Figures vii

List of Tables x

CHAPTER 1

Theory and Review 1

1.1 At-Line / In-Field Analysis 1

1.2 Near-Infrared Spectroscopy 2

1.2.1 Historical Review 3

1.2.2 Applications of SW-NIR Spectroscopy 4

1.2.3 Origin of NIR Spectral Transitions 5

1.2.4 Spectral Features of the NIR 10

1.2.5 NIR Sampling Methods 15

1.2.5.1 Transmission / Transflectance 15

1.2.5.2 Diffuse Reflectance 16

1.2.6 NIR Instrumentation 19

1.2.6.1 Fixed-Filter Photometers 20

1.2.6.2 Scanning Spectrophotometers 21

1.2.6.3 Photodiode Array Spectrometers 22

1.3 Mathematical Pretreatment Methods 24

1.3.1 Offset Subtraction 25

1.3.2 Second-Derivative Transformation 27

1.4 Multivariate Analysis Methods 31

1.4.1 Multiple Linear Regression 35

1.4.2 Partial Least Squares 37

1.5 Rationale for This Study 41

1.6 Notes to Chapter 1 42

CHAPTER 2

Instrument Design and Characterization (I) 49

2.1 Introduction 49

2.2 Instrument Design 50

2.3 Instrument Evaluation 53

2.3.1 Resolution 55

2.3.2 Baseline Noise 57

2.3.3 Stray Light 59

2.3.4 Dynamic Range 60

2.3.5 Performance Comparison Between the Portable NIR Spectrometer and a Commercially Available Laboratory Spectrophotometer. 65

2.4 Conclusions 77

2.5 Notes to Chapter 2 78

CHAPTER 3

Instrument Design and Characterization (II) 79

3.1 Introduction 79

3.2 Instrument Design 80

3.3 Instrument Evaluation 86

3.3.1 Baseline Noise 88

3.3.2 Stray Light 93

3.3.3 Resolution 95

3.3.4 Dynamic Range 97

3.4 Conclusions 100

3.5 Notes to Chapter 3 101

CHAPTER 4

Analysis of JP-4 Jet Aviation Fuel Using NIR Spectroscopy 102

4.1 Introduction 102

4.1.1 Background 103

4.1.2 Current Methods 104

4.2 Experimental 106

4.2.1 JP-4 Fuel Samples 106

4.2.2 Spectroscopy 109

4.2.3 Statistical Methodology 110

4.3 Results and Discussion 112

4.3.1 Spectroscopic Assignments 112

4.3.2 Multiple Linear Regression Analysis 117

4.3.3 Partial Least Squares Analysis 132

4.4 Conclusions 138

4.5 Notes to Chapter 4 140

CHAPTER 5

NIR Analysis of Xylene Isomers 143

5.1 Introduction 143

5.1.1 Background 143

5.2 Spectral Band Assignments 148

5.3 Experimental 148

5.3.1 Xylene Samples 149

5.3.2 Spectroscopy 151

5.3.3 Spectral Preprocessing 155

5.4 Results and Discussion 158

5.4.1 Multiple Linear Regression Analysis (MLR) 158

5.4.2 Partial Least Squares Analysis 163

5.4.3 Classical Least Squares 173

5.5 Conclusions 179

5.6 Notes to Chapter 5 181

BIBLIOGRAPHY 184

Appendix A

Portable NIR Schematics 193

Appendix B

Hamamatsu Photodiode Array - Data Acquisition Program 205

Appendix C

Reticon Photodiode Array - Data Acquisition Program 209

Appendix D

Instrument Control Software 214

List of Figures

Figure 1.1 NIR spectra of *n*-heptane, aniline and water. 12

Figure 1.2 Offset subtraction applied to simulated data. 26

Figure 1.3 Correlation plots of actual vs estimated concentration. 28

Figure 1.4 2nd derivative transformation of simulated spectra. 30

Figure 2.1 Portable NIR spectrometer. 51

Figure 2.2 Zero absorbance transmission spectrum. 54

Figure 2.3 Spectral resolution of portable NIR spectrometer. 56

Figure 2.4 Baseline noise evaluation of portable NIR spectrometer. 58

Figure 2.5 Stray light evaluation of portable NIR spectrometer. 61

Figure 2.6 Dynamic range determination. 63

Figure 2.7 Raw spectra of reference hydrocarbon standards. 67

Figure 2.8 Normalized spectra of reference hydrocarbon standards. . . . 69

Figure 2.9 Correlation plots for a) RON and b) MON. 72

Figure 2.10 Correlation plots for A) PON and B) vol % toluene. 73

Figure 2.11 Correlation plots for vol % a) isooctane and b) *n*-heptane. . . . 74

Figure 3.1 High resolution portable near-infrared spectrometer. 81

Figure 3.2 Observed intensity spectrum of portable NIR spectrometer. . . 87

Figure 3.3 Instrumental baseline noise (700 - 1100 nm). 89

Figure 3.4 Instrumental baseline noise (700 - 1000 nm). 91

Figure 3.5 Baseline noise improvement with signal-averaging. 92

Figure 3.6 Spectra used to calculate stray light intensity. 94

Figure 3.7 Resolution determination using argon emission spectrum. . . . 96

Figure 3.8 Dynamic range determination of portable NIR spectrometer. . 98

Figure 4.1 Absorption spectra of the 33 JP-4 jet fuel samples. 111

Figure 4.2 2nd derivative transformation of JP-4 absorption spectra. . . . 113

Figure 4.3 NIR absorption spectra of *2,2,4*-trimethylpentane. 116

Figure 4.4 NIR absorption spectra of *n*-heptane. 118

Figure 4.5 NIR absorption spectra of benzene. 119

Figure 4.6 Measured versus predicted volume percent aromatics. 123

Figure 4.7 Measured versus predicted volume percent saturates. 124

Figure 4.8 Measured versus predicted freezing point. 125

Figure 4.9 Correlation coefficient versus wavelength for % aromatics. . . 127

Figure 4.10 Volume percent aromatics - PRESS plot. 133

Figure 4.11 PLS loadings plot for volume percent aromatics. 134

Figure 4.12 PLS predicted volume percent aromatics. 137

Figure 5.1 NIR absorption spectra of the three xylene isomers. 150

Figure 5.2 Absorption spectra of the xylene mixtures. 154

Figure 5.3 Second-derivative transformation of the xylene mixtures. 157

Figure 5.4 Mean-centered, second-derivative spectra of the xylene mixtures. 159

Figure 5.5 Actual versus predicted volume percent *ortho*-xylene. 164

Figure 5.6 Actual versus predicted volume percent *meta*-xylene. 165

Figure 5.7 Actual versus predicted volume percent *para*-xylene. 166

Figure 5.8 PRESS plot - volume percent *ortho*-xylene. 167

Figure 5.9 *Ortho*-xylene -- PLS loadings for latent variable #1. 169

Figure 5.10 *Ortho*-xylene -- PLS loadings for latent variable #2. 170

Figure 5.11 *Ortho*-xylene -- PLS loadings for latent variable #3. 171

Figure 5.12 Reconstructed spectra of *ortho*-xylene from CLS analysis. . . . 176

Figure 5.13 Reconstructed spectra of *meta*-xylene from CLS analysis. . . . 177

Figure 5.14 Reconstructed spectra of *para*-xylene from CLS analysis. . . . 178

Figure A.1 Prototype NIR spectrometer - component layout. 194

Figure A.2 Schematic of light source control circuitry. 195

Figure A.3 Schematic diagram of data acquisition and transfer circuitry. . 196

Figure A.4 NIR spectrometer component layout. 197

Figure A.5 Portable NIR spectrometer electrical interconnections. 198

Figure A.6 Thermoelectric temperature controller board. 199

Figure A.7 Schematic of PDA thermoelectric temperature controller. 200

Figure A.8 Light source/shutter controller component layout. 201

Figure A.9 Schematic diagram of light source/shutter control circuitry. . . 202

Figure A.10 Analog-to-Digital converter component layout diagram. 203

Figure A.11 Schematic diagram of data acquisition control circuitry. 204

List of Tables

Table 1.1 Peak assignments for water, aniline and *n*-heptane. 13

Table 2.1 Instrument evaluation summary. 64

Table 2.2 Hydrocarbon mixture composition. 66

Table 2.3 Multiple linear regression analysis of hydrocarbon samples. . 70

Table 2.4 MLR calibration against component concentrations. 76

Table 3.1 Instrument evaluation summary. 99

Table 4.1 JP-4 round-robin analysis results. 108

Table 4.2 Primary C-H absorption bands in the NIR. 115

Table 4.3 MLR regression equations for JP-4 samples. 121

Table 4.4 MLR analysis results for JP-4 samples. 122

Table 4.5 Freezing point of selected hydrocarbons 130

Table 4.6 PLS analysis results for JP-4 samples. 136

Table 5.1 Xylene isomer quantitation capabilities. 147

Table 5.2 Xylene mixture composition. 152

Table 5.3 Concentration of the isomers in mixed xylenes. 153

Table 5.4 MLR regression equations for the three xylene isomers. 161

Table 5.5 MLR analysis results for the xylenes. 162

Table 5.6 PLS analysis results for the three xylene isomers. 172

Table 5.7 CLS analysis results for the xylenes. 175

Acknowledgements

The author wishes to express sincere appreciation to Professor James B. Callis for his guidance during all aspects of this work. His meticulous attention to detail during manuscript preparation was invaluable. Additionally, Dr.'s Gouterman, Kowalski, Krieger-Brockett, and Ruzicka, all of whom served on the authors dissertation committee, are thanked for their suggestions regarding this work.

Special thanks go to Major Darrell Hancock (USAF) for encouraging the author to pursue graduate study and to Dr. Jeffrey Kelly for his many hours of assistance on the hydrocarbon studies and for his guidance during the preparation of this manuscript. Dr.'s Lloyd Burgess and James van Zee, Sheldon Danielson, Roy Olund and Lon Buck are thanked for their indispensable work on the design and construction of the two instruments used during this work. Paul Aldridge, Dr. David Mayes, Eric Lindahl, James Roe, and the entire Callis research group who offered their time for discussions and constructive criticism are also thanked. Mary Beth Seasholtz is thanked for her assistance on the multivariate statistical analysis aspects of this research.

Dr. Ronald Butler and Mr. Steve Anderson, Wright-Patterson AFB, Ohio, are thanked for their work on obtaining the samples used in the aviation fuels round-robin analysis and for their participation in the analysis of the fuel samples. Thanks also to Mr. Richard Kiene of ARCO Petroleum Products Company, Mr. Jay Hebert of Chevron Research and Technology Co., Dr. Rocco DiFoggio and Mr. Baron Munchausen of Core Laboratories, Dr. Lawrence Altman of Mobil Research and

Development Corp., and Dr. Walter Hellmuth of Texaco Inc. for their participation in the round-robin analysis.

Finally, I wish to extend a very special thanks to my entire family for their love and encouragement throughout my schooling. I am especially grateful for the guidance given me by my father, Colonel Charles A. Lysaght, on the military aspects of graduate study in the Air Force and to my father-in-law, Howard E. Banta, for his countless hours of manuscript review and insightful suggestions. Without them, this work would not have been possible.

To my wife Kathryn

CHAPTER 1

Theory and Review

1.1 At-Line / In-Field Analysis

Typically, chemical analyses are performed by off-line techniques requiring manual sampling at the acquisition site and transport to a centralized laboratory. Laboratory analysis provides the advantages of highly qualified personnel, time-sharing use of expensive instruments, and economies of scale, but suffers a major disadvantage in the inevitable delay between sample-taking and receipt of the results (1,2). This delay not only reduces the number of samples that can be analyzed in a given time, but severely limits the possibilities of adjusting the outcome of a processing operation. In industry, this lack of rapid information feedback often results in a substandard product that must either be sold at a lower price, reprocessed, or discarded, resulting in increased "quality costs" of production.

The value of taking the measurement process out of the laboratory and placing it closer to the sampling site, has been recognized for many years (3). With ever-increasing international competition and costs of raw materials, cutting the expense of production is more important than ever. One solution to the higher cost problem is portable spectroscopic instrumentation capable of at-line and/or in-field analysis (4,5,6,7). Being able to perform at-line analyses allows the process engineer to affect the outcome of a process much more rapidly, thereby reducing the quality costs of production. Further, in the area of product

compliance monitoring, there are many advantages to in-field inspection. With the help of a field-portable instrument, quality assurance measurements can be performed at the site of delivery or location of use, where traditional analytical instrumentation is usually not available. Field testing may help to identify adulterated or otherwise substandard materials before their use. Early identification of substandard materials reduces the possibility that undesirable substances will enter the production process and adversely affect the quality cost of production. Additionally, in-field analysis can be used to assess the quality of the finished product prior to sale and thereby provide assurance to the end user. As will be shown, shortwave near-infrared spectroscopy is one technique that is ideally suited for adaptation into field-portable instrumentation for use both at-line and in-the-field.

1.2 Near-Infrared Spectroscopy

The near-infrared (NIR) is defined by the American Society for Testing and Materials (ASTM) as that part of the electromagnetic spectrum extending from 700 to 2500 nm. In recent years, the NIR has been divided into two subregions: a) the shortwave near-infrared (SW-NIR), covering the wavelength region 700 - 1100 nm, and b) the longwave near-infrared (LW-NIR), covering the wavelength region 1100 - 2500 nm. This subregion distinction is instrumental in nature, with silicon (Si) detectors being used in the SW-NIR and lead sulfide (PbS), germanium (Ge) or indium/gallium/arsenide (InGaAs) detectors being used in the LW-NIR.

1.2.1 Historical Review

The NIR spectral region was first observed in the year 1800 by Herschel, who noted the existence of radiation just beyond the visible which could blacken a photographic plate and raise the temperature of a thermometer (8). It was not until 1881 that Abney and Festing photographically measured the first near-infrared spectrum of an organic compound. The spectral range they measured was between 700 and 1200 nm (9), in what is today referred to as the SW-NIR. Much of the pioneering work in NIR spectroscopy was accomplished in the late 1800's and early 1900's by Donath (10), Puccianti (11,12), and Coblentz (13,14). In 1928, Brackett recorded the first high-resolution infrared spectrum of a large organic molecule (15) showing the overtone absorptions of the primary, secondary and tertiary hydrogen atoms attached to carbon (16). A review of the developments in the NIR as of 1952 was compiled by Lauer and Rosenbaum (17). Two other review articles on NIR were published in the following three years; the first dealing with spectral identification and analytical applications (18) and the second with instrumentation and technique (19). Up until that time, measurements in the NIR were carried out with glass-prism instruments and photographic detectors and were therefore limited to the spectral region 700 - 1600 nm. Commercial NIR instrumentation, which became available in the 1950's, used a lead sulfide photoconductive cell as the detector and extended the wavelength coverage out to 3 μ. At this point, quantitative analyses by NIR became possible. However, owing to the very low extinction coefficients

and the difficulty of interpreting the absorbance bands in terms of molecular structure, the technique was little used. NIR spectroscopy's real value as a routine analytical tool for compositional analysis became apparent in the 1960's, when Karl Norris began a series of investigations which showed how moisture, protein and fat content of wheat could be quantitated by diffuse reflectance measurements in the NIR (20). In the years following Norris' pioneering work, a tremendous surge in both research and industrial applications of NIR have been realized. Several excellent reviews discuss the history of NIR and present numerous applications where NIR has been successfully employed (16, 17,21,22,23).

1.2.2 Applications of SW-NIR Spectroscopy

The on-line analysis of caustic streams (24), clinical analyses (25,26), agricultural materials analysis (27,28,29), and determinations such as the fat content in milk (30), and the identity of functional groups in epoxy resins (31) have established NIR spectroscopy as a viable analytical method. Each of these analyses were accomplished in the long wavelength NIR (1100 - 2500 nm), where absorptions are due to the first and second overtones and combinations of the fundamental mid-IR molecular vibration bands (32). Absorptions in the short wavelength near-infrared (SW-NIR) region (700 - 1100 nm) of the spectrum arise from the third and fourth overtone vibrational stretches and have long been thought too weak to be of analytical importance. However, in 1983 Karl Norris pointed out the potential of the SW-NIR region of the spectrum for routine

compositional analysis, with greatly reduced sample preparation (33).

SW-NIR, when used in concert with multivariate statistical calibration to determine the quality parameters of various samples, has proven to be an extremely attractive region of the spectrum for chemical analysis. Determinations of the ethanol content of fermentation processes (34), the hydroxide concentration in caustic solutions (35), the progress of methyl methacrylate polymerization (36) and others, have been made with this approach. Additionally, SW-NIR spectroscopy can determine those quality parameters of a sample that may be indirectly related to the sample's chemical composition. Several consumer, chemical, and physical properties of commercial-grade gasoline samples (e.g. octane number, percent aromatics, percent saturates, percent olefinics, API gravity, among others) can be predicted on the basis of their absorption spectra in the wavelength region 660 to 1215 nm (37,38). Other physical properties such at the modulus of polymers (39), heat set of nylon (40), and molecular weight (41) have also been correlated to the sample's NIR spectra.

1.2.3 Origin of NIR Spectral Transitions

NIR is a form of absorption spectroscopy which provides information about molecular vibrational overtones and vibrational combinations. During the vibrational motion of atoms in a molecule, the associated charge distribution undergoes periodic change with time and, for heteroatomic species, generally

results in a change in dipole moment. To a first approximation, a vibrating molecule may be considered to be a simple harmonic oscillator. In the simple case of a diatomic molecule, the chemical bond between the two atoms is the restoring force acting on the atoms and is proportional to the displacement of the atoms from their equilibrium positions. The potential energy resulting from small displacements of a chemical bond is given by:

$$V(r) = \frac{k(r - r_e)^2}{2} \tag{1.1}$$

where $V(r)$ is the potential energy at displacement r, k is the force constant of the bond, and r_e is the equilibrium bond length. From the quantum mechanical treatment of a linear harmonic oscillator, the energy of vibration, E_{vib}, at any given time is restricted to discrete energy levels defined by:

$$E_{vib} = (v + \frac{1}{2})\, h\nu \tag{1.2}$$

where v is the vibrational quantum number (0, 1, 2, ...), h is Planck's constant (6.626×10^{-34} J s), and ν is the frequency of vibration in Hz. As a result, only discrete energy levels are allowed whose separation is equally spaced and given by:

$$\Delta E_v = h\nu \tag{1.3}$$

Further, the frequency of vibration of the simple harmonic oscillator can be calculated by:

$$\nu = \frac{1}{2\pi}\left(\frac{k}{m}\right)^{\frac{1}{2}} \tag{1.4}$$

where m is the mass. Similarly, the fundamental vibrational frequency, $\Delta\nu = 1$, for a diatomic molecule is given by:

$$\nu_0 = \frac{1}{2\pi}\left(\frac{k}{\mu}\right)^{\frac{1}{2}} \tag{1.5}$$

where μ is the reduced mass of the molecule:

$$\frac{1}{\mu} = \frac{1}{m_1} + \frac{1}{m_2} \tag{1.6}$$

In the harmonic oscillator approximation, quantum mechanical selection rules forbid transitions between nonadjacent energy levels, $\Delta v > \pm 1$, and interaction between different oscillators. If chemical bonds within molecules behaved strictly as ideal harmonic oscillators, only the mid-infrared fundamental vibrations ($\Delta v = 1$) would be observed and there would be no NIR transitions. However, the bonds within molecules are not ideal harmonic oscillators, and exhibit varying amounts of anharmonic behavior (42,43,44), which give rise to the overtone transitions observed in the NIR.

As mentioned earlier, the simple harmonic oscillator model holds only for small displacements of the atoms from their equilibrium positions. For larger displacements, the anharmonic behavior mentioned above must be taken into account. The Morse equation provides a reasonable description of molecular potential curves:

$$V(r) = D\left[1 - e^{-\beta(r-r_e)}\right]^2 \tag{1.7}$$

where D is the bond dissociation energy, and β is given by:

$$\beta = \nu_0\left(\frac{2\pi^2\mu}{Dhc}\right)^{\frac{1}{2}} \tag{1.8}$$

Substitution of the Morse equation (equation (1.7)) into the Schrödinger equation yields the following closed form expression for the vibrational energy levels:

$$E = \left(v + \frac{1}{2}\right)h\nu_0 - x_e h\nu_0\left(v + \frac{1}{2}\right)^2 \tag{1.9}$$

where x_e is called the anharmonicity constant and is given by:

$$x_e = \frac{h\nu_0}{4D} \tag{1.10}$$

Absorptions occurring in the NIR arise primarily from these "forbidden" transitions where $\Delta v \neq 1$, known as overtones, from combination vibrational transitions and, to a lesser extent, from low-lying electronic transitions (27,45,46,47). According to classical electrodynamics, any internal motion of a molecule that results in a change of its dipole moment will lead to the emission or absorption of radiation (48). Vibrational overtone bands occur when a molecular vibration is excited from the ground state, where the vibrational quantum number, v, is equal to 0, to a higher state where v is equal to 2 or greater. A transition from $v = 0 \rightarrow v = 2$ ($\Delta v=2$) is called the first overtone absorption band, a $\Delta v=3$ transition results in the second overtone absorption band, etc. These absorption bands are at a frequency slightly less than two, three, or more times the frequency of the fundamental vibration, due to the addition of anharmonicity terms described above. Likewise, combination absorption bands arise when two or more different molecular vibrational transitions occur simultaneously. Because, overtone and combination vibrational transitions are influenced by the same factors that affect the fundamental vibrational transitions occurring in the mid-IR, much of the information provided by IR spectroscopy is also obtained in the NIR -- at least for functional groups of the form X-H, where X is a much larger atom bound to the hydrogen (e.g. -O, -C, -N).

Because vibrations involving X-H occur at the highest frequencies of all the functional groups, their overtones also occur at the highest frequencies. This, together with the fact that the absorption coefficients decrease rapidly with

overtone number, dictates that most absorptions in the NIR are due to molecules containing hydrogen. Much of the work reported here deals with third overtone absorbances of C-H vibrations occurring between 850 nm and 950 nm, where the intensity of absorption is nearly one thousand times less intense than the corresponding fundamental transition occurring in the mid-IR. Such low absorptions allow measurements to be made over pathlengths of up to 20 cm, thereby enhancing the utility of NIR as a process analysis technique (49).

1.2.4 Spectral Features of the NIR

Precise band assignments in the NIR are extremely difficult to make owing to the breadth of the absorption bands, the high overlap between bands, and the large number of overtone and combinational bands appearing throughout the spectrum. It is possible to estimate the frequency of absorption for overtone and combination bands based on previously assigned fundamental absorptions for the same material. However, due to uncertainty in the anharmonicity of the vibration, and interference from other combinations or overtones which occur at the same frequency, these assignments are often uncertain. Because of these problems, NIR band assignments are usually made through the analysis of model compounds (50). Ideal model compounds are those that give only one or two major absorptions per overtone region, thereby making the band assignments relatively certain. Model compounds used in this work consisted of: a) benzene, toluene, and the three xylenes -- for assignment of the aromatic C-H vibrations and

verification of the methyl C-H vibration assignments; b) isooctane and n-heptane -- for the assignment of the methyl and methylene C-H vibrations; c) water -- for the assignment of the O-H vibrations; and d) aniline -- for assignment of the N-H vibrations and verification of the aromatic C-H vibration assignments.

As an illustration of the various overtone regions found in the NIR and their relative intensities, the spectra of three model compounds (water, aniline, and *n*-heptane) were taken using the same 1.0 cm pathlength cell and are presented in Figure 1.1a for the SW-NIR and in Figure 1.1b for the LW-NIR. As these figures show, the spectral information is generally repeated from one overtone to the next and the absorption intensities of each overtone region are approximately one order of magnitude less intense than the succeeding overtone region. The shape of the O-H combinational band at 1960 nm is distorted because of intense absorption that exceeded the linear dynamic range of the spectrometer. A summary of the various overtone absorption bands presented in Figure 1.1 is given in Table 1.1. The spectra of water and aniline are included for illustrative purposes only and are not discussed further.

The work presented here emphasizes hydrocarbon analysis. Consequently, a brief discussion about the NIR absorptions arising from the C-H bond provides a foundation for that analysis. The NIR spectrum of a fuel sample is dominated by aromatic, methyl and methylene C-H vibrations. When working in the SW-NIR spectral region, the third and fourth overtone and combinational regions are observed. The aromatic functional groups give rise to absorptions at 875 and 714

Figure 1.1 NIR spectra of *n*-heptane, aniline and water.

a) SW-NIR spectral region.

b) LW-NIR spectral region.

(—) *n*-heptane
(---) aniline
(-·-) water

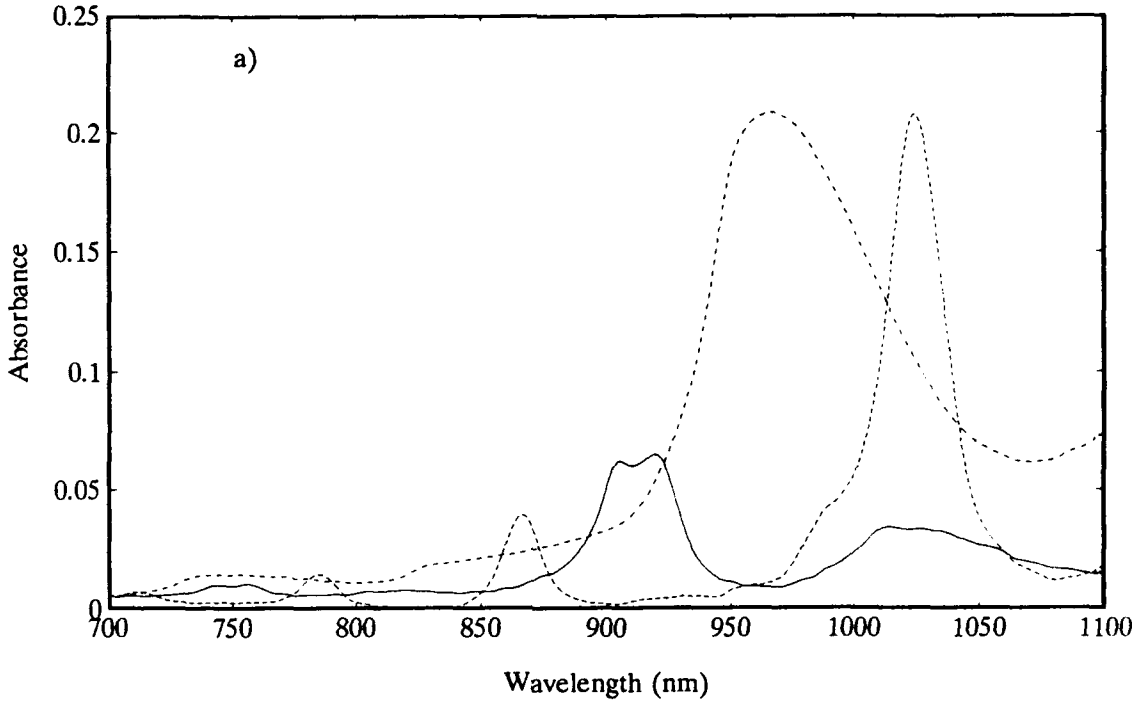
a)
Absorbance
0.25
0.2
0.15
0.1
0.05
0
700
750
800
850
900
950
1000
1050
1100
Wavelength (nm)

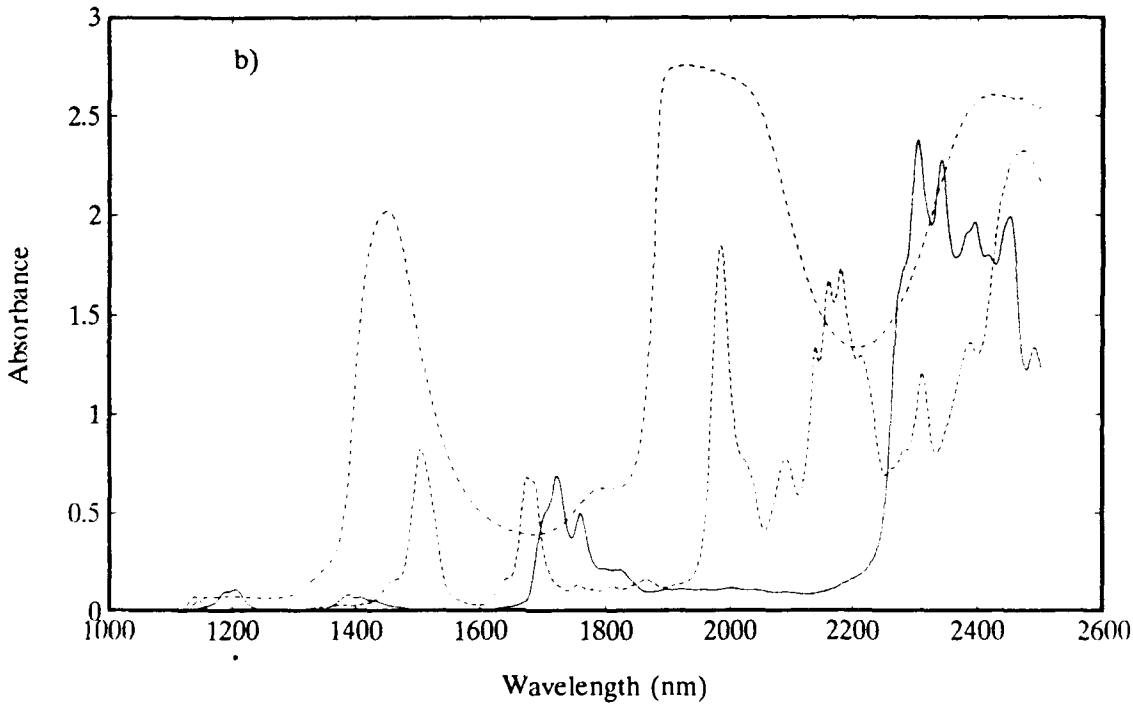
b)
Absorbance
3
2.5
2
1.5
1
0.5
0
1000
1200
1400
1600
1800
2000
2200
2400
2600
Wavelength (nm)

Table 1.1 Peak assignments for water, aniline and *n*-heptane.

NIR Overtone Absorption Band Assignments (Approximate Peak Maxima in nm)					
	Aromatic C-H	Methyl C-H	Methylene C-H	N-H	O-H
1st Overtone	1680	1700	1745	1540	1450
2nd Overtone	1145	1190	1210	1040	960
3rd Overtone	875	913	934	785	730
4th Overtone	714	746	762	not obs	not obs

nm, the methyl functional groups at 913 and 746 nm, and the methylene functional groups at 934 and 762 nm. As shown in Figure 1.1a, the fourth overtone absorptions (714 - 762 nm) are extremely weak and therefore are not often used in quantitative analysis. The third overtone region, which is nearly ten times more intense than the fourth overtone region, has a much higher signal-to-noise ratio and is therefore the overtone region most useful for quantitative analysis in the SW-NIR.

The LW-NIR contains both the first overtone (1680 - 1745 nm) and second overtone (1145 - 1210 nm) regions of the C-H vibrational bands, both of which have been used successfully for quantitative analysis. Due to sampling considerations and the optical density of the sample under investigation, one overtone region may be preferred over the other. For samples with high molar absorptivities or for analytes at high concentration, the linear dynamic range of the spectrometer may be exceeded in the first overtone region, making the second overtone region the preferable one for analysis. However, for samples with low molar absorptivities, or for analytes at extremely low concentration, the first overtone region will provide higher signal-to-noise -- making its selection the preferred one. Because virtually the same information is available in each overtone region, it is possible to use successive overtone regions in place of serial dilutions when studying samples of widely varying concentration. As the linear dynamic range of the spectrometer is exceeded with increasing concentration in the lower overtone regions, analysis in the higher overtone regions may be preferable to

sample dilution.

It has been shown that NIR spectroscopy is a viable analytical technique and, in common with other techniques, has both advantages and disadvantages associated with its use. For those applications where NIR spectroscopy can be employed, sample preparation and instrumental costs can be reduced, and analysis is more rapid.

1.2.5 NIR Sampling Methods

Three sampling techniques are commonly employed for measurement in the NIR. The choices are: transmission, transflectance or diffuse reflectance. The preferred method is often dictated by the optical properties of the sample being studied.

1.2.5.1 Transmission / Transflectance

The techniques of transmission and transflectance are used when the sample being studied is optically "clear". For these samples the absorbance of radiation by a molecule may be defined as:

$$A = \log_{10} \frac{I_0}{I} \qquad (1.11)$$

where A is the absorbance, I_0 is the intensity of incident radiation impinging on the sample and I is the intensity of radiation exiting the sample. The absorbance of

the analyte may then be related to its concentration, using the Beer-Lambert relationship:

$$A = abc \tag{1.12}$$

where a is the molar absorptivity in liters per mole centimeter, b is the pathlength or thickness of the sample in centimeters, and c is the concentration of analyte in moles per liter.

For transflectance measurements, a diffuse reflector or polished surface is placed behind the sample compartment, causing the incident radiation to traverse the sample twice. This technique is most easily implemented using a concentric bifurcated fiber-optic bundle for sample illumination and to pick-up the transflected light for return to the spectrometer. Here the center bundle of fibers is usually used to illuminate the sample, while the outer bundle is used for signal pick-up. In the transflectance configuration, the pathlength for clear solutions, using a mirror reflector, is twice that for normal transmission measurements and often best for analytes at low concentrations or for analytes with relatively low molar absorptivities. Provided the sample is not highly scattering, the Beer-Lambert relationship will apply.

1.2.5.2 Diffuse Reflectance

Diffuse reflectance measurements are used when the sample being probed is highly-scattering or is optically "opaque", *i.e.,* little or no radiation passes

completely through the sample without being scattered or absorbed. With samples such as these, normal transmission measurements are not possible and the absorbance of the analyte must be related to the intensity of radiation being reflected from the sample (51,52,53,54). This light contains both specular and diffuse components. The specular component arises from reflection at the surfaces of the sample and the sample holder without undergoing absorbance. The relationship between the angle of incident light, θ_1, and the angle of reflected light, θ_2, is very well-characterized and is governed by Snell's law:

$$n_1 \sin\theta_1 = n_2 \sin\theta_2 \qquad \textbf{(1.13)}$$

where n_1 and n_2 are the indices of refraction of adjacent media and are related to the velocity, v, of light passing through the media by $n = c/v$. The diffuse component arises from incident radiation that penetrates the surface of the sample, undergoes multiple scattering events in which partial absorption occurs, with subsequent reemission from the front surface of the sample. It is the diffusely-reflected radiation which contains chemical information about the sample and is a result of the partial absorptions occurring near the surface of the sample. In diffuse reflectance spectroscopy, the intensity of light reflected by the sample is used to calculate a pseudo-absorbance, A_R, and is given by:

$$A_R = Log \frac{R_0}{R} \qquad \textbf{(1.14)}$$

where R_0 is the reflected intensity from a non-absorbing, highly-scattering standard (a ceramic tile is often used) and R is the intensity of reflected radiation from the surface of the sample. Despite the fact that the pseudo-absorbance has been routinely applied in the analysis of NIR diffuse reflectance data, there is no established theory to relate it to concentration. Instead, various linearization techniques such as the Kubelka-Munk function (54) and the Beer-Lambert relationship (53) have been used to approximate analyte concentration based on the measured pseudo-absorbance. Using the Beer-Lambert relationship, concentration may be related to pseudo-absorbance by:

$$c\ a\ \bar{d} = Log\ \frac{R_0}{R} \qquad \textbf{(1.15)}$$

where c is the concentration of analyte, a is the molar absorptivity and $\bar{d}$ is the average penetration thickness. Due to the nature of the materials being investigated, the studies we conducted did not use the reflectance sampling technique and instead used both transmission and transflectance sampling techniques.

Most spectrometers employed in the NIR spectral region behave linearly, with concentration up to absorbances of 1.5 to 2.0, depending on the dynamic range and intensity of stray light of the spectrometer. All of the applications presented here assume such linearity and therefore compliance with the Beer-Lambert relationship. The above assumption should apply to analytes present in

low concentration and/or for analytes with relatively low molar absorptivities, such as the hydrocarbon samples studied here.

1.2.6 NIR Instrumentation

Advances in instrumentation over the past three decades (55) have made analyses in the NIR region of the spectrum extremely attractive and readily available. Tungsten-halogen light sources provide high levels of illumination throughout the NIR spectral region and, with silicon for the SW-NIR and lead sulfide, germanium and indium-gallium-arsenide for the LW-NIR, detectors now give signal-to-noise ratios as high as 100,000:1. Wavelength dispersion can be accomplished using concave holographic gratings, blazed at a wavelength optimized for the NIR, providing high light gathering power with minimal defects and optical aberrations. The ability to easily interface NIR instruments with optical fibers that can transmit SW-NIR radiation over several hundred meters permits remote sensing in harsh or otherwise inaccessible environments (56,57). This, coupled with the relatively low cost of NIR instrumentation, are contributing factors to the rapid growth of this technology.

There are three types of instruments typically employed in the NIR: fixed-filter photometers, scanning monochromators, and photodiode array spectrometers. All are examples of single-beam instruments which require separate determinations of I and I_0 (or R and R_0), as compared to dual-beam instruments where I and I_0 (R and R_0) are measured simultaneously. Each

instrument has advantages and disadvantages associated with it that often dictate which will be used for a particular application.

1.2.6.1 Fixed-Filter Photometers

Fixed-filter photometers have seen use in the NIR spectral region for more than 30 years and have earned the reputation as the workhorse of NIR in many process analytical applications (58). In this technique, interference filters are sequentially placed in the optical beam path of the photometer, allowing signal detection at a series of discrete wavelengths. Filters are chosen based on an initial full-spectrum analysis of the sample, to determine those regions of the spectrum which are highly correlated to the constituents of interest. These instruments commonly have anywhere from 3 to 15 filters, one or more of which are dedicated to wavelength standardization and/or intensity normalization. The use of reference wavelengths has been shown to be effective in removing the effects of baseline offsets and sloping baselines (59). Filter photometers are capable of taking measurements in either transmission, reflectance or transflectance configurations -- making them quite versatile for a number of different applications.

Industrial photometer applications are described by Winson (60) and Brown (61). The ability to easily thermostat the photometer and sample compartment is advantageous for making measurements where temperature effects, *e.g.*, aqueous solutions, are important. A limiting factor in the use of filter photometers lies in the fact that the measurements are made at a series of discrete

wavelengths only, thereby limiting the photometers ability to identify the presence of outliers or sample contamination.

1.2.6.2 Scanning Spectrophotometers

Scanning spectrophotometers record entire spectral regions and therefore provide the advantage of data analysis by full-spectrum techniques (see section 1.4, 1.4.1). This is especially important for the analysis of complex mixtures involving multiple analytes having overlapping absorption bands. Today's state-of-the-art scanning NIR spectrophotometers (e.g. The LT Industries Quantum 1200, the Guided Wave 300P and the NIRSystems 6500) consist of a mechanically scanned holographic grating for wavelength dispersion and a single detector for signal measurement. After the incident light is dispersed, the monochromatic radiation is allowed to interact with the sample in either a transmission, reflectance or transflectance sampling configuration. The transmitted/reflected light is then detected and converted to absorbance. Despite the high cost (implying high performance) of scanning spectrophotometers, their long-term stability in the process environment has been called into question (49,62). Problems associated with the presence of moving components, such as mechanical wear, temperature stability and reproducibility, all serve to degrade long-term performance characteristics. Difficulties associated with wavelength reproducibility were recently described by Baughman, et al., (63), who illustrated spectral shifts between "identical" instruments, as well as for an individual instrument over time.

Despite wavelength calibration at a reference wavelength of 1410.8 nm, spectral shifts of 1 - 2 nm were observed at the 1152 nm absorption band of chloroform for three different instruments of the same make and model. Not only were there shifts in wavelength, but the absorption profile, *i.e.*, bandwidth and peak intensity, varied from one instrument to another. This change in absorption profile was attributed to differences in detector time response from one instrument to the next. Variability in spectral shape, such at that described here, not only degrade the performance of analyte prediction, but make the calibration transfer between instruments extremely difficult, if not impossible. For applications demanding high wavelength precision and repeatability, instruments employing a mechanically-scanned grating and detector with unpredictable speed of response may not be appropriate.

1.2.6.3 Photodiode Array Spectrometers

Photodiode array-based spectrometers provide the benefit of full-spectrum analysis techniques without the use of a mechanically-scanned grating. Here, incident light is passed through, or reflected from, the sample before wavelength dispersion. Wavelength dispersion may be accomplished with either a plane diffraction grating, in which case additional collimating optics must be employed (see Chapter 2), or with a concave holographic grating, which serves to both collimate and disperse the incident radiation (see Chapter 3). The dispersed radiation is then focused on the image plane of a linear photodiode array (PDA)

for spectral readout. Each photodiode acts as an exit slit, recording spectral information at different wavelengths. PDA's typically employed for spectroscopic measurements have between 35 and 1024 photodiodes and, depending on the linear dispersion of the grating being employed, can easily give a spectral resolution of a few nanometers.

A major benefit of working in the SW-NIR is the ability to employ silicon PDA's (64,65) and/or charge transfer device (CTD) detectors (66,67). Several recent articles have detailed the benefits of PDA spectrometers for making measurements in the SW-NIR region of the spectrum (4,68,69). The advantages of a PDA-based system, over a conventional scanning monochromator, include the elimination of all critically-aligned moving parts and the ability to simultaneously acquire the entire spectral region of interest. This latter feature is known as the *multichannel advantage* and results in a significant decrease in spectral acquisition time and/or an increase in the signal-to-noise (S/N) ratio of the measurement (70). Because there are no moving parts in a PDA-based spectrometer (except the light source shutter, if included), wavelength stability and system durability are greatly enhanced.

For a number of reasons, a PDA-based design was chosen for the development of the field-portable NIR spectrometer described in this work. First, and most important, was the elimination of the mechanically-scanned grating, thereby reducing the effects of movement on critically-aligned optical components. This not only reduces the instrument's susceptibility to vibration, but ensures long-

term wavelength reproducibility. Second, the PDA spectrometer can be made several times smaller and lighter than a scanning spectrophotometer, giving better system portability. Finally, the cost of a PDA-based spectrometer is several times less than that of a scanning spectrophotometer.

1.3 Mathematical Pretreatment Methods

When assuming the applicability of the Beer-Lambert relationship, *i.e.*, that concentration is proportional to absorbance, any changes in absorbance not directly related to changes in concentration will induce an error in the calculated concentration. One feature common to nearly all NIR analyses is a baseline offset between spectra, causing an apparent change in absorption intensities. Several factors which contribute to this offset are accentuated due to the single-beam nature of most NIR spectrophotometers. These factors include: a) an inability to reproducibly place the sample cuvette from one measurement to the next; b) changes in index of refraction between samples; and c) differences in scattering coefficients of the samples under study. Because changes in absorption due to baseline offset are confounded with changes in absorption due to varying concentration, it is necessary to apply some form of mathematical pretreatment to remove the baseline offset present in the spectral data before conducting multivariate statistical analysis. Two common pretreatments applied to NIR spectral data are offset subtraction and derivative transformation.

1.3.1 Offset Subtraction

Offset subtraction is straight-forward and computationally very simple. For a given series of spectra, a wavelength exhibiting little or no absorbance and minimal slope is chosen as the normalization wavelength. The intensity at this wavelength is then subtracted from all other wavelengths, with each spectrum considered separately. The effect is to normalize each of the spectra to a common wavelength, from which intensity changes at other wavelengths can be related to concentration through the Beer-Lambert relationship. Provided the baseline has minimal slope throughout all the spectra, offset subtraction is an effective way to remove baseline drift. When the slope of the baseline is non-zero and changing from one spectrum to the next, offset subtraction will only be useful for a localized region of the spectrum and may not effectively negate the effects of baseline drift throughout the spectral region.

The effect of offset subtraction is illustrated in Figure 1.2 for a series of simulated spectra to which two percent random noise has been added. The raw data set (Figure 1.2a) shows a variable baseline offset on the order of 0.01 absorbance units, not atypical for single-beam NIR spectrometers. This variability in absorbance intensities, due to baseline offset, is confounded with the absorption intensities due to the three chemical species with absorption maxima at channel numbers 50, 120 and 170 -- making it impossible to calculate a linear relationship between absorbance and concentration. By selecting a region of constant slope and minimum absorbance, it is possible to remove the baseline offset from each

Figure 1.2 Offset subtraction applied to simulated data.

a) Raw spectral data.

b) Spectra normalized to data channel 45.

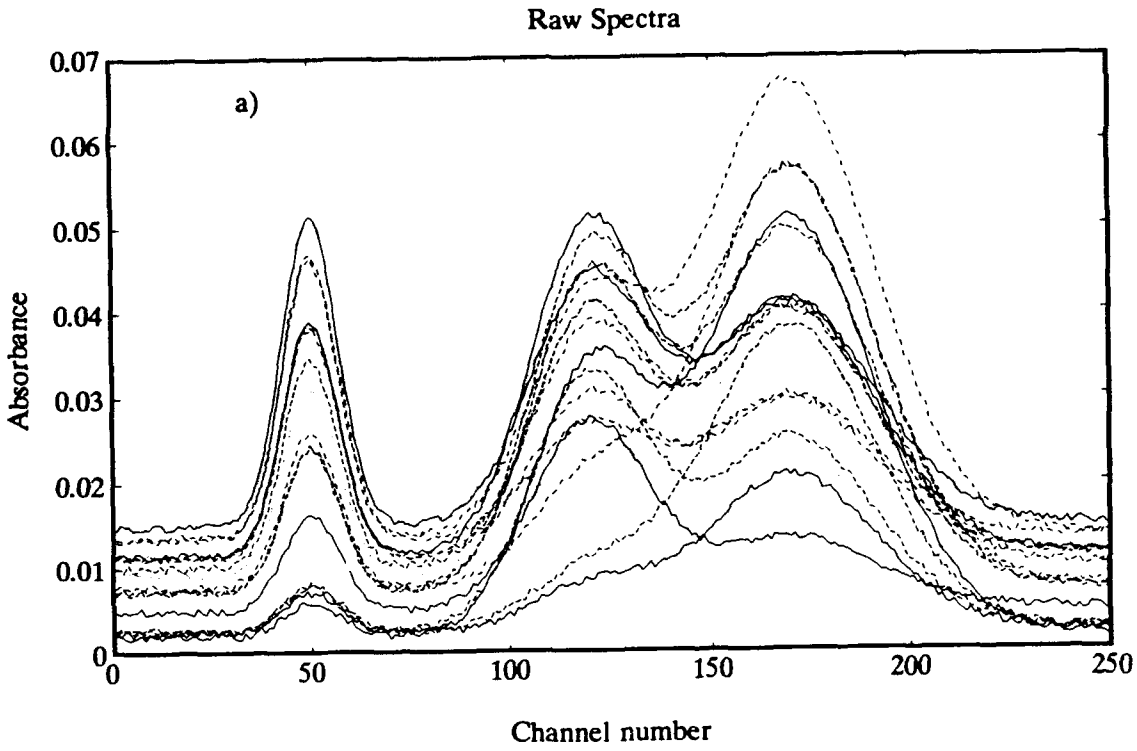
Raw Spectra
a)
Absorbance
0.07
0.06
0.05
0.04
0.03
0.02
0.01
0
0
50
100
150
200
250
Channel number

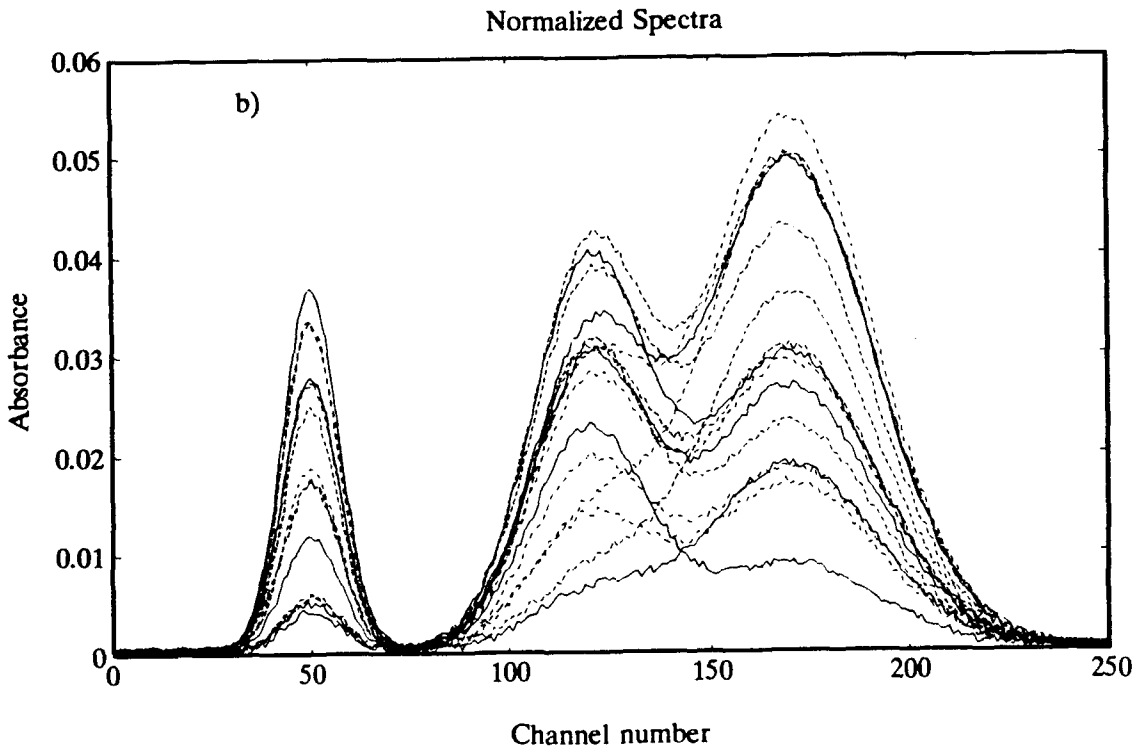
Normalized Spectra
b)
Absorbance
0.06
0.05
0.04
0.03
0.02
0.01
0
0
50
100
150
200
250
Channel number

of the spectra, leaving behind the chemical absorbance of the individual species. For this data set, channel number 45 was chosen as the normalization wavelength and its value subtracted from all other channel numbers. The changes in intensity of the absorption peaks (channels 50, 120 and 170) due to varying concentration are much more evident after offset subtraction (Figure 1.2b) and better correlated with concentration than is the case with the raw data. To demonstrate the utility of offset subtraction, an MLR analysis (see section 1.4, 1.4.1) was performed on both the raw spectra (Figure 1.2a) and the normalized spectra (Figure 1.2b). A one-wavelength regression, using the concentration of the center peak as the independent variable, gave SEE values of 0.007 for the raw spectra and 0.0007 for the normalized spectra. Multiple R values were 0.9445 for the raw spectra and 0.9994 for the normalized spectra (see section 1.4 for a discussion on SEE and multiple R). Correlation plots of regression-estimated versus actual concentration (Figure 1.3) help to visualize the improvement in calibration results using offset subtraction (regression results using the normalized spectra are indicated by the symbol 'o' in part b). Despite the relatively large amount of noise in the data (2%), excellent correlations to concentration are obtained using the normalized data.

1.3.2 Second-Derivative Transformation

Second-derivative transformation is usually preferred over offset subtraction, since it removes the effects of a sloping baseline as well as any offset. Second-derivative transformation of NIR spectra has been widely reported in the literature

Figure 1.3 Correlation plots of actual vs estimated concentration.

a) One-wavelength regression results using the raw spectra.

b) One-wavelength regression results following data pretreatment.

(∘) Offset subtraction.

(⋆) Second-derivative transformation.

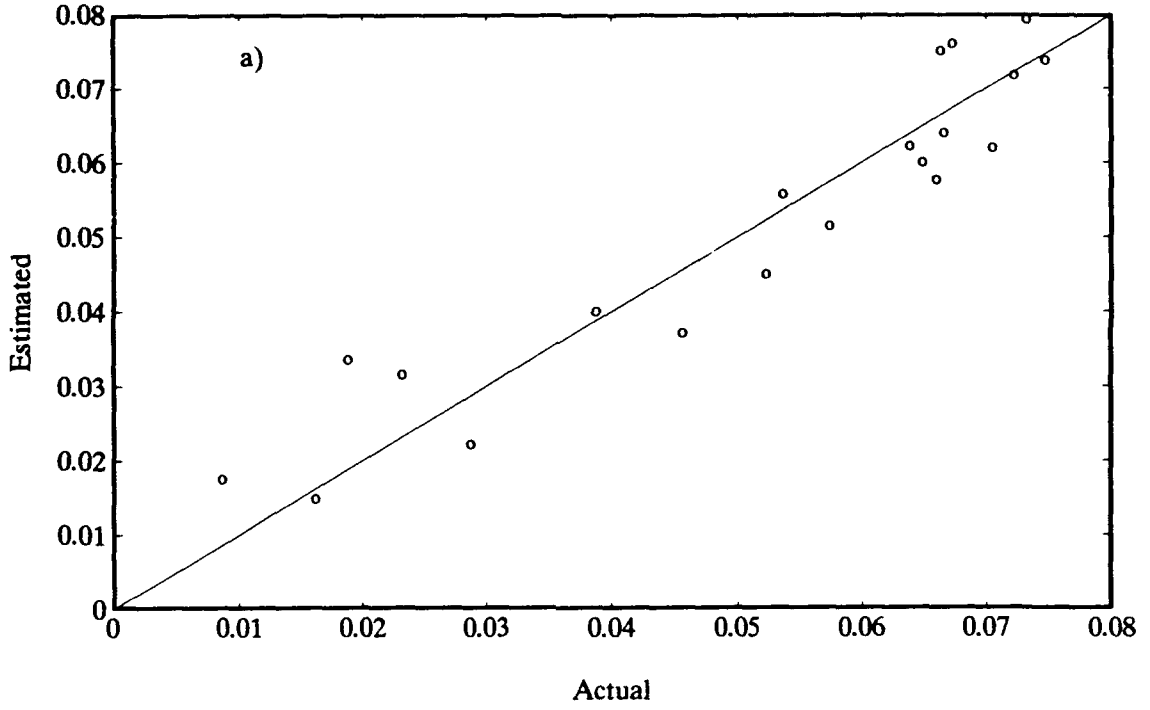
a)
Estimated
Actual
0
0.01
0.02
0.03
0.04
0.05
0.06
0.07
0.08

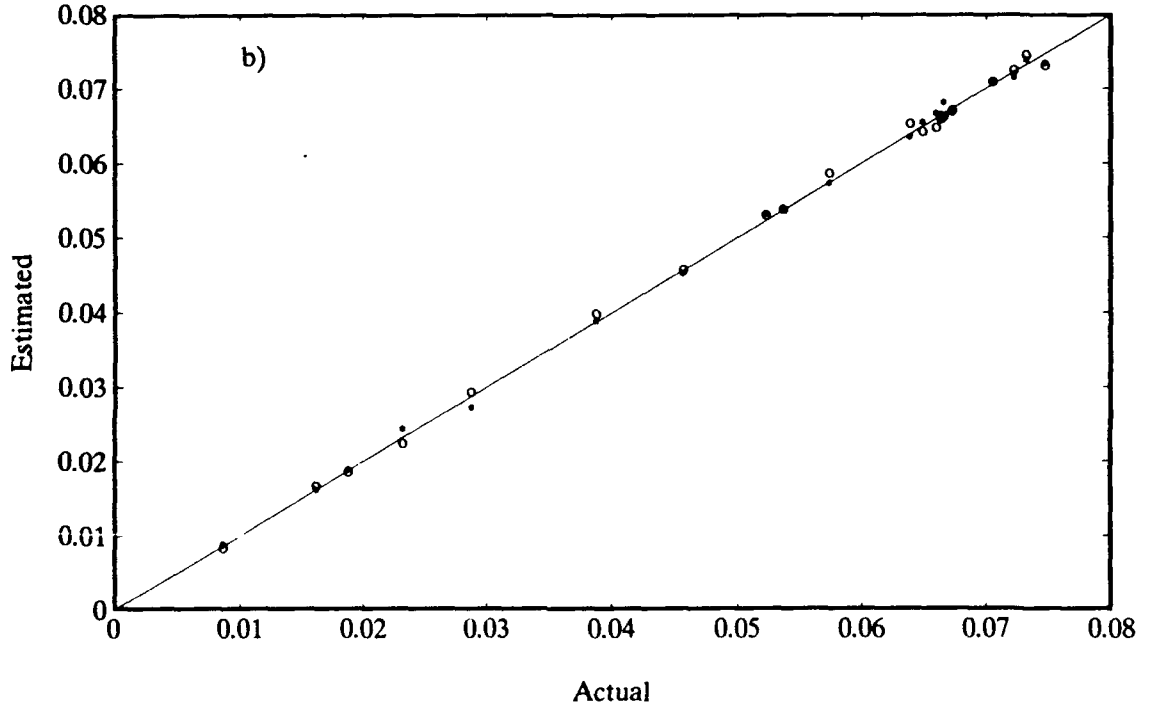
b)
Estimated
Actual
0
0.01
0.02
0.03
0.04
0.05
0.06
0.07
0.08

(27). For digital data, such as that presented here, the second-derivative can be estimated using a finite difference approximation (71):

$$f''(x_n) \approx \frac{f_{n+g} - 2f_n + f_{n-g}}{g^2} \tag{1.16}$$

where f_n is the intensity at the nth wavelength and g is the distance between the data points or gap size of the derivative. Prior to calculating the second-derivative, it is recommended the data be smoothed, e.g. using the Savitsky-Golay algorithm (72), in order to reduce the possibility of random noise distorting the derivative. The second-derivative of the data set presented in Figure 1.2a was calculated using equation (1.15), employing a smoothing window (segment) of 15 and a gap of 25. The effect of using a relatively large window and gap value is to remove much of the 2 percent noise in the data. The resultant spectra, (Figure 1.4), show quite nicely the absence of any baseline offset, with the intensity changes at each of the absorption peaks being due to varying concentration alone.

The same MLR analysis, as presented in the previous section, was accomplished using the second-derivative of the simulated spectra. For this analysis, the SEE was 0.0008 and the Multiple R was 0.9993. Because there was no change in baseline slope and the only difference from one spectra to the next was a baseline offset, the performance of offset subtraction and second-derivative normalization should be nearly identical. A correlation plot of regression-estimated versus actual concentration (Figure 1.3b) shows equally good results as that

Figure 1.4 2nd derivative transformation of simulated spectra.

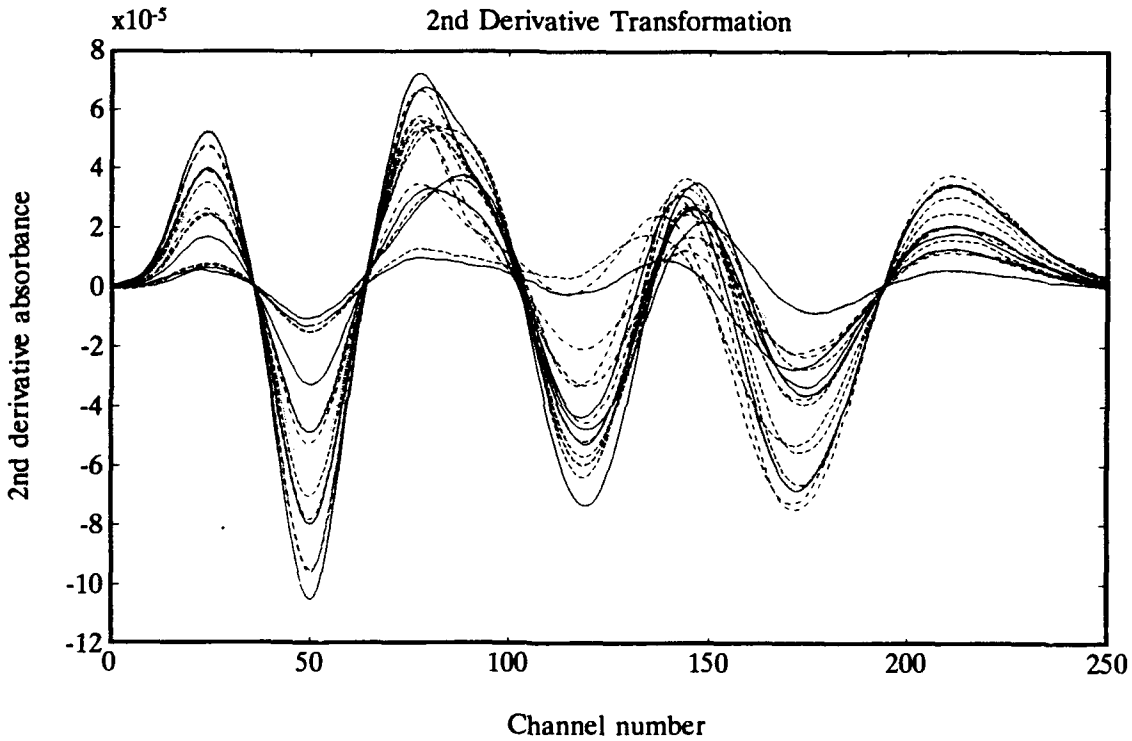
2nd Derivative Transformation
x10-5
8
6
4
2
0
-2
-4
-6
-8
-10
-12
0
50
100
150
200
250
2nd derivative absorbance
Channel number

obtained using the normalized data.

1.4 Multivariate Analysis Methods

To clarify the discussion that follows, it is useful to develop a common notation. Boldface, upper case, italic letters are used for matrices, *i.e.*, ***R,E,C***, boldface, lower case, italic letters are used for vectors, *i.e.*, ***r,e,c***, a superscript ^{T} is used for the transpose of matrices and vectors, and lower case, italic characters are used for scalars, *i.e.*, *r,e,c*. All matrices and vectors are expressed in column format.

Although NIR spectroscopy is a low-resolution technique distinguished by broad and severely overlapping absorption bands, definitive relationships between spectral features and sample properties (constituents) can often be obtained through the use of multivariate statistical calibration (73). Two approaches have been applied for the multivariate analysis of NIR spectra: a) wavelength selection methods (Multiple Linear Regression - MLR), where only a few wavelength channels are used (27,74,75) and b) full-spectrum methods, where the entire NIR spectrum is used. The work presented in this dissertation employed both MLR and the full-spectrum approach of Partial Least Squares (PLS1) (73,76,77,78). In both techniques, analysis is based on one constituent at a time, with multiple constituents being considered independently of one another. Regardless of the multivariate technique being employed, the goal of the analysis is to establish a relationship between the sample property of interest, *c*, and the

sample's instrumental response, $\boldsymbol{r}$ such that:

$$c = \boldsymbol{rb} + e = \sum_{j=1}^{N} r_j b_j + e \tag{1.17}$$

where $\boldsymbol{b}$ is a transformation vector relating concentration to instrumental response over j wavelength channels and e is an error term. For MLR, $\boldsymbol{b}$ will usually contain only a few non-zero elements, *i.e.*, only a few sensing channels will be used in the regression analysis, whereas for PLS, $\boldsymbol{b}$ is of full dimension. Whether using a wavelength selection or a full-spectrum technique, the method development stage is a three-step process; calibration, validation and prediction.

The object of the calibration phase is to determine $\boldsymbol{b}$ so as to provide the optimal prediction of property c, given spectrum $\boldsymbol{r}$. This is done using a calibration set which consists of a number of samples chosen for their ability to provide a reasonable representation of the sample universe. For each of these samples the following measurements must be made: a) the spectral responses, arranged as a matrix $\boldsymbol{R}$ of dimensions m x j, where m is the number of samples and j is the number of independent wavelength channels measured, and b) the sample property (as measured by a standard reference method), arranged as a vector $\mathbf{c}$ of dimensions m x 1. The calibration problem is posed as follows: given the calibration set $\{\boldsymbol{c}, \boldsymbol{R}\}$, find the optimal estimate for $\boldsymbol{b}$, using:

$$\boldsymbol{c} = \boldsymbol{Rb} + \boldsymbol{e} \tag{1.18}$$

The solution for ***b***, will depend on the multivariate technique being used, and is discussed in the following sections.

In the prediction phase, the constituent value for an unknown sample is determined directly from equation (1.18), using the regression vector calculated during the calibration phase. It is important to ensure that the unknown sample being evaluated is similar to, and falls within, the constituent make-up of the calibration samples. Should this not be the case, the predicted constituent error will be larger than those for samples within the range of the calibration set. It is often possible to identify future samples that do not belong to the same constituent make-up of the calibration samples by examination of the spectral residuals.

In order to evaluate the quality of the calibration model, it is necessary to validate its performance before using it for prediction of unknown samples. In the validation phase, the model developed during calibration is used to predict the constituent values of a second set of *m* samples, also having known constituent values. These predicted values are then compared with the known constituent values, thereby providing an indication on the quality of the calibration model. Evaluation of the performance of the model is usually judged on a number of statistical parameters, including multiple correlation coefficient, ***MR***, and standard error of prediction, SEP (79). ***MR*** is an indication of how much of the variance is accounted for by the regression and is given by:

$$MR = \frac{\sum_{i=1}^{m} (\hat{c}_i - \bar{c})^2}{\sum_{i=1}^{m} (c_i - \bar{c})^2} \tag{1.19}$$

where: $\hat{c}_i$ is the estimated constituent value for the ith sample as determined from the calibration analysis, c_i is the actual constituent value for the ith sample as determined from the reference analytical measurement, and $\bar{c}$ is the mean of the estimated constituent values. The SEP is given by:

$$SEP = \sqrt{\frac{\sum_{i=1}^{m} (\hat{c}_i - c_i)^2}{m - 1}} \tag{1.20}$$

It is desired that the ***MR*** value approach unity, indicating a high degree of correlation, and the SEP value approach the standard error in the reference method, indicating minimum error in the estimated constituent values when compared to the actual values. When it is impossible or impractical to obtain a second data set of known constituents, a cross-validation technique may be used to validate the model (80). In cross-validation, all but one sample of the calibration set is used to determine the prediction equation, which is then used as a test case for prediction of the constituent value of the omitted sample. This technique of "leave-one-out" is then repeated for each sample in the original calibration set, resulting in a set of predicted values of each constituent for each

sample. Provided the SEP falls within acceptable prediction limits, the model calculated in the calibration phase may be used to predict the constituent values of unknown samples.

1.4.1 Multiple Linear Regression (MLR)

MLR uses a wavelength selection method, where only those wavelengths which describe the maximum variance in the response matrix are retained in the calibration model (81,82,83). This procedure has the advantages of rapid method development, the ability to ignore regions of the spectrum where the linear model does not hold, and ready interpretation of how the method works, based on the specific wavelengths chosen. The disadvantages of wavelength selection include a limited outlier detection capability and loss of the signal-averaging advantages of full-spectrum techniques (84).

Several wavelength selection methods are available for choosing those wavelengths to be used in the regression analysis (85,86). The most straight-forward, and the one used here, selects wavelengths based on maximum correlation between spectral response and analyte concentration. Once a wavelength is chosen, the variance associated with its correlation is removed from both the concentration vector and the spectral data matrix. The next wavelength chosen is the one having the highest correlation based on this reduced data space. The F-test is used to decide whether or not the most recently chosen wavelength should be retained and future wavelengths investigated. Caution must

be exercised to avoid retaining too many wavelengths with resultant overfitting. In the validation phase, evaluation of the predictive ability of the model, as a function of the number of wavelengths retained, will indicate when overfitting occurs. When wavelengths which incorporate noise into the model are chosen, the predictive ability of the model will begin to degrade. This is a good indication that too many wavelengths have been retained.

Typically, one of three methods are used to arrive at the optimum wavelengths used in the regression equation; all possible regressions, backward elimination, and forward selection. In all possible regressions, 2^n possible subsets of n regressors (wavelengths) must be evaluated. For data sets commonly encountered in the NIR, this may entail the evaluation of 2^{700+} wavelength combinations and is too computationally intensive to be of practical use. For large data sets, it is possible to restrict the number of regressors to a smaller subset, thereby retaining some of the advantages of the all possible regressions technique. The technique of backward elimination is a procedure for searching for the "optimum" subset of wavelengths without evaluating all 2^n possible combinations. With this technique, the regression begins with all n regressors in the model, which are then removed one at a time so as to reduce the value of the SEP statistic. Variables continue to be removed until the value of the SEP statistic begins to increase. The variables remaining are then used in the calibration model for future predictions. Again, depending on the number of variables present in the data set, backward elimination tends to be quite computationally intensive. The third

technique, and the one used here, is forward selection or stage-wise MLR (87). It involves choosing those wavelengths, one at a time, which best correlate the response matrix (**R**) to the concentration or quality parameter vector (**c**).

The stage-wise MLR algorithm used here was written in the MATLAB programming environment (88) at the Center for Process Analytical Chemistry - University of Washington, Seattle, WA.

1.4.2 Partial Least Squares (PLS)

The full-spectrum technique of partial least squares was used for data analysis in Chapters 4 and 5 and is briefly described below. The PLS algorithm used (PLS1), is that reported by Haaland and Thomas (80) and summarized by Pell (89) and it is from these references that much of the following discussion was derived.

In PLS, the decomposition of the data matrix in the calibration phase is performed in such a way as to arrive at a solution that is optimized for prediction of the constituent value being considered. As such, the spectral data matrix, **R**, can be represented as follows:

$$\boldsymbol{R} = \boldsymbol{TP} + \boldsymbol{E_R} \tag{1.21}$$

where $\boldsymbol{T}$ is a matrix of intensities (scores), $\boldsymbol{P}$ is a set of loading vectors, and $\boldsymbol{E_R}$ is a matrix of spectral residuals not fit by the PLS model. This basis set of full-spectrum loading vectors is composed of linear combinations of the original

calibration spectra. The scores represent the intensities of each of the loading vectors which are needed to reconstruct the calibration spectra. The PLS1 algorithm for calibration consists of six steps as summarized below:

STEP 1. Calculate the weight loading vector, $\hat{\mathbf{w}}_h$:

$$\hat{\boldsymbol{w}}_h = \frac{\boldsymbol{R}^T\boldsymbol{c}}{\boldsymbol{c}^T\boldsymbol{c}} \tag{1.22}$$

where $\hat{\boldsymbol{w}}_h$ is the least squares estimate of the pure component spectrum with the first normalized weight vector, $\hat{\boldsymbol{w}}_1$, a weighted average of the centered calibration spectra. Subsequent weight vectors are calculated so as to be mutually orthogonal.

STEP 2. Calculate the score (latent variable) vector, $\hat{t}_h$ by projecting $\boldsymbol{R}$ onto the loading calculated in step 1:

$$\hat{t}_h = \frac{\boldsymbol{R}\hat{\boldsymbol{w}}_h}{\hat{\boldsymbol{w}}_h^T\hat{\boldsymbol{w}}_h} = \boldsymbol{R}\hat{\boldsymbol{w}}_h \tag{1.23}$$

STEP 3. Relate the score vector to concentration using a linear least-squares regression:

$$\hat{v}_h = \frac{\hat{t}_h^T c}{\hat{t}_h^T \hat{t}_h} \tag{1.24}$$

where $\hat{v}_h$ is similar to the regression coefficients relating concentration to spectral intensity in the MLR method.

STEP 4. Calculate the PLS loading vector for R:

$$\hat{p}_h = \frac{R^T \hat{t}_h}{\hat{t}_h^T \hat{t}_h} \tag{1.25}$$

STEP 5a. Calculate the spectral residuals:

$$E_R = R - \hat{t}_h \hat{p}_h^T \tag{1.26}$$

STEP 5b. Calculate the concentration residuals:

$$e_c = c - \hat{v}_h \hat{t}_h \tag{1.27}$$

STEP 6. Substitute E_R for R and e_c for c in step 2 and increment h. Repeat steps 1 through 5 for the desired number of loading vectors.

Prediction of the constituent value, for a future unknown sample, requires the calculation of the vector of regression coefficients, **b**, from the pseudoinverse of the response matrix, $\mathbf{R}^+$, and the constituent matrix as follows:

$$b = R^+ c \tag{1.28}$$

where $\mathbf{R}^+$ is obtained from the PLS algorithm (90) as follows:

$$R^+ = TS^{-1}W^T$$

T is the score matrix and **W** the weights for the independent block.

Once the vector of regression coefficients is calculated, the constituent value of the unknown sample may be calculated directly:

$$\hat{c} = r^*_{unk}\, b \tag{1.30}$$

where r^*_{unk} is the scaled response vector for the unknown sample and is given by:

$$r^*_{unk} = \frac{r_{unk} - \bar{r}}{s_R} \tag{1.31}$$

where $\mathbf{r}_{unk}$ is the response vector of the unknown sample, $\hat{\mathbf{r}}$ is the mean response vector, and $\mathbf{s}_R$ is the variance in **R**.

The PLS1 method, in which only one constituent value at a time is used, was employed throughout this work and is the only PLS technique discussed here. The PLS1 algorithm was implemented in the MATLAB programming environment (88) with software written at the Center for Process Analytical Chemistry - University of Washington, Seattle, WA.

1.5 Rationale for This Study

The demand for rapid chemical analysis and information feedback in today's rapidly changing environment has created a need for rugged, field-portable instruments capable of performing the necessary analyses in-field and away from the traditional centralized laboratory. The ability to make the required measurements on-site not only enhances quality control, but can often prevent the manufacture of substandard products. The research presented in the following chapters describes the first compact and truly portable SW-NIR spectrometer capable of performing what has traditionally been a laboratory-only analysis, "in-the-field". The discussions that follow demonstrate that SW-NIR spectroscopy can be performed just as effectively away from the laboratory as in it. This thesis is supported in several application studies, where the performance of the portable SW-NIR spectrometer is compared to commercially available state-of-the-art SW-NIR spectrophotometers.

1.6 Notes to Chapter 1

1. Callis, J.B., Illman, D.L., Kowalski, B.R., *Anal. Chem.*, **1987**, 59, 624A.

2. Riebe, M.T., Eustace, D.J., *Anal. Chem.,* **1990**, 62, 65A.

3. Clevett, K.J., *Process Analyzer Technology*, John Wiley: New York, 1986.

4. Aldridge, P.K., Callis, J.B., Burns, D.H., *J. Liquid Chromatogr.,* **1990**, 13, 2829.

5. Lysaght, M.J., van Zee, J.A., Callis, J.B., *Rev. Sci, Instrum.*, **1991**, 62, 507.

6. Lysaght, M.J., Danielson, J.D.S., Callis, J.B., *CPAC Publication Announcement #106,* **1991**, 1, 1.

7. Aldridge, P.K., Callis, J.B., Burns, D.H., *Manuscript in preparation*.

8. Herschel, W., *Philos. Trans.*, **1800**, 90, 225.

9. Abney, W., Festing, E.R., *Phil. Trans.,* **1881**, 172, 887.

10. Donath, B., *Ann. Physik,* **1896**, 58, 609.

11. Puccianti, L., *Physik. Z.*, **1899-1900**, 49, 494.

12. Puccianti, L., *Nuovo Cimento*, **1900**, 11, 141.

13. Coblentz, W.W., *Investigation of Infrared Spectra, Part 1*, Carnegie Institution, Washington, D.C., **1905**.

14. Coblentz, W.W., Natl. Bur. Standards (U.S.), *Special Publication No. 418*, **1921**.

15. Brackett, F.S., *Proc. Natl. Acad. Sci. (U.S.)*, **1928**, 14, 857.

16. Wheeler, O.H., *Chem. Rev.*, **1959**, 59, 642.

17. Lauer, J.L., Rosenbaum, E.J., *Appl Spectrosc.*, **1952,** 6, 29.

18. Kaye, W.I., *Spectrochim. Acta.*, **1954**, 6, 257.

19. Kaye, W.I., *Spectrochim. Acta.*, **1955**, 7, 181.

20. Stark, E., Luchter, K., Margoshes, M., *Appl. Spectrosc. Rev.*, **1986**, 22, 335.

21. Goddu, R.F., *Advan. Anal. Chem. Instr.*, **1960,** 1, 347.

22. Kaye, W.I., *The Encyclopedia of Spectroscopy,* **1960**, Clark, G.L., Ed., Reinhold, NY, 494.

23. Whetsel, K.B., *Encyclopedia of Industrial Chemical Analysis, Vol. 2*, **1966,** Snell, F.D., Ed., Wiley-Interscience, NY, 648.

24. Watson, E. Jr., Baughman, E.H., *Spectroscopy,* **1987**, 2, 44.

25. Jobsis, F.F., *Science*, **1977**, 198, 1264.

26. Peuchant, E., Salles, C., Jensen, R., *Anal. Chem.*, **1987**, 59, 816.

27. Williams, P.C., and Norris, K.H., *Near-Infrared Technology in the Agricultural and Food Industries*, American Association of Cereal Chemists, Inc., St. Paul, Minnesota **1987**.

28. Robert, P., Bertrand, D., Devaux, M.F., *Anal. Chem.*, **1987**, 59, 2187.

29. Watson, C.A., *Anal. Chem.*, **1977**, 49, 837A.

30. Biggs, D.A., *Assoc. Off. Anal. Chem.,* **1983**.

31. Dannenberg, H., *SPE Transactions,* **1963,** 1, 78.

32. Weyer, L.G., *Appl. Spectrosc. Rev.*, **1985**, 21, 1.

33. Norris, K.H., *NATO Adv. Study Inst. Sec. A,* **1983**, 46, 471.

34. Cavinato, A.G., Mayes, D.M., Ge, Z., Callis, J.B., *Anal. Chem.*, **1990**, 62, 1977.

35. Phelan, M.K., Barlow, C.H., Kelly, J.J., Jinguji, T.M., Callis, J.B., *Anal. Chem.*, **1989**, 61, 1419.

36. Aldridge, P.K., Burns, D.H., Kelly, J.J., Callis, J.B., *CPAC Publication # 101*, **1991**, 1, 1.

37. Kelly, J.J., Barlow, C.H., Jinguji, T.M., Callis, J.B., *Anal. Chem.*, **1989**, 61, 313.

38. Kelly, J.J., Callis, J.B., *Anal. Chem.*, **1990**, 62, 1444.

39. Miller, C.E., *Doctoral Dissertation*, University of Washington, Seattle, WA, **1989**.

40. Ghosh, S., Rodgers, J.E., *Textile Res. J.*, **1985**, 9, 556.

41. Honigs, E.E., Hirschfeld, T.B., Hieftje, G.M., *Anal. Chem.*, **1985**, 57, 443.

42. Colthup, N.B., Daly, L.H., Wiberly, S.E., *Introduction to Infrared and Raman Spectroscopy, 2nd edition*, **1975**, Academic: NY.

43. Sverdlov, L.M., Kovner, M.A., Krainov, E.P., *Vibrational Spectra of Polyatomic Molecules*, **1974**, John Wiley and Sons, NY.

44. Wilson, E.B., Decius, J.C., Cross, P.C., *Molecular Vibrations*, **1955**, McGraw-Hill, NY.

45. Wetzel, D.L., *Anal. Chem.*, **1983**, 55(12), 1165A.

46. Weyer, L.G., *Appl. Spectrosc. Rev.*, **1985**, 21, 1.

47. Stark, E., Luchter, K., Margoshes, M., *Appl. Spectrosc. Rev.*, **1986**, 22(4), 335.

48. Herzberg, G., *Infrared and Raman Spectra*, **1945**, Van Nostrand Reinhold Co., NY, NY, 239.

49. Baughman, E.H., Mayes, D.M., *Amer. Lab.*, **1989**, 10, 54.

50. Miller, C.E., Edelman, P.G., Ratner, B.D., Eichinger, B.E., *Appl. Spectrosc.*, **1990**, 4, 581.

51. Birth, G.S., Hecht, H.G., in *Near Infrared Analysis in the Agricultural and Food Industries, Chapter 1*, **1987**, P.W.Williams and K. Norris, Eds.; American Association of Cereal Chemists: St. Paul, MN.

52. Kortum, G., *Reflectance Spectroscopy: Principles, Methods, Applications*, Springer-Verlag, NY, **1969**.

53. Wendlandt, W.W., Hecht, H.G., *Reflectance Spectroscopy*, Elving, P.J., Kolthoff, I.M., Eds., Interscience Publishers, NY, **1966**.

54. Kubelka, P., Munk, F., *Z. Tech. Phys.*, **1931**, 12, 593.

55. McClure, W.F., in *Near-Infrared Technology in the Agricultural and Food Industries*, P. Williams, and K. Norris, Eds., American Association of Cereal Chemists, Inc., St. Paul, Minnesota, **1987**.

56. Archibald, D.D., Miller, C.E., Lin, L.T., Honigs, D.E., *Appl. Spectrosc.*, **1988**, 42, 1549.

57. Buchanan, B.R., *Doctoral Dissertation*, University of Washington, Seattle, WA, **1987**.

58. Moessner, R.C., Russell, D.A., *ISA Proceedings Report #90-486*, **Oct 1990**, 691.

59. Hindle, P.H., Roberts, D.L., *An Introduction to Infrared Absorption Gauging*, **1987**, September, Tobacco Reporter.

60. Winson, R.J., *Coating Measurement and Control*, Advances in Pressure Sensitive Tape Technology, Technical Seminar Proceedings, **1987**.

61. Brown, G.K., *Coatweight and Film Thickness Measurement Using Near Infrared Techniques*, 1987 Air Knife Coating Seminar, **1987**, TAPPI Seminar Notes, 87.

62. Wilks, P.A., *Infrared in the Real World: FT-IR Versus IR in Process Monitoring*, Spectroscopy, 1(4), 42.

63. Baughman, E.H., Vickers, G.H., Mayes, D.M., *Effect of Wavelength on Prediction Errors in the NIR*, **1990** Pittsburgh Conference, NY, Paper # 526.

64. Jones, D. G. *Anal. Chem.* **1985**, 57, 1057A.

65. Jones, D.G., *Anal. Chem.*, **1985**, 57, 1207A.

66. Sweedler, J.V., Jalkian, R.D., Denton, M.B., *Appl. Spectrosc.*, **1989**, 43, 953.

67. Epperson, P.M., Sweedler, J.V., Bilhorn, R.B., Sims, G.R., Denton, M.B., *Anal. Chem.*, **1988**, 60, 327A.

68. Sedlmair, J., Ballard, S.G., Mauzerall, D.C., *Rev. Sci. Instrum.*, **1986**, 57, 2995.

69. Mayes, D.M., Callis, J.B., *Appl. Spectrosc.*, **1989**, 43, 27.

70. James, J.F., Sternberg, R.S., *The Design of Optical Spectrometers*, **1969,** Chapman and Hall Ltd. London, England.

71. Mathews, J.H., *Numerical Methods*, Prentice-Hall, NJ, **1987**, 279.

72. Savitsky, A., Golay, M., *Anal. Chem.*, **1964**, 36, 1627.

73. Beebe, K.R., Kowalski, B.R., *Anal. Chem.*, **1987**, 59, 1007A.

74. Brown, C.W., Obremski, R.J., *Appl. Spectrosc. Rev.*, **1984**, 20, 373.

75. Martens, H., Naes, T., *Trends Anal. Chem.*, **1984**, 3, 204.

76. Geladi, P., Kowalski, B.R., *Anal. Chim. Acta*, **1986**, 185, 1.

77. Stone, M., *J. R. Statistical Soc., B*, **1974**, 36, 111.

78. Sharaf, M.A., Illman, D.L., Kowalski, B.R., *Chemometrics*, John Wiley and Sons: NY, 1986.

79. Hruscha, W.R. in *Near Infrared Analysis in the Agricultural and Food Industries,* **1985**, P.W. Williams and K. Norris, Eds.; American Association of Cereal Chemists: St. Paul, MN, 35.

80. Haaland, D.M., Thomas, E.V., *Anal. Chem.*, **1988**, 60, 1193.

81. Brown, C.W., Lynch, P.F., Obremski, R.J., Lavery, D.S., *Anal. Chem.*, **1982**, 54, 1472.

82. Kisner, H.J., Brown, C.W., Kavarnos, G.J., *Anal. Chem.*, **1983**, 55, 1694.

83. Maris, M.A., Brown, C.W., Lavery, D.S., *Anal. Chem.*, **1983**, 55, 1694.

84. Haaland, D.M., Easterling, R.G., *Appl. Spectrosc.*, **1980**, 34, 539.

85. Kowalski, K.G., *Chemometrics and Intelligent Laboratory Systems*, **1990**, 9, 177.

86. Phelan, M.K., *Doctoral Dissertation*, University of Washington, Seattle, WA, **1990**.

87. Draper, N., Smith, H., *Applied Regression Analysis 2nd Edition*, John Wiley and sons, NY, **1981**.

88. *PC-MATLAB for 80386-based MS-DOS Personal Computers*, Version 3.5e, The Math Works Inc., **1989**.

89. Pell, R.J., *Doctoral Dissertation*, University of Washington, Seattle, WA, **1990**.

90. Veltkamp, D., Gentry, D., *PLS 2-Block Modeling: User's Manual Version 3.1,* **1988**, Center for Process Analytical Chemistry, University of Washington, Seattle, WA.

CHAPTER 2

Instrument Design and Characterization (I)

2.1 Introduction

The focus of this chapter is the design, construction and evaluation of a prototype instrument capable of in-field fuels analysis. First, we consider the requirements for a rugged, field-portable, and user-friendly instrument capable of accomplishing laboratory-quality measurements in-the-field. Next, subsystems needed to achieve the design goals are described, such as optical interfaces, light source intensity feedback stabilization, and software for data acquisition and display. Finally, the performance of the resultant instrument is assessed. Described here is a low resolution, fiber-optic, field-portable spectrometer for measurement in the shortwave near-infrared (SW-NIR) region of the spectrum (680 - 1050 nm). The instrument, controlled by a 12-Mhz laptop computer (Toshiba - model 3100e), costs approximately $5,000 in parts, weighs 23 pounds and is about the size of a 6" thick briefcase. The spectrometer uses the single reversed-beam measurement principle by employing a grating-based spectrograph for wavelength dispersion and a silicon photodiode array as detector. The instrument is evaluated in terms of resolution, baseline noise, stray light, and dynamic range. Instrument performance is compared with a commercially available SW-NIR mechanically scanned spectrophotometer (Near Infrared Systems - model 6250) (1).

2.2 Instrument Design

A drawing (Figure 2.1a) and block diagram (Figure 2.1b) show the prototype instrument configured for reflectance/transflectance measurements. In this configuration, light from the source is focused onto one end of a bifurcated fiber bundle (Sterngold Corporation; 6 mm outside bundle diameter, 2 mm inside bundle diameter, 1 m in length) using two 15 mm focal length lenses. The return portion of the fiber bundle is connected to the spectrograph using a fiber-optic coupler configured with a 1 mm wide entrance slit. Wavelength dispersion is accomplished using an 8 cm focal length fiber-optic spectrograph (PTR Optics Corporation - model 830) equipped with an 830 grooves/mm diffraction grating, operating in the first order and optimized for wavelengths between 680 and 1050 nm. With this configuration, a dispersion of 315 nm/inch is achieved. The dispersed radiation is focused horizontally on a silicon photodiode array (PDA) for spectral readout. The detector used is a 35-element charge storage PDA (Hamamatsu - model #C2333), with individual detector elements 4.5 mm high and 0.93 mm wide (2). The PDA is not cooled; however, noise and interference is reduced by isolating the PDA from the instrument electronics by placing it in a 1/8"-thick aluminum housing. A diagram of the instrument's system components is presented in Figure A.1 (Appendix A).

The light source, located in a 1.75" height compartment beneath the computer, is a 5.5 watt tungsten-halogen bulb (Eveready - model #HPR36). To maintain the light source at a constant intensity, a separate silicon photodiode

Figure 2.1 Portable NIR spectrometer.

a) Drawing of portable NIR spectrometer.

b) Block diagram of portable NIR spectrometer.

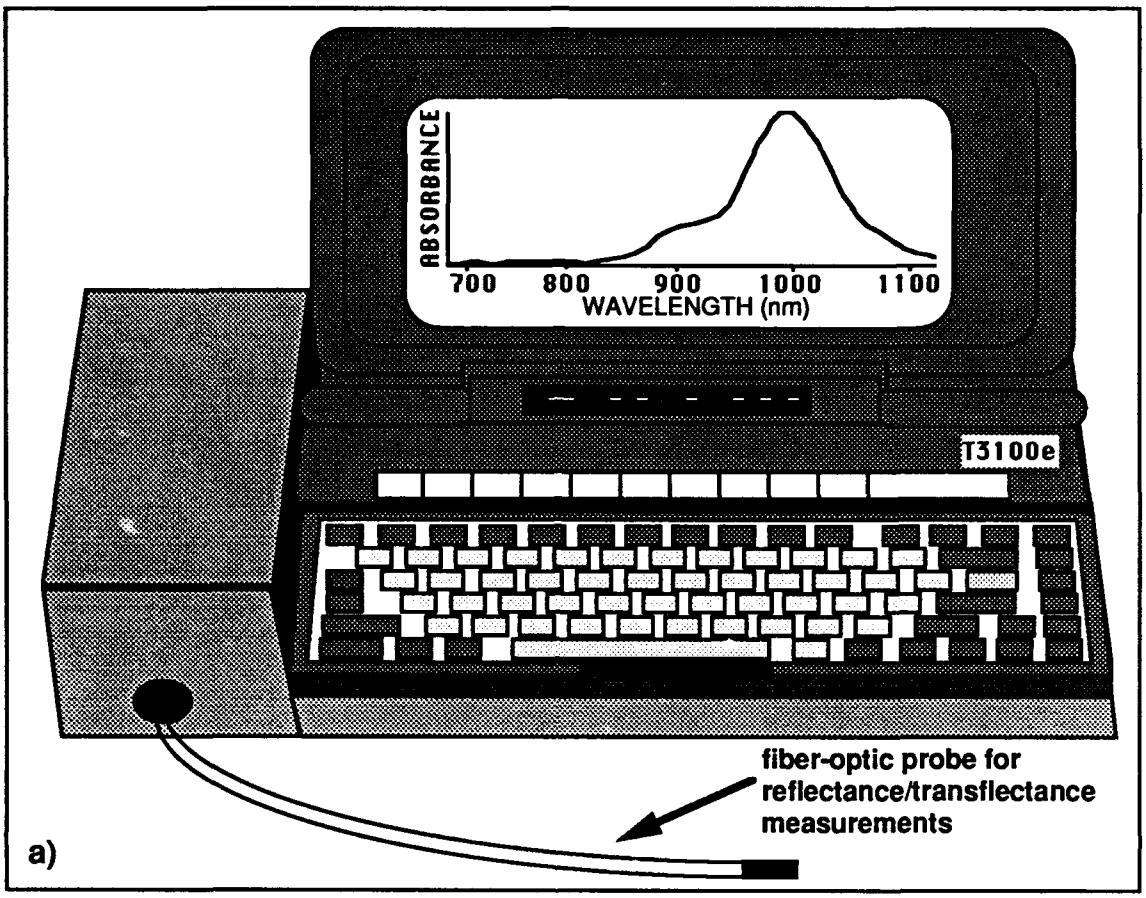
ABSORBANCE
700
800
900
1000
1100
WAVELENGTH (nm)
T3100e
fiber-optic probe for
reflectance/transflectance
measurements
a)

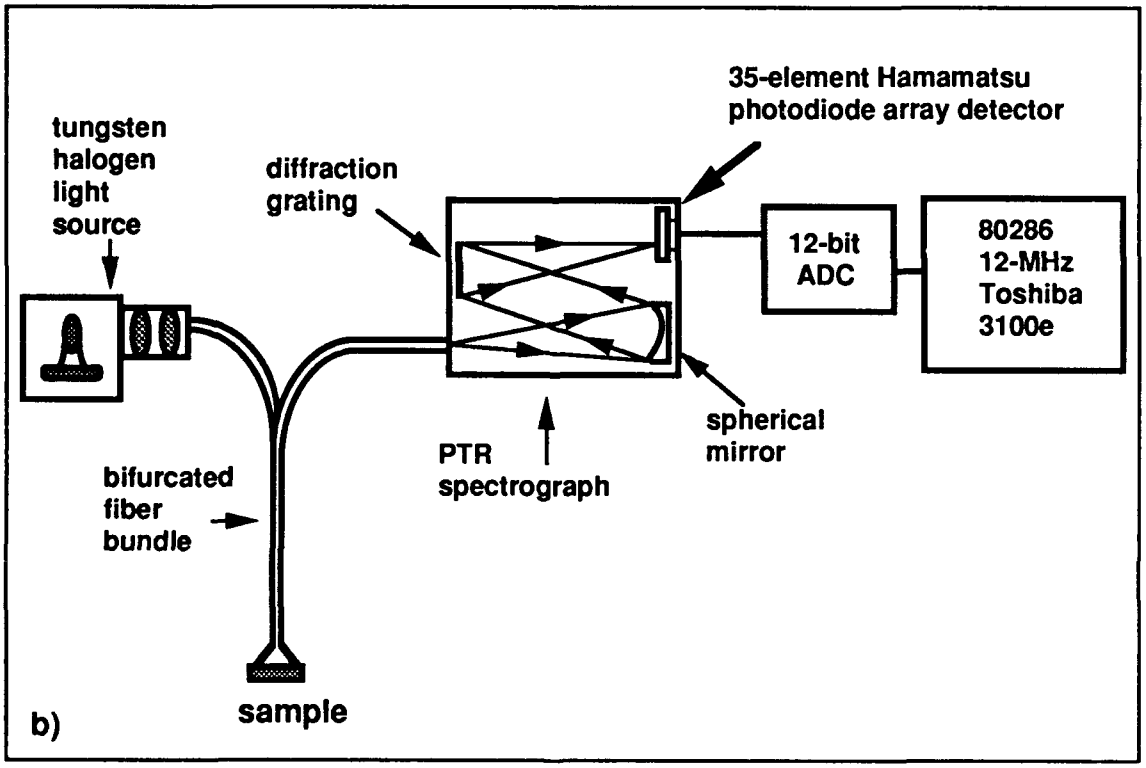
35-element Hamamatsu
photodiode array detector
tungsten
halogen
light
source
diffraction
grating
12-bit
ADC
80286
12-MHz
Toshiba
3100e
spherical
mirror
PTR
spectrograph
bifurcated
fiber
bundle
sample
b)

monitors the photon output of the lamp, providing continuous optical stabilization feedback. Initial setting of the light source intensity is computer-controlled through the use of a digitally controlled potentiometer (Xicor - model X9104P - E^2POT^{TM}). Before each series of measurements is taken, the light source intensity is adaptively adjusted by the E^2POT to 90% of detector saturation. This provides a near-maximum allowable returned light intensity when passed through a suitable blank chosen for its similarity in optical transmission to the sample. Once the maximum intensity of returned light is determined, the E^2POT maintains this resistance value for subsequent sample measurements. This adaptive adjustment allows optimization of the S/N ratio for samples of differing extinction coefficients and/or refractive index. As a result, maximum dynamic range can be maintained. A schematic of the circuitry used to control the light source and provide continuous optical stabilization feedback is given in Figure A.2 (Appendix A).

Digitization of the spectral signal is accomplished by means of a 12-bit successive approximation analog-to-digital (A/D) converter (Burr Brown - model ADC674A). In an effort to provide universal compatibility with any laptop computer and because a majority of laptop computers lack an expansion slot, a decision was made to avoid use of the Toshiba's expansion slot and instead input the data through the ubiquitous parallel printer port. Accordingly, the 12-bit data is temporarily split into three 4-bit values, using two multiplexers (Texas Instruments - model 74LS153) for input through the parallel printer port of the laptop computer. It was necessary to split the data into three 4-bit values in order to make use of

the five pins on a standard parallel printer port capable of data input. Once the data is read into the computer, the three 4-bit values are recombined to the original 12-bit data values. A schematic detailing the circuitry required to accomplish the data acquisition and transfer is given in Figure A.3 (Appendix A).

Data acquisition was performed with assembler code (see Appendix B) while data analysis and display was accomplished using software written in Microsoft QuickBasic (ver. 4.5). The software was written such that relatively untrained field-personnel could operate the instrument with little or no supervision. Instrumental parameters such as lamp intensity, number of scans for signal averaging, and integration time are preset to optimal values, but may be changed by the operator as desired. All changes to original settings are accomplished by pressing a single function key, followed with computer prompts to guide the operator through the changes. Stage-wise multiple linear regression (MLR) analysis was carried out on a laboratory IBM-AT compatible computer, using software purchased from Near Infrared Systems (3).

2.3 Instrument Evaluation

The transmission spectra at zero absorbance, I_0, of any system is influenced by many factors, but especially by lamp emission intensity, throughput of the monochromator, and quantum efficiency of the detector. The transmission spectra, at zero absorbance, of the prototype instrument is presented in Figure 2.2. The abrupt decrease in intensity at 700 nm is due to a 675 nm long

Figure 2.2 Zero absorbance transmission spectrum.

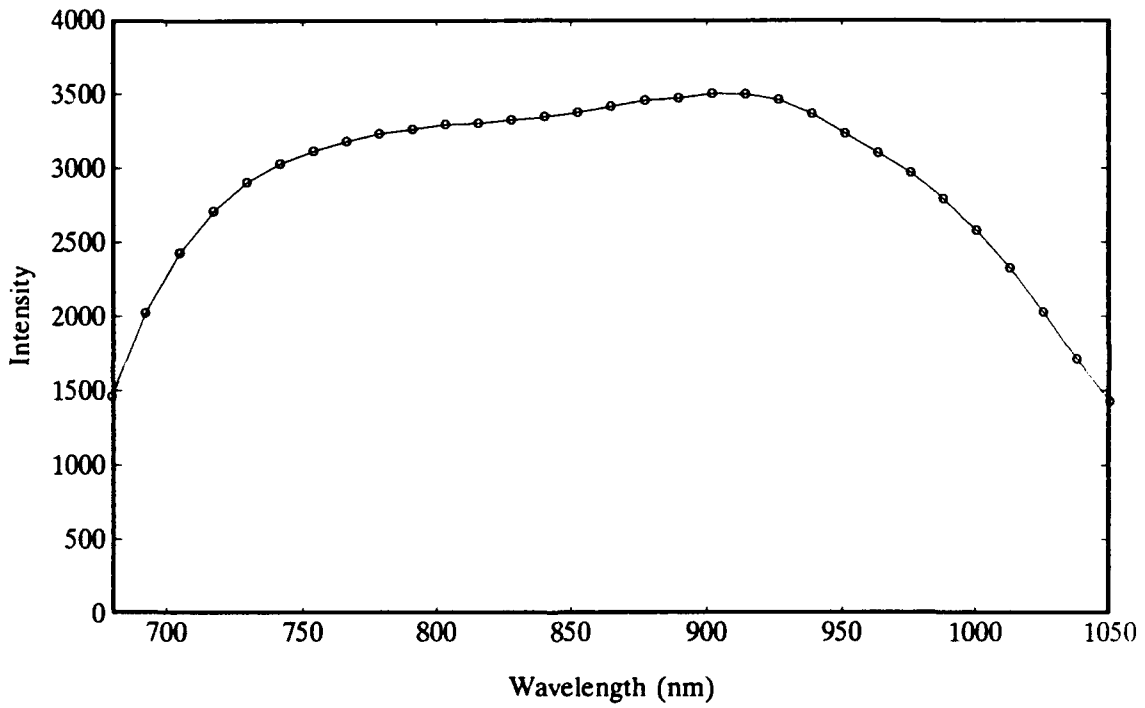
4000
3500
3000
2500
2000
1500
1000
500
0
Intensity
700
750
800
850
900
950
1000
1050
Wavelength (nm)

wave pass filter (Corion - model LG-675-S) inserted to remove the overlapping second-order visible radiation. The falloff in intensity at wavelengths above 950 nm is due, primarily, to the well-known decrease in quantum efficiency of silicon-based detectors (4).

2.3.1 Resolution

The spectral resolution of the instrument was determined by examining the response to narrow-band radiation emitted from a 0.25m grating monochromator (Bausch & Lomb - Model #33-86-40-01, entrance slit - 1 mm, exit slit - 1 mm, bandpass 6.5 nm) using the full-width/ half-maximum criterion. The output of the monochromator was coupled to the entrance slit of the spectrograph by means of the fiber-optic bundle described earlier. With the entrance slit-width of the spectrograph set to 1 mm, the resolution of the instrument is approximately 25 nm (Figure 2.3). Theoretically, the resolution for an instrument with a linear dispersion of 315 nm/inch and an entrance slit width equal to the width of a single diode is twice that of the width, or, in this case, 24.8 nm. Though the resolution is rather low, and the data somewhat under-sampled, the spectral resolution is sufficient to distinguish between the C-H overtone absorptions of the aromatic (875 nm), methyl (913 nm), and methylene (934 nm) functional groups in hydrocarbons and hydrocarbon mixtures (Figure 2.3). Here, the methylene C-H overtone absorption serves to broaden the right-hand side of the methyl C-H absorption, as seen near the peak maxima between 913 and 934 nm.

Figure 2.3 Spectral resolution of portable NIR spectrometer.

a) Resolution determination using full-width/half-maximum criterion of adjacent spectral peaks. Resolution is calculated to be 25 nm.

b) SW-NIR spectra of unleaded gasoline.

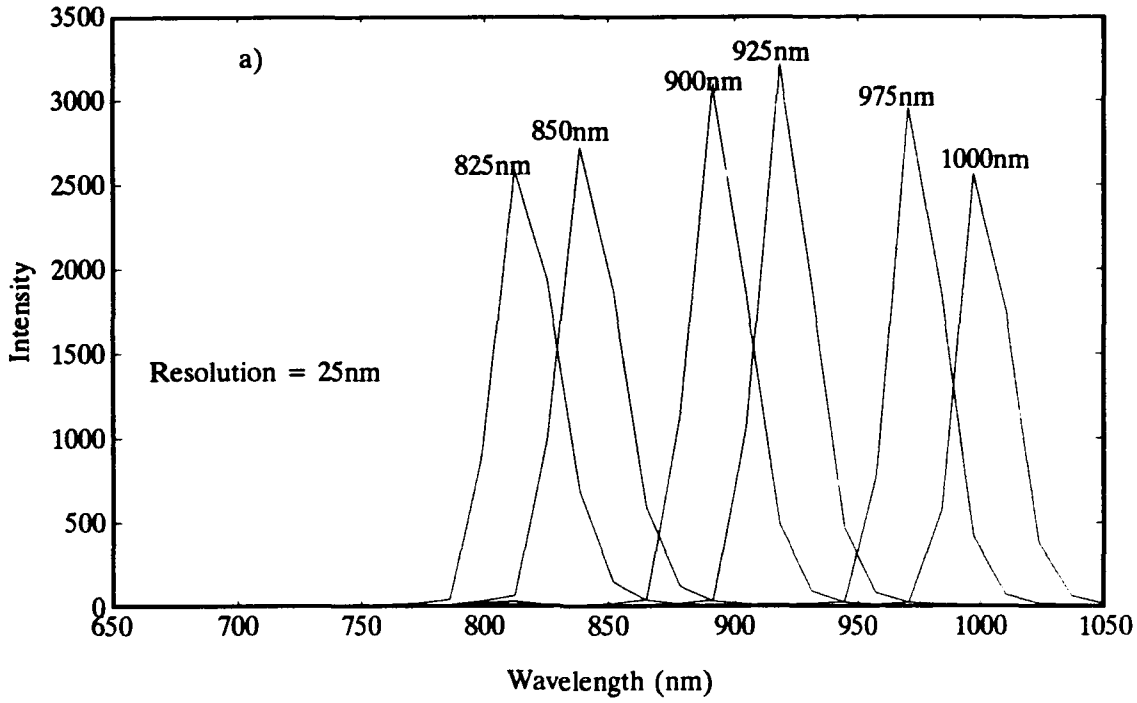
a)
825nm
850nm
900nm
925nm
975nm
1000nm
Resolution = 25nm
Intensity
Wavelength (nm)
3500
3000
2500
2000
1500
1000
500
0
650
700
750
800
850
900
950
1000
1050

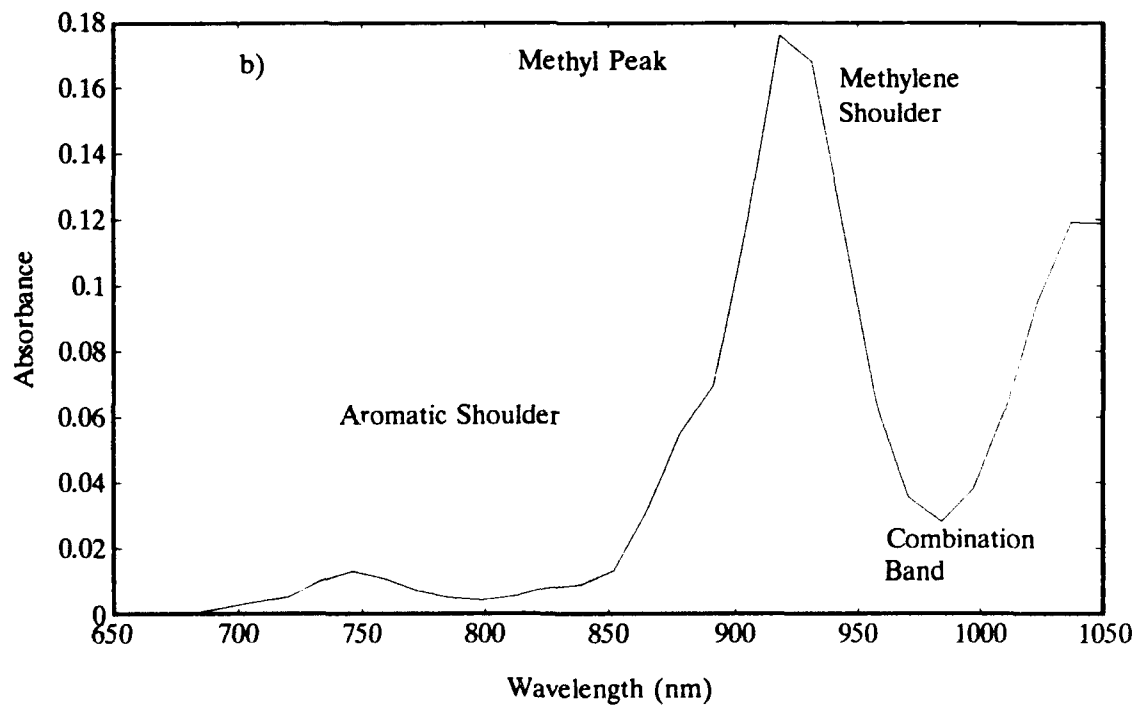
b)
Methyl Peak
Methylene Shoulder
Aromatic Shoulder
Combination Band
Absorbance
Wavelength (nm)
0.18
0.16
0.14
0.12
0.1
0.08
0.06
0.04
0.02
0
650
700
750
800
850
900
950
1000
1050

2.3.2 Baseline Noise

The baseline noise level of an instrument can be calculated by taking the log ratio of two successive spectral measurements of an air blank. Prior to calculating the log ratio, the dark current must be subtracted from each of the blanks (5). Since silicon detectors are photoelectron noise-limited at high light levels (6), the baseline noise for a given wavelength will be proportional to the square root of the intensity of incident light, as well as the quantum efficiency at that wavelength. For the photoelectron noise-limited case, the baseline noise should decrease by $(N)^{1/2}$, where N is the number of signal-averaged scans taken (7). Figure 2.4a shows the baseline noise for 1 scan (35ms acquisition time) to have an RMS value of 1.25 X 10^{-4} absorbance units (AU). It is encouraging to see that when 100 scans are averaged (3.5 s acquisition time) the baseline noise improves by one order of magnitude, to an RMS value of 1.24 X 10^{-5} AU (Figure 2.4b).

A baseline noise comparison of the portable spectrometer with the commercial spectrophotometer was accomplished by measuring the noise level of the commercial instrument under both equal acquisition time (3.5 sec) and equal number of averaged scans (100 scans). The commercial spectrophotometer was able to average 7 scans in 3.5 seconds giving an RMS baseline noise level of 3.33 X 10^{-4} AU. For the same acquisition time, the portable spectrometer showed a twenty-seven fold improvement in baseline noise levels compared to the commercial instrument. It should be noted that were the commercial spectrophotometer data smoothed, so that it had the equivalent of 35 channels,

Figure 2.4 Baseline noise evaluation of portable NIR spectrometer.

a) Baseline noise for 1 scan.
(35.0 ms data acquisition)

b) Baseline noise for 100 scans.
(3.5 s data acquisition)

Root Mean Square (RMS) noise characteristics:

1 scan	1.25×10^{-4} AU
100 signal-averaged scans	1.24×10^{-5} AU

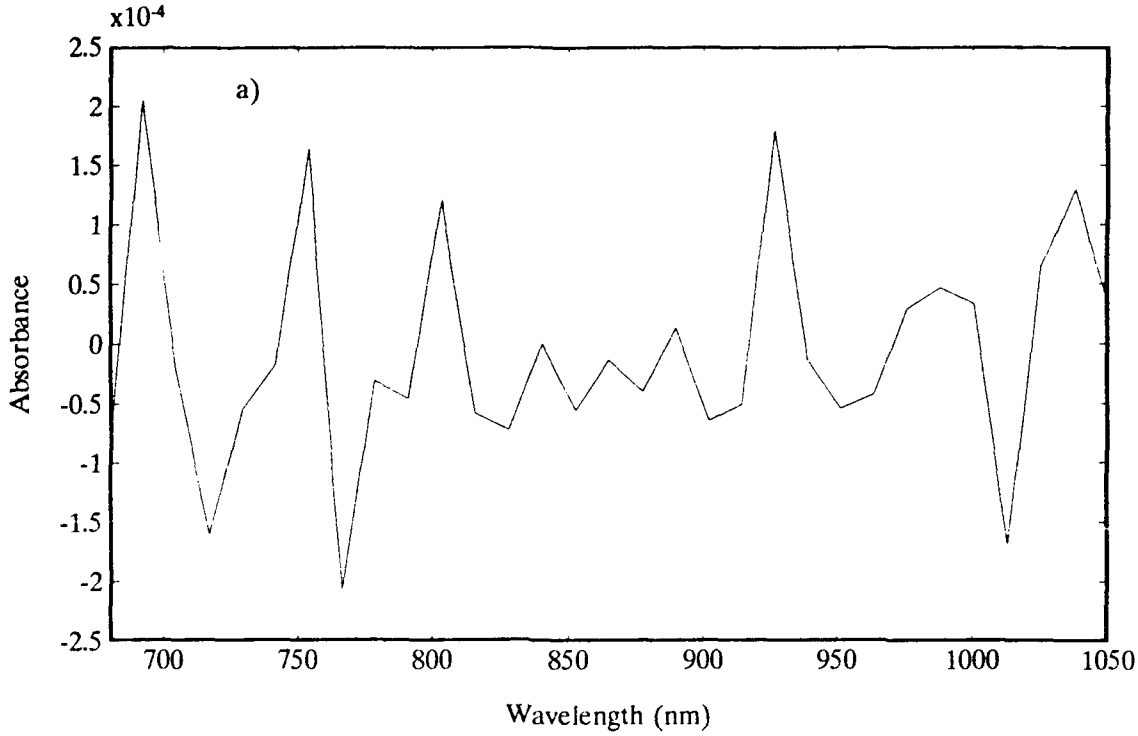
x10-4
a)
Absorbance
2.5
2
1.5
1
0.5
0
-0.5
-1
-1.5
-2
-2.5
700
750
800
850
900
950
1000
1050
Wavelength (nm)

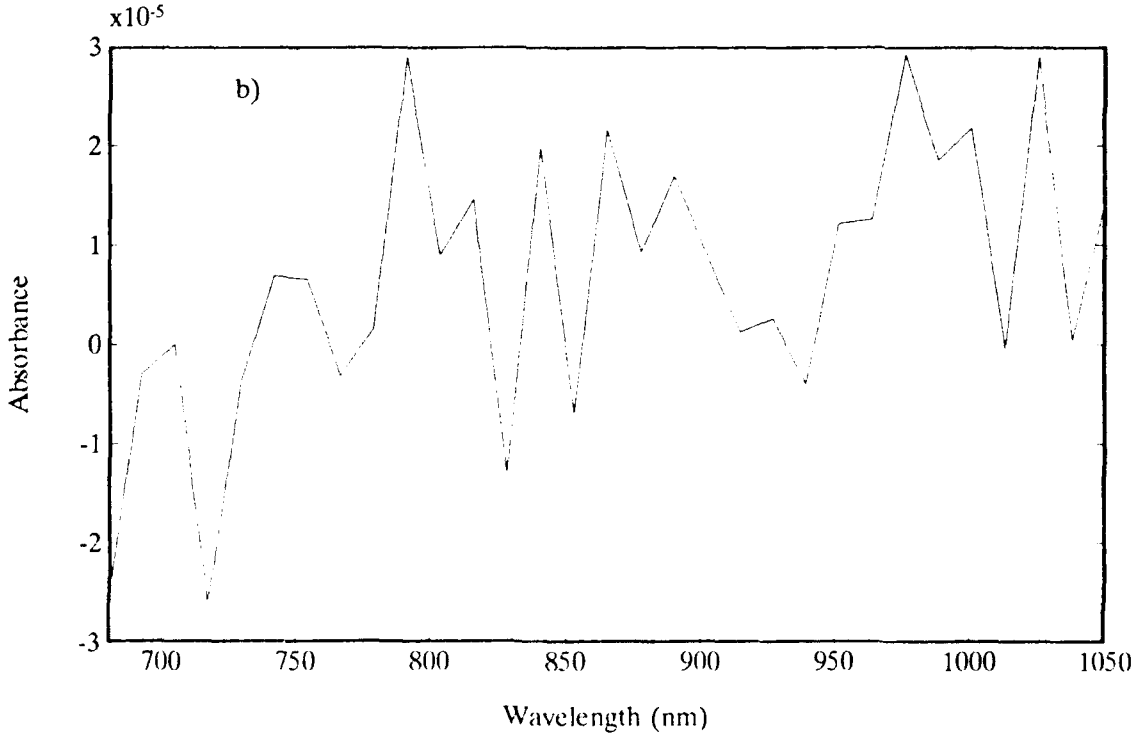
x10-5
b)
Absorbance
3
2
1
0
-1
-2
-3
700
750
800
850
900
950
1000
1050
Wavelength (nm)

the baseline noise level would have decreased by a factor of $(500/35)^{1/2} \approx 3.8$. This would result in an RMS value of 8.8×10^{-5} AU, still 7 times greater than that for the portable spectrometer. For an equal number of averaged scans (100), the commercial instrument required 47 seconds and had an RMS baseline noise value of 9.56×10^{-5} AU. Again, when the commercial spectrophotometer data is reduced to the equivalent of 35 channels, the equivalent RMS baseline noise value is 2.51×10^{-5} AU. For equal number of scans, the portable spectrometer showed a two-fold improvement in baseline noise level and a thirteen-fold time advantage over the commercial spectrometer.

2.3.3 Stray Light

To determine the amount of stray light present in the prototype instrument, monochromatic light was used at a series of wavelengths in the region between 680 and 1050 nm. The response was measured at those wavelengths, as well as the baseline response over the entire spectral region (8). The stray light (SL) was then calculated as follows:

$$SL = \frac{(I_0 - D)}{(I_P - D)} \tag{2.1}$$

where $\mathbf{I_0}$ is the baseline intensity, **D** is the dark current, and $\mathbf{I_p}$ is the peak intensity of monochromatic light. Monochromatic light was furnished by two Jarrell-Ash 0.25m monochromators (Model #82-410), arranged in series, to form a double

monochromator. Entrance and exit slits were set to provide a 10 nm bandpass. The exit slit of the second monochromator was coupled directly to the entrance slit of the spectrograph by a fiber-optic bundle. Spectral measurements were taken every 100 nm (Figure 2.5), giving a stray light intensity of 0.1%, typical for a single monochromator system. Methods usually used for stray light determination, such as those published by the American Society for Testing and Materials (ASTM) (9,10) could not be employed as there are no reference standards listed for measuring stray light in the 700 - 1100 nm region.

2.3.4 Dynamic Range

Absorption spectra of ten benzene/carbon tetrachloride mixtures were measured in order to determine the dynamic range of the portable spectrometer. Samples were gravimetrically prepared using a Sartorius balance accurate to 0.1 mg, with spectral measurements made immediately after sample preparation to minimize any effects due to evaporation. Concentration of benzene in the ten standards ranged from 100 weight percent (11.247 molar) to 0.212 weight percent (0.043 molar). Measurements were made in a transflectance configuration through a 2.0-cm cuvette, using the bifurcated fiber bundle described earlier as the optical interface. By placing a diffuse reflector behind the cuvette, the light beam was made to traverse the sample twice, making the effective path length of the measurement 4.0-cm. To compare results with the commercial spectrophotometer on an equal acquisition-time basis, spectral measurements were performed with

Figure 2.5 Stray light evaluation of portable NIR spectrometer.

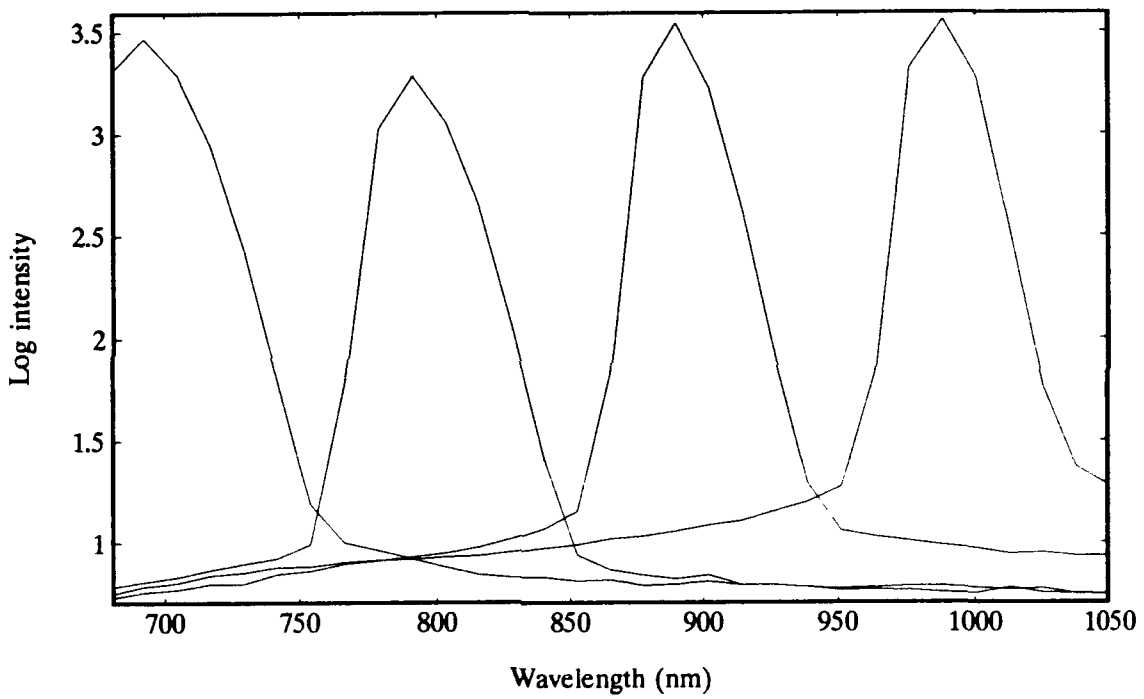
3.5
3
2.5
2
1.5
1
Log intensity
700
750
800
850
900
950
1000
1050
Wavelength (nm)

30 seconds acquisition time (375 scans), The high standard (pure benzene), as well as each of the four lowest standards, was measured three times to determine the reproducibility of the measurement technique.

One-wavelength regression models were used to calculate the estimated benzene concentrations following spectral normalization to 778 nm (a non-absorbing wavelength in the NIR). This procedure compensated for variations in sample placement. Plots of log actual concentration versus log estimated concentration are shown in Figure 2.6a for the portable spectrometer and in Figure 2.6b for the commercial spectrophotometer. The detection limit of benzene (based on a standard error of prediction greater than two standard deviations) using the portable spectrometer is approximately 0.063 molar, while that for the commercial spectrophotometer is approximately 0.107 molar. For our instrument, the theoretical detection limit for benzene, based on its molar extinction coefficient and the minimum resolution of a 12-bit A/D converter (1 part in 4095), is 0.025 molar. As shown in Figure 2.6, both instruments attained a dynamic range of approximately three orders of magnitude, with the portable spectrometer able to estimate the lower concentrations slightly better than the commercial spectrophotometer. This observation can be attributed to the better signal-to-noise (S/N) ratio of the portable spectrometer, which becomes especially important at low signal levels.

Table 2.1 summarizes the evaluation of the instrument and includes some of the physical characteristics of the instrument.

Figure 2.6 Dynamic range determination.

a) Portable NIR spectrometer.

b) Commercial spectrophotometer.

Comparison of the two instruments using the prediction of percent benzene in carbon tetrachloride by multiple linear regression.

	Portable NIR Spectrometer	Commercial Spectrophotometer
Slope:	0.996	1.008
R^2:	0.999	0.993

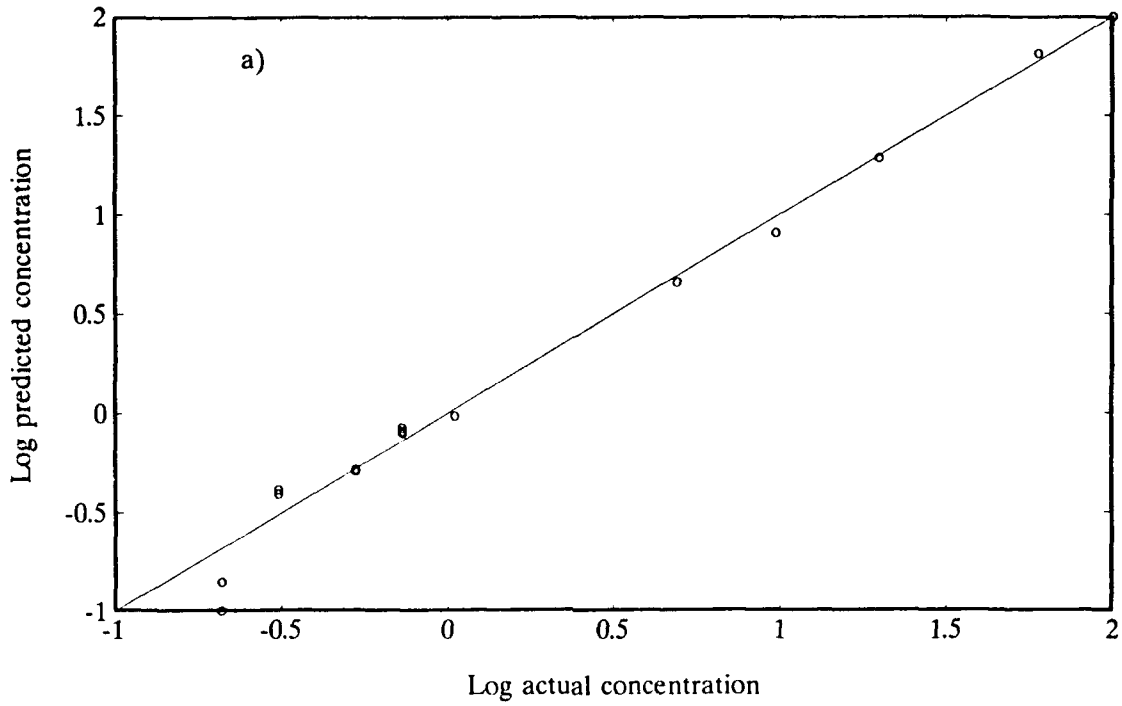
a)
Log predicted concentration
Log actual concentration
2
1.5
1
0.5
0
-0.5
-1
-1
-0.5
0
0.5
1
1.5
2

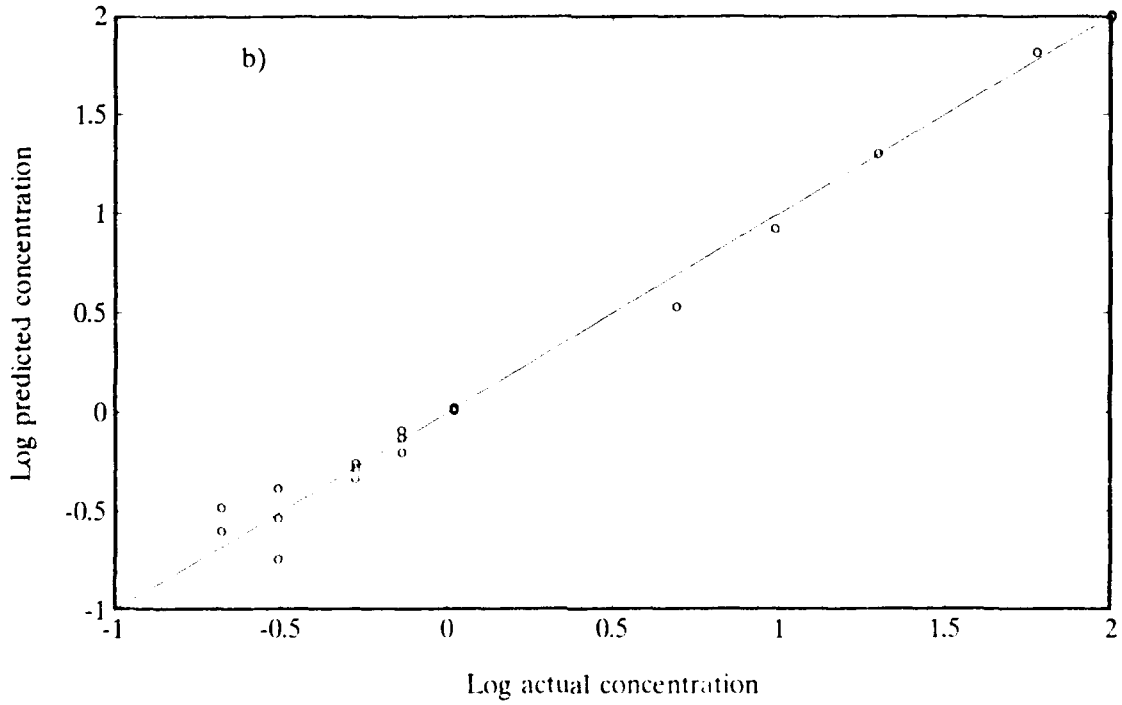
b)
Log predicted concentration
Log actual concentration
2
1.5
1
0.5
0
-0.5
-1
-1
-0.5
0
0.5
1
1.5
2

Table 2.1 Instrument evaluation summary.

Resolution	25 nm
Baseline Noise	1.24×10^{-5} AU
Stray Light	0.1 %
Dynamic Range	3 orders
Cost in Parts	$5,000.00
Weight	23 lbs.
Size	6" X 14" X 17"

2.3.5 Performance Comparison Between the Portable NIR Spectrometer and a Commercially Available Laboratory Spectrophotometer.

As a test of the performance of the instrument, we measured the NIR spectra of 28 hydrocarbon mixtures in an attempt to correlate various quality parameters of the sample mixtures with their spectra. The hydrocarbon mixtures, consisting of varying amounts of toluene, isooctane and n-heptane, are specified by the ASTM (11) for use in calibrating octane engines. The mixtures utilized gave a range of research octane number (RON) from 65.2 to 113.7 and a range of motor octane number (MON) from 57.8 to 100.8. Pump octane number (PON), the numerical average of the RON and PON values, is the quality parameter of most interest to consumers (see Table 2.2). The portable spectrometer was operated in a transflectance configuration, while the commercial spectrophotometer used a transmission configuration. Measurements were made through a 2.00 cm cuvette at room temperature using an air blank as the reference. Figure 2.7 shows the raw data of: a) the portable spectrometer, and b) the commercial spectrophotometer. The baseline offset shown in the data was primarily a result of an inability to reproducibly place the sample cuvette from one measurement to the next and, to a lesser extent was due to varying indices of refraction from one sample to another. The sudden decrease in absorption intensity at 850 nm, seen in the spectra obtained on the portable spectrometer (Figure 2.7a), was an aberration which apparently arose from the difference in refractive index between

Table 2.2 Hydrocarbon mixture composition.

Sample Number	Volume Percent			Octane Number		
	Toluene	Isooct.	n-Hept.	RON	MON	PON
1	50.0	0.0	50.0	65.2	57.8	61.5
2	52.0	0.0	48.0	67.8	60.1	64.0
3	54.0	0.0	46.0	70.3	62.2	66.3
4	56.0	0.0	44.0	72.9	64.4	68.7
5	58.0	0.0	42.0	75.5	66.5	71.0
6	60.0	0.0	40.0	77.9	68.5	73.2
7	62.0	0.0	38.0	80.3	70.5	75.4
8	64.0	0.0	36.0	82.7	72.5	77.6
9	66.0	0.0	34.0	85.0	74.4	79.7
10	68.0	0.0	32.0	87.3	76.1	81.7
11	70.0	0.0	30.0	89.5	77.9	83.7
12	72.0	0.0	28.0	91.5	79.5	85.5
13	74.0	0.0	26.0	93.4	81.1	87.3
14	74.0	2.0	24.0	94.8	82.7	88.8
15	74.0	4.0	22.0	96.0	84.1	90.1
16	74.0	5.0	21.0	96.7	84.9	90.8
17	74.0	6.0	20.0	97.2	85.5	91.4
18	74.0	8.0	18.0	98.3	87.0	92.7
19	74.0	10.0	16.0	99.6	88.5	94.1
20	74.0	12.0	14.0	101.0	90.0	95.5
21	74.0	14.0	12.0	102.5	91.7	97.1
22	74.0	15.0	11.0	103.3	92.5	97.9
23	74.0	16.0	10.0	104.2	93.4	98.8
24	74.0	18.0	8.0	106.1	95.1	100.6
25	74.0	20.0	6.0	108.0	96.8	102.4
26	74.0	22.0	4.0	109.9	98.2	104.1
27	74.0	24.0	2.0	111.8	99.5	105.7
28	74.0	26.0	0.0	113.7	100.8	107.3

Figure 2.7 Raw spectra of reference hydrocarbon standards.

a) Portable NIR spectrometer.

b) Commercial spectrophotometer.

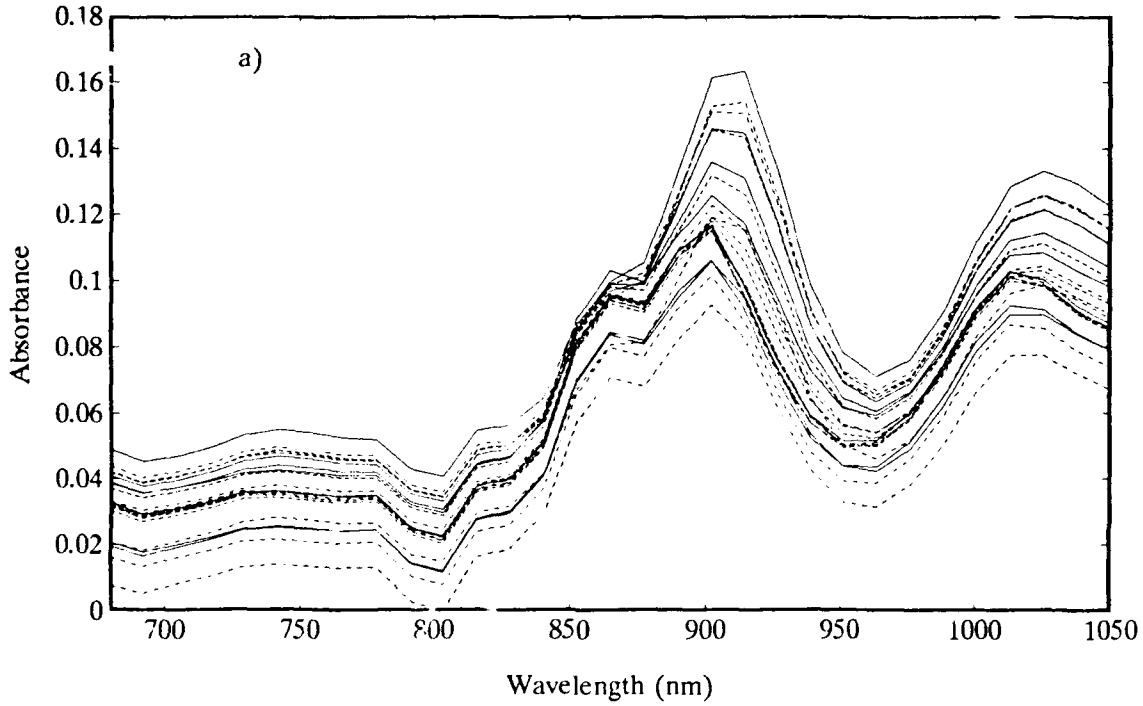
a)
Absorbance
0.18
0.16
0.14
0.12
0.1
0.08
0.06
0.04
0.02
0
700
750
800
850
900
950
1000
1050
Wavelength (nm)

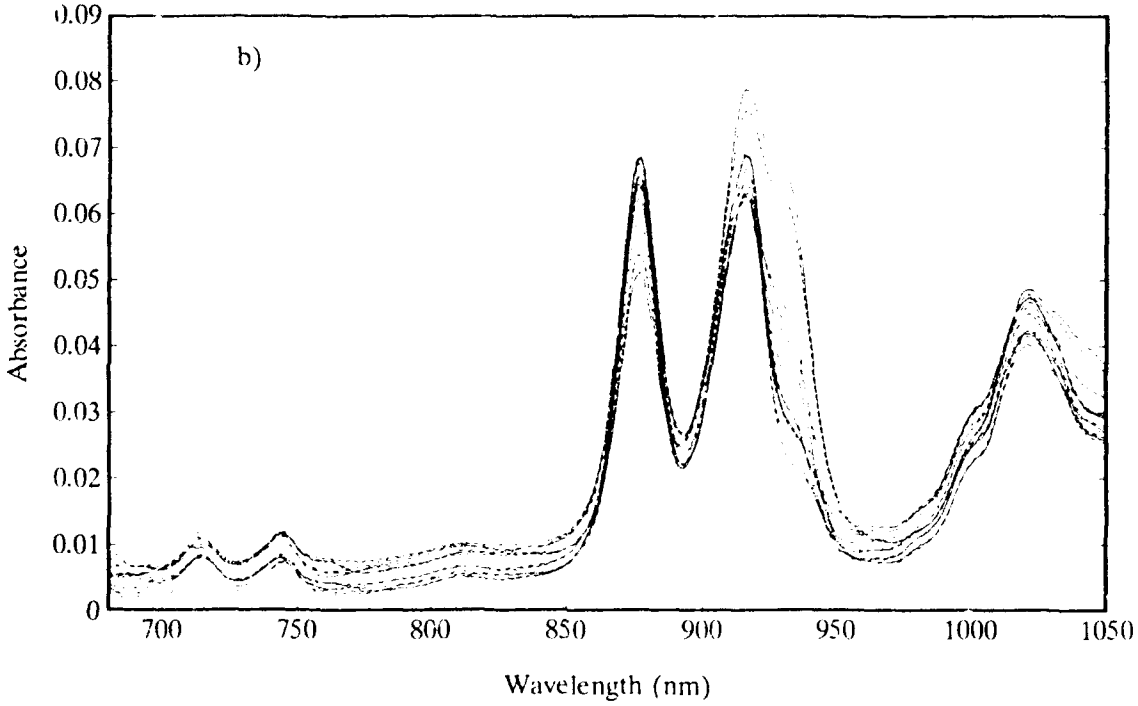
b)
Absorbance
0.09
0.08
0.07
0.06
0.05
0.04
0.03
0.02
0.01
0
700
750
800
850
900
950
1000
1050
Wavelength (nm)

the hydrocarbon samples and the air blank used as reference. When carbon tetrachloride was used as the reference, this undesired feature disappeared. The technique of offset subtraction was applied to both data sets in order to better compare instrument performance. It was performed by subtracting the absorbance at 825 nm from the absorbance values at all other wavelengths. This wavelength was chosen for normalization since hydrocarbons have minimal absorbance at 825 nm and any changes in intensity are a result of the offset mentioned above. Figure 2.8 shows the normalized spectra of: a) the portable spectrometer and b) the commercial spectrophotometer. The very low resolution of the portable instrument is apparent from these figures. Stage-wise MLR was performed over the wavelength region 680 - 1050 nm in order to find correlations between various spectral features and several independently-measured constituent values. Each of the regression equations calculated used a three-wavelength model. Correlations to RON, MON, PON, and volume percent of the three components were calculated and the standard error of calibration (SEC) and multiple correlation coefficients (R^2) determined (Table 2.3). The predictive capability of the model was determined from a cross-validation estimate where all, but one, of the samples in the calibration set were used to determine the prediction equation. The equation was then used to predict the constituent values of the omitted sample (12). This technique of "leave-one-out" was then repeated for each sample in the original calibration set, resulting in a set of predicted values for each constituent. The standard errors of prediction (SEP) were then calculated

Figure 2.8 Normalized spectra of reference hydrocarbon standards.

a) Portable NIR spectrometer.

b) Commercial spectrophotometer.

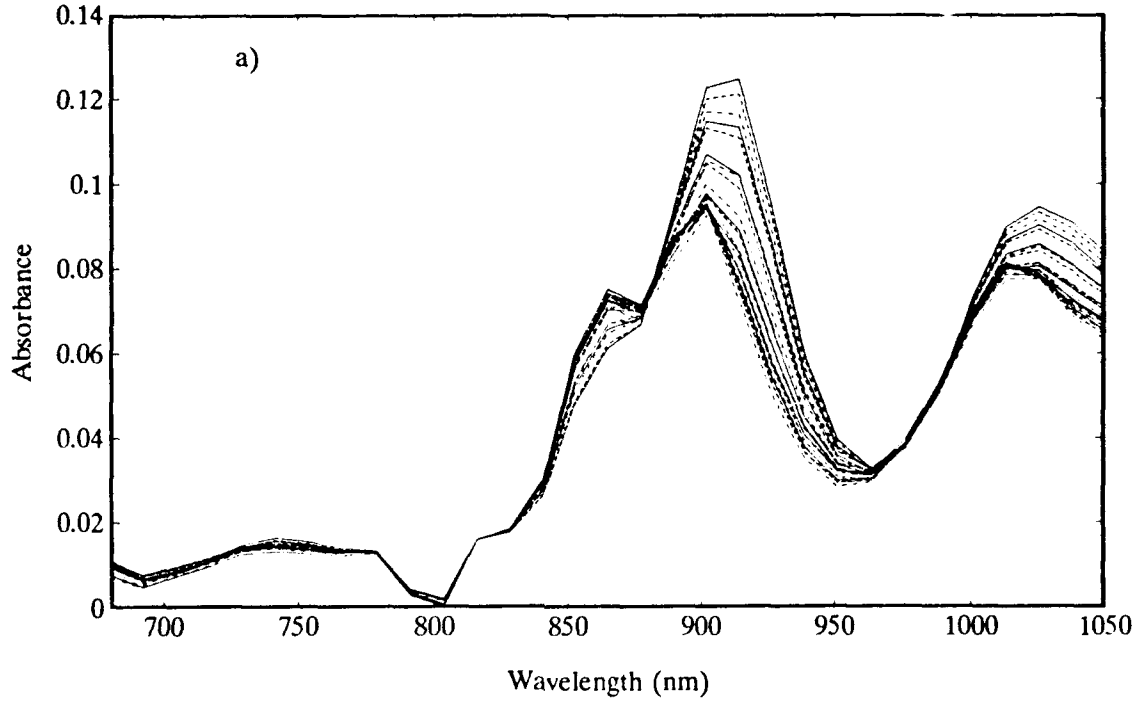
a)
Absorbance
0.14
0.12
0.1
0.08
0.06
0.04
0.02
0
700
750
800
850
900
950
1000
1050
Wavelength (nm)

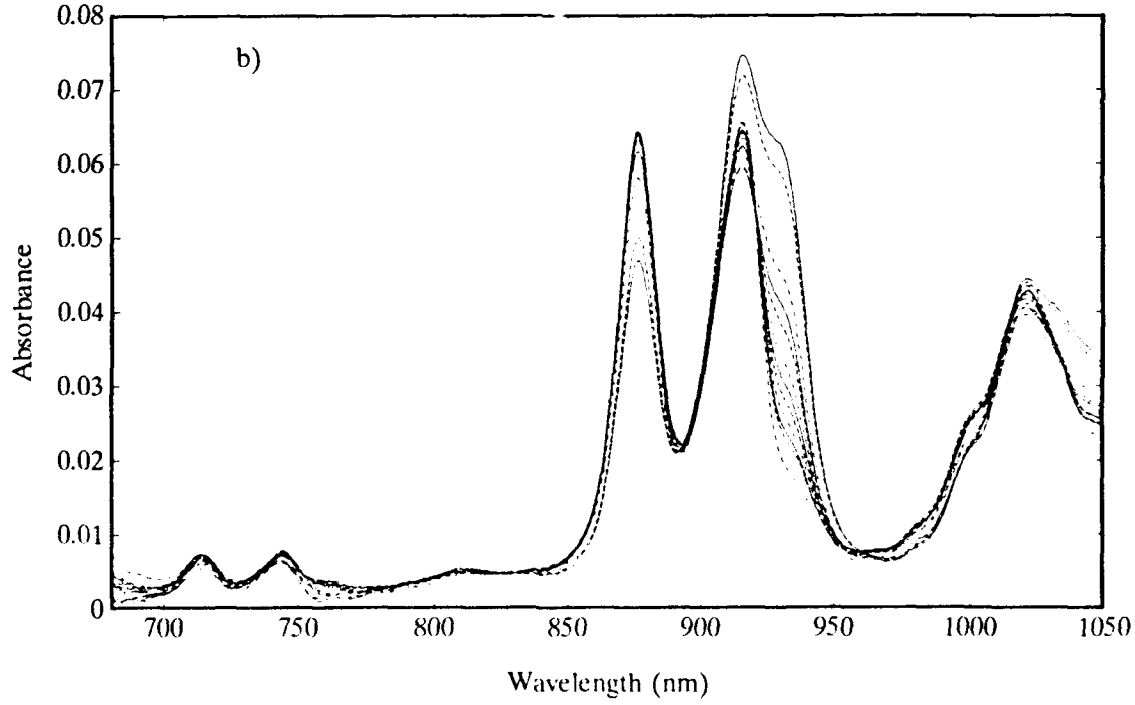
b)
Absorbance
0.08
0.07
0.06
0.05
0.04
0.03
0.02
0.01
0
700
750
800
850
900
950
1000
1050
Wavelength (nm)

Table 2.3 Multiple linear regression analysis of hydrocarbon samples.

	Portable NIR Spectrometer		
	SEC	R^2	SEP
RON	0.591	0.9992	0.791
MON	0.429	0.9995	0.499
PON	0.448	0.9995	0.551
Volume % Toluene	0.173	0.9998	0.247
Volume % Isooctane	0.921	0.9951	1.218
Volume % n-Heptane	0.346	0.9998	0.499
	Commercial Laboratory Instrument		
	SEC	R^2	SEP
RON	0.645	0.9990	0.844
MON	0.390	0.9996	0.544
PON	0.328	0.9997	0.583
Volume % Toluene	0.271	0.9995	0.368
Volume % Isooctane	0.762	0.9966	0.901
Volume % n-Heptane	0.232	0.9999	0.280

using equation 2.2 and are presented in Table 2.3.

$$SEP=\sqrt{\frac{\sum(D-\bar{D})^2}{(N-1)}} \tag{2.2}$$

where **D** is the difference between predicted and actual value, $\bar{\mathbf{D}}$ is the mean difference, and **N** is the number of samples.

As can be seen from the SEC, SEP and correlation coefficient values, the portable spectrometer performed as well as the commercial spectrophotometer, despite having a resolution of 25 nm -- 3.5 times worse than that of the commercial instrument. Correlation values approaching unity, such as those seen here, are indicative of a high degree of linearity between the spectral features and constituent values of the data set. This high degree of linearity is apparent in the correlation plots of RON, MON, PON, and volume percents of toluene, isooctane and *n*-heptane shown in Figure 2.9, Figure 2.10, and Figure 2.11 from data obtained using the portable spectrometer. Though not shown here in graphical form, the correlation plots of data obtained using the commercial spectrophotometer showed equally good correlations and are omitted as unnecessary. The somewhat poorer performance in the prediction of volume percent isooctane is due to the severe overlap between isooctane and *n*-heptane in the methyl absorption peak. The prediction of *n*-heptane is not hindered by this overlap because it can be correlated with the methylene absorption, which is much stronger in *n*-heptane than in isooctane. The portable spectrometer performed

Figure 2.9 Correlation plots for a) RON and b) MON.

RON - Research octane number.

MON - Motor octane number.

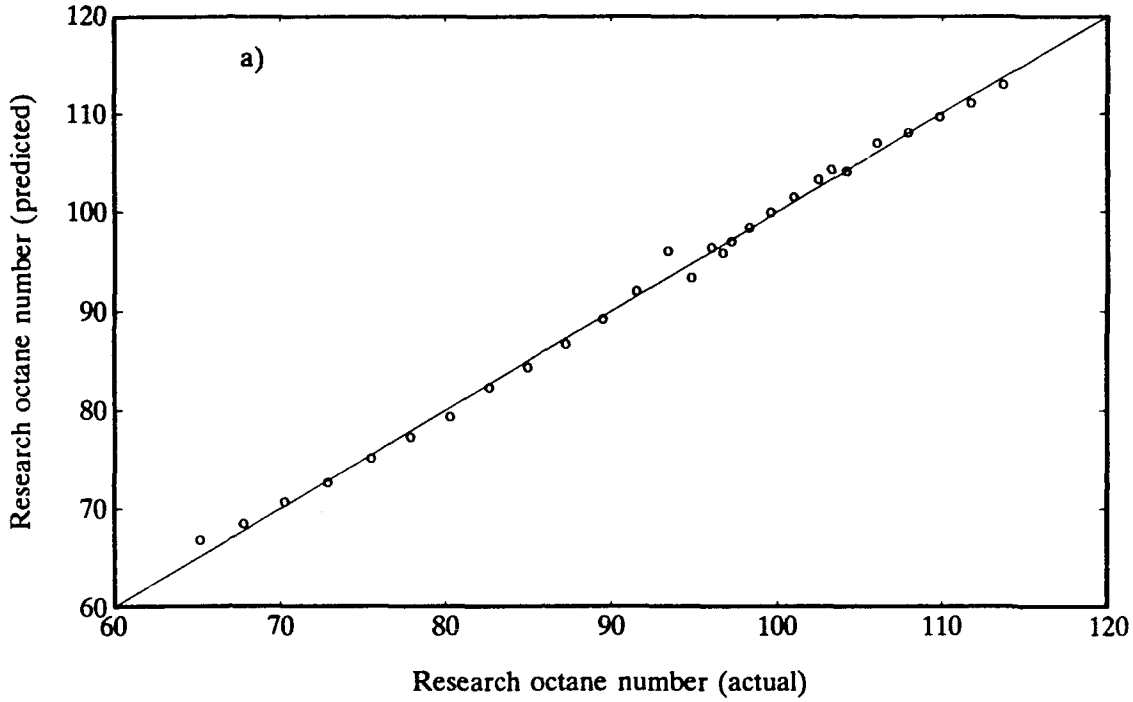
a)
Research octane number (predicted)
Research octane number (actual)
60
70
80
90
100
110
120

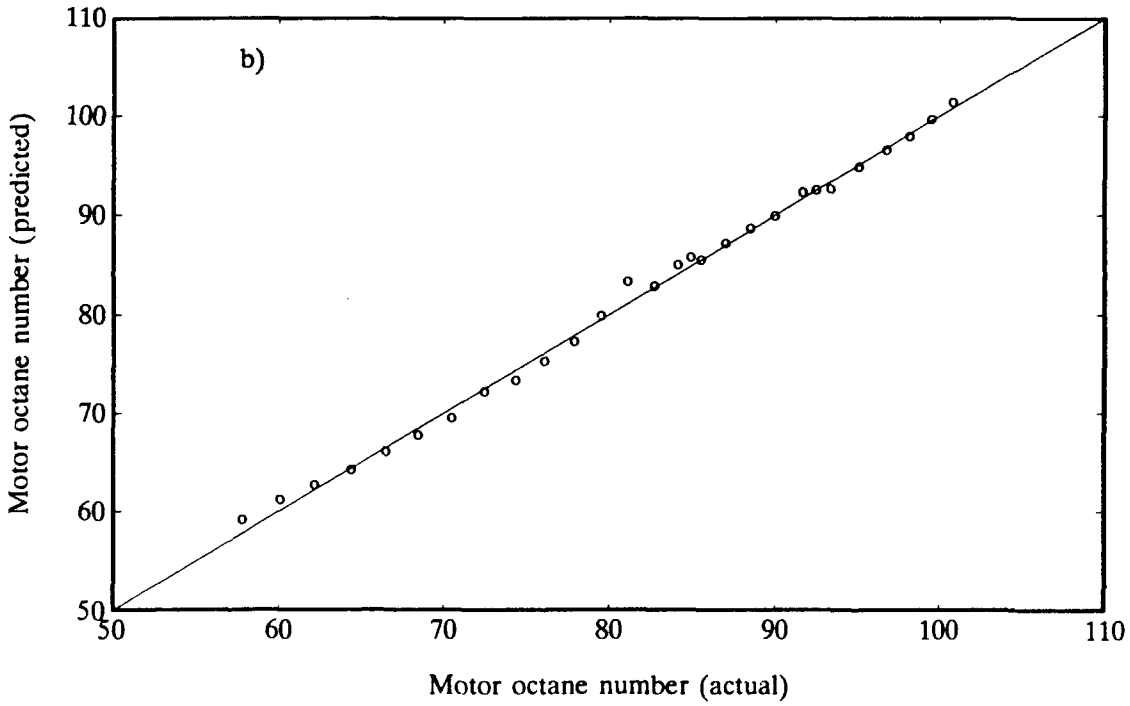
b)
Motor octane number (predicted)
Motor octane number (actual)
50
60
70
80
90
100
110

Figure 2.10 Correlation plots for A) PON and B) vol % toluene.

PON - Pump octane number.

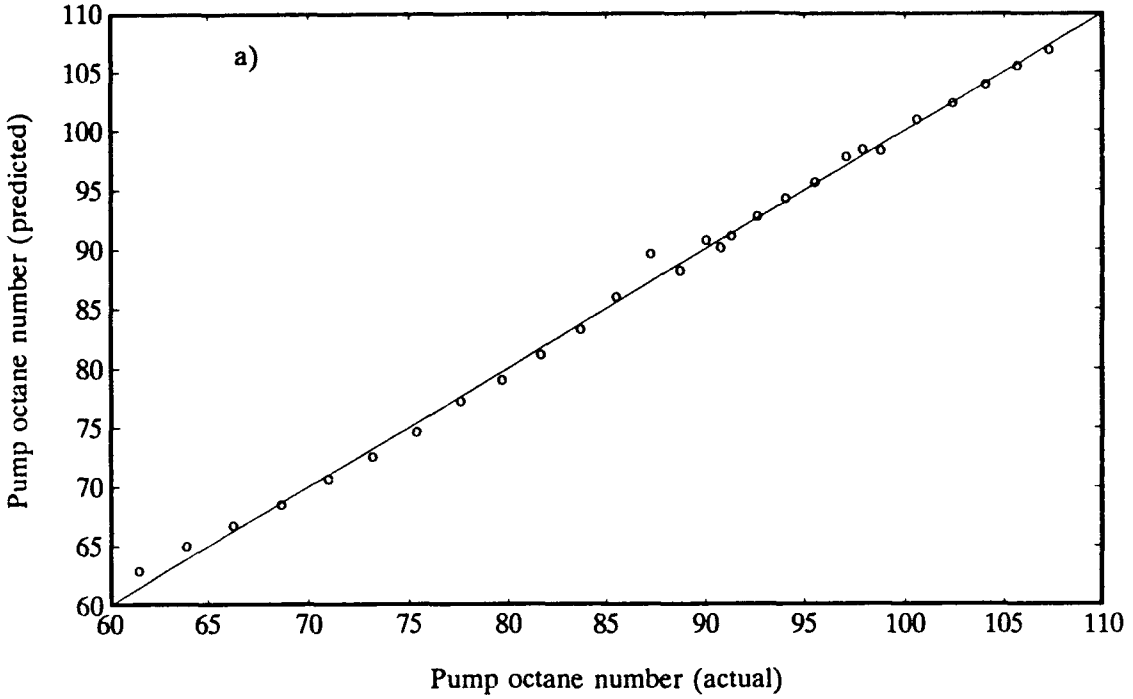
a)
Pump octane number (predicted)
Pump octane number (actual)
60
65
70
75
80
85
90
95
100
105
110

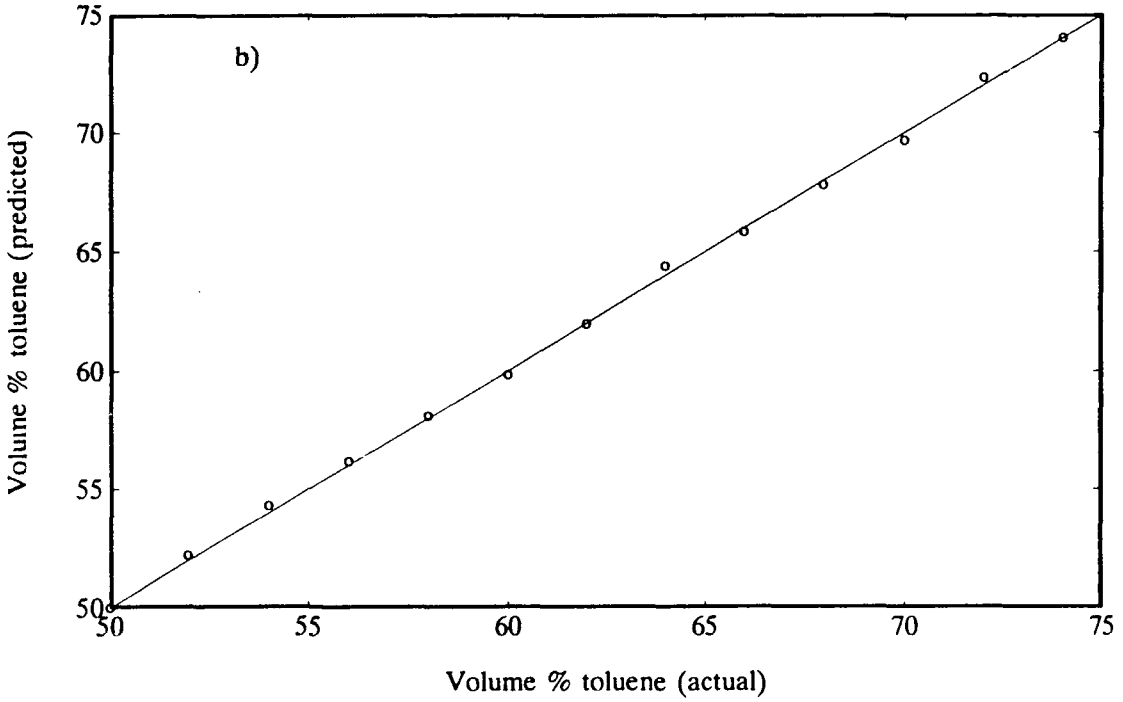
b)
Volume % toluene (predicted)
Volume % toluene (actual)
50
55
60
65
70
75

Figure 2.11 Correlation plots for vol % a) isooctane and b) *n*-heptane.

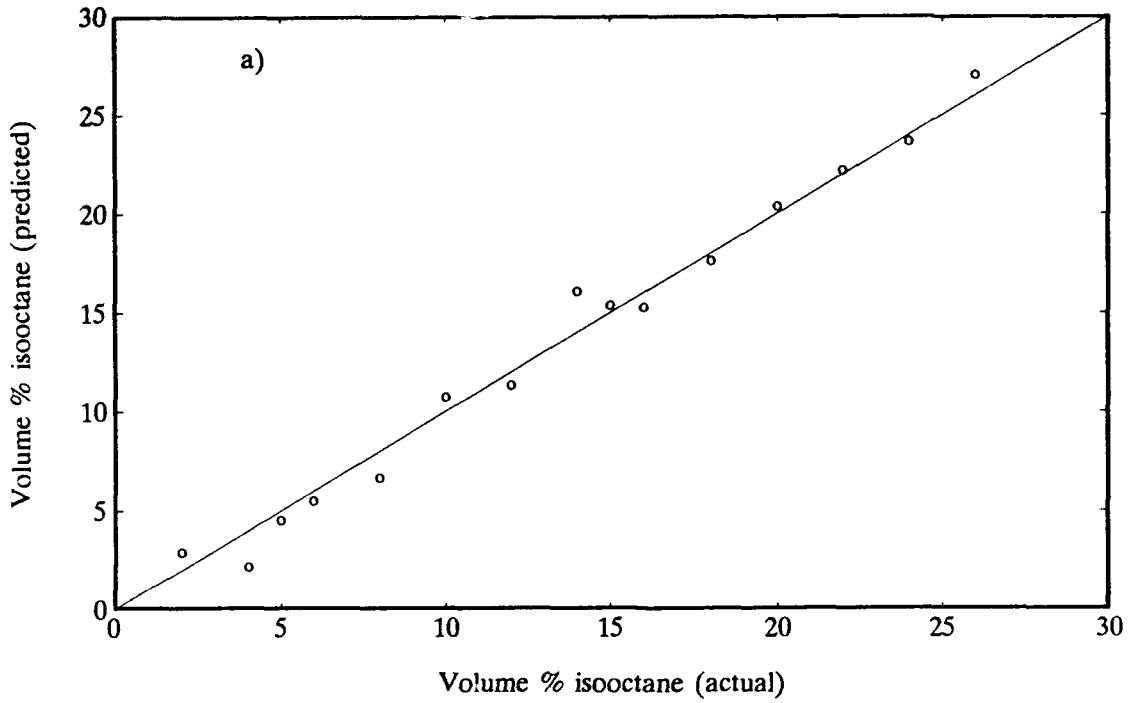
a)
Volume % isooctane (predicted)
Volume % isooctane (actual)
0
5
10
15
20
25
30

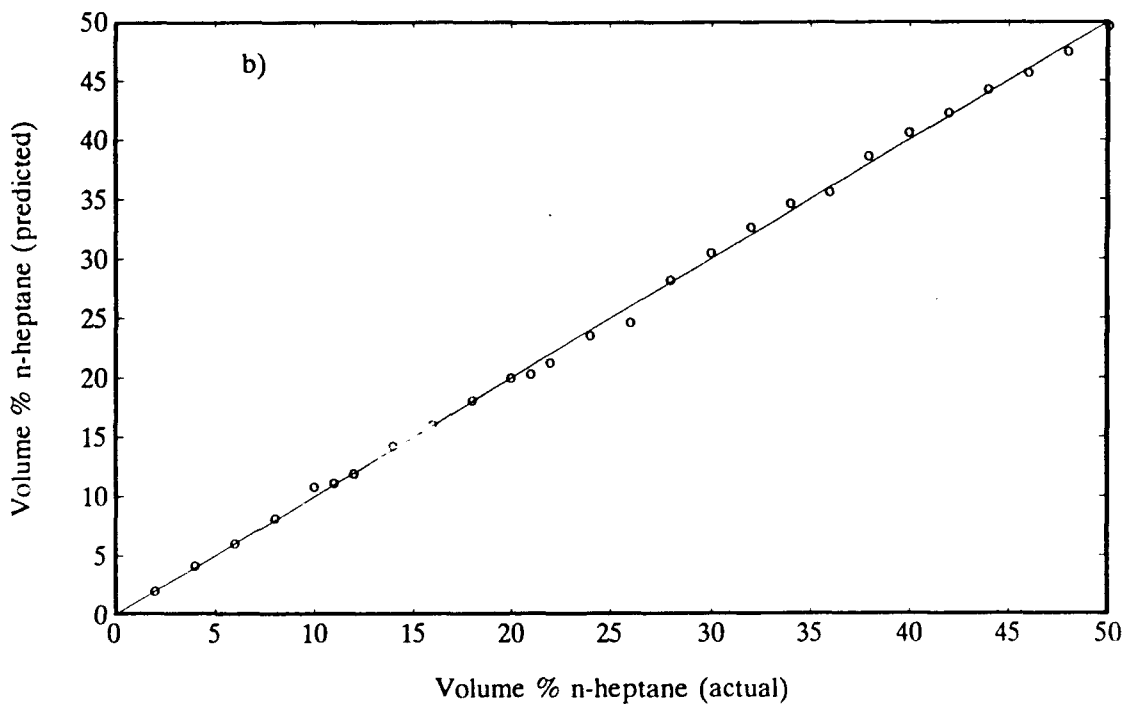
b)
Volume % n-heptane (predicted)
Volume % n-heptane (actual)
0
5
10
15
20
25
30
35
40
45
50

slightly better than the scanning spectrophotometer in the prediction of RON, MON, PON, and volume percent toluene. This can be attributed to the higher S/N ratio of the portable spectrometer. For the prediction of volume percent isooctane and volume percent *n*-heptane, however, the scanning spectrophotometer performs slightly better. This is attributed to its higher resolution and an inability of the portable spectrometer to resolve the severe overlap of the methyl and methylene functional groups. The low resolution did not hinder the portable spectrometer in the prediction of volume percent toluene, as the 875 nm aromatic C-H stretch is far enough removed from the methyl and methylene absorptions to adequately distinguish the aromatic absorption.

To see if the three octane numbers could be predicted directly from the known concentrations of toluene, isooctane, and *n*-heptane, an MLR analysis was conducted using the concentration matrix as the independent variable. Though slightly worse than the spectral analysis presented above, calibration against the volume percents of the three constituents worked very well. The results of this analysis are presented in Table 2.4 for both the calibration analysis (SEC values) as well as the cross-validation analysis (SEP values). For the prediction of all three octane numbers, the order of independent variable selection was, *n*-heptane, followed by isooctane, and then toluene. This is not surprising, as the concentration of *n*-heptane is varying throughout all 28 samples, while the concentration of both toluene and isooctane is held constant for approximately half the calibration samples.

Table 2.4 MLR calibration against component concentrations.

	SEC	R^2	SEP	R^2
RON	0.709	0.9987	0.812	0.9989
MON	0.366	0.9996	0.418	0.9995
PON	0.500	0.9993	0.569	0.993

Though not considered in this analysis, volume-of-mixing effects could be degrading the performance of the MLR analysis. The slight non-linear behavior observed in Figure 2.9, Figure 2.10 and Figure 2.11 may be a result of a volume increase or decrease of mixing not taken into account in this analysis.

2.4 Conclusions

The results shown here demonstrate the potential of a field-portable near-infrared spectrometer. The higher S/N ratios of silicon PDA's and the wavelength stability and system reliability, which result from having no moving parts in the instrument, clearly demonstrate its advantages over traditional scanning spectrophotometers. However, as was seen with the prediction of volume percent isooctane and volume percent *n*-heptane, the spectral resolution of the portable spectrometer needed improvement in order to have utility for the analysis of mixtures with severely overlapping peaks. This, along with numerous other instrumental improvements whose need became apparent as a result of the evaluation of this instrument, are presented in Chapter 3.

2.5 Notes to Chapter 2

1. Lysaght, M.J., van Zee, J.A., Callis, J.B., *Rev. Sci. Inst.*, **1991**, 2, 507.

2. Hamamatsu Technical Data Sheet No. S-501-02, **1987**, 2.

3. NIR Spectral Analysis Software, Ver. 3.07, NIRSystems, Silver Spring Maryland, **1989**.

4. Janesick, J.R., Elliott, T., Collins, S., Blouke, M.M., Freeman, J., *Optical Engineering*, **1987**, 26, 692.

5. Landa, I., *Rev. Sci. Instrum.*, **1979**, 50(1), 34.

6. Talmi, Y., *Appl. Spectrosc.*, **1982**, 36(1), 1.

7. Bilhorn, R. B., Epperson, P. M., Sweedler, J. V., Denton, M. D., *Appl. Spectrosc.*, **1987**, 41(7), 1125.

8. Kaye, W., *Anal. Chem.*, **1981**, 53, 2201.

9. *"Designation: E275-83," in Annual Book of ASTM Standards,* (ASTM Press, Philadelphia, Pennsylvania), **1990**, 14.01, 64.

10. *"Designation: E387-84," in Annual Book of ASTM Standards,* (ASTM Press, Philadelphia, Pennsylvania), **1990**, 14.01, 96.

11. *"Annex 2 - Reference Materials and Blending Accessories", in Annual Book of ASTM Standards*, (ASTM Press, Philadelphia, Pennsylvania), **1988**, 5.01, 128.

12. Haaland, D.M., Thomas, E.V., *Anal. Chem.*, **1988**, 60, 1202.

CHAPTER 3

Instrument Design and Characterization (II)

3.1 Introduction

The prototype instrument presented in Chapter 2 clearly demonstrated the feasibility and utility of a field-portable near-infrared (NIR) spectrometer. Though possessing performance characteristics comparable to an existing commercial laboratory instrument, the evaluation of the prototype instrument highlighted several areas for improvement, resulting in the design and construction of a second generation portable NIR spectrometer (1). The focus of this chapter is the design and performance evaluation of the upgraded portable NIR spectrometer. The new instrument allows sample measurements to be made in reflectance, transmission, and transflectance modes in order to analyze a wider selection of samples. It has a wavelength range of 700 - 1100 nm, improved spectral resolution and reduced stray light intensity. These improvements were accomplished by: a) incorporating a 1024-element photodiode array detector to increase resolution; b) temperature stabilizing the photodiode array, using a thermoelectric cooler to yield a higher signal-to-noise ratio (S/N); c) including a shutter to allow the light source to remain on continuously, for greater source stability; d) adding a 16-bit analog-to-digital (A/D) converter, to increase dynamic range; e) performing wavelength dispersion using a concave holographic grating, to reduce stray light; and f) modifying the software to improve the instrument

control, data acquisition and display, and user interface. The instrument now weighs 2 pounds more than the prototype instrument due to changes in the spectrometer portion of the instrument, but remains the size of a thick briefcase. The performance of this improved portable NIR spectrometer is compared with state-of-the-art, commercially available Near-Infrared (NIR) spectrometers in Chapters 4 and 5.

3.2 Instrument Design

A drawing (Figure 3.1a) and block diagram (Figure 3.1b) show the portable NIR spectrometer configured for transmission measurements. Light from the 5.5 watt tungsten light source is focused onto one end of a fiber-optic bundle (Sterngold Corporation; 1 mm outside bundle diameter and 12" in length) using two 15 mm focal length lenses. Light exiting the opposite end of the fiber bundle is collimated, using another 15 mm focal length lens, before it passes through the sample. The transmitted light is then refocused onto one end of a second fiber-optic bundle, using a fourth 15 mm focal length lens. The opposite end of this fiber bundle is connected to the spectrometer by means of a fiber-optic coupler configured with a 50 micron wide by 2.5 mm high entrance slit. The fiber-optic bundle is reshaped to a slit geometry to better match the spectrometer/detector optical configuration. Wavelength dispersion is accomplished using an 97.4 mm focal length spectrograph (American Holographic - model Chemspec 100S), with a 520 grooves/mm concave holographic grating, operating in the first order and

Figure 3.1 High resolution portable near-infrared spectrometer.

a) Drawing of portable NIR spectrometer.

b) Block diagram of portable NIR spectrometer configured for transmission measurements.

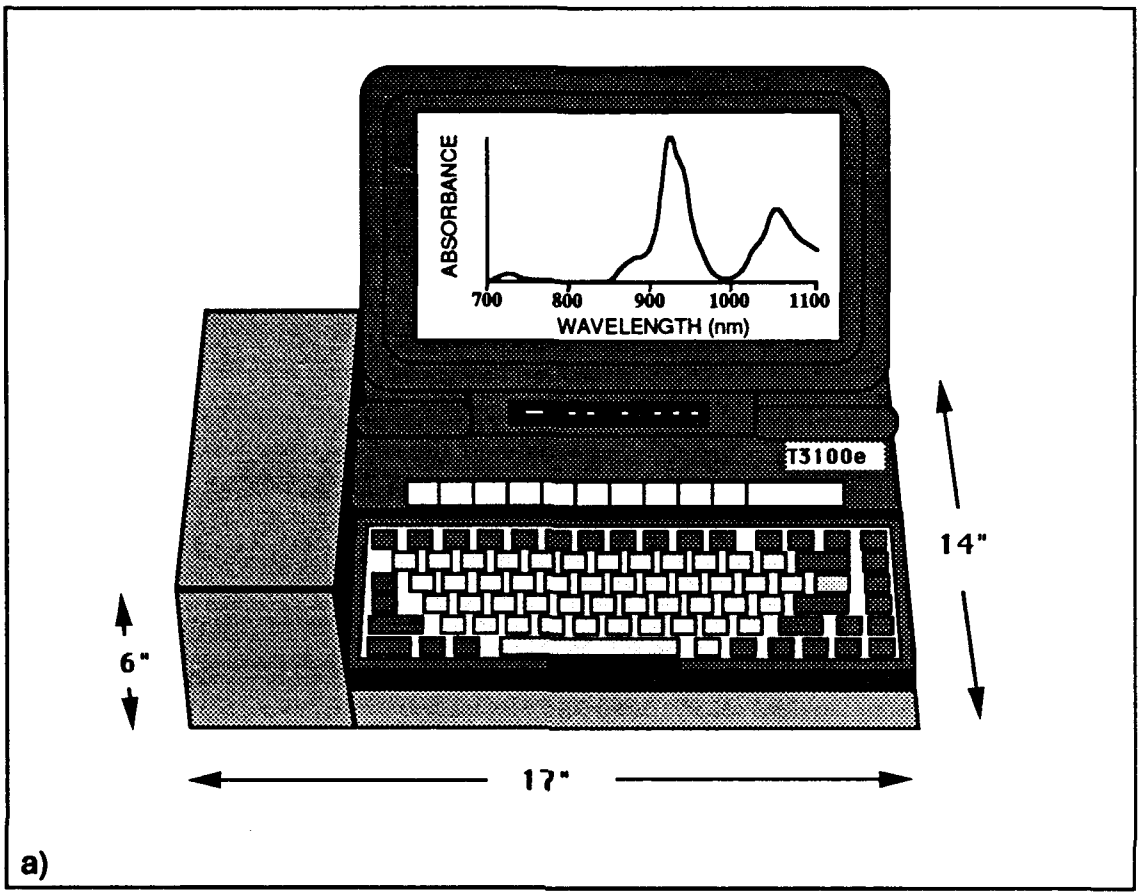
ABSORBANCE
700
800
900
1000
1100
WAVELENGTH (nm)
T3100e
14"
6"
17"
a)

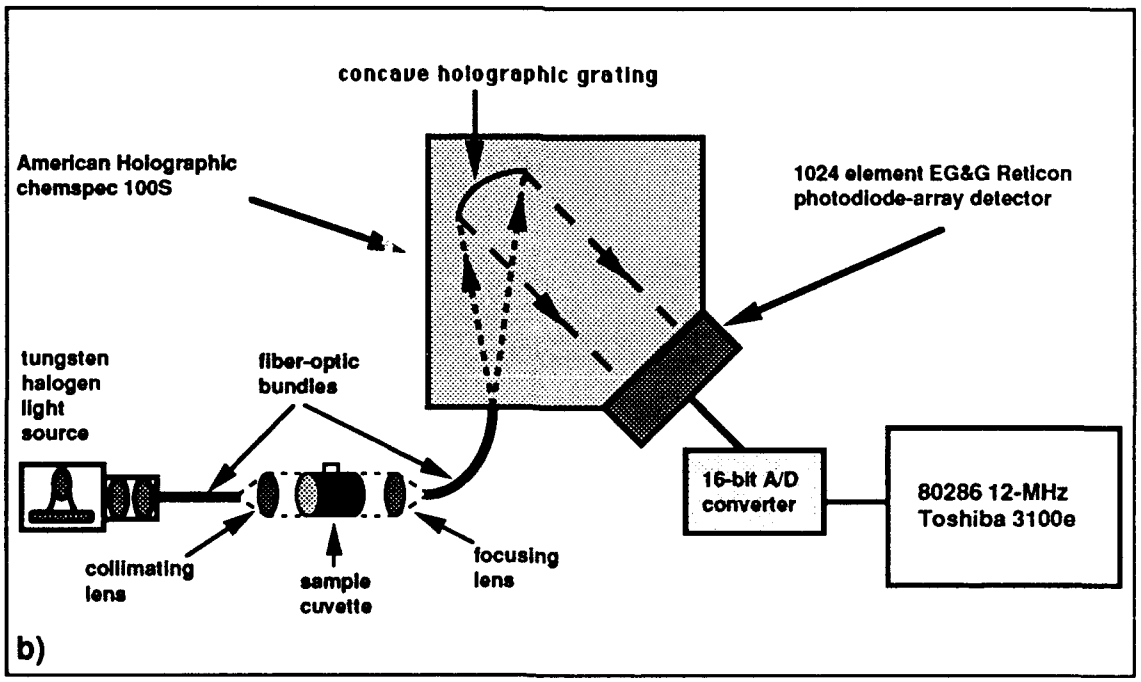
concave holographic grating
American Holographic
chemspec 100S
1024 element EG&G Reticon
photodiode-array detector
tungsten
halogen
light
source
fiber-optic
bundles
16-bit A/D
converter
80286 12-MHz
Toshiba 3100e
collimating
lens
sample
cuvette
focusing
lens
b)

optimized for the wavelength region 600 - 1000 nm. With this configuration, a reciprocal dispersion of 16 nm/mm is achieved. The dispersed radiation is focused onto a photodiode array (PDA) detector for spectral readout. To record the spectral region from 700 to 1100 nm, it was necessary to re-orient the grating from its preset position to perform wavelength detection in the region 600 - 1000 nm. A diagram of the instrument's system components can be found in Appendix A - Figure A.4. With this arrangement, all preprocessing of the analog signal is accomplished in the shielded portion of the instrument case, located on the left-hand side of the instrument. This minimizes the length of the cable the analog signal is transported over, thereby minimizing external noise and interference. Figure A.5 (Appendix A) diagrams the system's electrical interconnections. A single AC (110 Volts) input line powers both the instrument and the laptop computer. DC voltages of +/- 15 volts, + 5 volts and ground are generated by a switching power supply fused at 1.5 amps.

The detector is a 1024-element charge-storage silicon PDA (EG&G Reticon - model RL1024S) (2). Individual detector elements are 2.5 mm high and 25 microns wide, giving a pixel/aspect ratio of 100:1. PDA detectors with high aspect ratios, such as that used here, are ideally suited for spectroscopic measurements due to their increased full-well charge capacity and optical match to the spectrometer entrance slit, thereby resulting in higher S/N levels. The charge capacity of the Reticon RL1024S array is 10^8 electrons per detector element, giving a theoretical S/N ratio of $(10^8)^{1/2}$ or 10,000:1 for a single readout. In practice, S/N

ratios for measurements made in the NIR (700 - 1100 nm) are not quite this good at wavelengths beyond 975 nm, due to the decreases in reflectivity of the grating and in quantum efficiency of the silicon detector. As a result, at the longer wavelengths, the detector elements are not filled to capacity, which causes the S/N ratio for this spectral region to be lower. However, using signal-averaging, the S/N ratio can easily be improved to 40,000:1, for the spectral range 700 - 1000 nm, by co-adding 100 scans. To provide long-term stability, the PDA is temperature-stabilized by a thermoelectric module (Melcor - model CP1.4-35-06L). Detector temperature is sensed with dual linear temperature transducers (Analog Devices - model AD590KF) and is maintained at the operator-selected set point by a high-gain proportional feedback controller. The complementary twin totem-pole output stage provides bipolar drive to the thermoelectric module, allowing regulation below, at, or above ambient temperature. The thermoelectric cooler component layout is given in Figure A.6 (Appendix A), with interconnections as shown in Figure A.7 (Appendix A). In this configuration, the single-stage Peltier cooler has an operating range of 0° C to 45° C, with a step resolution of 0.5° C, and a regulated reproducibility of ± 0.1° C. Detector temperature is computer-controlled and requires less than two minutes to stabilize after initial setting or adjustment.

The light source and feedback control module has been previously described (3) and was presented in Chapter 2. Briefly, this assembly consists of a 5.5 watt tungsten-halogen bulb (Eveready - model #HPR36), equipped with a

where $\mathbf{I_{ref}}$ is the reference spectral intensity, $\mathbf{I_{sam}}$ is the sample spectral intensity, $\mathbf{D_{ref}}$ is the reference dark current reading, and $\mathbf{D_{sam}}$ is the sample dark current reading. By recording a dark current reading immediately before each spectral measurement, system drift is minimized. A component layout diagram of the circuitry used to control the light source and shutter, as well as to provide continuous optical-stabilization feedback to the light source, is shown in Figure A.8 (Appendix A). A schematic of the component interconnections is given in Figure A.9 (Appendix A).

The spectral signal is digitized using a 16-bit successive approximation A/D converter (Burr Brown - model ADC700JH). Timing and digital input-output (I/O) is provided by a timer/counter and digital I/O board (Real Time Devices - model TC24), located in the half-height expansion slot of the laptop computer. The analog signal voltage exported from the Reticon PDA is amplified by a factor of two, using a low-noise, high-speed operational amplifier (Burr Brown - model OPA37). Rejection of ground-loop noise, a critical consideration in maintaining a full 16 bits of dynamic range, is accomplished by operating the amplifier in differential mode. A sample and hold (Burr Brown - model SHC5320KH) maintains a constant signal voltage during the 15 microsecond conversion time of the A/D converter. To minimize memory effects, the diode array is operated continuously; when data is required, the program synchronizes itself to the array frame clock, which is generated by the digital I/O interface. This interface provides all communication between the computer and the spectrometer. A component layout

diagram (Figure A.10 - Appendix A) and schematic (Figure A.11 - Appendix A) present the circuitry required to accomplish the data acquisition and transfer.

Data acquisition is performed with assembler code (see Appendix C), while data analysis and display is accomplished with software written in Microsoft QuickBasic version 4.5 (see Appendix D). As with the software used to control the prototype instrument, the software was written in such a way as to require the minimum amount of input from the operator for ease of operation during in-field conditions, where the expertise associated with the central laboratory may not be available. As before, optimal instrument parameters are preset to aid the untrained operator. For the trained operator, instrument parameters now under user control include the following: number of scans for signal-averaging, integration time, lamp intensity, detector temperature and amount of pixel binning. Again, the overriding goal during the software development stage was to make the instrument as user-friendly as possible. System diagnostics for monitoring wavelength reproducibility, source intensity fluctuations, signal-to-noise ratio, and individual pixel reproducibility statistics have been incorporated in the data acquisition program to allow the operator to assess day-to-day performance changes in the instrument.

3.3 Instrument Evaluation

The single beam transmission spectrum of the instrument, at zero absorbance, is presented in Figure 3.2. As before, the wavelength dependence of the baseline noise is a product of lamp emission, throughput of the

Figure 3.2 Observed intensity spectrum of portable NIR spectrometer.

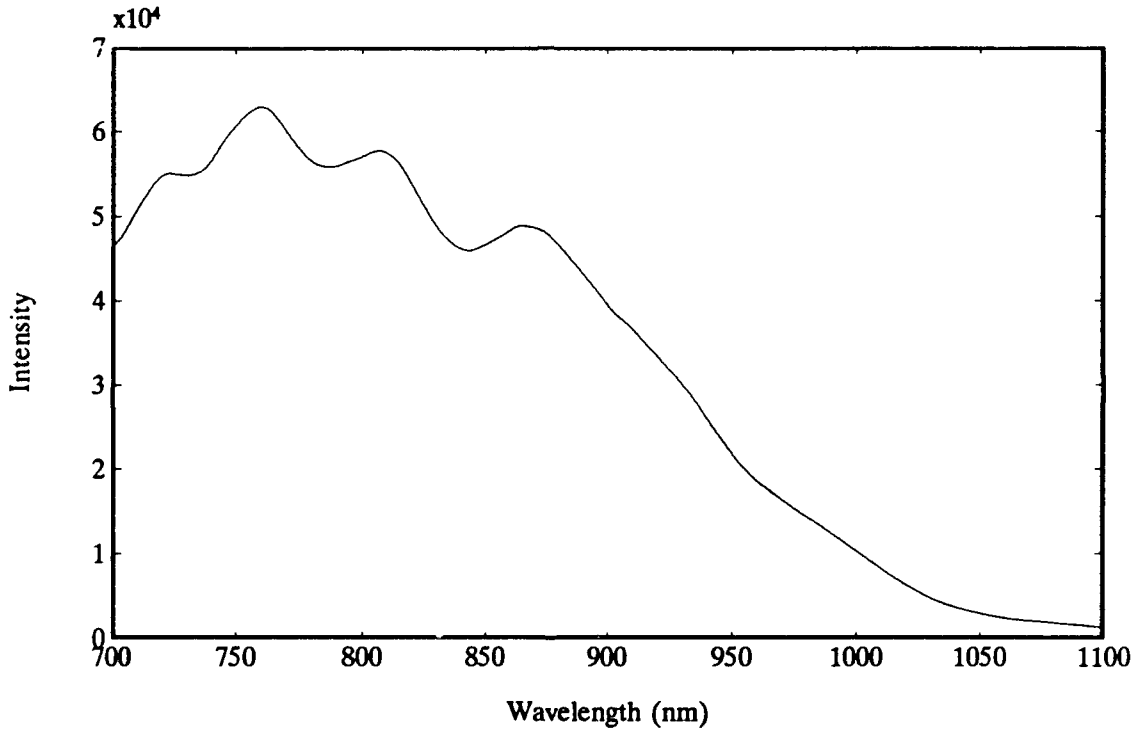
x10⁴
7
6
5
4
3
2
1
0
Intensity
700
750
800
850
900
950
1000
1050
1100
Wavelength (nm)

monochromator, and quantum efficiency of the detector. The rapid decrease in measured intensity at wavelengths above 850 nm is due primarily to the fall-off in quantum efficiency of silicon-based detectors at longer wavelengths, as noted earlier (4). A 675 nm longwave-pass filter (Corion - model LG-675-S), placed between the grating and the detector, to remove the overlapping second-order visible radiation, is responsible for the decrease in intensity at wavelengths below 720 nm. The oscillating pattern observed in the 700 to 900 nm region is due to the thick oxide layer on the surface of the PDA. This layer acts as an interference coating, giving a pattern with a spatial period of approximately 50 nm. Unfortunately, the exact nature of the pattern is strongly dependent on temperature. It is largely eliminated by detector temperature regulation.

3.3.1 Baseline Noise

The baseline noise of the portable NIR spectrometer was calculated by taking the log ratio of two successive spectral measurements (minus the dark current) of an air blank (equation (3.1)) (5). Figure 3.3 shows typical baseline noise plots for; a) a single scan (47 ms acquisition time) and b) 100 signal-averaged scans (4.7 s acquisition time). For 1 scan, the spectrometer has a root-mean-square (RMS) noise level of 1.28 X 10^{-3} absorbance units (AU) over the wavelength region 700 -1100 nm. As mentioned earlier, the decrease in quantum efficiency of the detector beyond 850 nm prevents the overall S/N ratio from reaching the theoretically calculated value of 10,000:1. When 100 scans are signal-

Figure 3.3 Instrumental baseline noise (700 - 1100 nm).

after:

a) 1 scan.

b) 100 signal-averaged scans.

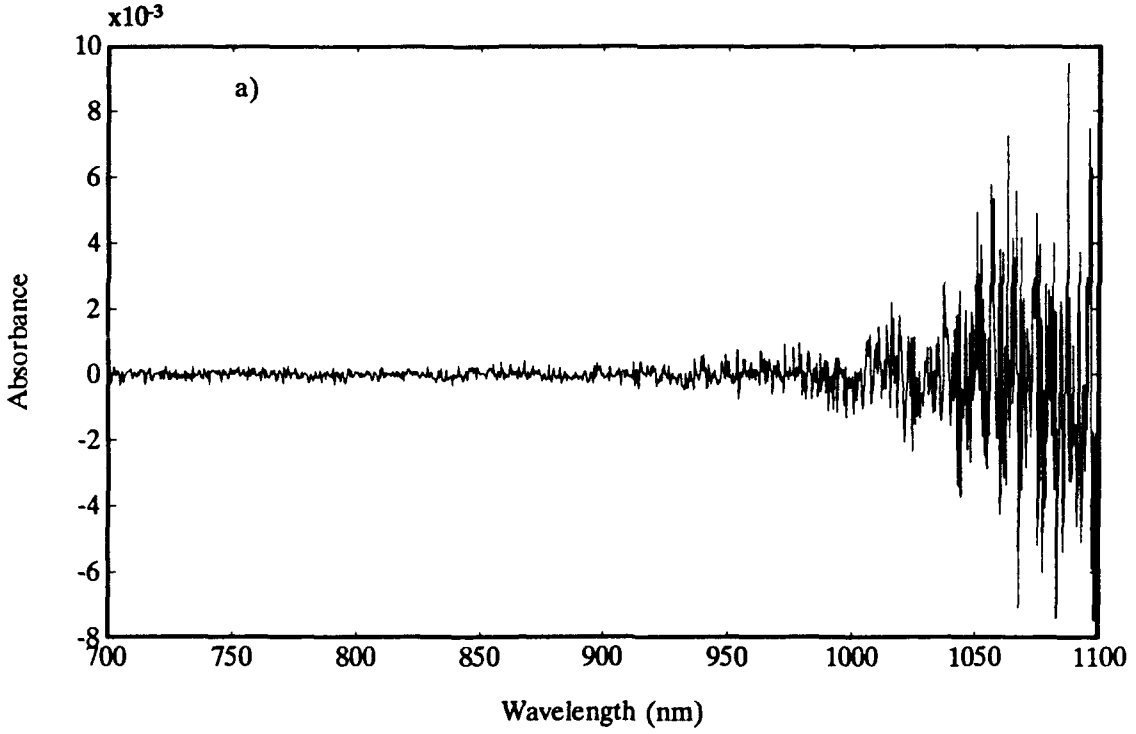
x10-3
a)
Absorbance
10
8
6
4
2
0
-2
-4
-6
-8
700
750
800
850
900
950
1000
1050
1100
Wavelength (nm)

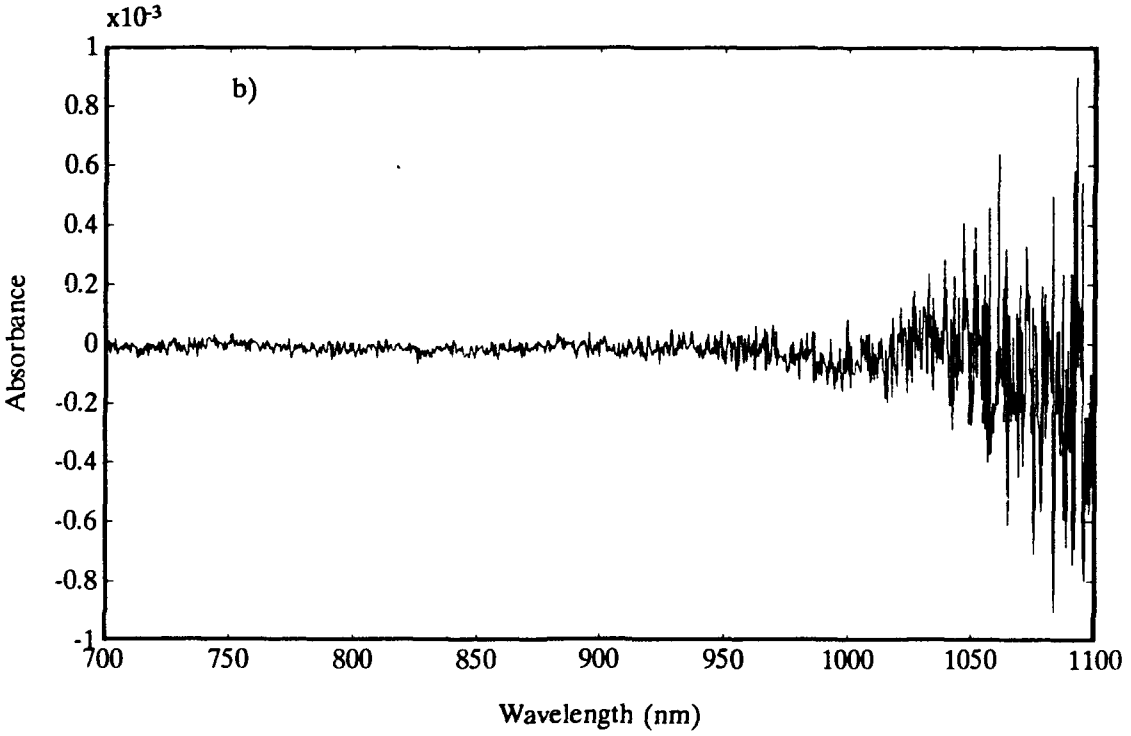
x10-3
b)
Absorbance
1
0.8
0.6
0.4
0.2
0
-0.2
-0.4
-0.6
-0.8
-1
700
750
800
850
900
950
1000
1050
1100
Wavelength (nm)

averaged, the baseline noise improves by one order of magnitude, to an RMS value of 1.27 X 10^{-4} AU. As can be seen in Figure 3.3, the baseline noise steadily degrades at wavelengths above 850 nm. Examining only the 700 - 1000 nm region, as is often the case in SW-NIR spectroscopy, the baseline noise improves to 2.55 X 10^{-5} AU (39,000:1 S/N ratio) for 100 scans (Figure 3.4). This is a slight degradation in S/N compared to the prototype instrument using a 35-element PDA and is due to the reduced full-well capacity of the individual diodes of the Reticon PDA.

As mentioned earlier, because the major noise contributed by silicon detectors is random, it is expected that the baseline noise can be improved by signal-averaging. By this means, the noise should decrease by $(N)^{1/2}$, where N is the number of signal-averaged scans taken (6,7). Figure 3.5a is a log-log plot of baseline noise versus the square root of the number of signal-averaged scans for the full spectral range of 700 - 1100 nm. The log of baseline noise shows a linear decrease as the number of signal-averaged scans is increased from one to eighty. Beyond eighty scans, long-term thermal drift in dark current predominates and no further decreases are observed. An effective way to reduce the long-term thermal drift is to periodically take dark current measurements during the reference and sample spectral acquisitions. By recording a series of 10 dark current measurements, followed by 10 reference or sample scans, it is possible to signal-average over 150 scans before thermal drift predominates. This is illustrated in Figure 3.5b where the linear region of the curve extends beyond 150 scans.

Figure 3.4 Instrumental baseline noise (700 - 1000 nm).

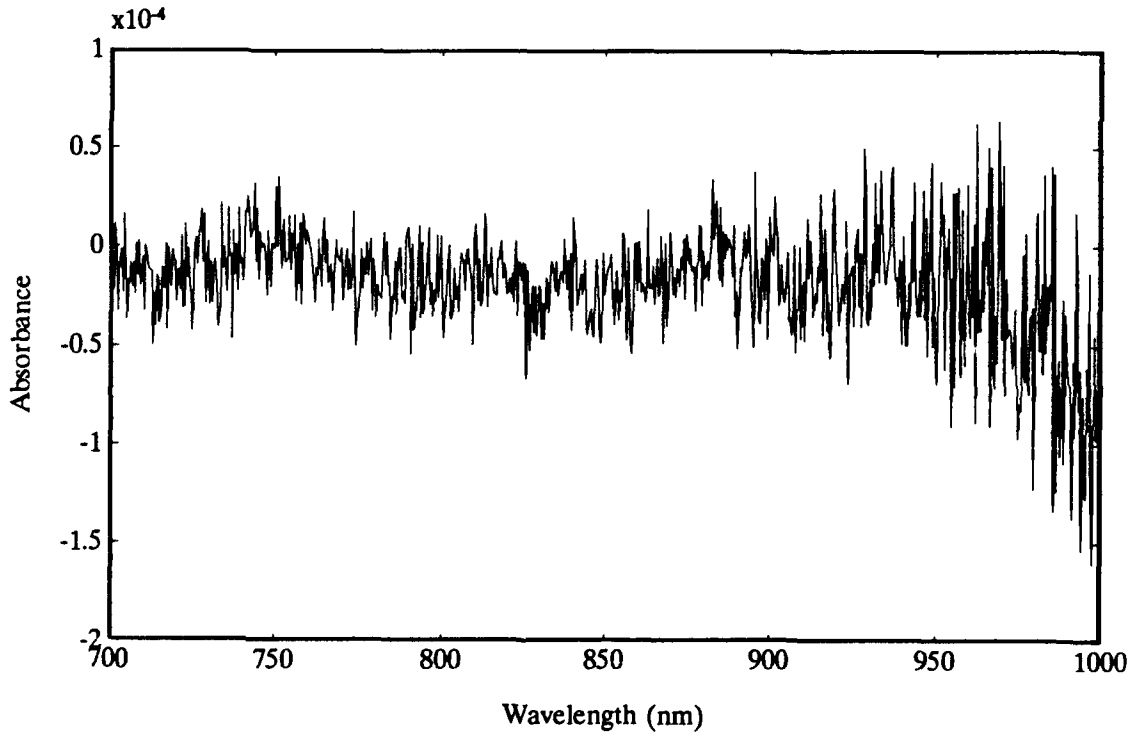
x10-4
1
0.5
0
-0.5
-1
-1.5
-2
Absorbance
700
750
800
850
900
950
1000
Wavelength (nm)

Figure 3.5 Baseline noise improvement with signal-averaging.

a) Single subtraction of dark current.

b) Subtraction of dark current after multiples of 10 signal-averaged scans.

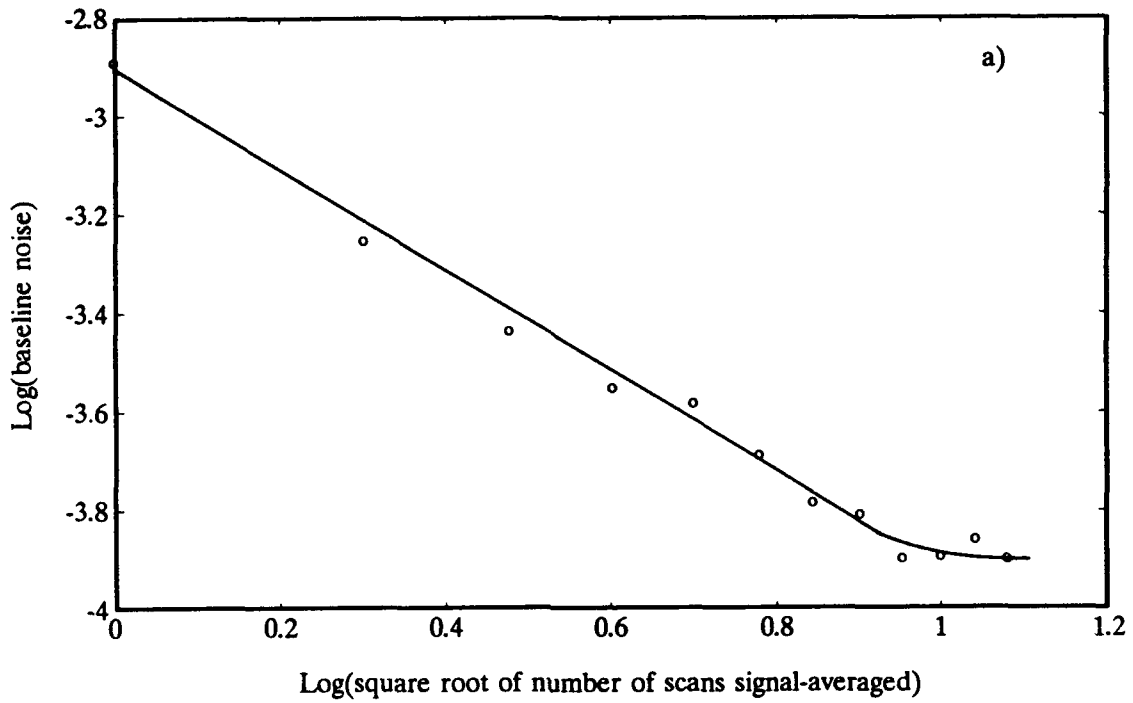
a)
-2.8
-3
-3.2
-3.4
-3.6
-3.8
-4
0
0.2
0.4
0.6
0.8
1
1.2
Log(baseline noise)
Log(square root of number of scans signal-averaged)

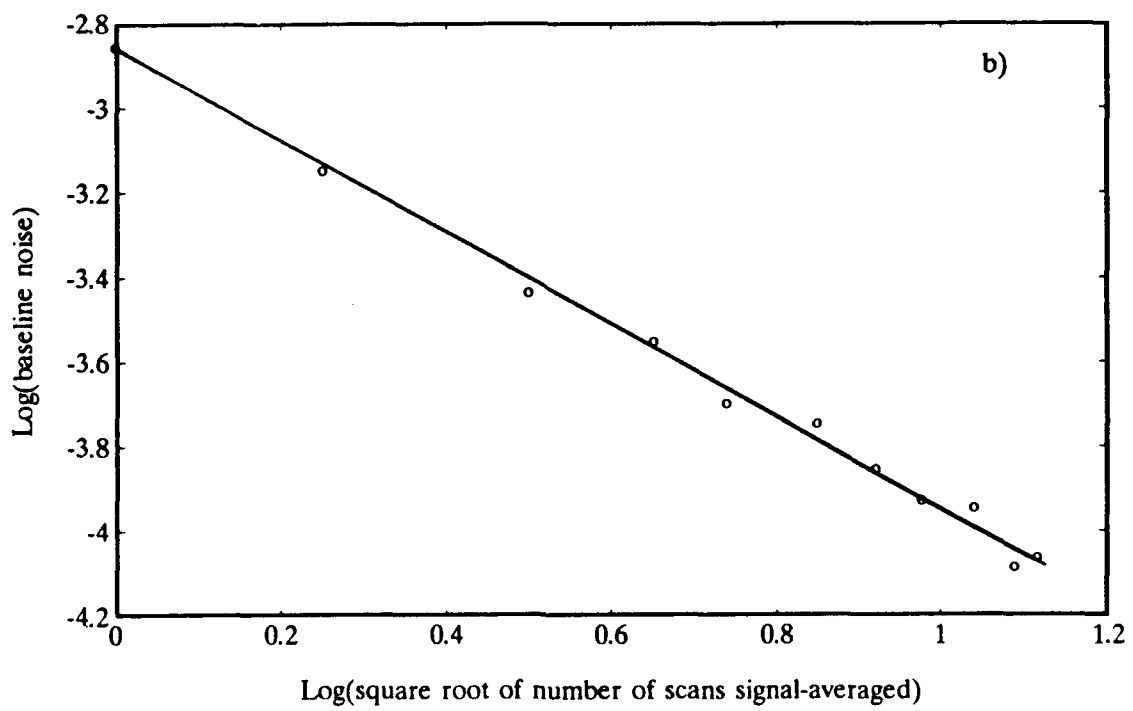
b)
-2.8
-3
-3.2
-3.4
-3.6
-3.8
-4
-4.2
0
0.2
0.4
0.6
0.8
1
1.2
Log(baseline noise)
Log(square root of number of scans signal-averaged)

Overall, the baseline noise level of the portable NIR spectrometer is on the same order as that of state-of-the-art spectrophotometers currently available (8,9).

3.3.2 Stray Light

To determine the amount of stray light present in the portable NIR spectrometer, monochromatic light at a series of wavelengths between 700 and 1000 nm was measured and ratioed against the response over the entire spectral region (Figure 3.6) (the same procedure as was used with the prototype instrument) (10). The stray light intensity was then calculated as the ratio of maximum peak intensity at a given wavelength to overall baseline intensity. The monochromatic light used as the source was obtained by placing two single 0.25 m monochromators (Jarrel Ash - Model 82-410) in series, with slits set for a 7 nm bandpass. The exit slit of the second monochromator was coupled directly to the entrance slit of the spectrograph by a fiber-optic bundle similar to that described earlier. Intensity spectra were taken every 100 nm of excitation, in order to calculate the stray light intensity at various wavelengths. The maximum stray light present in the system is given by the horizontal line in Figure 3.6 and represents a stray light intensity of 0.05%. This two-fold reduction in stray light intensity over the earlier version of the instrument is a result of baffling placed inside the spectrograph and replacement of the spherical mirror / plane diffraction grating combination with a concave holograph grating for wavelength dispersion.

Figure 3.6 Spectra used to calculate stray light intensity.

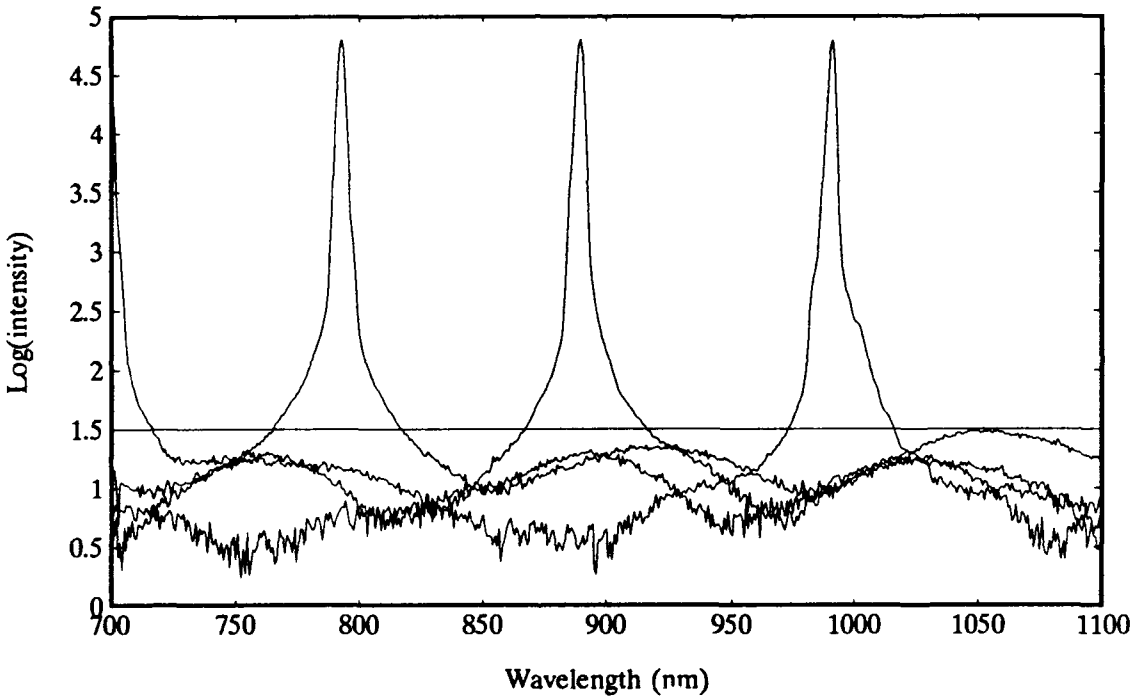
5
4.5
4
3.5
3
2.5
2
1.5
1
0.5
0
Log(intensity)
700
750
800
850
900
950
1000
1050
1100
Wavelength (nm)

3.3.3 Resolution

The most significant improvement over the prototype instrument was an increase in spectral resolution by replacing the 35-element PDA with a 1024-element PDA. The resolution of the instrument was determined using full width/half-maximum criteria at several wavelengths. An argon emission source, coupled to the entrance slit of the spectrometer via the 12" fiber-optic bundle described earlier, was used to generate several narrow-band peaks. With the entrance slit width of the spectrometer set to 50 microns, the resolution of the instrument is observed to be approximately 3 nm, based on full-width/half-maximum of the emission lines at 763 nm, 811 nm, and 912 nm (Figure 3.7). This represents an eight-fold improvement in spectral resolution over the prototype instrument. Theoretically, the resolution of an instrument with a linear dispersion of 16 nm/mm and an entrance slit width equal to twice the width of a single diode will be four times that of the width, or, in this case, 1.6 nm. Due to lateral charge spreading (5, 6), however, the actual line width is typically found to be 2-3 times greater than 1.6 nm, which agrees with our observed spectral width of 3 nm. The asymmetry in the spectral lines, appearing at longer wavelengths as shown in Figure 3.7, is due to a slight curvature in the focal plane of the spectrometer. This curvature makes the alignment process a compromise, preventing optimum alignment at all wavelengths.

Figure 3.7 Resolution determination using argon emission spectrum.

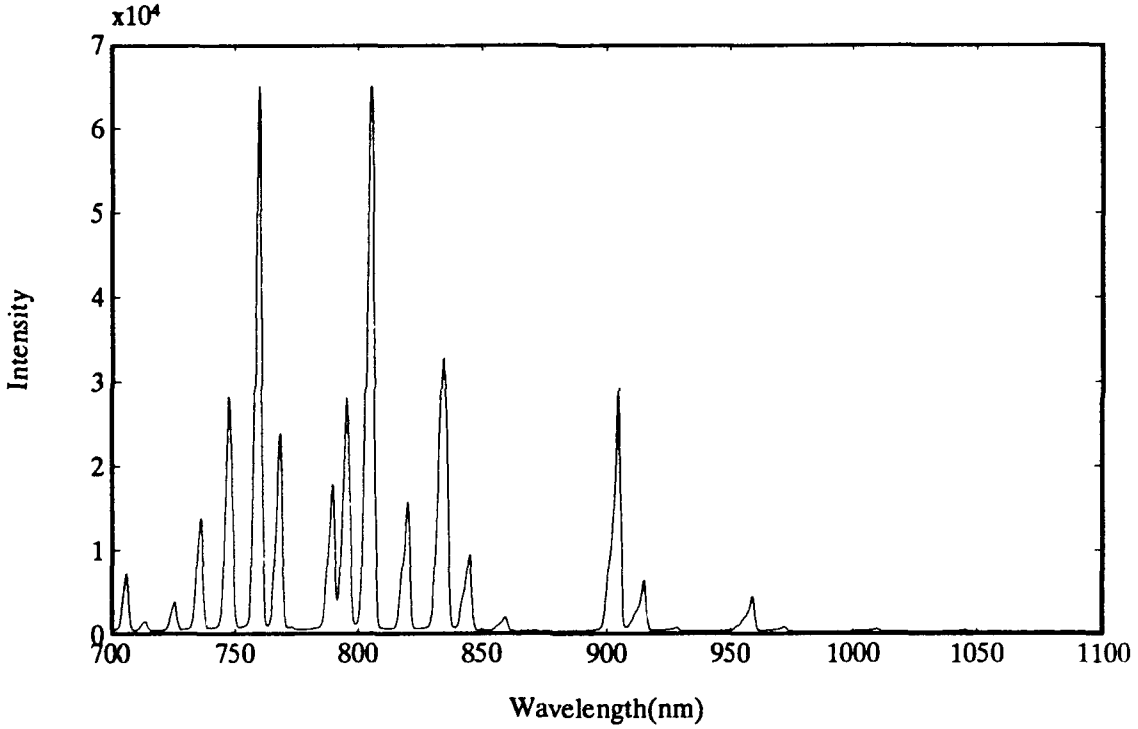
x10⁴
7
6
5
4
3
2
1
0
Intensity
700
750
800
850
900
950
1000
1050
1100
Wavelength(nm)

3.3.4 Dynamic Range

The absorption spectra of a series of zinc-*2,3*-naphthalocyanine in dimethyl sulfoxide (DMSO) mixtures were measured in order to determine the dynamic range of the portable NIR spectrometer (Figure 3.8a). The zinc-*2,3*-naphthalocyanine high standard solution was prepared gravimetrically (±0.1 mg accuracy) with the lower concentration solutions obtained by serial dilution. Concentration of the zinc-*2,3*-naphthalocyanine solutions ranged from 3.25×10^{-8} molar to 3.248×10^{-5} molar. Measurements were made using a 3.0-second acquisition time (64 scans) in transmission mode through a 1.0-cm cuvette. The absorption at 767 nm was measured as a function of zinc-*2,3*-naphthalocyanine concentration and demonstrated good compliance with the Beers-Lambert law up to an absorbance of 1.5 AU (Figure 3.8b). For this region the data is quite linear, with an R^2 value of 0.9997. This gives a dynamic range of three orders of magnitude and is in accordance with the excellent S/N ratio (39,000:1) and reasonably low stray light level (0.05%) of the spectrometer.

Table 2.1 is a summary of instrument performance, as discussed above, together with a list of physical characteristics. As stated previously, the improved portable NIR spectrometer attained an eight-fold improvement in spectral resolution, a two-fold reduction in stray light intensity, no change in dynamic range and a two-fold degradation in S/N when compared to the prototype instrument.

Figure 3.8 Dynamic range determination of portable NIR spectrometer.

a) Zinc-*2,3*-naphthalocyanine spectra used to determine dynamic range.

b) Absorbance at 767 nm -vs- zinc-*2,3*-naphthalocyanine concentration.

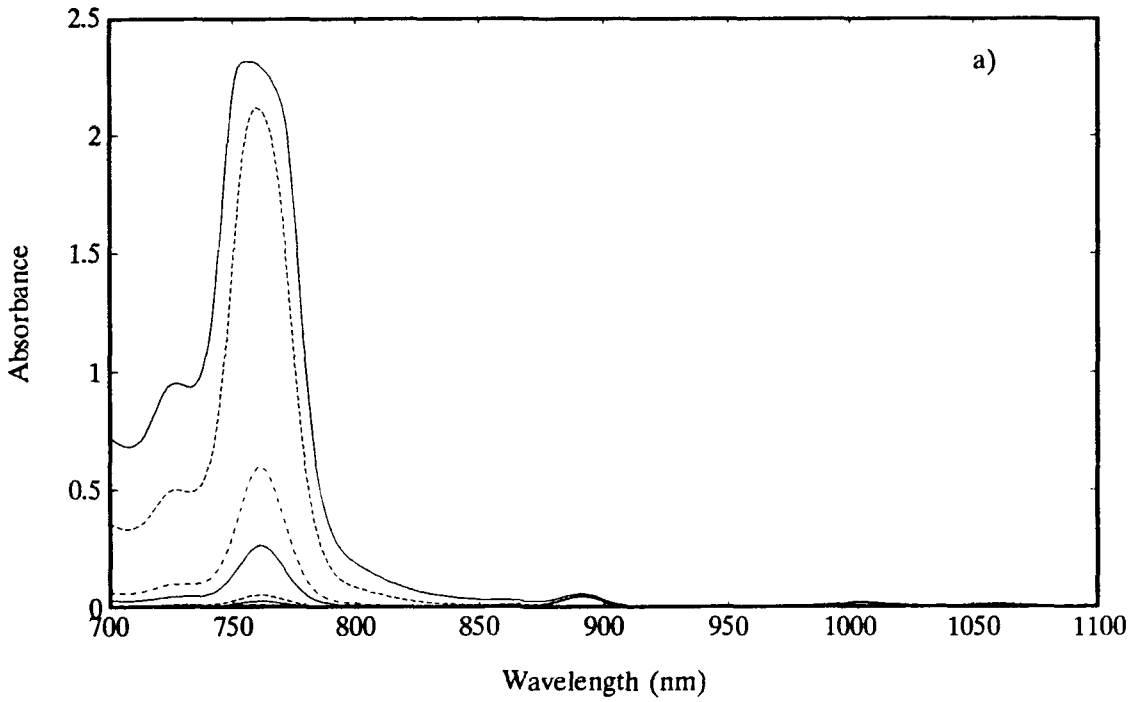
a)
Absorbance
2.5
2
1.5
1
0.5
0
700
750
800
850
900
950
1000
1050
1100
Wavelength (nm)

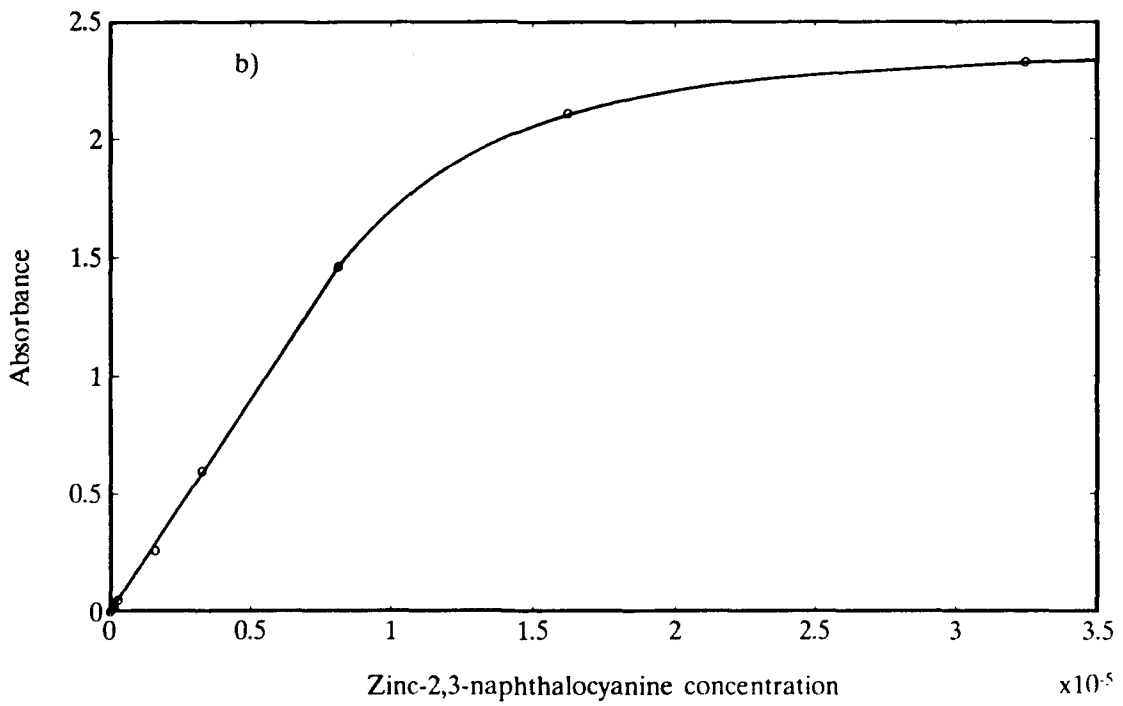
b)
Absorbance
2.5
2
1.5
1
0.5
0
0
0.5
1
1.5
2
2.5
3
3.5
Zinc-2,3-naphthalocyanine concentration
x10-5

Table 3.1 Instrument evaluation summary.

Baseline Noise	2.55×10^{-5} AU
Stray Light	0.05 %
Resolution	3 nm
Dynamic Range	3 orders
Cost in Parts	$7,000.00
Weight	25 lbs.
Size	6" X 14" X 17"

3.4 Conclusions

This version of the portable NIR spectrometer, with a concave holographic grating - PDA detector combination yields an extremely reliable and rugged spectrometer, with no critically-aligned moving parts. With the improvements of higher resolution and reduced stray light, its performance is comparable to state-of-the-art NIR spectrophotometers currently on the market and allows what has been traditionally a laboratory-only analysis to be conducted in-field or at-line. The ability to take measurements on-site, in distant locations, and/or over long-distance fiber-optics has the potential to revolutionize many areas of process monitoring and in-field analysis. Applications of this instrument and performance comparisons with commercially available NIR spectrophotometers will be presented in Chapters 4 and 5.

3.5 Notes to Chapter 3

1. Lysaght, M.J., Danielson, J.D.S., Callis, J.B., *CPAC Publication Announcement # 106*, **1991**, 1, 1.

2. EG&G Reticon Data Book, Image Sensing Products, **1989**, 39.

3. Lysaght, M.J., van Zee, J.A., Callis, J.B., *Rev. Sci. Inst.*, **1991**, 2, 507.

4. Janesick, J.R., Elliott, T., Collins, S., Blouke, M.M., Freeman, J., *Optical Engineering*, **1987**, 26, 692.

5. Landa, I., *Rev. Sci. Instrum.*, **1979**, 50(1), 34.

6. Talmi, Y., *Appl. Spectrosc.*, **1982**, 36(1), 1.

7. Bilhorn, R.B., Epperson, P.M., Sweedler, J.V., Denton, M.D., *Appl. Spectrosc.*, **1987**, 41(7), 1125.

8. Mayes, D.M., Callis, J.B., *Appl. Spectrosc.*, **1989**, 43, 27.

9. Tong, L., Lysaght, M.J., Kelly, J.J., Callis, J.B., *HP Application Note, Performance Evaluation of the HP-8452A with NIR Modification*, to be published.

10. Kaye, W., *Anal. Chem.*, **1981**, 53, 2201.

CHAPTER 4

Analysis of JP-4 Jet Aviation Fuel Using NIR Spectroscopy

4.1 Introduction

As a test to demonstrate the capabilities of the portable NIR spectrometer in a real-world analysis situation which has field applications, this chapter focuses on the spectrophotometric determination of the major hydrocarbon classes and the freezing point of JP-4 jet aviation fuel. The enormous volume of jet fuel required by both military and civil aviation has resulted in an increased research effort to establish faster, more accurate and more cost-effective analysis techniques. From a military standpoint, quality-assurance measurements are vitally important for determining the quality of fuels supplied by the producer and the status of stored fuels. Additionally, rapid field-determinations are critical during deployed operations, as well as for assessment of captured fuels during combat operations. From an industrial standpoint, the need is for rapid, on-line analysis procedures during fuel production.

The ability of the portable NIR spectrometer to perform rapid and in-field analysis of aviation fuel (1), is evaluated through a comparison with the ability of two commercially available near-infrared (NIR) spectrophotometers to perform the same analysis in the laboratory (2).

4.1.1 Background

Since May of 1951, the primary jet fuel used by the United States Air Force (USAF) has been JP-4 (NATO F-40), as governed by specification MIL-T-5624N (3). During the distillation of crude oil, a wide cut is taken of the distillate to produce JP-4. This cut includes both the naphtha (gasoline) and kerosene fractions and results in a mixture that is roughly 50 to 60 percent gasoline and 40 to 50 percent kerosene. The cost of production, as well as the performance of the fuel, is directly related to its chemical composition. A typical JP-4 fuel sample consists of 82 to 92 percent saturates, 7 to 17 percent aromatics and less than 1 percent olefinics. Current specifications for JP-4 limit the total aromatics to below 25 percent by volume and total olefinics to below 5 percent by volume (4).

There are two basic reasons for the limitation on aromatic content. First, of the four major hydrocarbon types present in jet fuel (aromatics, olefins, paraffins, and cycloparaffins), aromatics have the poorest combustion performance. From a military standpoint, this incomplete combustion results in a black-colored exhaust enhancing the possibility of visual identification by enemy aircraft during combat operations. As the concentration of aromatics are reduced, the performance of the fuel increases, exhaust color is minimal and visual sightings by enemy aircraft are limited to distances less than 2 to 4 miles. Second, aromatics tend to dissolve the gaskets, sealants, and hoses currently used in many aircraft fuel systems (3). Certain elastomers used in the production of these fuel system components exhibited complete failure after prolonged exposure to fuels with aromatic

concentrations greater than 30 percent. The current specification limit of 25 percent decreases the occurrence of such problems.

The limitation on percent olefins is based on the fact that olefins tend to have the poorest long-term stability, due to the presence of unsaturated carbon-carbon bonds. As the degree of unsaturation increases, the chemical reactivity of the molecule leads to polymerization, resulting in the formation of undesirable gums and resins during fuel storage which can cause fuel flow problems during flight.

4.1.2 Current Methods

With aircraft performance so closely linked to the chemical composition of its fuel, analysis of fuels has become the focus of a great deal of research and quality control measurements. Tests approved by the American Society of Testing and Materials (ASTM) are used to evaluate the quality of aviation fuel. These tests, including API gravity, Reid Vapor pressure, viscosity, sulfur content, freezing point and total aromatics, aliphatics, and olefinics are extremely time-consuming to carry-out, require a relatively large sample volume, and must be performed in centralized testing facilities operated by highly-trained personnel. Analyses such as these cannot readily be used for rapid quality-assurance tests or as on-line methods for rapid information feedback desired in modern refineries.

Of the ASTM tests listed above, the determination of hydrocarbon classes by the fluorescence indicator adsorption (FIA) method (ASTM D-1319) (5) is one

of the most time-consuming and least precise. For samples such as the aviation fuels described here, consisting of 10 - 20 % aromatics and 80 - 90 % saturates (< 1 % olefinics), ASTM published reproducibility values (defined at the 95% confidence level) for the three hydrocarbon classes are as follows: a) volume percent aromatics -- 2.5 % absolute; b) volume percent saturates -- 4.0 % absolute; and c) volume % olefinics -- 1.7 % absolute. Campbell et al. (6) and Norris and Rawdon (7) cite numerous shortcomings of the FIA analysis, including operator and column substrate dependent variations, as well as the poor resolution and long analysis time (≈ 2 hrs) of the method. Alternative techniques that have been proposed for the determination of hydrocarbon classes include nuclear magnetic resonance (NMR) (8,9), high-performance liquid chromatography (HPLC) (10,11), gas chromatography (GC) (12,13), supercritical fluid chromatography (SFC) (6,27) and mass spectroscopy (MS) (14). While each of the above techniques are more precise than the FIA analysis, all require expensive instrumentation operated by highly trained personnel. One technique that shows promise, is an HPLC method that uses an olefin-selective column, coupled with a dielectric constant detector (10,15). Although accurate to within 1 percent absolute when complex solutions of hydrocarbon standards are analyzed, this technique requires a skilled operator and considerable analysis time.

In this chapter, near-infrared (NIR) spectroscopy is evaluated for the rapid and non-destructive determination of volume percents of the hydrocarbon classes, as well as freezing point, for a series of JP-4 fuels. This region of the spectrum is

particularly attractive for fuel analysis because most of the absorption bands occurring in the NIR spectral region arise from overtones or combinations of carbon-hydrogen stretching vibrations of the hydrocarbon constituents of the fuel. In addition, the C-H vibrations on different functional groups occupy a different, but reproducible position in the spectrum, while remaining reasonably independent of the remainder of the molecule (16,17). Finally, the absorptivities of these bands are proportional to the concentration of the absorbing group, e.g., aromatic, olefinic, methylene or methyl C-H's. As a result, NIR spectroscopy is well-suited to analyses of hydrocarbon-based samples.

The studies detailed here demonstrate the utility of the statistical methods of multiple linear regression (MLR) and partial least squares (PLS) in correlating the volume percentages of saturates and aromatics, as well as the freezing point of JP-4 fuels, with their respective NIR spectra. Although the field-portable NIR spectrometer developed here operates only in the SW-NIR, both the SW-NIR and the LW-NIR have been examined to compare their utility in predicting the above mentioned properties.

4.2 Experimental

4.2.1 JP-4 Fuel Samples

A JP-4 jet fuel round-robin sample exchange was organized between the Center for Process Analytical Chemistry (CPAC) at the University of Washington,

Seattle, WA, and laboratories at ARCO Petroleum Products Company, Chevron Research and Technology Co., Core Laboratories, Mobil Research and Development Corp., Texaco Inc., and the USAF. The USAF Wright Aeronautical Laboratories at Wright-Patterson Air Force Base, Dayton, Ohio delivered a set of thirty-three JP-4 fuel samples to each of the laboratories for blind testing. Samples were shipped and stored in dark, tightly-stoppered Qorpak bottles sealed with teflon tape. For each sample, all six laboratories made the following determinations: freezing point (ASTM test D2386 -Freezing Point of Aviation Fuels) (18), volume percent aromatics, and volume percent saturates (ASTM test D1319 - Hydrocarbon Types in Liquid Petroleum Products by Fluorescent Indicator Adsorption) (5). The analyses were completed in triplicate at each of the six laboratories, resulting in a total of 18 analyses per sample per determination. Included with each set of fuel samples were three reference hydrocarbon mixtures to validate laboratory analysis results. However, the results obtained from one of the six laboratories showed a consistently low bias of nearly two percent absolute when compared to the average values calculated from the 15 replicate measurements made by the other five laboratories. For this reason, results obtained from this laboratory were not used in the following analyses. Table 4.1 is a summary of the results from the round-robin sample exchange. The average of the 15 replicate measurements, as well as their associated standard deviations, are given for each of the 33 fuel samples, as well as the three hydrocarbon standards. Standard deviation values were calculated according to the following

Table 4.1 JP-4 round-robin analysis results.

(Constituent values represent the average of 15 replicate measurements with associated standard deviations. Shaded samples represent reference standards.)

N.A. = Not Applicable - Sample #30 was reported as having a freezing point below -80 ^{0}C. The actual freezing point was not determined. This sample was not used in the regression analysis.

Sample Number	Percent Aromatics	Std. Dev.	Percent Saturates	Std. Dev.	Freezing Point	Std. Dev.
1	12.65	0.52	86.26	0.66	-61.84	1.36
2	14.89	0.43	84.04	0.49	-59.10	1.59
3	14.59	0.56	84.18	1.09	-55.80	1.63
4	11.81	0.59	87.19	0.62	-62.73	1.29
5	13.36	0.58	85.66	0.66	-57.19	1.49
6	12.34	0.64	86.57	0.60	-58.48	1.62
7	10.54	0.64	88.08	0.78	-71.59	1.41
8	12.41	0.94	86.23	0.77	-60.63	1.56
9	8.26	0.61	90.55	0.78	-59.57	2.28
10	10.94	0.73	87.81	0.71	-59.77	1.48
11	12.07	0.82	86.95	0.93	-55.71	2.05
12	11.90	0.29	87.12	0.43	-66.32	1.36
13	5.68	0.61	92.72	0.76	-44.66	2.09
14	15.39	0.95	82.67	1.46	-38.33	1.87
15	12.39	0.95	86.69	0.87	-63.27	1.42
16	11.64	0.65	87.30	0.84	-60.96	1.35
17	14.55	0.86	84.49	0.86	-60.19	1.23
18	12.42	1.14	86.51	1.00	-66.07	1.91
19	12.60	1.15	86.34	1.22	-63.50	1.84
20	12.30	1.06	86.88	1.06	-62.98	1.35
21	11.13	0.62	88.02	0.66	-61.97	1.37
22	14.46	0.80	84.69	0.69	-60.27	1.23
23	12.60	0.99	86.42	0.97	-63.43	1.70
24	12.73	0.97	86.33	1.01	-62.01	1.44
25	11.32	1.02	87.72	0.99	-68.28	1.65
26	12.66	0.89	86.36	0.87	-61.43	1.25
27	11.64	1.03	87.34	1.00	-62.17	1.26
28	10.09	1.23	88.97	1.25	-60.68	1.44
29	14.93	0.68	83.99	0.81	-64.13	1.49
30	15.18	1.25	83.92	1.35	-80.00	N.A.
31	8.64	0.65	90.34	0.64	-70.95	1.62
32	10.17	0.74	88.72	1.05	-59.89	1.33
33	11.11	0.75	87.79	0.87	-62.32	1.39
34	10.86	0.69	87.92	0.68	-62.20	1.23
35	11.90	0.82	87.03	0.97	-61.22	1.81
36	25.74	0.65	70.66	1.43	-34.86	0.64

equation:

$$\sigma_s = \sqrt{\left(\frac{\sum_{i=1}^{N} (s_i - \bar{s})^2}{N - 1} \right)} \tag{4.1}$$

where σ_s is the calculated standard deviation, s_i are the individual measurements, $\bar{s}$ is the average of the 15 measurements, and N is the number of measurements. The hydrocarbon standards (samples 13, 14 and 36) were not identified by sample number during the round-robin analysis.

As previously noted, JP-4 fuels are limited by specification to 5 percent olefinic content. In practice, JP-4 fuels are found to contain much less than 5 percent olefinics in order to preclude non-acceptance. The fuel samples used in this study contained less than 1 percent olefins and as a result, the level of percent olefins were either not detected or simply reported as less than 1 percent in the fluorescence indicator absorption analyses performed by the round-robin members. The NIR analysis presented here has therefore been limited to percent aromatics, percent saturates and freezing point predictions.

Samples were stored at 4°C until analyzed. Before analysis by NIR spectroscopy, samples were warmed to room temperature.

4.2.2 Spectroscopy

For each sample, near-infrared transmission spectra were obtained in both

the short-wavelength (700 - 1100 nm) and a portion of the long-wavelength (1100 - 1500 nm) spectral regions. Using a 2.00-cm sample cuvette, short-wavelength spectra were acquired on both the portable NIR spectrometer (Figure 4.1a) and a Hewlett Packard (HP) 8452A Diode Array spectrometer (Figure 4.1b) operated in transmission mode. The portable NIR spectrometer acquired spectra at a data rate of 20 spectra/sec and consisted of 1012 data points covering the wavelength region 700-1100 nm (0.4 nm per data point). The HP spectrometer acquired spectra at a data rate of 10 spectra/sec and consisted of 201 data points covering the same spectral range (2.0 nm per data point). The HP spectrometer was interfaced to an IBM AT microcomputer for data acquisition and statistical analysis. Long-wavelength spectra (Figure 4.1c) were acquired on a NIRSystems (Model 6250) scanning-spectrophotometer operated in transmission mode using a 1.00-cm sample cuvette. Spectra were acquired at a data rate of 2 spectra/sec and consisted of 201 data points covering the wavelength region 1100 - 1500 nm (2 nm per data point). In all cases, spectra were the result of averaging 64 scans, with sample measurements referenced against air.

4.2.3 Statistical Methodology

Stage-wise multiple linear regression and partial least squares analyses were performed on each of the NIR spectral data sets using an IBM 386 microcomputer and chemometrics software written in the MATLAB programming environment (19) at CPAC. Statistical analyses were performed on the data after second-

Figure 4.1 Absorption spectra of the 33 JP-4 jet fuel samples.

a) Portable NIR spectrometer.

b) Hewlett Packard spectrometer.

c) NIRSystems spectrophotometer.

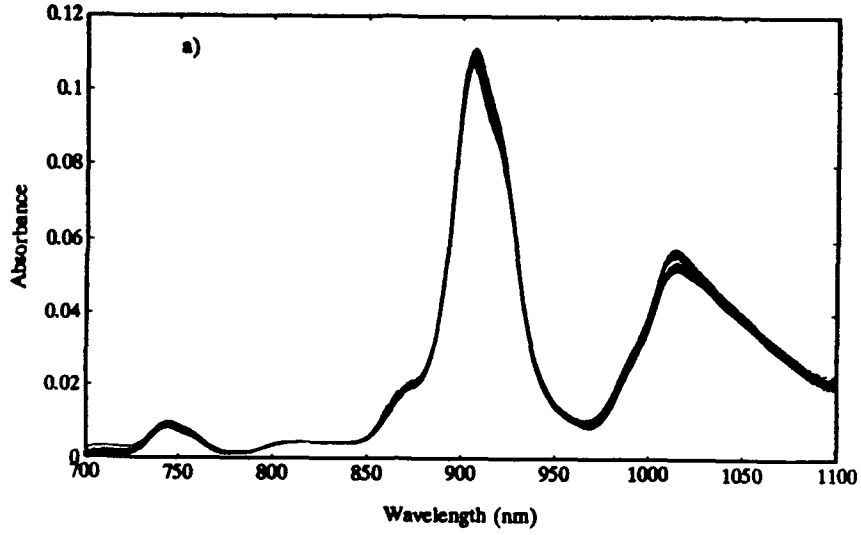
a)
Absorbance
0.12
0.1
0.08
0.06
0.04
0.02
0
700
750
800
850
900
950
1000
1050
1100
Wavelength (nm)

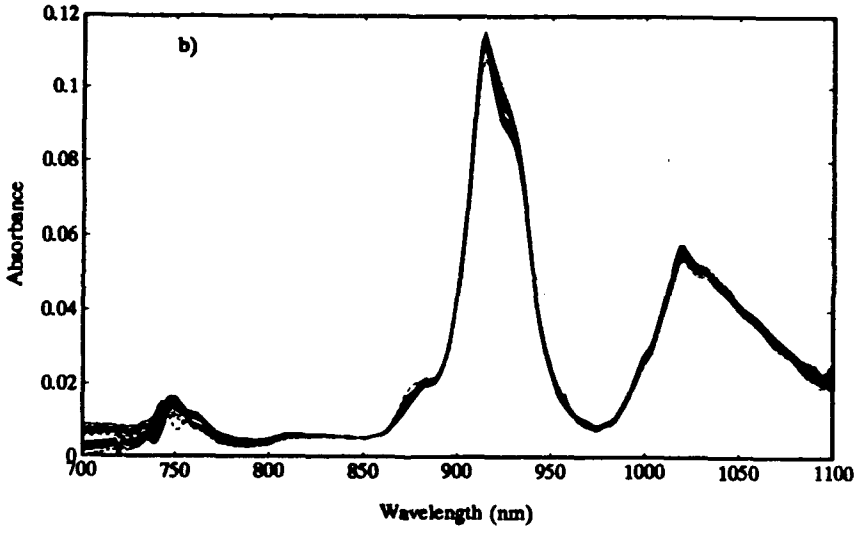
b)
Absorbance
0.12
0.1
0.08
0.06
0.04
0.02
0
700
750
800
850
900
950
1000
1050
1100
Wavelength (nm)

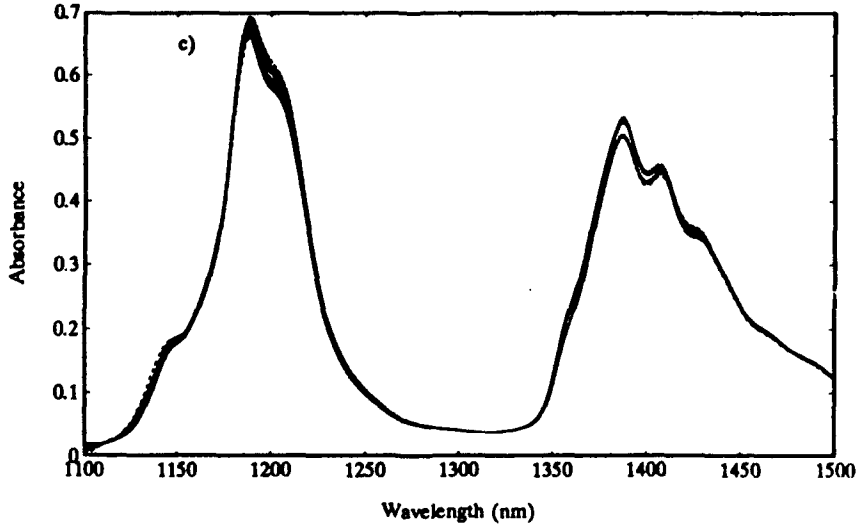
c)
Absorbance
0.7
0.6
0.5
0.4
0.3
0.2
0.1
0
1100
1150
1200
1250
1300
1350
1400
1450
1500
Wavelength (nm)

derivative transformation to remove any variance due to baseline offset. The second-derivative transformation was calculated using software written in MATLAB, employing a window of 7 and a gap of 0 data points for the LW-NIR spectral region and a window of 5 and a gap of 0 data points for the SW-NIR spectral region. It was necessary to use a larger second-derivative window on the LW-NIR spectral region due to the lower spectral resolution (7 nm) of the NIRSystems spectrophotometer. The second-derivative transformation of the JP-4 spectra are presented in Figure 4.2a for the portable NIR spectrometer (SW-NIR), Figure 4.2b for the HP spectrometer (SW-NIR) and in Figure 4.2c for the NIRSystems spectrophotometer (LW-NIR).

Both the partial least squares and stage-wise multiple linear regression analyses provided estimates of the standard error of calibration (SEC), correlation coefficient (R^2), and standard error of prediction (SEP) for each constituent. SEP values were determined by "leave-one-out" cross-validation (20).

4.3 Results and Discussion

4.3.1 Spectroscopic Assignments

The absorption bands seen in Figure 4.1 are typical of hydrocarbon-based samples and are the result of overlap between the overtone and combination bands of the various hydrocarbon species present in JP-4. Because absorbance in the NIR is primarily due to functional group type, remaining largely independent

Figure 4.2 2nd derivative transformation of JP-4 absorption spectra.

a) Portable NIR spectrometer.

b) Hewlett Packard spectrometer.

c) NIRSystems spectrophotometer.

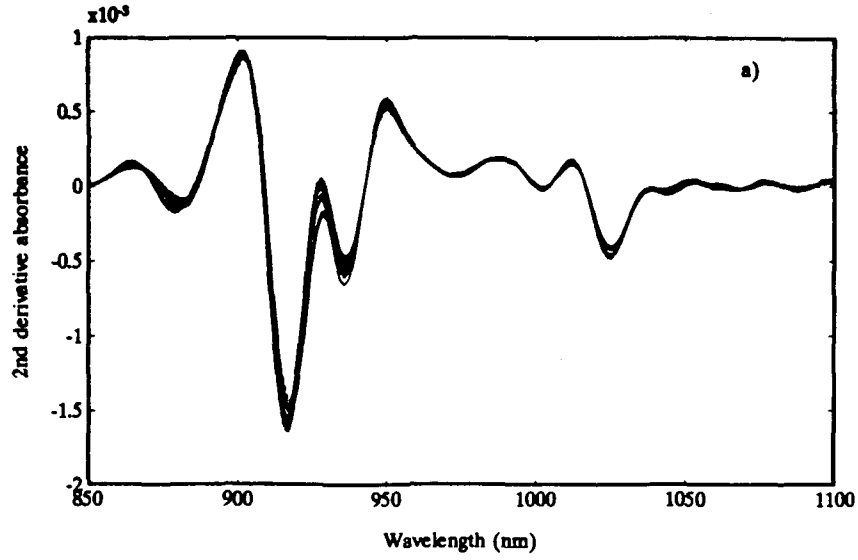
x10⁻³
a)
2nd derivative absorbance
Wavelength (nm)

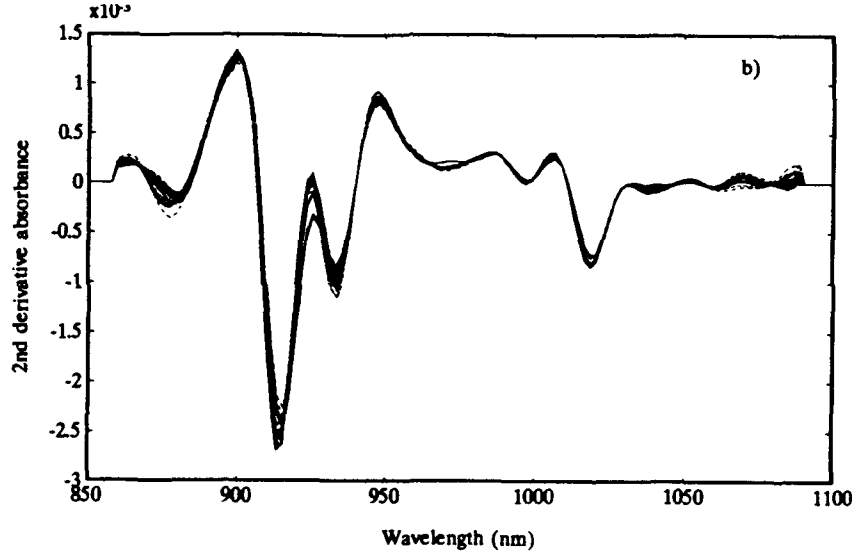
x10⁻³
b)
2nd derivative absorbance
Wavelength (nm)

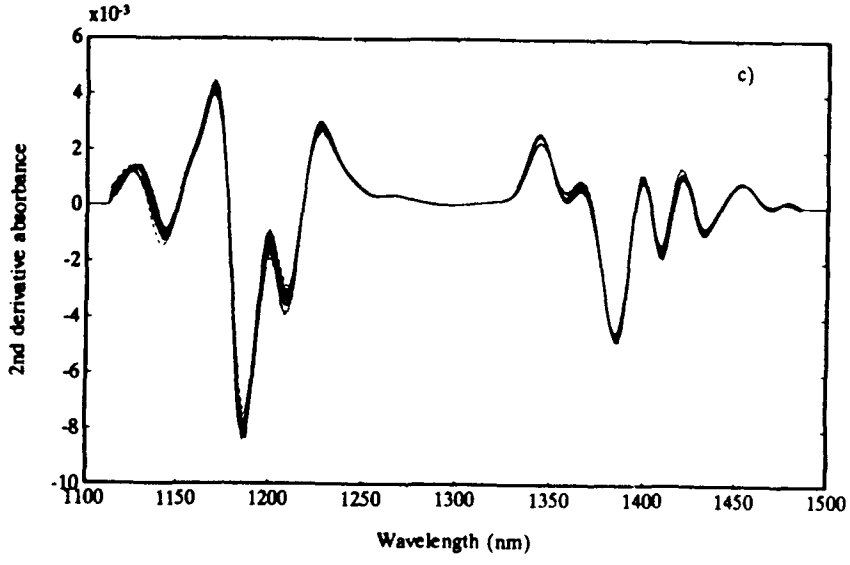
x10⁻³
c)
2nd derivative absorbance
Wavelength (nm)

of the rest of the molecule, absorption bands arise from the three major functional constituents (aromatic, methyl and methylene) present in the fuel.

In the NIR spectral region, weak absorptions by hydrocarbon C-H bonds arise from overtones and combinations of the fundamental molecular vibrations occurring in the mid-infrared region. Of primary importance to hydrocarbon studies are the overtones of the symmetric and antisymmetric C-H stretching vibrations. The symmetric stretching becomes comparatively weaker and the antisymmetric dominates at higher overtones. In addition, combination bands of stretching with bending vibrations in methyls and stretching with scissoring vibrations in methylenes are found in the NIR, but these are somewhat less intense than overtone bands in the SW-NIR. Olefins and aromatics exhibit similar C-H overtones in the NIR, but their combination bands are barely detectable. General assignments of the NIR absorption peaks to specific overtones and combinations of C-H fundamental frequencies have been proposed by Weyer (16) and Wheeler (16, 17). Table 4.2 is a summary of these assignments for the broad hydrocarbon C-H absorptions observed in gasoline in the NIR spectral region (21,22).

Further confirmation of the absorption band assignments for JP-4 can be made by comparing the NIR spectra with a series of hydrocarbon standards. Figure 4.3a represents the SW-NIR spectrum, and Figure 4.3b the (LW-NIR) spectrum, of *2,2,4*-trimethylpentane (isooctane) which consists of 15 methyl C-H's and only 3 methylene C-H's. The weak absorbance at 934 (1210) nm, due to the methylene C-H's, is seen as a shoulder to the much stronger absorbance centered

Table 4.2 Primary C-H absorption bands in the NIR.

	Aromatic	**Methyl**	**Methylene**
1st Overtone	1680	1700	1745
Combination	1435	1397	1405
2nd Overtone	1145	1190	1210
Combination	not obs	1015	1053
3rd Overtone	875	913	934
4th Overtone	714	746	762

Note: Wavelength values are in nanometers and represent the peak maxima of the absorption band.

Figure 4.3 NIR absorption spectra of *2,2,4*-trimethylpentane.

a) SW-NIR spectral region.

b) LW-NIR spectral region.

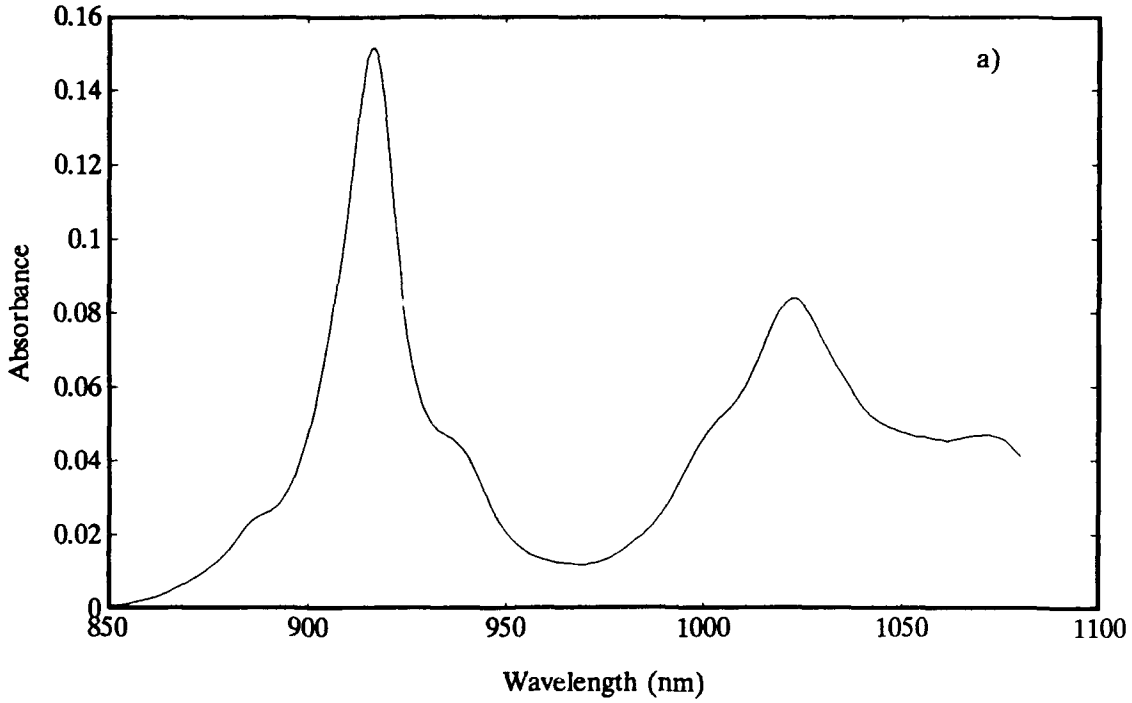
a)
Absorbance
0.16
0.14
0.12
0.1
0.08
0.06
0.04
0.02
0
850
900
950
1000
1050
1100
Wavelength (nm)

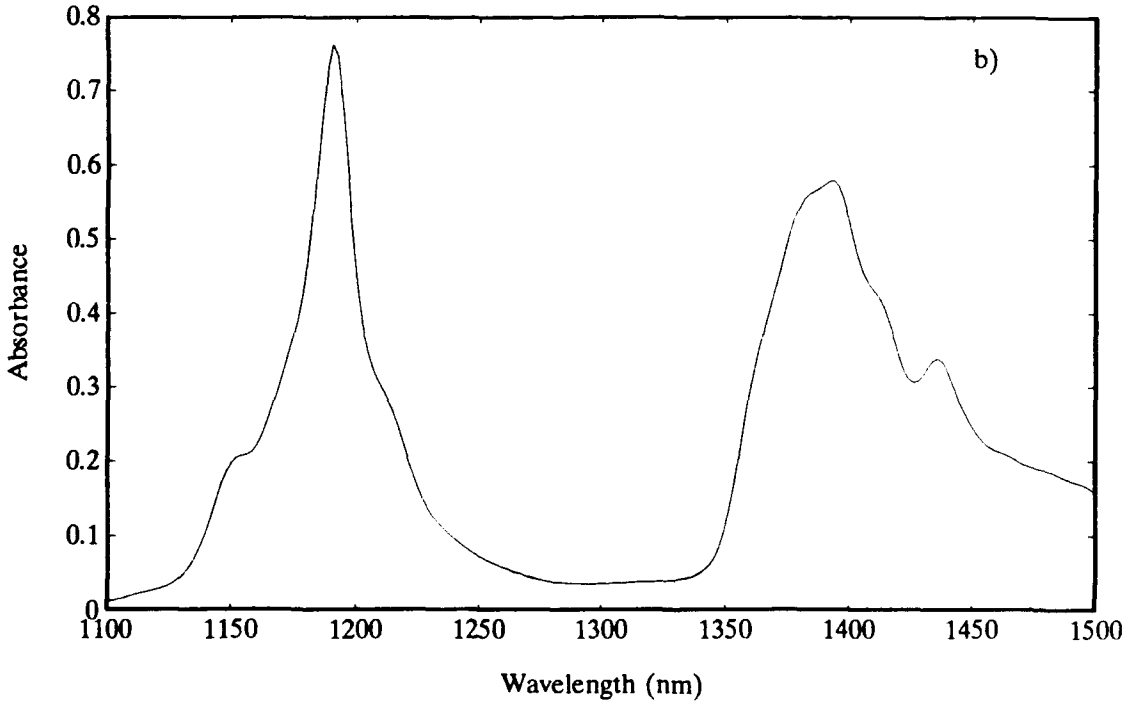
b)
Absorbance
0.8
0.7
0.6
0.5
0.4
0.3
0.2
0.1
0
1100
1150
1200
1250
1300
1350
1400
1450
1500
Wavelength (nm)

at 913 (1190) nm, due to the methyl C-H's. Figure 4.4a shows the SW-NIR spectrum, and Figure 4.4b the (LW-NIR) spectrum, of *n*-heptane with 10 methylene C-H's and 6 methyl C-H's. Here the methylene peak at 934 (1210) nm is slightly stronger than the methyl peak at 913 (1190) nm (23,24). Benzene, Figure 4.5, shows a single peak centered at 875 (1145) nm, well separated from the alkanes. The above assignments are for the third (second) overtone antisymmetric stretch region. The combinational regions from 980 - 1100 nm and (1320 - 1500 nm) have not yet been assigned. Though not used for analysis in this study because of their extremely weak intensities, the fourth-overtone C-H stretches of the aromatic, methyl, and methylene functional groups are observed at 716 nm, 746 nm, and 762 nm respectively.

4.3.2 Multiple Linear Regression Analysis

Stage-wise multiple linear regression (MLR) was conducted on the second-derivative transformation of both the SW-NIR and the LW-NIR spectral data sets. Linear regression equations of the form given in equation (4.2) were determined for the 3 constituents; volume percent aromatics, volume percent saturates and freezing point:

$$c = b_0 + b_1 * r_1(\lambda_1) + b_2 * r_2(\lambda_2) + \ldots + b_n * r_n(\lambda_n) \qquad \textbf{(4.2)}$$

where c is the constituent value, b_0 is an offset constant, b_n is the regression coefficient at wavelength n, r_n is the 2nd derivative absorbance at wavelength n, and

Figure 4.4 NIR absorption spectra of *n*-heptane.

a) SW-NIR spectral region.

b) LW-NIR spectral region.

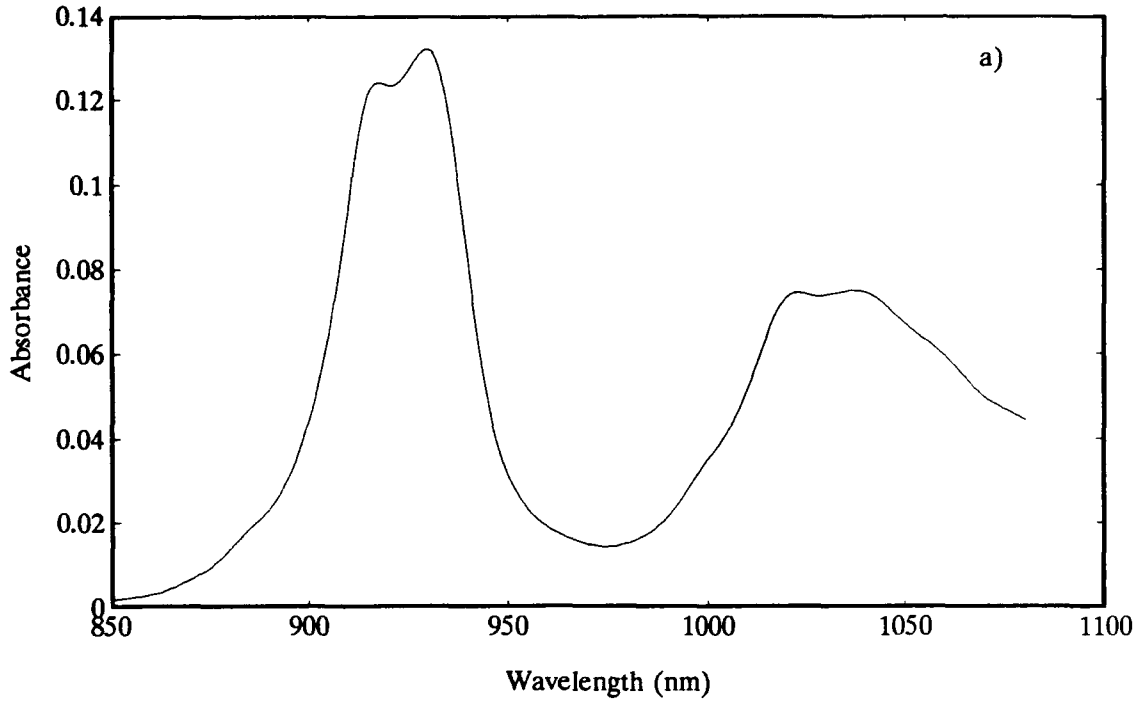
a)
Absorbance
0.14
0.12
0.1
0.08
0.06
0.04
0.02
0
850
900
950
1000
1050
1100
Wavelength (nm)

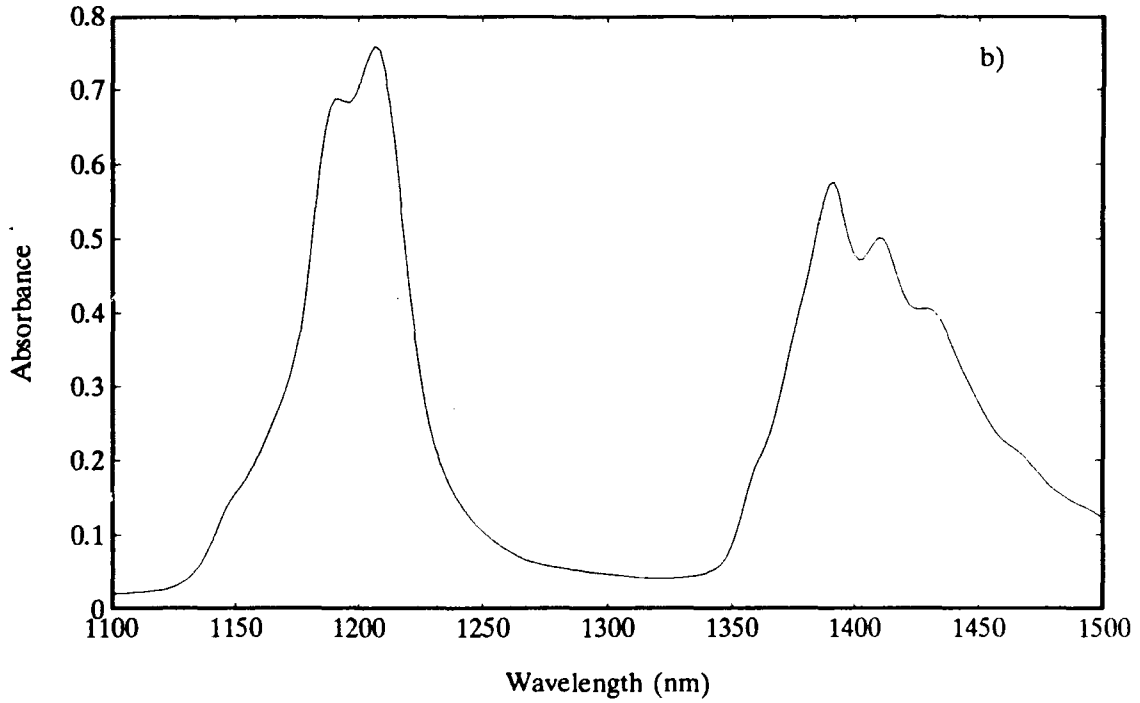
b)
Absorbance
0.8
0.7
0.6
0.5
0.4
0.3
0.2
0.1
0
1100
1150
1200
1250
1300
1350
1400
1450
1500
Wavelength (nm)

Figure 4.5 NIR absorption spectra of benzene.

a) SW-NIR spectral region.

b) LW-NIR spectral region.

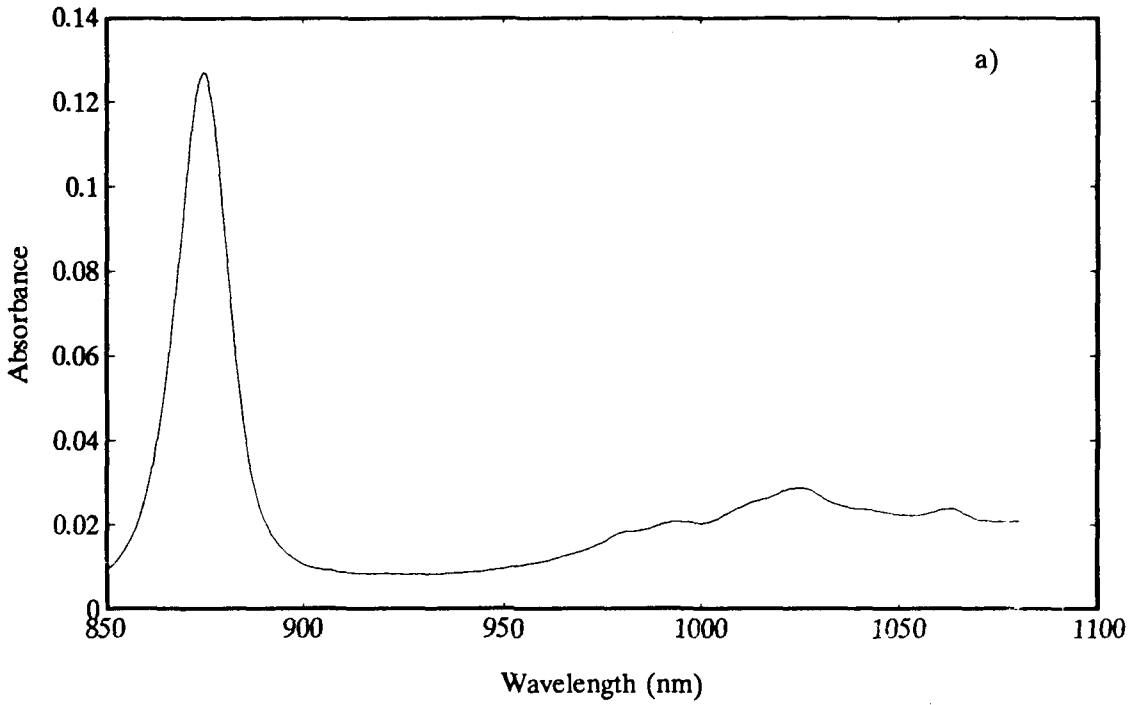
a)
Absorbance
0.14
0.12
0.1
0.08
0.06
0.04
0.02
0
850
900
950
1000
1050
1100
Wavelength (nm)

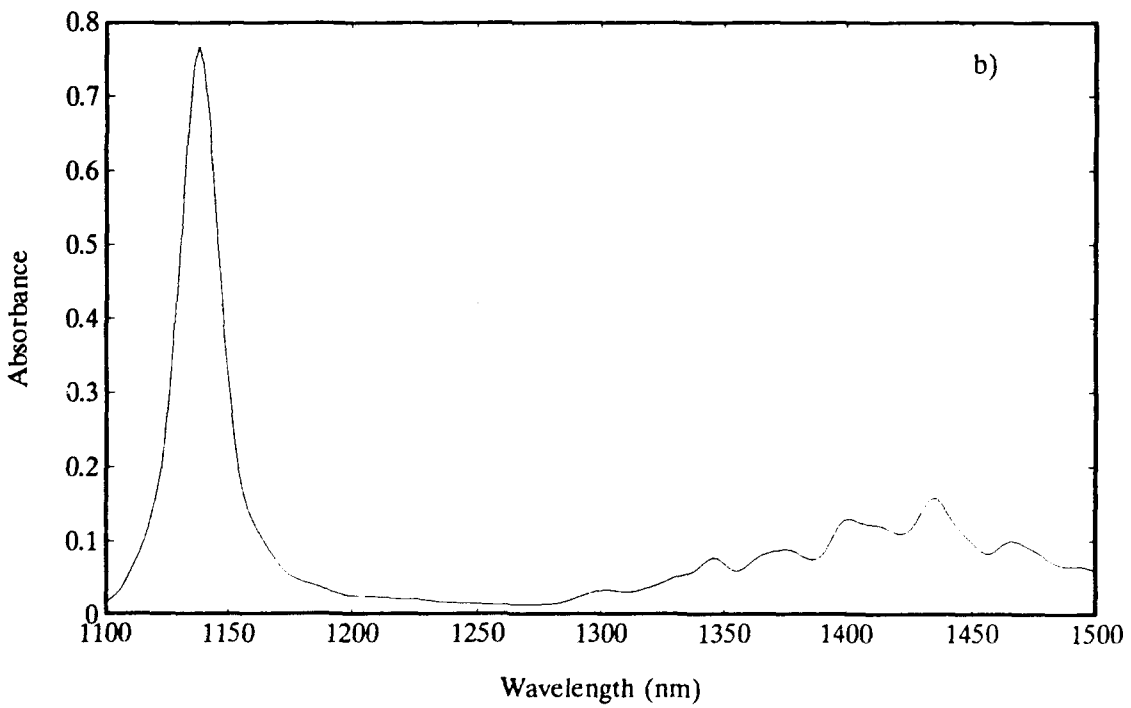
b)
Absorbance
0.8
0.7
0.6
0.5
0.4
0.3
0.2
0.1
0
1100
1150
1200
1250
1300
1350
1400
1450
1500
Wavelength (nm)

λ_n is the wavelength chosen by the step-forward regression analysis technique described in Chapter 1. The constituent values employed were the averages of the values determined by the round-robin laboratories as listed in Table 4.1. The MLR analysis results are presented before the partial least squares analysis results for reasons of convenience and interpretability. Examination of the wavelengths chosen by MLR, allows the analyst to rationalize the correlations on the basis of "first-principles".

Table 4.3 presents the three-wavelength regression equations determined by step-forward MLR for each of the three constituents. The calibration and prediction results for these models are given in Table 4.4. As can be seen from this data, both regions of the NIR performed comparably, with standard errors of estimate and prediction amounting to less than 1 percent for both aromatics and saturates and less than 2.5°C for freezing point. These values are well below published ASTM repeatability values (5,18) and might at first suggest that the limiting error in the NIR analysis is not due to the error in the reference analytical methods. However, the fact that the NIR prediction values are lower than the ASTM repeatability figures is explained by taking into account the fact that the NIR analysis was based on the average values obtained from the round-robin analysis, with standard errors of the mean significantly lower than ASTM repeatability values. Figure 4.6 presents lab plots of the actual versus regression estimated volume percent aromatics for; a) the portable NIR spectrometer, b) the HP spectrometer and c) the NIRSystems spectrophotometer. Figure 4.7 and Figure 4.8 present the

Table 4.3 MLR regression equations for JP-4 samples.

	Portable NIR Spectrometer (SW-NIR)						
	K_0	K_1	λ_1	K_2	λ_2	K_3	λ_3
Volume % Aromatics	20.8	-1905.1	882	976.2	1092	596.1	1070
Volume % Saturates	107.0	1972.1	882	-502.3	1100	2345.7	823
Freezing Point	-6.0	-930.5	905	1530.2	1029	-2867.4	866
	HP 8452 Spectrometer (SW-NIR)						
	K_0	K_1	λ_1	K_2	λ_2	K_3	λ_3
Volume % Aromatics	8.6	-547.6	882	8219.4	854	-2796.9	886
Volume % Saturates	59.8	1668.7	882	2275.0	988	470.7	944
Freezing Point	-66.4	8639.3	1028	4216.1	890	-3544.1	1052
	NIRSystems Spectrophotometer (LW-NIR)						
	K_0	K_1	λ_1	K_2	λ_2	K_3	λ_3
Volume % Aromatics	11.0	-250.7	1144	-1105.0	1454	6912.0	1314
Volume % Saturates	6.1	110.1	1144	-366.1	1386	-75.7	1190
Freezing Point	53.5	-7370.1	1300	313.5	1190	-661.1	1404

Table 4.4 MLR analysis results for JP-4 samples.

	Portable NIR Spectrometer (SW-NIR)			
	Calibration		Cross-Validation	
	SEE	R^2	SEP	R^2
Vol % Aromatics	0.54	0.94	0.81	0.90
Vol % Saturates	0.56	0.92	0.82	0.90
Freezing Point	1.89	0.86	2.28	0.81
	HP 8452A Spectrometer (SW-NIR)			
	Calibration		Cross-Validation	
	SEE	R^2	SEP	R^2
Vol % Aromatics	0.66	0.91	0.85	0.86
Vol % Saturates	0.68	0.91	0.84	0.85
Freezing Point	1.89	0.87	1.96	0.85
	NIRSystems Spectrophotometer (LW-NIR)			
	Calibration		Cross-Validation	
	SEE	R^2	SEP	R^2
Vol % Aromatics	0.51	0.95	0.91	0.86
Vol % Saturates	0.57	0.94	0.94	0.85
Freezing Point	1.80	0.88	2.47	0.76

Figure 4.6 Measured versus predicted volume percent aromatics.

a) Portable NIR spectrometer.

b) Hewlett Packard spectrometer.

c) NIRSystems spectrophotometer.

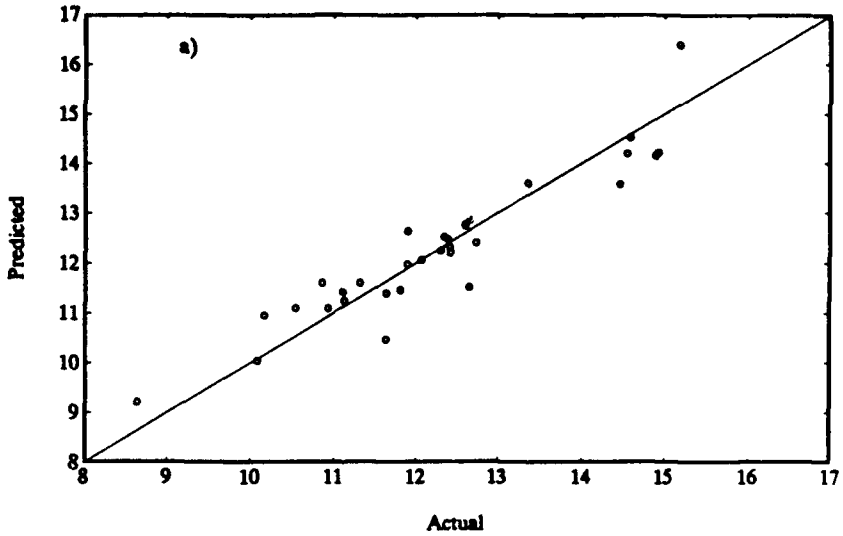
a)
Predicted
Actual
8
9
10
11
12
13
14
15
16
17

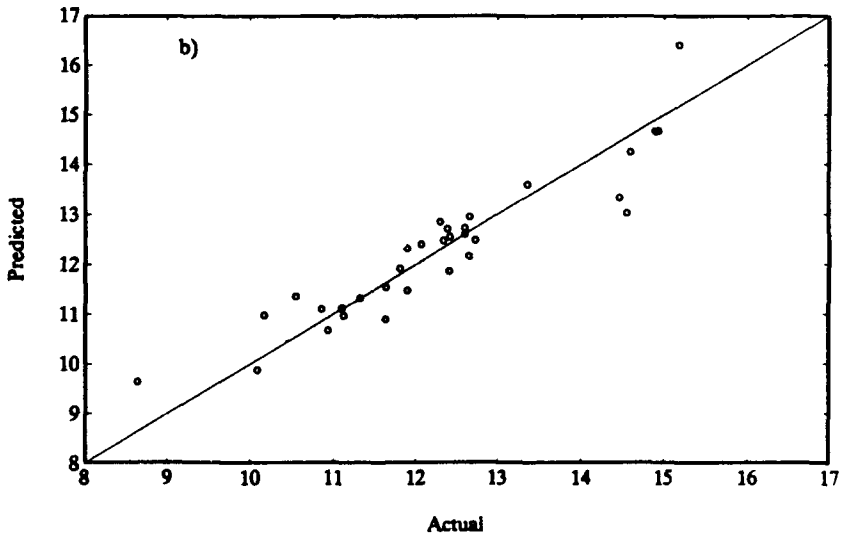
b)
Predicted
Actual
8
9
10
11
12
13
14
15
16
17

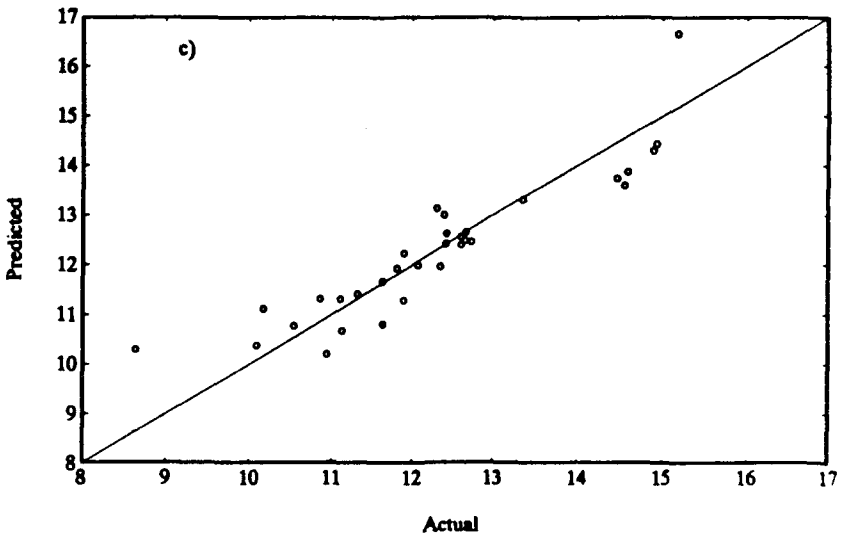
c)
Predicted
Actual
8
9
10
11
12
13
14
15
16
17

Figure 4.7 Measured versus predicted volume percent saturates.

a) Portable NIR spectrometer.

b) Hewlett Packard spectrometer.

c) NIRSystems spectrophotometer.

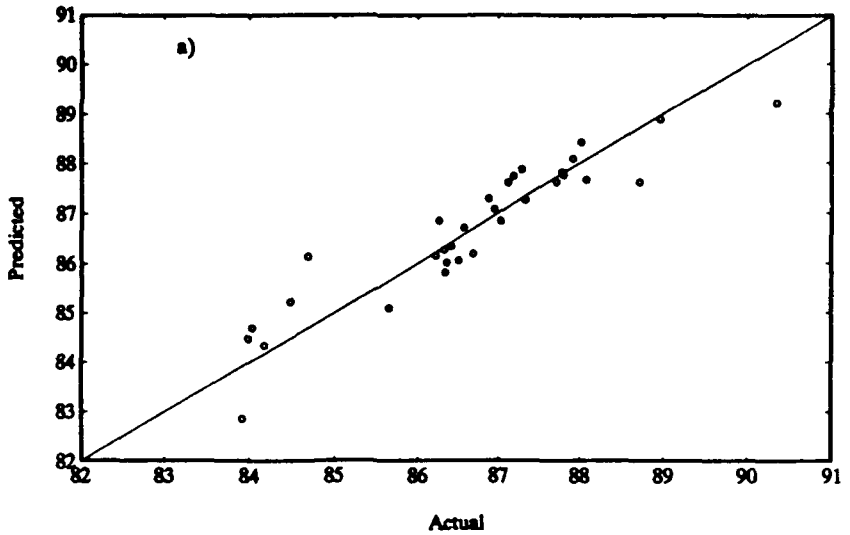
a)
Predicted
Actual
82
83
84
85
86
87
88
89
90
91

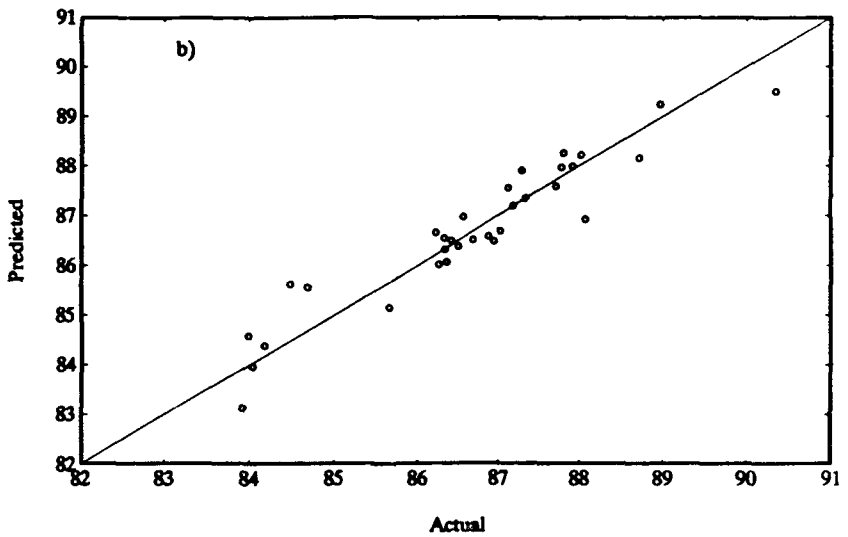
b)
Predicted
Actual
82
83
84
85
86
87
88
89
90
91

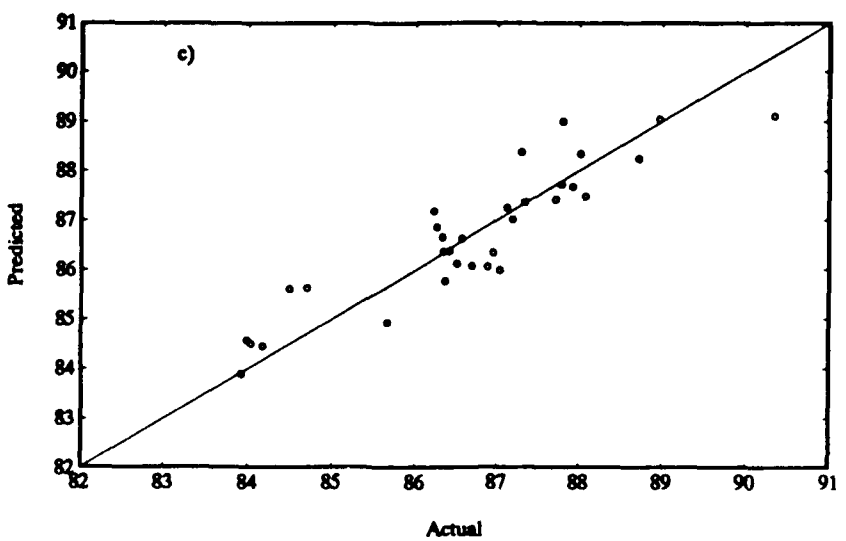
c)
Predicted
Actual
82
83
84
85
86
87
88
89
90
91

Figure 4.8 Measured versus predicted freezing point.

a) Portable NIR spectrometer.

b) Hewlett Packard spectrometer.

c) NIRSystems spectrophotometer.

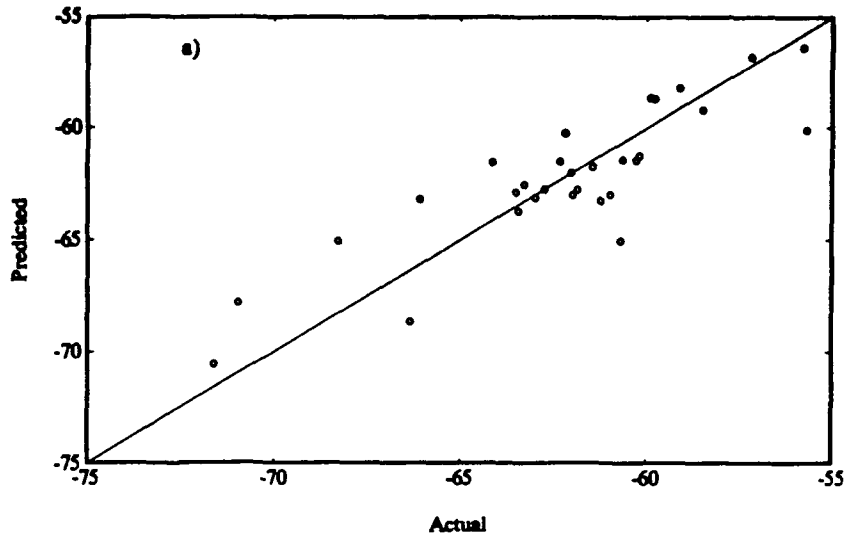
a)
Predicted
Actual
-55
-60
-65
-70
-75
-75
-70
-65
-60
-55

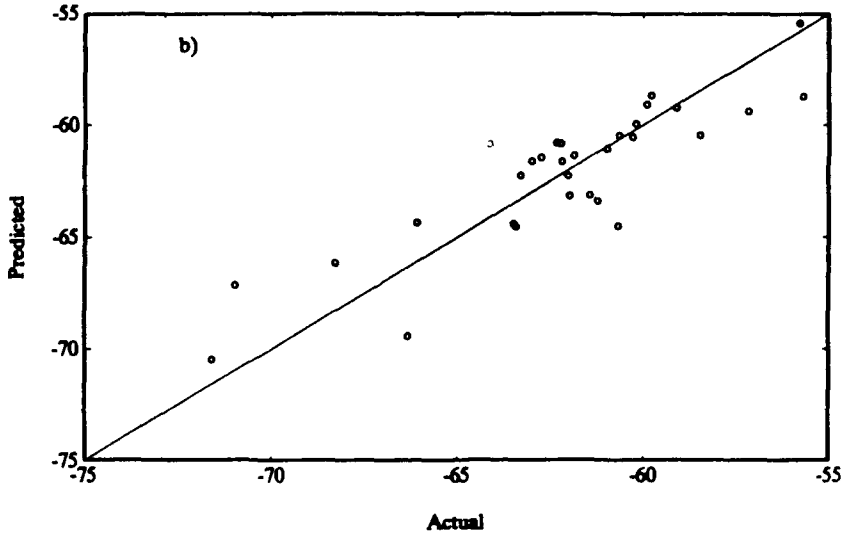
b)
Predicted
Actual
-55
-60
-65
-70
-75
-75
-70
-65
-60
-55

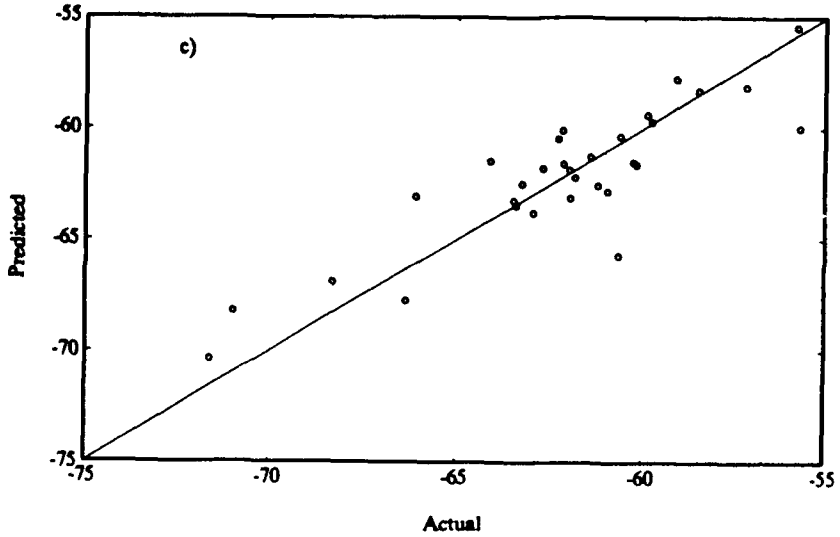
c)
Predicted
Actual
-55
-60
-65
-70
-75
-75
-70
-65
-60
-55

corresponding results for volume percent saturates and freezing point, respectively.

In both spectral regions, the first wavelength chosen for percent aromatics, as well as percent saturates, corresponds to an aromatic overtone absorption peak (occurring at 882 nm for the SW-NIR and 1144 nm for the LW-NIR). The sign of the correlation coefficient is negative for percent aromatics and positive for percent saturates. This is easily explained from the fact that the JP-4 samples consist almost exclusively of aromatics and saturates and contain virtually no olefinics. This results in closure between the two constituents (aromatics and saturates) and, for a given calibration wavelength, the correlation coefficients should be opposite in sign. This is verified by calculating the correlation coefficient between percent aromatics and percent saturates, as determined by the reference method. For this sample set the correlation coefficient is -0.9963. Evidently, the single most informative wavelength is the one corresponding to the aromatic CH. This is understandable because 882 and 1144 nm are in the most isolated bands in the spectrum. In contrast, saturates have both methyl and methylene functional groups in varying amounts. Therefore, a more economical description of the saturates is in terms of their complement to the aromatics.

A plot of correlation coefficient versus wavelength, after a one-wavelength regression, helps to visualize those regions of the spectrum that most highly correlate to a given constituent. Figure 4.9 presents plots of correlation coefficient, or R value, versus wavelength for percent aromatics for each of the three instruments. To aid the comparison between correlation coefficient and

Figure 4.9 Correlation coefficient versus wavelength for % aromatics.

a) Portable NIR spectrometer.

b) Hewlett Packard spectrometer.

c) NIRSystems spectrophotometer.

Note: The dashed spectrum in each plot represents an overlaid calibration sample.

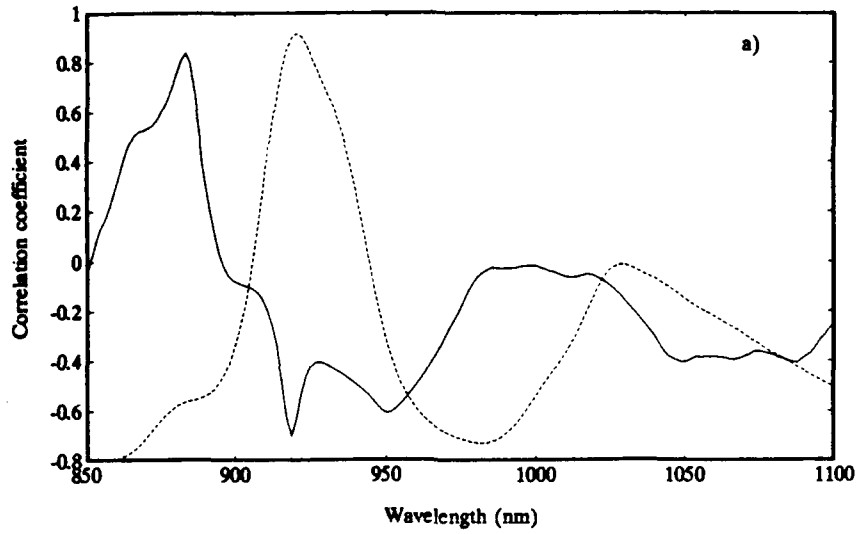
a)
Correlation coefficient
Wavelength (nm)
1
0.8
0.6
0.4
0.2
0
-0.2
-0.4
-0.6
-0.8
850
900
950
1000
1050
1100

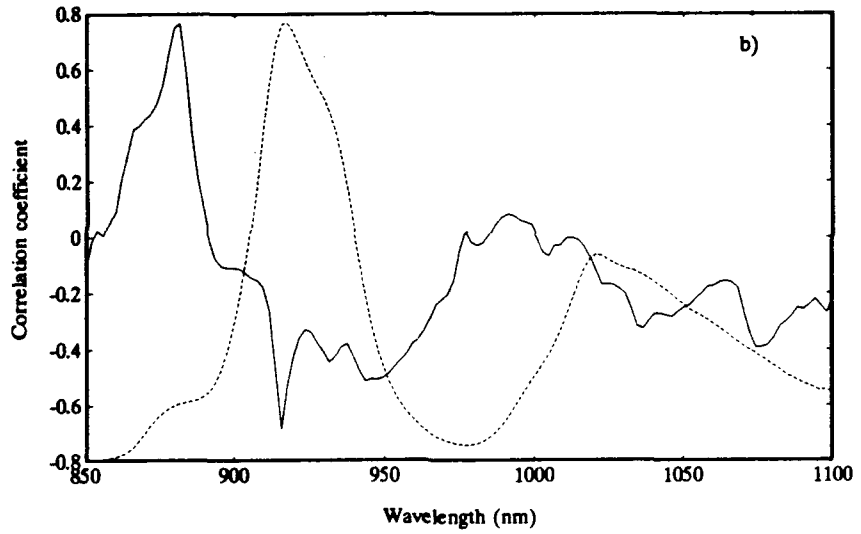
b)
Correlation coefficient
Wavelength (nm)
0.8
0.6
0.4
0.2
0
-0.2
-0.4
-0.6
-0.8
850
900
950
1000
1050
1100

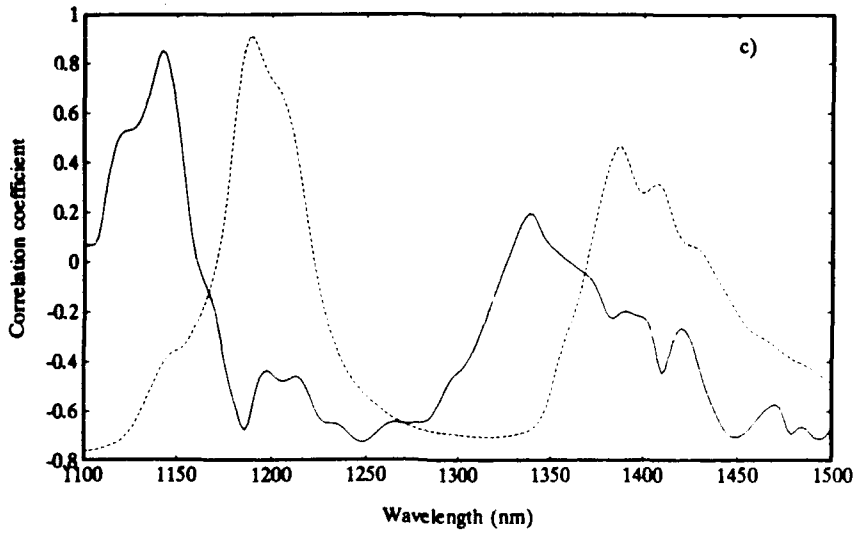
c)
Correlation coefficient
Wavelength (nm)
1
0.8
0.6
0.4
0.2
0
-0.2
-0.4
-0.6
-0.8
1100
1150
1200
1250
1300
1350
1400
1450
1500

wavelength, a calibration spectrum has been overlaid on each plot. As can be seen from these figures, there is a strong positive correlation with the aromatic absorption band (SW-NIR: 860 - 890 nm and LW-NIR: 1130 - 1160) and a negative correlation with the saturates region (SW-NIR: 900 - 950 and LW-NIR: 1175 - 1225).

For the SW-NIR prediction of both aromatics and saturates, the second wavelength chosen corresponds to a region of minimum absorbance and is thought to be correcting for residual baseline offset or differences in refractive index between samples. The effect of refractive index on NIR baselines has been demonstrated for the analysis of a polymerization process (25). In the LW-NIR prediction, the second wavelength chosen for percent aromatics (1454 nm) is in the aromatic portion of the combination band with a positive correlation. The second wavelength chosen for percent saturates (1386 nm) is in the methyl portion of the combination band with a positive correlation. It should be noted that the wavelengths chosen by the MLR analysis are consistent with what one would expect based on assignment of the absorption peaks.

At this point, it is appropriate to ask: at what level of precision in the NIR does measurement become limiting? A glance at the SW-NIR regression results shows that 90% of the correlation and, therefore 90% of the error, is contributed by the intensity measurement at 882 nm. The second-derivative intensity is approximately 3×10^{-4} at this wavelength for a sample with 15% aromatics. The precision in the air-vs-air baseline at this wavelength is approximately 1.0×10^{-5}. Thus, the expected absolute precision in the absorbance measurement is 0.2%.

When this is compared with the absolute error of 1.25% (1σ) in the reference aromatic determination, as reported by the ASTM, and the SEP value of 0.8% from the MLR analysis, the relative precision in the absorbance is not limiting. Yet another interesting point is the comparison of the regression equation for gasoline versus that for JP-4 in the prediction of percent aromatics (22). The first wavelength chosen for both data sets corresponds to the second overtone aromatic absorption band -- 1144 nm for JP-4 and 1151 nm for gasoline. Though these represent completely different types of fuel and were analyzed on spectrometers with different bandwidths, both data sets result in similar regression equations -- suggesting the possibility of a more universal calibration equation.

As shown in Table 4.3, freezing point is positively correlated with the methyl (890, 1028 and 1190 nm) and negatively correlated with the methylene (1052 and 1404 nm) absorption bands. As with any family of hydrocarbons, as the branching increases resulting in higher methyl and lower methylene content, van der Waals forces decrease causing a decrease in freezing point (26). As shown in Table 4.5, the addition of methyl groups to benzene causes a substantial decrease in freezing point. Likewise, as methyl groups are added to the straight-chain alkanes, thereby reducing the number of methylene hydrogens, freezing point is reduced significantly. Although freezing point does not appear to be correlated to aromatics, it undoubtedly is correlated to the degree and type of substitution of the aromatic ring. The lower multiple R values associated with freezing point are, in all likelihood, due to the lack of precision in the reference method. On-going

Table 4.5 Freezing point of selected hydrocarbons

Hydrocarbon	Molecular Weight	Freezing Point
Aromatic Hydrocarbons		
Benzene C_6H_6	78.11	5.5
Toluene $C_6H_5CH_3$	92.14	-95.0
1,3-dimethylbenzene 1,3-$(CH_3)_2C_6H_4$	106.17	-47.9
1,3,5-trimethylbenzene 1,3,5-$(CH_3)_3C_6H_3$	120.19	-44.7
Saturated Hydrocarbons		
Octane $CH_3(CH_2)_6CH_3$	114.23	-56.8
2,2,4-trimethylpentane $(CH_3)_2CHCH_2C(CH_3)_3$	114.23	-107.4
Decane $CH_3(CH_2)_8CH_3$	142.28	-29.7
3-methyldecane $C_7H_{15}CH(CH_3)C_2H_5$	156.31	-92.9

research at the USAF Wright Aeronautical Laboratories is concentrating on obtaining more accurate freezing point determinations so as to determine whether the limiting factor in the estimation of freezing point is the NIR spectral analysis or the reference method. Despite the somewhat lower multiple R values, the SEE and SEP values obtained from both statistical analyses are within the published ASTM reproducibility value of 2.5^0, suggesting the feasibility of NIR analysis for the estimation of freezing point of JP-4.

In the calibration phase, the portable NIR spectrometer produced SEE values which are 20% lower than for the HP spectrometer and 10% higher than the NIRSystems spectrophotometer. The 20% improvement over the HP spectrometer is attributed to the higher signal-to-noise ratio of the portable NIR spectrometer (2.55×10^{-5} versus 6.00×10^{-5}) (27). The fact that the NIRSystems spectrophotometer, operating in the LW-NIR, performed somewhat better than the portable NIR spectrometer is not surprising since the second-overtone absorptions are six to seven times more intense than the third-overtone absorptions resulting, in higher signal-to-noise ratios. However, in the prediction phase, the portable NIR spectrometer performed slightly better than the HP spectrometer and approximately 10% better than the NIRSystems spectrophotometer. In light of the 10% relative error in the reference measurements, the performance differences between the three instruments are not significant. On the basis of the MLR analysis, the portable NIR spectrometer was able to perform the in-field analysis at a level of precision comparable to that of either of the laboratory instruments.

4.3.3 Partial Least Squares Analysis

To corroborate the results of the MLR analysis, the sample data set was also analyzed by applying the method of partial least squares to both the SW-NIR and LW-NIR data sets.

By evaluating the predictive error of the PLS model as a function of the number of independent variables, the proper number of independent variables to retain can be determined. The point at which the predictive error goes through a minimum indicates the proper number of variables to retain. Retaining fewer than this number results in a model that does not sufficiently describe the data set, while retaining more than this number results in a model that is overfit and incorporates system noise. Evaluation of the prediction residual sum of squares (PRESS) (28) from the PLS analysis of the data sets, indicates that four independent variables are needed to describe the maximum amount of variance in the data set. Figure 4.10 presents the PRESS results from the analysis of the SW-NIR spectral data for percent aromatics and shows a minimum at four latent variables.

The PLS analysis performed somewhat better than the MLR analysis, with an improvement of approximately 10% in the SW-NIR and 20% in the LW-NIR for both SEE and SEP values. A comparison of the PLS X-block loadings from the auto-scaled data set provides a sense of the spectral components inherent in the analysis of the three constituents. The PLS X-block loadings for the first latent variable are presented in Figure 4.11 for volume percent aromatics. Apparent from

Figure 4.10 Volume percent aromatics - PRESS plot.

PRESS plot generated using SW-NIR spectra of the JP-4 fuels taken on the portable NIR spectrometer.

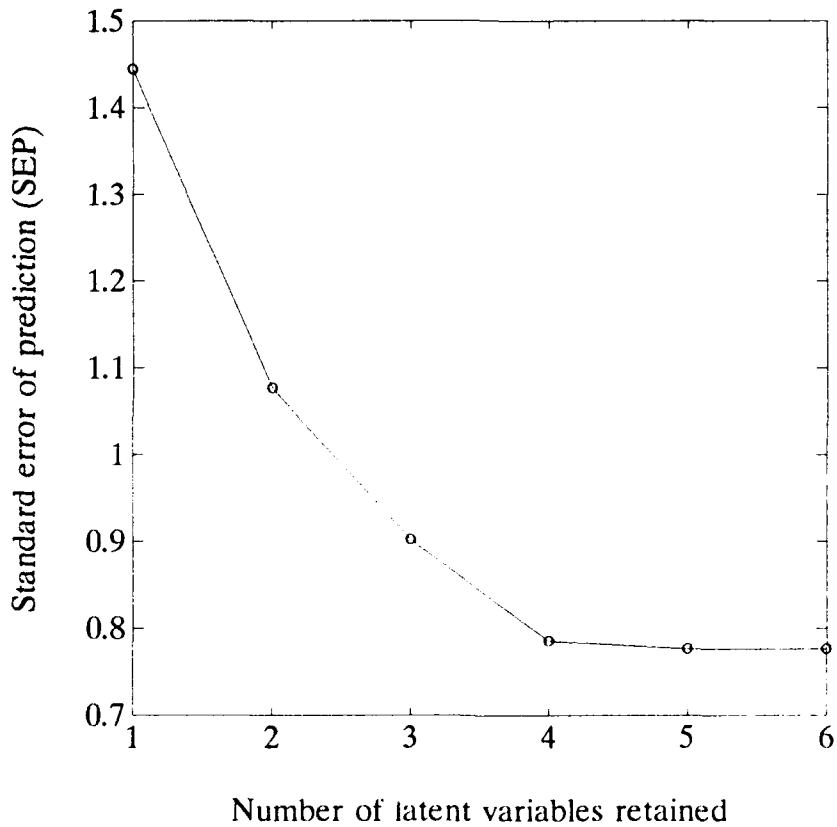
1.5
1.4
1.3
1.2
1.1
1
0.9
0.8
0.7
1
2
3
4
5
6
Standard error of prediction (SEP)
Number of latent variables retained

Figure 4.11 PLS loadings plot for volume percent aromatics.

a) Portable NIR spectrometer.

b) Hewlett Packard spectrometer.

c) NIRSystems spectrophotometer.

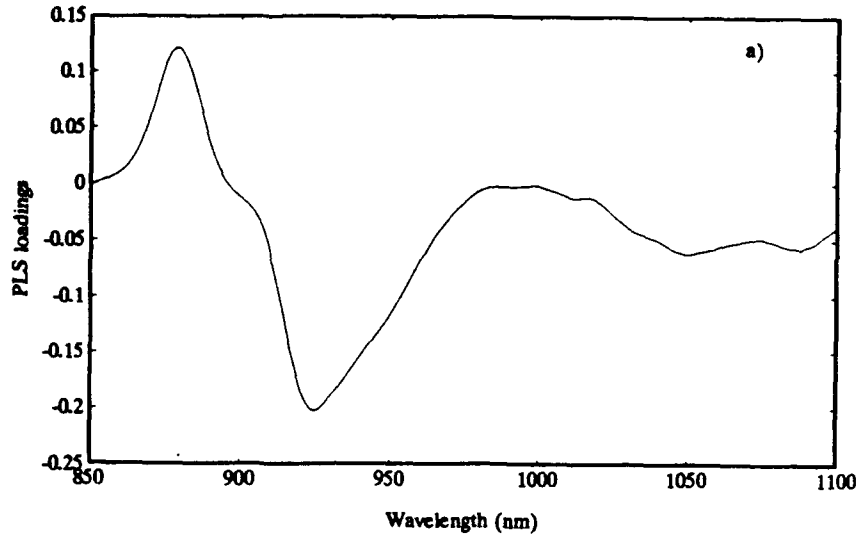
a)
PLS loadings
0.15
0.1
0.05
0
-0.05
-0.1
-0.15
-0.2
-0.25
850
900
950
1000
1050
1100
Wavelength (nm)

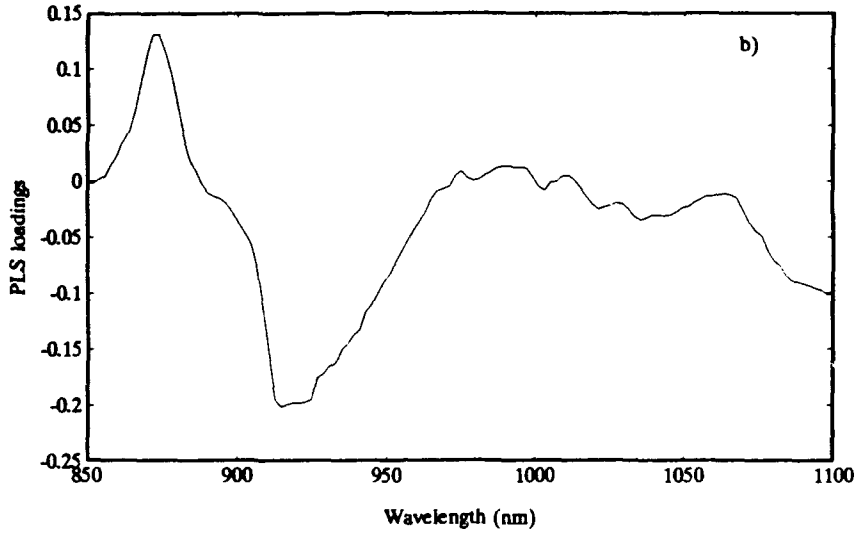
b)
PLS loadings
0.15
0.1
0.05
0
-0.05
-0.1
-0.15
-0.2
-0.25
850
900
950
1000
1050
1100
Wavelength (nm)

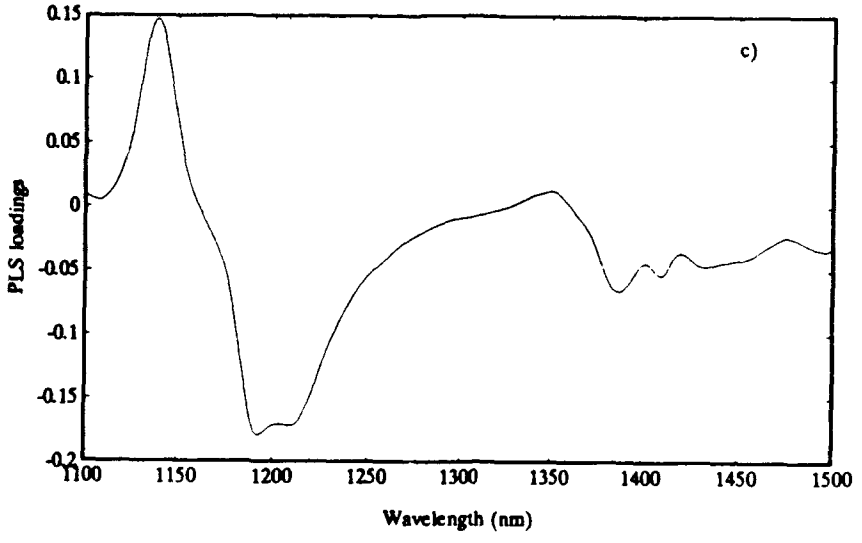
c)
PLS loadings
0.15
0.1
0.05
0
-0.05
-0.1
-0.15
-0.2
1100
1150
1200
1250
1300
1350
1400
1450
1500
Wavelength (nm)

these plots is the positive correlation with the aromatic overtone C-H absorbance and the negative correlation with the methyl and methylene overtone C-H absorption band. For both the SW-NIR and the LW-NIR, the PLS X-block loading of the first latent variable is very similar to the correlation spectrum from the MLR analysis (Figure 4.9). The first latent variable in the analysis of both spectral regions is found to have a strong correlation with aromatic absorptions, and the information is used positively for aromatics and negatively for saturates in the correlations. Additional latent variables continue this same theme of positively correlating with spectral regions of the constituent hydrocarbon and negatively with spectral regions corresponding to the functional groups of the other hydrocarbon classes. The importance of the above observation is that the PLS analysis selects the appropriate spectral features that one would select based on the first principles of absorption spectroscopy.

A summary of the PLS regression statistics is presented in Table 4.6. As can be seen from these results, the standard error of estimate, as well as the standard error of prediction, are less than 1 percent for volume percent aromatics and volume percent saturates and less than 2.5°C for freezing point. As in the MLR analysis, the standard error of prediction (SEP) values were generated using a "leave-one-out" cross-validation technique for prediction. Again each of these values is within the range of published ASTM repeatability values. Lab plots of an autoscaled, four latent variable PLS analysis for volume percent aromatics are presented in Figure 4.12. As with the MLR analysis, the limiting error in the PLS

Table 4.6 PLS analysis results for JP-4 samples.

	Portable NIR Spectrometer (SW-NIR)			
	Calibration		Cross-Validation	
	SEE	R^2	SEP	R^2
Vol % Aromatics	0.51	0.85	0.73	0.88
Vol % Saturates	0.51	0.85	0.73	0.89
Freezing Point	1.55	0.72	2.28	0.78
	HP 8452A Spectrometer (SW-NIR)			
	Calibration		Cross-Validation	
	SEE	R^2	SEP	R^2
Vol % Aromatics	0.55	0.84	0.78	0.86
Vol % Saturates	0.55	0.84	0.78	0.86
Freezing Point	1.69	0.71	2.49	0.73
	NIRSystems Spectrophotometer (LW-NIR)			
	Calibration		Cross-Validation	
	SEE	R^2	SEP	R^2
Vol % Aromatics	0.32	0.95	0.69	0.89
Vol % Saturates	0.32	0.95	0.70	0.89
Freezing Point	1.64	0.73	2.25	0.78

Figure 4.12 PLS predicted volume percent aromatics.

a) Portable NIR spectrometer.

b) Hewlett Packard spectrometer.

c) NIRSystems spectrophotometer.

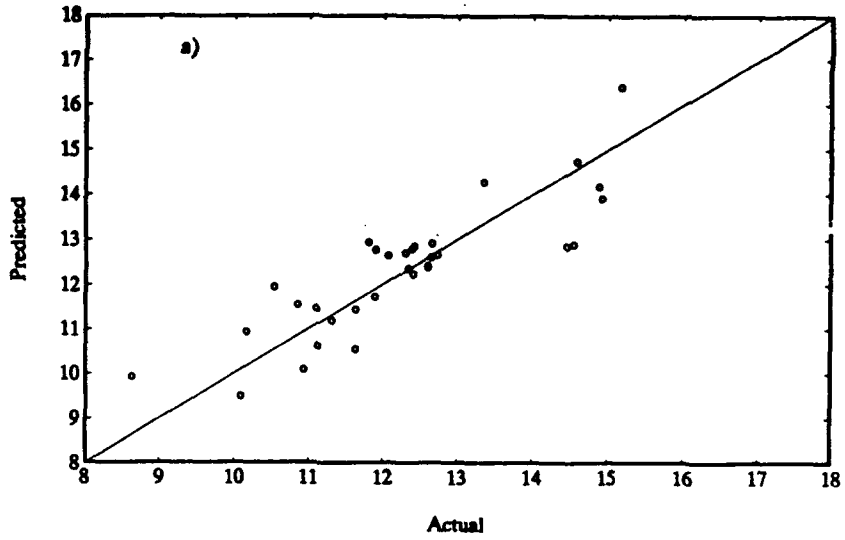
a)
Predicted
Actual
8
9
10
11
12
13
14
15
16
17
18

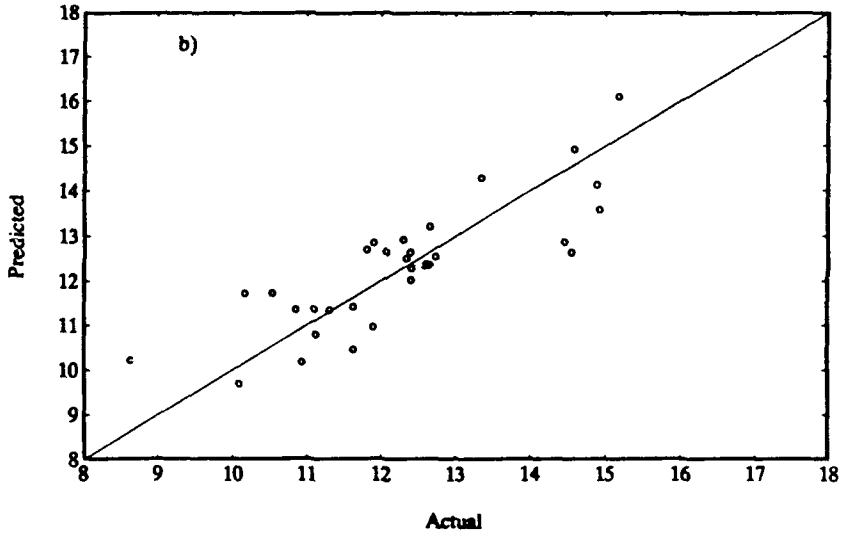
b)
Predicted
Actual
8
9
10
11
12
13
14
15
16
17
18

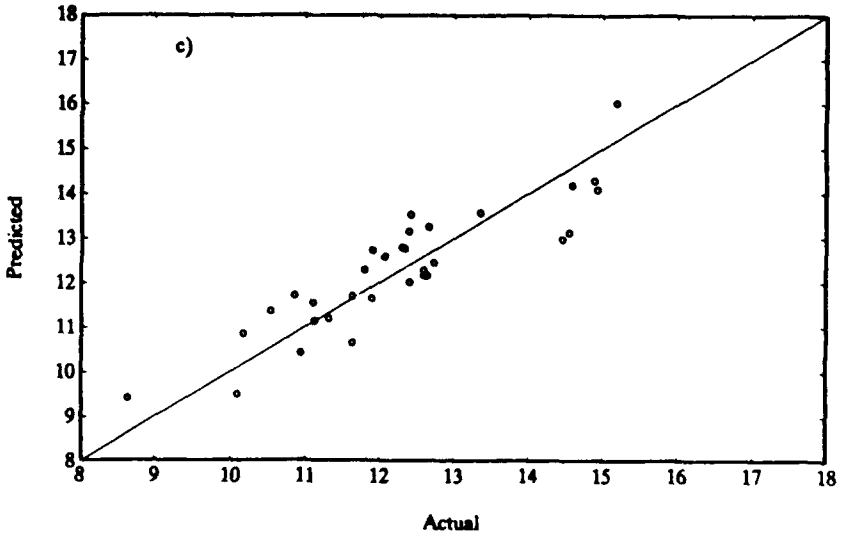
c)
Predicted
Actual
8
9
10
11
12
13
14
15
16
17
18

analysis appears to be due to the inaccuracy of the reference analytical methods.

For the PLS analysis, the portable NIR spectrometer performed slightly better than the HP spectrometer. As with the MLR analysis, this is expected due to the higher signal-to-noise ratio of the portable NIR spectrometer. Though not performing as well as the NIRSystems spectrophotometer (LW-NIR) in the calibration phase, the portable NIR spectrometer (SW-NIR) performed just as well as the NIRSystems spectrophotometer in the prediction phase. As was the case with the MLR analysis, the portable NIR spectrometer was able to perform the in-field analysis at a level of precision comparable with either of the laboratory instruments.

4.4 Conclusions

Near-infrared spectroscopy is an analytical technique ideally suited for the analysis of hydrocarbon samples. Not only is the rapid and simultaneous determination of the major hydrocarbon classes as well as the freezing point of JP-4 jet fuels possible, but the errors in the NIR predicted values (< 1.0% for percent aromatics and percent saturates and < 2.5°C for freezing point) are less than published ASTM reproducibility values and are an indication of the merit of this technique. One of the major goals of this research was to develop an instrument capable of performing jet fuel analysis just as accurately in-the-field as is possible in the laboratory. This was indeed shown to be the case by both the MLR and the PLS analyses, where the portable NIR spectrometer performed as well as, and in

some cases better than, both the HP diode array spectrometer and the NIRSystems scanning spectrophotometer.

It is important to emphasize that the results obtained here are based upon calibration against a limited number of samples and that future results will be valid only for unknowns which belong to the calibration set. For example, all of the samples tested had low levels of olefinics. Thus, it cannot be guaranteed that good results will be obtained for high olefinic samples. However, it should be noted here that NIR spectroscopy has been used successfully in the prediction of olefinic content of finished gasolines (22) and certainly should be capable of determining olefin content of aviation fuels also.

The major limitation of this analysis technique is its dependency on accurately determined reference values from which a calibration model is developed. Improvements in the NIR prediction of fuel properties will require reference analysis methods more accurate than the fluorescence indicator method and the present freeze point determination method on which these analyses were based.

4.5 Notes to Chapter 4

1. Lysaght, M.J., Danielson, J.D.S., Callis, J.B., *CPAC Publication Announcement # 106*, **1991,** 2, 1.

2. Lysaght, M.J., Kelly, J.J., Callis, J.B., *CPAC Publication Announcement # 102*, **1991**, 1, 1.

3. Martel, C.R., *Military Jet Fuels, 1944-1987: Report # AFWAL-T R-87-2062*, Aero Propulsion Lab, AFWAL/POSF, Wright-Patterson Air Force Base, OH **1987**.

4. *Aviation Fuels and Their Effects on Engine Performance*, Ethyl Corporation, contract No. 52-202, Department of the Navy, Bureau of Aeronautics, **1951**.

5. *1990 Annual Book of ASTM Standards*; American Society for Testing and Materials: Philadelphia, PA, **1990**, 05.01, 509.

6. Campbell, R.M., Djordjevic, N.M., Markides, K.E., Lee, M.L., *Anal. Chem.,* **1988**, 60, 356.

7. Norris, A.T., Rawdon, M.G., *Anal. Chem.,* **1984**, 56, 1767.

8. Petrakis, L., Allen, D.T., Gavalas, G.R., Gates, B.C., *Anal. Chem.,* **1983**, 55, 1557.

9. Caswell, K.A., Glass, T.E., Swann, M., Dorn, H.C., *Anal. Chem.,* **1989**, 61, 206.

10. Hayes, P.C., Jr., Anderson, S.D., *Anal. Chem.,* **1985**, 58, 2384.

11. Miller, R.L., Ettre, L.S., Johansen, N.G., *J. Chromatogr.*, **1983**, 264, 19.

12. Durand, J.P., Boscher, Y., Petroff, N., Berthelin, M., *Journal of Chromatography,* **1987**, 395, 229.

13. Szakasits, J.J., Robinson, R.E., *Anal. Chem.*, **1991**, 63, 114.

14. Ozubko, R.S., Clungston, D.M., Furimsky, E., *Anal. Chem.,* **1981**, 53, 183.

15. Hayes, P.C., Jr., Anderson, S.D., *Anal. Chem.*, **1985**, 57, 2094.

16. Weyer, L.G., *Appl. Spectrosc. Rev.,* **1985**, 19, 1.

17. Wheeler, O.H., *Chem. Rev.,* **1959**, 59, 629.

18. *1990 Annual Book of ASTM Standards*; American Society for Testing and Materials: Philadelphia, PA, **1990**, 05.02, 157.

19. *PC-MATLAB for 80386-based MS-DOS Personal Computers*, Version 3.5e, The Math Works Inc., **1989**.

20. Haaland, D.M., Thomas, E.V., *Anal. Chem.*, **1988**, 60, 1202.

21. Kelly, J.J., Barlow, C.H., Jinguji, T.M., Callis, J.B., *Anal. Chem.*, **1989**, 61, 313.

22. Kelly, J.J., Callis, J.B., *Anal. Chem.*, **1990**, 62, 1444.

23. Fox, J.J., Martin, A.E., *Proc. R. Soc. London*, **1938**, A167, 257.

24. Fox, J.J., Martin, A.E., *Proc. R. Soc. London*, **1938**, A175, 208.

25. Aldridge, P.K., *Doctoral Dissertation*, University of Washington, Seattle, WA, **1991**.

26. Morrison, R.T., Boyd, R.N, *Organic Chemistry, Third Edition,* **1974**, Allyn and Bacon, Inc., Boston, 85.

27. Tong, L., Lysaght, M.J., Kelly, J.J., Callis, J.B., *HP Application Note, Performance Evaluation of the HP8452A with NIR Modification*, to be published.

28. Sharaf, M.A., Illman, D.L., Kowalski, B.R., *Chemometrics*, John Wiley & Sons, NY, **1986**.

CHAPTER 5

NIR Analysis of Xylene Isomers

5.1 Introduction

This chapter presents the shortwave near-infrared analysis of mixtures of the three xylene isomers: *ortho*-xylene, *meta*-xylene, and *para*-xylene. Its purpose is to further demonstrate the capabilities of the portable NIR spectrometer, and to compare the performance of partial least squares, multiple linear regression and classical least squares methods of data analysis. The xylene isomers were chosen as the sample system for two reasons. First, the high degree of spectral overlap between the three isomers will provide a definite test of performance of the various multivariate statistical methods. Second, the importance of the xylenes in the petroleum industry, as well as their value as a chemical commodity, necessitates a rapid method for quantitative analysis. Current approaches to this problem require a time-consuming chromatographic separation prior to quantitation (1,2).

A final aspect of this study involved a comparison of the performance of the portable NIR spectrometer with that of the NIR Systems 6250 mechanically-scanned spectrophotometer.

5.1.1 Background

The existence of the xylenes was first reported in 1840, when Gerhardt and Cahours (3) successfully isolated what they thought to be a single compound from the distillation of cuminic acid in an excess of lime. It was not until thirty-

seven years later that the xylenes were proven to exist in the three isomeric forms of *ortho*-, *meta*-, and *para*-xylene, by Fittig (4), and Jacobsen (5). Although the importance of the xylenes as solvents was immediately recognized, the need for the xylene isomers in pure form was not apparent until the mid-twentieth century. The first isomer to achieve commercial significance was *ortho*-xylene. Phthalic anhydride, used in the manufacture of plasticizers, alkyd resins, and polyester resins (6), is produced by the direct oxidation of *ortho*-xylene. Current annual demand for phthalic anhydride in the US alone, is over 500,000 metric tons. The primary use for *para*-xylene is in the production of polyester fibers, where the key adduct, terephthalic acid, is produced by the direct oxidation of *para*-xylene (7). Current US production of terephthalic acid stands at over 3 million metric tons per year. *Meta*-xylene is the least used of the three xylene isomers, with a total US demand of only 35,000 metric tons per year. Primary uses for *meta*-xylene include: the production of isophthalic acid, for use in the manufacture of polyester resins and alkyd resins (8); the synthesis of *meta*-xylidine for the production of the anaesthetic, xylocaine; and for the manufacture of insect repellents and flavoring materials (6). Due to the difficulty in separating *meta*-xylene from ethylbenzene, much of the *meta*-rich fraction is used in motor gasoline blends, where it has a valuable effect in improving octane ratings (9).

Prior to 1945, coal carbonization was the primary source of the xylenes. In the years following 1945, a gradual switch was made to the recovery of the xylenes from petroleum. Today, the xylenes are predominantly derived from catalytic

reformate and pyrolysis gasoline. Catalytic reformate is made by subjecting the petroleum naphtha to the Zelinski reaction (10), using either the 'Platforming' process (11) or the 'Powerforming' process (12). The Zelinski reaction consists of exposing the petroleum fraction to high pressure and temperature (approximately 500 ^{0}C) in the presence of a catalyst, usually platinum or palladium. Under these conditions, the hydrogen atoms of the various naphthalenic hydrocarbons are detached, resulting in conversion to benzene, toluene and the C_8 alkyl benzenes. Pyrolysis gasoline is the liquid-stream by-product from the steam-cracking of refinery gas, naphtha or gas oil (9). Recovery of the aromatic compounds from petroleum may be achieved by a variety of techniques including: fractional distillation, solvent extraction, extractive distillation, azeotropic distillation, solid adsorption, and crystallization. The method used depends on the source of the feedstock and relative proportions of the major components. Once the aromatics are separated from the feedstock, further separation is required for recovery of the individual xylenes. *Para*-xylene (99.5% pure) is usually recovered by either a solid adsorption process or crystallization (13,14). *Meta*-xylene is obtained using a multistage extractor, in which a complex with hydrofluoric acid and boron trifluoride is formed. After separation from the other aromatics, decomposition at moderate temperatures (< 100 ^{0}C) produces 99.5% pure *meta*-xylene (6). *Ortho*-xylene is separated using fractional distillation (15). Despite the fact that much research has gone into the separation of the three isomers, a rapid technique for quantifying the individual isomers in mixed xylenes is lacking.

The American Society for Testing and Materials (ASTM) provides an established procedure for xylene isomer analysis by gas chromatography, ASTM Test D2306 (16). With this test, either packed or capillary columns can be used to effect isomer separation, with detection provided by either thermal conductivity or flame ionization detectors. The quantification of the isomers is based on a peak height or peak area comparison with a chromatogram of synthetic reference samples at known concentration. Another test, proposed for adoption by the ASTM, is based on infrared spectroscopy in the wavelength region 12 to 15 microns (17). The ASTM published repeatability / reproducibility values (defined at the 95% confidence level) for these techniques are given in Table 5.1.

The quantitative analysis of two of the xylene isomers in the presence of other methylated benzenes, using both fourier transform infrared (FT-IR) and UV spectroscopy, has been reported by Brown *et al.* (18). The FT-IR analysis consisted of mixtures of *para*-xylene and *meta*-xylene in the presence of pseudocumene (*1,2,4*-trimethylbenzene). For the UV analysis, sample mixtures consisted of two of the xylene isomers in the presence of toluene. The SEP values from a cross-validation factor analysis, retaining three eigenvectors, are reported in Table 5.1.

The research presented here describes a rapid spectroscopic method of analysis for determining the relative amounts of the three xylene isomers, to a precision of less than 0.50 % absolute.

Table 5.1 Xylene isomer quantitation capabilities.

ASTM Repeatability / Reproducibility Values				
	Infrared Analysis		Gas Chromatography Analysis	
	Repeat-ability	Reproduc-ibility	Repeat-ability	Reproduc-ibility
o-Xylene	1.2 %	2.3 %	0.9 %	1.7 %
m-Xylene	2.4 %	4.2 %	0.8 %	2.4 %
p-Xylene	0.7 %	1.4 %	0.7 %	1.2 %

Standard Error of Prediction (Cross-Validation)		
	FT-IR Spectroscopy	UV Spectroscopy
o-Xylene	Not Reported	1.2 %
m-Xylene	1.4 %	1.3 %
p-Xylene	3.5 %	0.7 %

5.2 Spectral Band Assignments

From the discussion on spectroscopic assignments presented in Chapter 4, and previous work by Henry (19,20,21), Nakagaki, and Hanazaki (22,23), it is possible to assign the NIR absorption bands observed for the three xylene isomers. The C-H third-overtone region extends from approximately 850 - 940 nm. The aromatic C-H stretch gives rise to a single absorption band at approximately 878 nm. Depending on the local environment of the aromatic C-H, *i.e.*, location of the two methyl groups attached to the aromatic ring, there is a 3.6 nm shift in peak maxima position. The peak maxima is at 877.1 nm for *ortho*-xylene, 878.2 nm for *meta*-xylene, and 880.7 nm for *para*-xylene.

For *meta*-xylene and *para*-xylene, the two methyl groups attached to the aromatic ring give rise to a single and rather wide absorption band centered at 912.7 nm and 913.4 nm, respectively. Work by Henry (19), suggests that the two methyl groups of *meta*- and *para*-xylene are nearly free rotors having equivalent C-H bonds. This would explain the single methyl peak observed at 913 nm. However, the adjacent methyl groups in *ortho*-xylene have a high barrier to internal rotation. As a result, two peaks (with intensities in the ratio 2:1) are expected for *ortho*-xylene, with the less intense peak at the higher frequency.

5.3 Experimental

Spectra of the pure-components were taken on both the portable NIR spectrometer (resolution = 3 nm) and the commercial scanning spectrophotometer

(resolution = 7 nm) to demonstrate the spectral similarities between the three isomers. The NIR spectra of the three xylenes are presented in Figure 5.1a, for the portable NIR spectrometer, and in Figure 5.1b, for the scanning spectrophotometer. The improved resolution of the portable spectrometer over the scanning spectrophotometer, is evident from the absorption band at 915 nm. For the portable spectrometer, this band begins to separate into two distinct peaks, whereas for the scanning spectrophotometer the band appears as a major peak at 920 nm, with a shoulder at 910 nm. The major spectral differences between the three xylenes are: a) the splitting of the third-overtone methyl C-H absorption for *ortho*-xylene at 915 nm, b) differences in the combination region (970 - 1070 nm) between *ortho*-xylene and the other two isomers and, c) a 3.6 nm spectral shift in the location of the third-overtone aromatic C-H absorption at 878 nm.

5.3.1 Xylene Samples

Two sets of 40 samples, consisting of varying amounts of the three xylene isomers, were made using reagent grade *ortho*-xylene, *meta*-xylene, and *para*-xylene, as obtained from Aldrich Chemical Company. The initial set of samples prepared are referred to as Data Set A. Data Set B was prepared 30 days later, using the same concentration constraints as those applied to Data Set A. The concentrations ranged from 12.818 - 37.032 volume percent *ortho*-xylene, 38.200 - 62.485 volume percent *meta*-xylene, and 12.880 - 36.656 volume percent *para*-xylene. Actual concentrations for both sets of xylene mixtures are listed in

Figure 5.1 NIR absorption spectra of the three xylene isomers.

a) Portable NIR spectrometer.

b) Commercial scanning spectrophotometer.

(—) *ortho*-xylene

(····) *meta*-xylene

(---) *para*-xylene

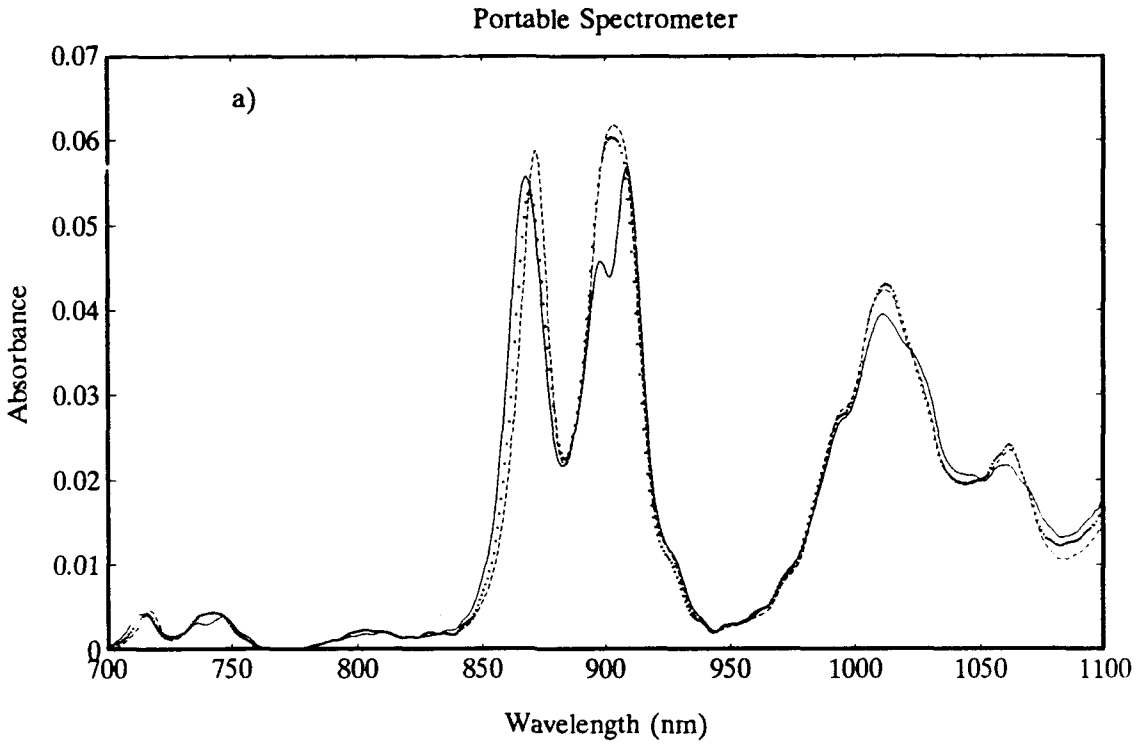
Portable Spectrometer
a)
Absorbance
0.07
0.06
0.05
0.04
0.03
0.02
0.01
0
700
750
800
850
900
950
1000
1050
1100
Wavelength (nm)

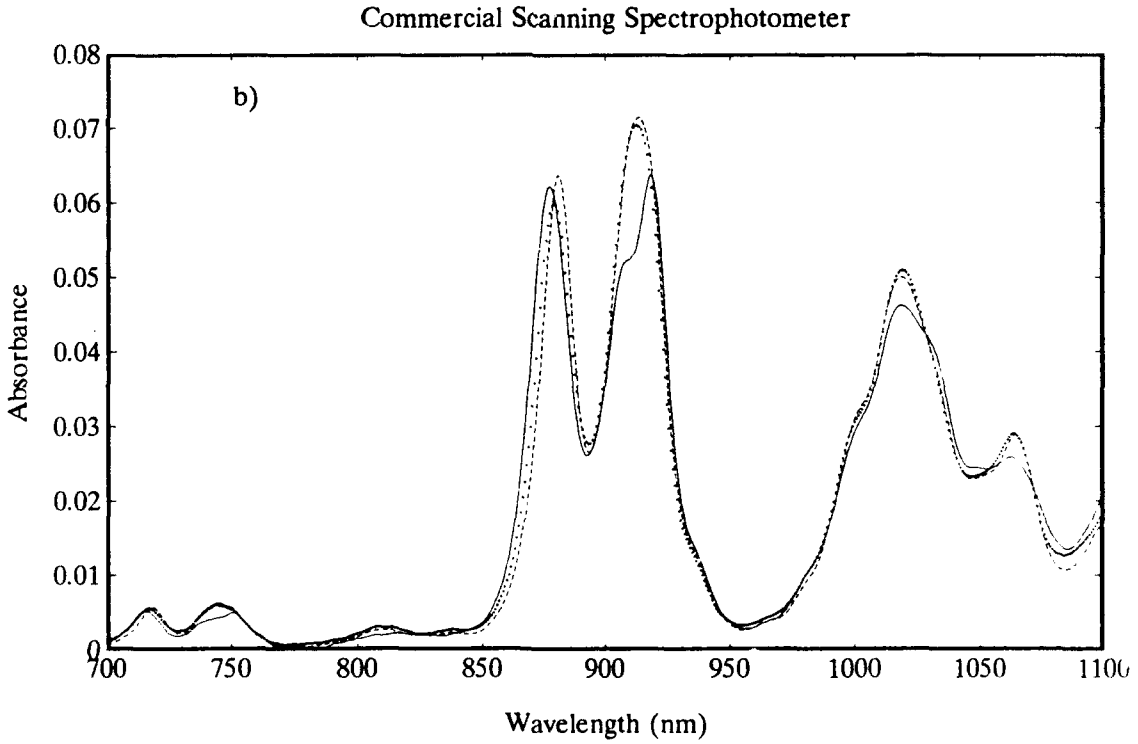
Commercial Scanning Spectrophotometer
b)
Absorbance
0.08
0.07
0.06
0.05
0.04
0.03
0.02
0.01
0
700
750
800
850
900
950
1000
1050
1100
Wavelength (nm)

Table 5.2, with the high and low concentration values for each of the three components highlighted. Samples were gravimetrically prepared using a Sartorius balance accurate to 0.1 mg, with subsequent volume percent calculations based on room temperature density values (*ortho*-xylene: 0.8802 g/ml, *meta*-xylene: 0.8642 g/ml, *para*-xylene: 0.8611 g/ml).

The xylene mixtures prepared in this study, were designed to span the concentration ranges of the three isomers found in major petroleum sources. Additionally, they encompass the concentration ranges given by the equilibrium considerations, valid for xylenes from reformate and pyrolysis gasoline as shown in Table 5.3 (24). The ratio 25:50:25 (*ortho*-xylene:*meta*-xylene:*para*-xylene) was used as the mean concentration ratio for the three isomers, with the samples spanning a range of ± 12 percent absolute for each of the three isomers. A range extending beyond those given in Table 5.3 was used to provide a wide enough concentration range for calibration that would include that encountered from all sources. The concentration values used for sample preparation were calculated using a random number generator, with the mean concentration ratio and concentration range listed above as constraints. The inner correlations for the three constituents were calculated, with the highest correlation being -0.5302.

5.3.2 Spectroscopy

Absorption spectra of the two xylene data sets were obtained on the portable spectrometer (Figure 5.2a), as well as on the scanning spectrophotometer

Table 5.2 Xylene mixture composition.

Sample #	Data Set A			Data Set B		
	o-Xylene	*m*-Xylene	*p*-Xylene	*o*-Xylene	*m*-Xylene	*p*-Xylene
1	12.899	62.223	24.879	12.818	62.485	24.697
2	16.073	60.300	23.628	15.980	60.013	24.007
3	14.941	59.288	25.771	15.207	58.763	26.030
4	19.073	57.904	23.024	19.524	57.809	22.667
5	20.993	58.421	20.587	20.882	58.165	20.953
6	17.402	57.198	25.401	18.877	60.133	20.989
7	23.912	56.877	19.211	23.523	55.219	21.258
8	21.964	56.552	21.484	21.784	54.197	24.018
9	20.143	54.987	24.870	19.422	52.820	27.758
10	16.967	54.364	28.669	17.226	53.971	28.803
11	26.167	53.969	19.864	26.394	53.797	19.809
12	28.592	53.731	17.677	29.079	53.718	17.203
13	24.116	53.046	22.839	23.406	54.594	22.001
14	21.232	52.139	26.629	20.811	51.481	27.709
15	28.361	52.308	19.331	28.822	51.952	19.226
16	24.468	51.294	24.238	24.992	50.406	24.602
17	32.383	51.364	16.253	32.557	50.904	16.539
18	34.786	51.201	14.013	35.296	50.608	14.096
19	19.440	50.080	30.480	19.908	49.593	30.499
20	27.875	50.205	21.921	28.364	50.074	21.563
21	36.941	50.179	12.880	37.032	49.859	13.109
22	21.634	48.967	29.399	21.558	49.025	29.417
23	24.340	49.110	26.550	23.884	49.421	26.695
24	31.859	49.284	18.857	32.582	48.660	18.758
25	34.351	49.363	16.286	34.463	49.053	16.484
26	30.406	48.146	21.448	30.717	47.764	21.519
27	23.260	47.073	29.667	23.139	47.098	29.763
28	26.734	47.198	26.068	27.158	46.789	26.053
29	29.193	47.432	23.375	29.695	46.783	23.523
30	20.192	49.283	30.525	21.660	46.142	32.198
31	32.894	46.281	20.825	33.293	46.170	20.537
32	25.092	45.051	29.857	25.197	45.031	29.773
33	28.995	44.219	26.786	28.519	44.119	27.362
34	31.276	43.966	24.758	31.371	43.994	24.635
35	23.525	42.987	33.488	23.676	42.836	33.488
36	27.344	42.873	29.783	27.267	42.556	30.177
37	29.220	42.007	28.773	28.811	41.824	29.365
38	25.629	40.963	33.408	25.564	40.654	33.782
39	25.073	40.098	34.829	25.174	39.809	35.017
40	25.773	38.622	35.605	25.145	38.200	36.656

Table 5.3 Concentration of the isomers in mixed xylenes.

Concentration of the Xylenes From Various Sources				
	Catalytic Reforming	Steam Cracking	Dispropor-tionation	Coke Oven
o-Xylene	20 - 24	13	24	15 - 20
m-Xylene	36 - 41	24	50	42 - 44
p-Xylene	16 - 20	11	26	15 - 17

Equilibrium Concentration of C_8 alkyl Benzenes				
Temp. ^{0}K	Ethyl Benzene	*o*-Xylene	*m*-Xylene	*p*-Xylene
500	3.1	20.4	52.8	23.2
700	8.3	22.4	47.8	21.5
900	13.2	23.1	43.9	19.8
1000	15.5	23.2	42.3	19.0
1100	17.6	23.3	40.8	18.3
1200	19.6	23.2	39.5	17.7
1300	21.5	23.1	38.3	17.1
1400	23.2	23.0	37.2	16.6
1500	24.6	22.9	36.4	16.1

Figure 5.2 Absorption spectra of the xylene mixtures.

a) Portable NIR spectrometer.

b) Commercial scanning spectrophotometer.

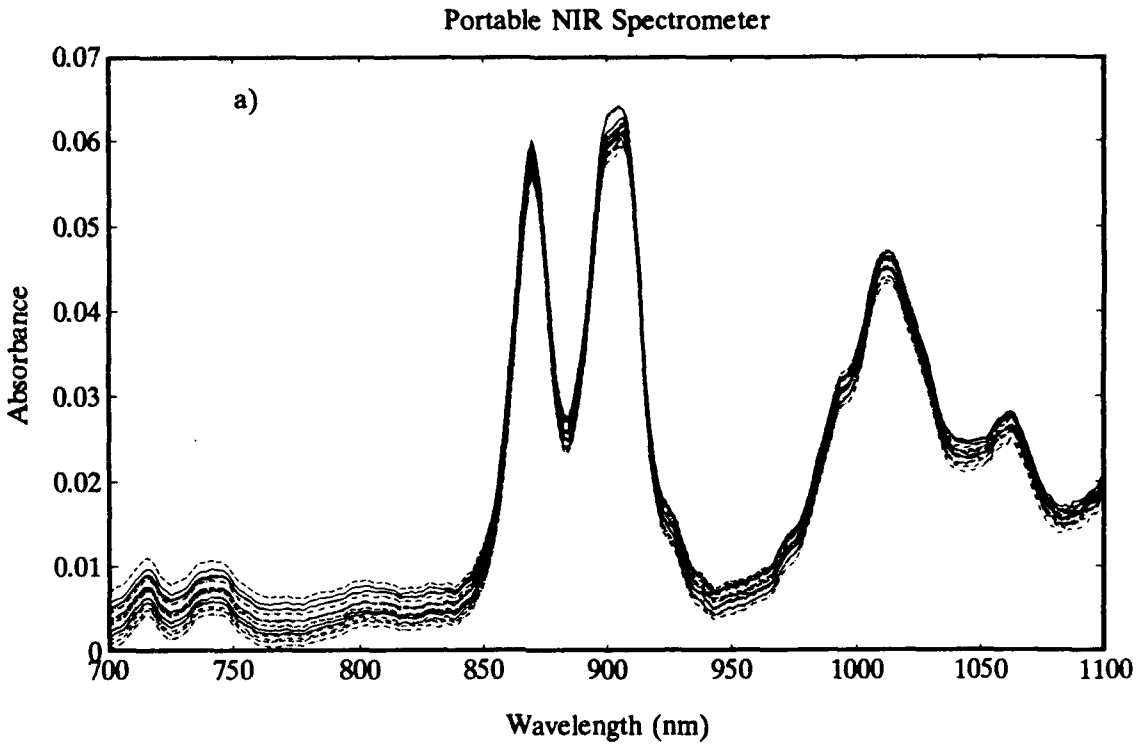
Portable NIR Spectrometer
a)
Absorbance
0.07
0.06
0.05
0.04
0.03
0.02
0.01
0
700
750
800
850
900
950
1000
1050
1100
Wavelength (nm)

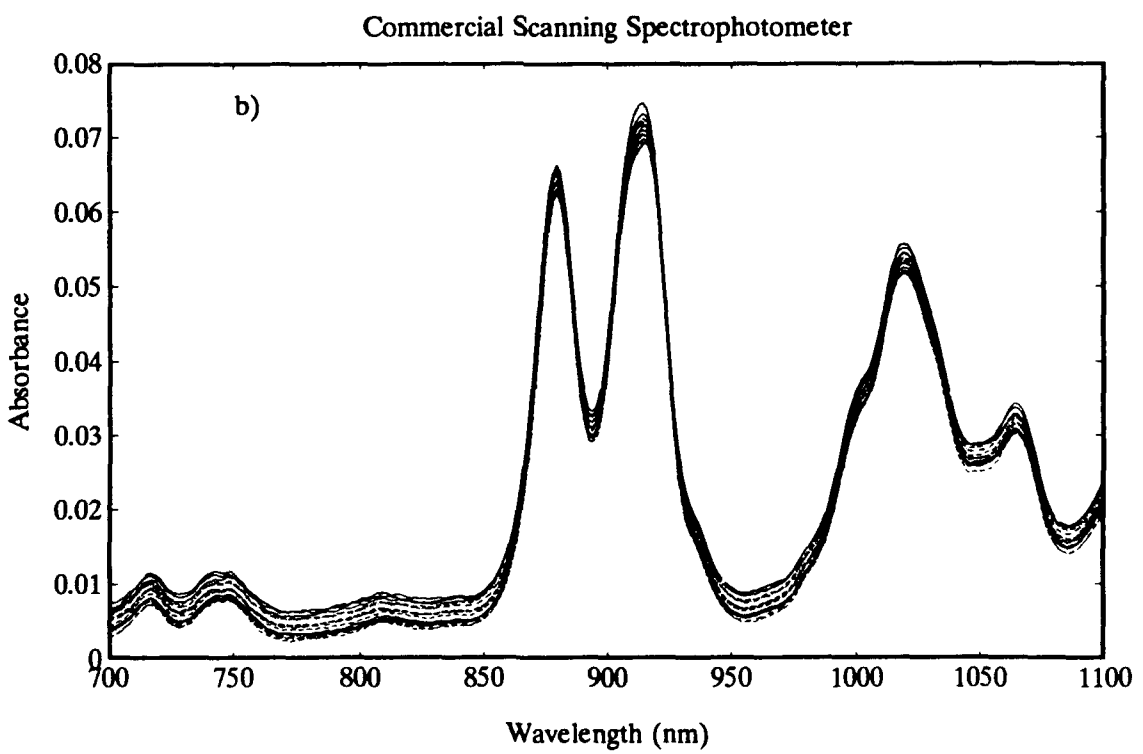
Commercial Scanning Spectrophotometer
b)
Absorbance
0.08
0.07
0.06
0.05
0.04
0.03
0.02
0.01
0
700
750
800
850
900
950
1000
1050
1100
Wavelength (nm)

(Figure 5.2b). The portable spectrometer was operated in transmission mode, using a 2.00-cm sample cuvette. Spectra were the result of averaging 64 scans, acquired at a data rate of 20 scans/sec (50 msec integration time), and consisted of 1012 data points covering the wavelength region 700 - 1100 nm (0.4 nm per data point). Detector temperature was stabilized at 10 ^{0}C for all spectral measurements. The scanning spectrophotometer was operated in transflectance mode, using a 1.00-cm sample cuvette (total pathlength 2.00-cm). Again, spectra were the result of averaging 64 scans, acquired at a data rate of 2 scans/sec, and consisted of 506 data points covering the wavelength region 700 - 1100 nm (0.80 nm per data point). The slightly higher absorbance values of the scanning spectrophotometer are due to differences in pathlength of the cuvette being used, and a less well-defined pathlength resulting from the transflectance sampling mode.

Spectral measurements were made immediately after sample preparation, to minimize any effects due to evaporation. Sample measurements made on both instruments were taken at room temperature and were referenced against carbon tetrachloride. The two data sets were prepared and analyzed 30 days apart, in order to evaluate instrumental drift as well as the long-term prediction capability of the multivariate statistical models.

5.3.3 Spectral Preprocessing

Both offset subtraction (see Chapter 1 - Section 1.3.1) and second-derivative transformation (see Chapter 1 - Section 1.3.2) were applied to the

spectral data sets prior to multivariate statistical analysis. In all cases, analysis of spectra following second-derivative transformation gave better results than using offset subtraction. It is the data-preprocessing technique used in these studies.

Various second-derivative smoothing-window and gap values were investigated to determine the optimum data-preprocessing to apply to the spectral data. Data Set A was used for this study. Following data-preprocessing, a full cross-validation analysis, using each of the multivariate statistical methods mentioned earlier, was performed and the standard error of prediction and multiple correlation coefficients were calculated. The data-preprocessing parameters resulting in the lowest SEP and highest multiple correlation coefficients were used for subsequent analysis. For the spectra acquired on the portable spectrometer, the optimum window/gap combinations for the PLS analysis were: a) *ortho*-xylene - 17/5, b) *meta*-xylene - 9/5, and c) *para*-xylene - 9/5, and for the MLR analysis: a) *ortho*-xylene - 17/21, b) *meta*-xylene - 25/5, and c) *para*-xylene - 5/9. For the analysis of the spectra acquired on the scanning spectrophotometer, the optimum window/gap combinations for the PLS analysis were: a) *ortho*-xylene - 17/13, b) *meta*-Xylene - 25/9, and c) *para*-xylene - 25/9 and for the MLR analysis: a) *ortho*-xylene - 5/13, b) *meta*-xylene - 21/9, and c) *para*-xylene - 9/13. For the most part, optimum performance was obtained with a small second-derivative gap, while being much less sensitive to the degree of smoothing (window) used.

A second-derivative transformation of the spectra given in Figure 5.2 was performed to remove the baseline offset present in the spectral data. Figure 5.3

Figure 5.3 Second-derivative transformation of the xylene mixtures.

a) Portable NIR spectrometer.

b) Commercial scanning spectrophotometer.

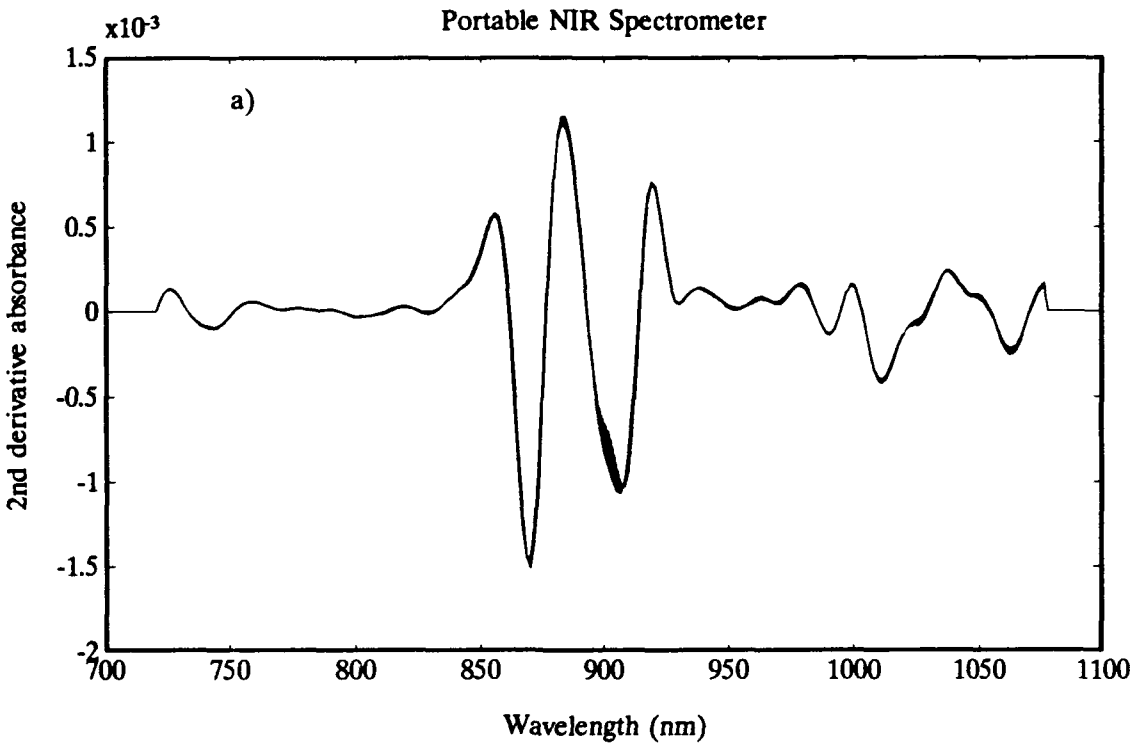
Portable NIR Spectrometer
x10-3
a)
2nd derivative absorbance
1.5
1
0.5
0
-0.5
-1
-1.5
-2
700
750
800
850
900
950
1000
1050
1100
Wavelength (nm)

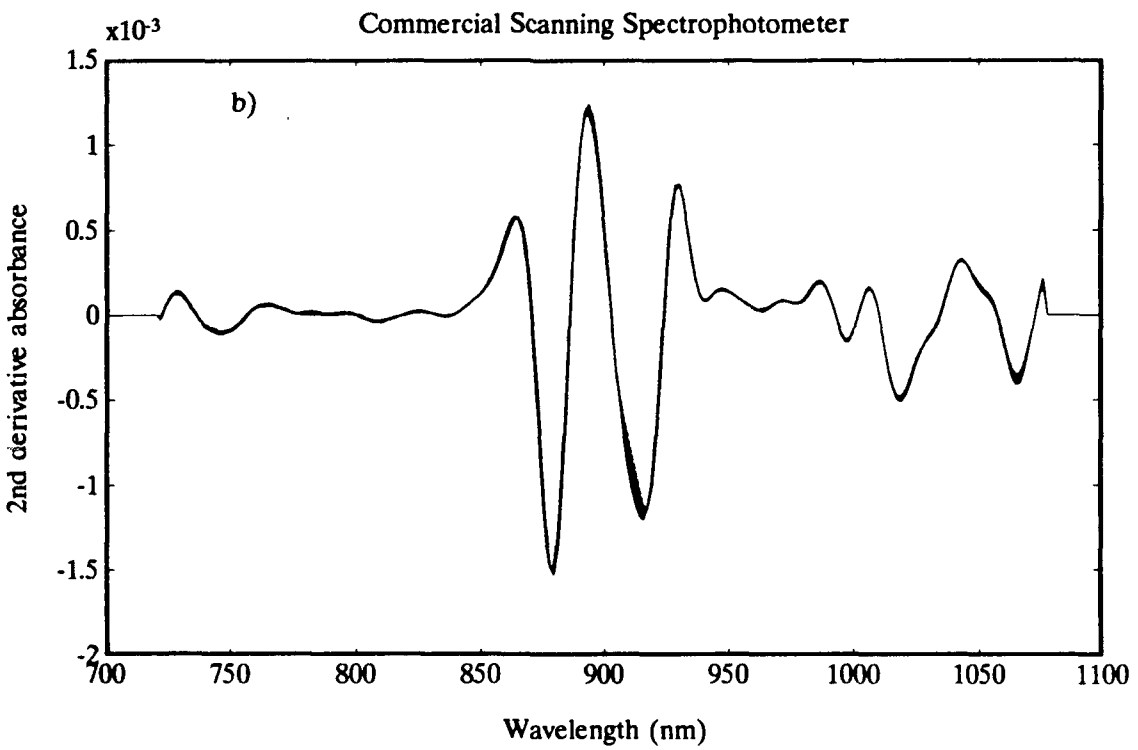
Commercial Scanning Spectrophotometer
x10-3
b)
2nd derivative absorbance
1.5
1
0.5
0
-0.5
-1
-1.5
-2
700
750
800
850
900
950
1000
1050
1100
Wavelength (nm)

presents the second-derivative spectra for: a) the portable spectrometer and b) the scanning spectrophotometer, calculated using a window of 9 and a gap of 5. To enhance the differences between the spectra, the second-derivative spectra were mean-centered. Here, the mean spectra is subtracted from each of the spectra, leaving only the difference between the individual spectra and the mean spectra. The mean-centered, second-derivative spectra are given in Figure 5.4 for: a) the portable spectrometer and b) the scanning spectrophotometer. Though small in intensity, differences in both the third-overtone aromatic C-H region (860 -890 nm) and the third-overtone methyl C-H region (900 - 930 nm) are apparent. The higher signal-to-noise ratio of the portable spectrometer is nicely shown in the wavelength region 725 - 850 nm. Also apparent from these plots, are an increased number of zero-crossings, between 950 and 1075 nm, for the portable spectrometer, further indicating its improved signal-to-noise ratio.

5.4 Results and Discussion

5.4.1 Multiple Linear Regression Analysis (MLR)

Stage-wise multiple linear regression (see Chapter 1 - Section 1.4.1) was applied to the spectral data sets obtained on both the portable spectrometer and the scanning spectrophotometer. Three-wavelength regression equations, of the form given in equation (1.17), were determined for the volume percents of the three xylene isomers. Wavelength selection was by the step-forward technique

Figure 5.4 Mean-centered, second-derivative spectra of the xylene mixtures.

a) Portable NIR spectrometer.

b) Commercial scanning spectrophotometer.

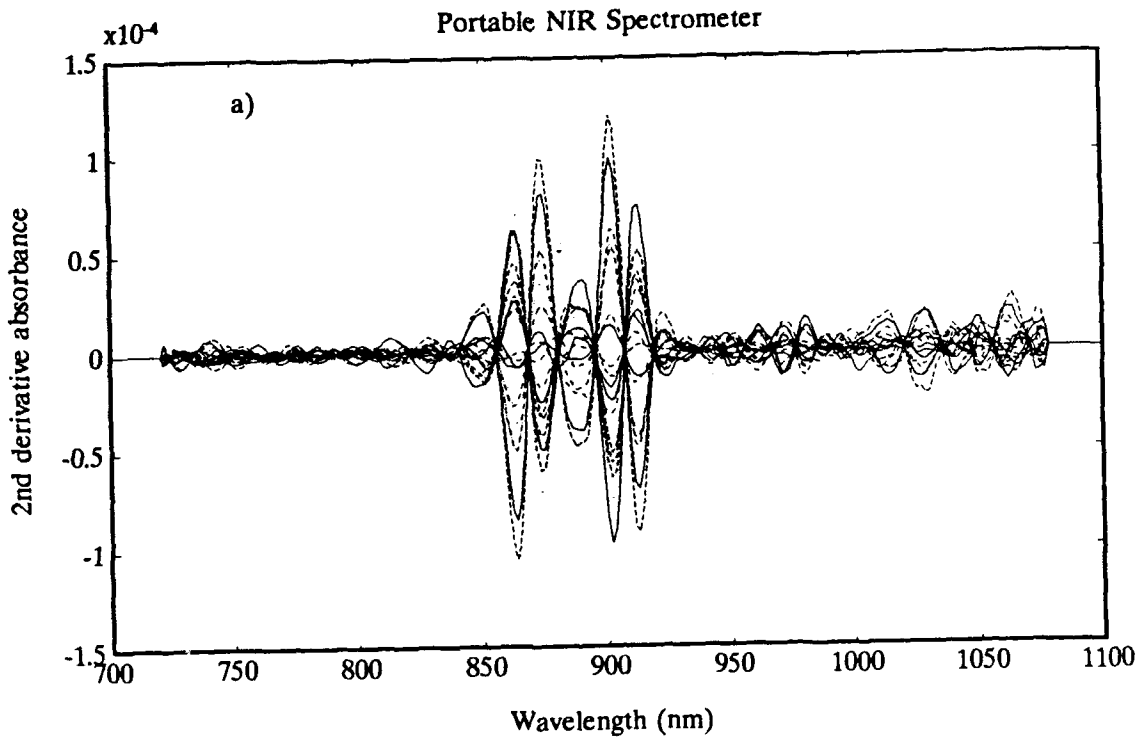
Portable NIR Spectrometer
x10-4
a)
1.5
1
0.5
0
-0.5
-1
-1.5
2nd derivative absorbance
700
750
800
850
900
950
1000
1050
1100
Wavelength (nm)

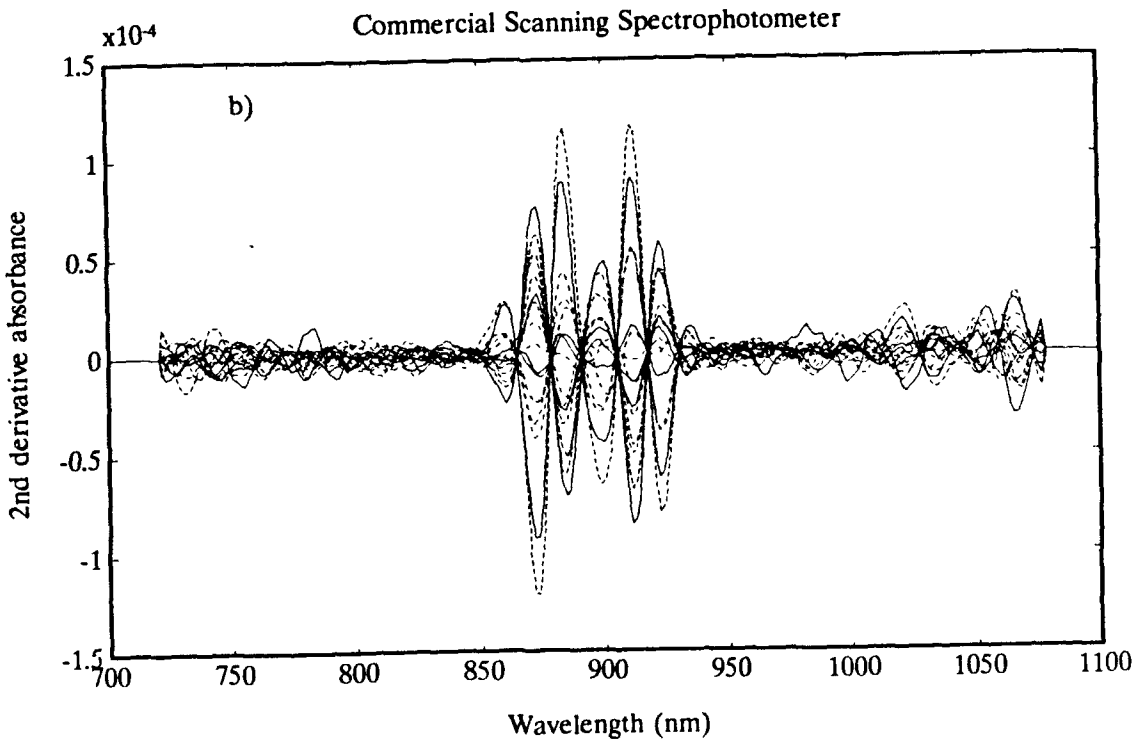
Commercial Scanning Spectrophotometer
x10-4
b)
1.5
1
0.5
0
-0.5
-1
-1.5
2nd derivative absorbance
700
750
800
850
900
950
1000
1050
1100
Wavelength (nm)

described in Chapter 1. Table 4.3, Table 5.4 gives the regression equations for each of the isomers. For *ortho*-xylene each of the wavelengths chosen corresponds to the methyl peak. This is to be expected, as the major difference between *ortho*-xylene and the other two isomers, is in the spectral split of the methyl peak, as described earlier. In contrast, the first wavelength chosen for both *meta*-xylene and *para*-xylene corresponds to the aromatic peak. Again, this is not surprising, as the only significant difference between *meta*-xylene and *para*-xylene is a 2 nm shift in the position of the aromatic C-H absorption. Likewise, the position of the aromatic C-H absorption for *ortho*-xylene is blue-shifted an additional 2 nm, providing further distinction between the three xylene isomers. Subsequent wavelengths make use of the subtle differences between the isomers in the methyl C-H absorption and the shoulders of the aromatic C-H peak. The third wavelength chosen for *meta*-xylene, using the portable spectrometer (765 nm), is near the baseline and is presumably correcting for differences in refractive index between samples (25). The second wavelength chosen for *para*-xylene, using the scanning spectrometer (1022 nm), corresponds to the methyl C-H combinational band (26,27). Results of the regression analysis are presented in Table 2.3, Table 5.5 for both calibration and prediction. For this analysis, not only was a cross-validation analysis performed, but a double-blind prediction analysis using xylene set A to predict xylene set B was accomplished. As seen from this data, the portable spectrometer performed two to four times better than the scanning spectrophotometer, depending on the constituent being evaluated.

Table 5.4 MLR regression equations for the three xylene isomers.

	Portable NIR Spectrometer			
	K_0	K_1 (λ_1)	K_2 (λ_2)	K_3 (λ_3)
o-Xylene	25.162	455647.58 (902 nm)	-240379.99 (918 nm)	303697.40 (921 nm)
m-Xylene	-163.22	-394412.92 (894 nm)	425019.99 (883 nm)	404170.82 (765 nm)
p-Xylene	61.82	1002365.05 (891 nm)	-2583706.83 (912 nm)	2056450.88 (868 nm)
	Commercial Scanning Spectrophotometer			
	K_0	K_1 (λ_1)	K_2 (λ_2)	K_3 (λ_3)
o-Xylene	88.00	467365.37 (910 nm)	-206155.82 (902 nm)	24.3777.60 (931 nm)
m-Xylene	398.13	-1446493.71 (890 nm)	-1242471.54 (934 nm)	-499092.38 (878 nm)
p-Xylene	-209.32	-488568.41 (879 nm)	1019170.34 (1022 nm)	-583216.54 (882 nm)

Table 5.5 MLR analysis results for the xylenes.

	Portable NIR Spectrometer					
	Calibration		Cross-Validation		Prediction (A predict B)	
	SEE	R^2	SEP	R^2	SEP	R^2
o-Xylene	0.170	0.9996	0.190	0.9996	0.284	0.9986
m-Xylene	0.377	0.9979	0.433	0.9977	0.593	0.9960
p-Xylene	0.369	0.9978	0.435	0.9976	0.621	0.9952
	Commercial Scanning Spectrophotometer					
	Calibration		Cross-Validation		Prediction (A predict B)	
	SEE	R^2	SEP	R^2	SEP	R^2
o-Xylene	0.280	0.9988	0.388	0.9988	0.560	0.9967
m-Xylene	1.313	0.9742	1.612	0.9764	2.216	0.9283
p-Xylene	0.938	0.9858	1.163	0.9846	1.674	0.9697

Correlation plots of actual versus predicted concentration for *ortho*-xylene (Figure 5.5), *meta*-xylene (Figure 5.6), and *para*-xylene (Figure 5.7) are presented to graphically compare the performance of the two instruments. The superior performance of the portable spectrometer is obvious from these figures and is attributed to its higher signal-to-noise ratio and spectral resolution, which results in improved differentiation of the highly overlapping absorption peaks of the three isomers.

5.4.2 Partial Least Squares Analysis

To further evaluate the ability of NIR to predict the composition of mixed xylenes, the spectral data sets were evaluated using the multivariate statistical analysis technique of partial least squares (see Chapter 1 - Section 1.4.2). The proper number of latent variables to retain was determined by examining the predictive error of the PLS model as a function of the number of independent variables retained. Figure 4.10, Figure 5.8 presents the PRESS results (28) from the cross-validation analysis of the SW-NIR spectral data for volume percent *ortho*-xylene. As indicated here, the minimum in the standard error of prediction occurs at three latent variables, suggesting that the proper number of latent variables to retain is three. The improvement in SEP between two and three latent variables is relatively small, indicating that a majority of the variance is described by the first two latent variables. To aid in the determination of the proper number of latent variables, the PLS loadings of each of the latent variables were examined. Plots

Figure 5.5 Actual versus predicted volume percent *ortho*-xylene.

a) Portable spectrometer.

b) Scanning spectrophotometer.

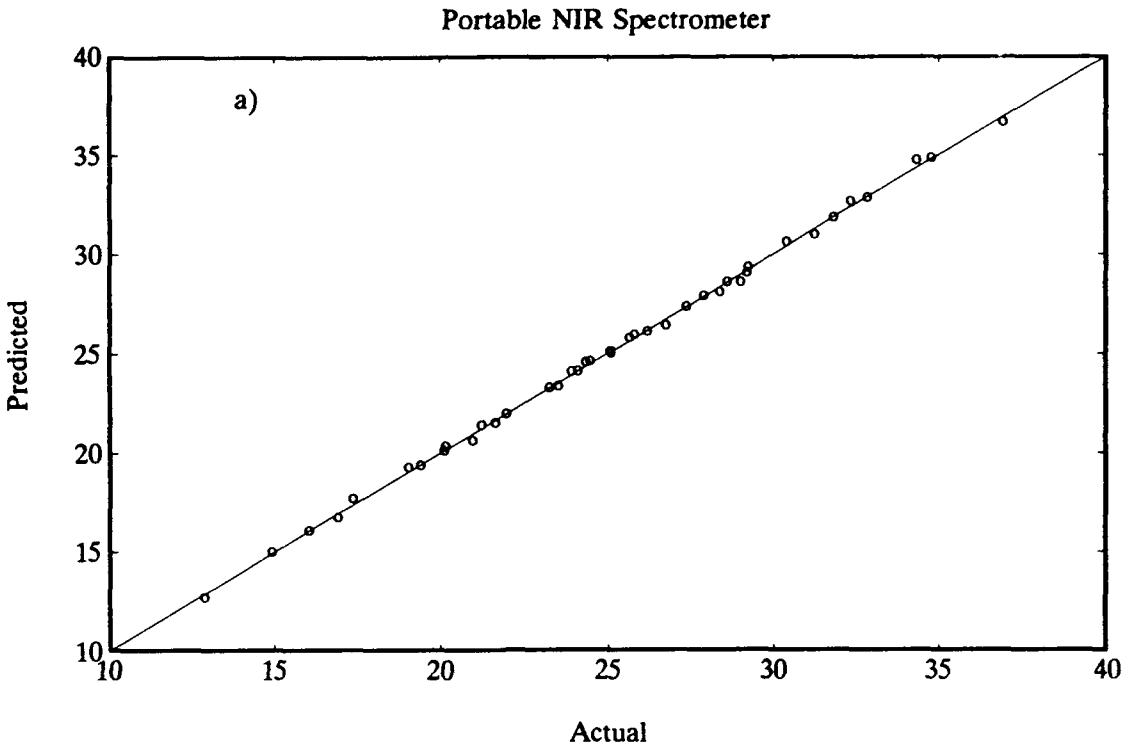
Portable NIR Spectrometer
a)
Predicted
Actual
10
15
20
25
30
35
40

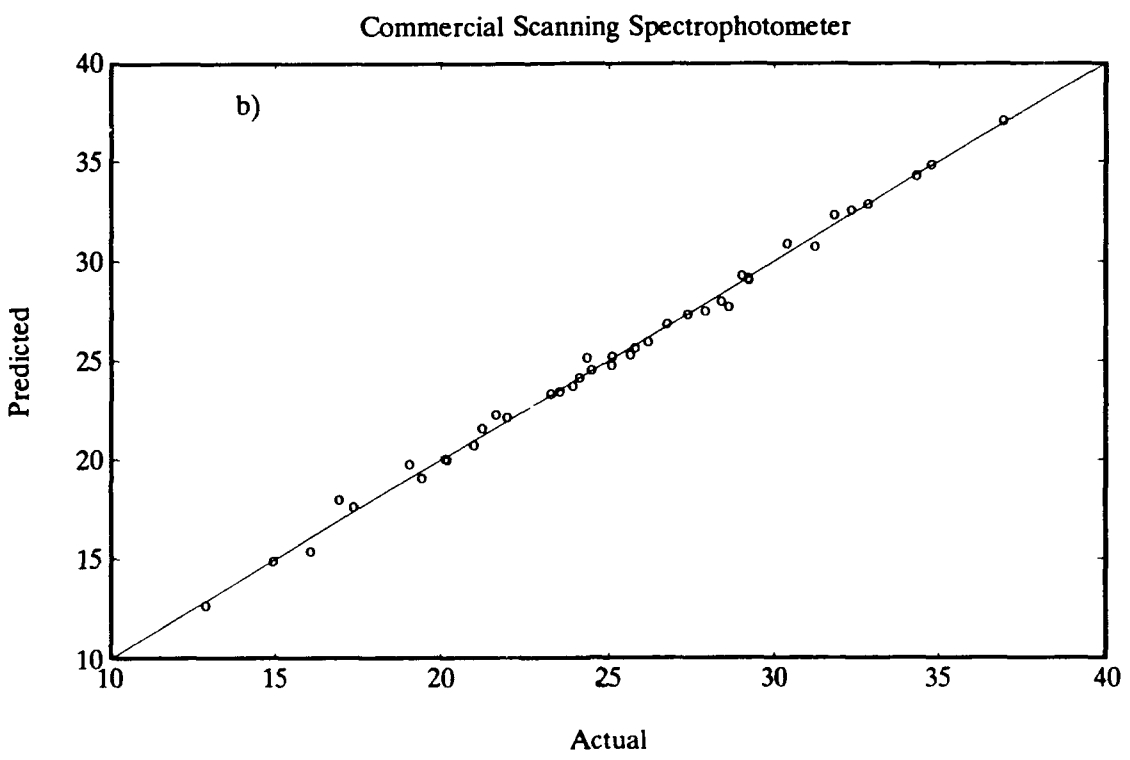
Commercial Scanning Spectrophotometer
b)
Predicted
Actual
10
15
20
25
30
35
40

Figure 5.6 Actual versus predicted volume percent *meta*-xylene.

a) Portable spectrometer.

b) Scanning spectrophotometer.

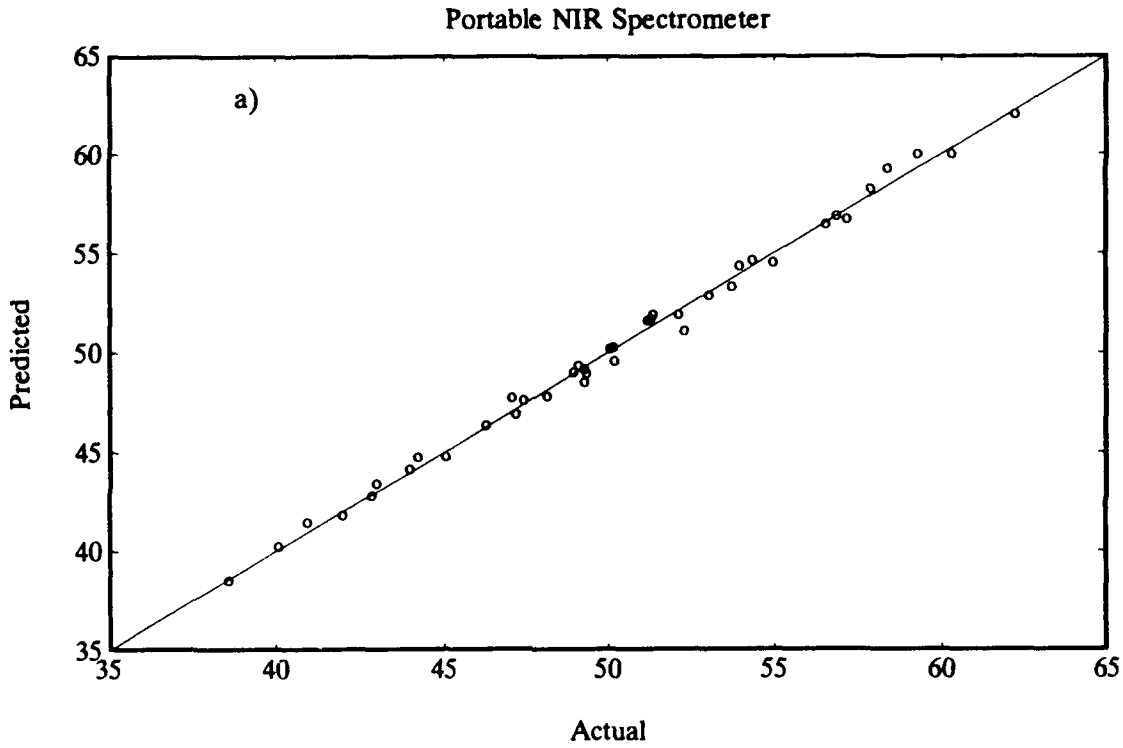
Portable NIR Spectrometer
a)
Predicted
Actual
35
40
45
50
55
60
65

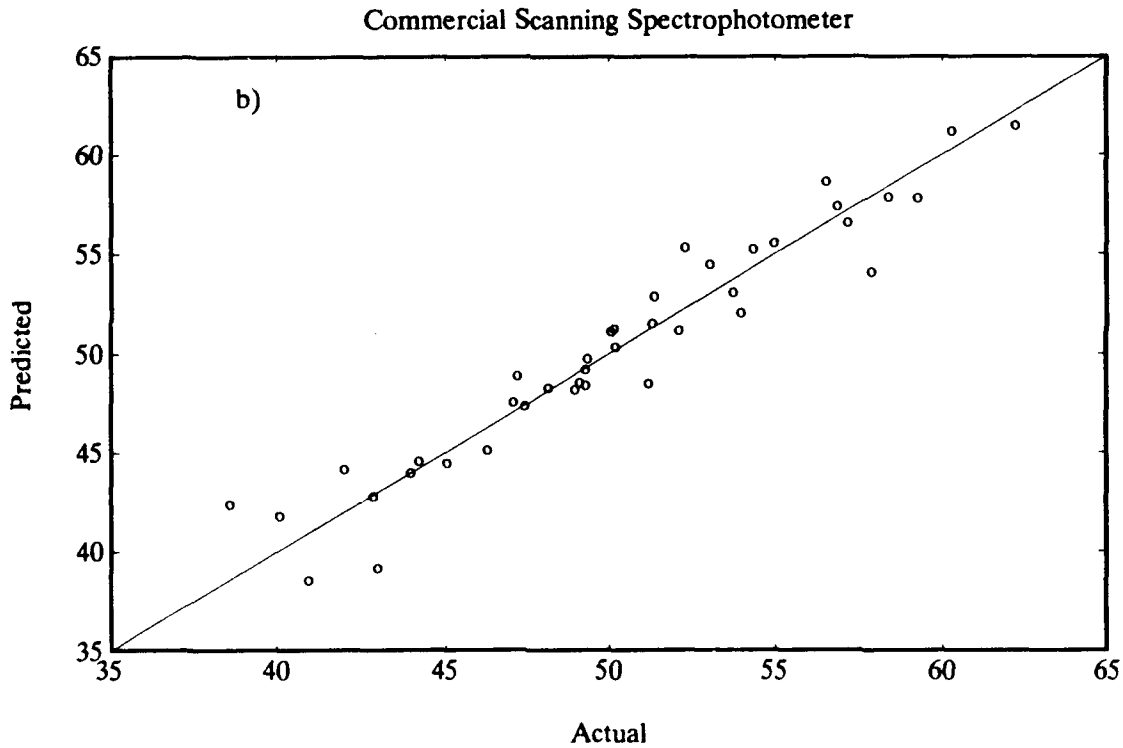
Commercial Scanning Spectrophotometer
b)
Predicted
Actual
35
40
45
50
55
60
65

Figure 5.7 Actual versus predicted volume percent *para*-xylene.

a) Portable spectrometer.

b) Scanning spectrophotometer.

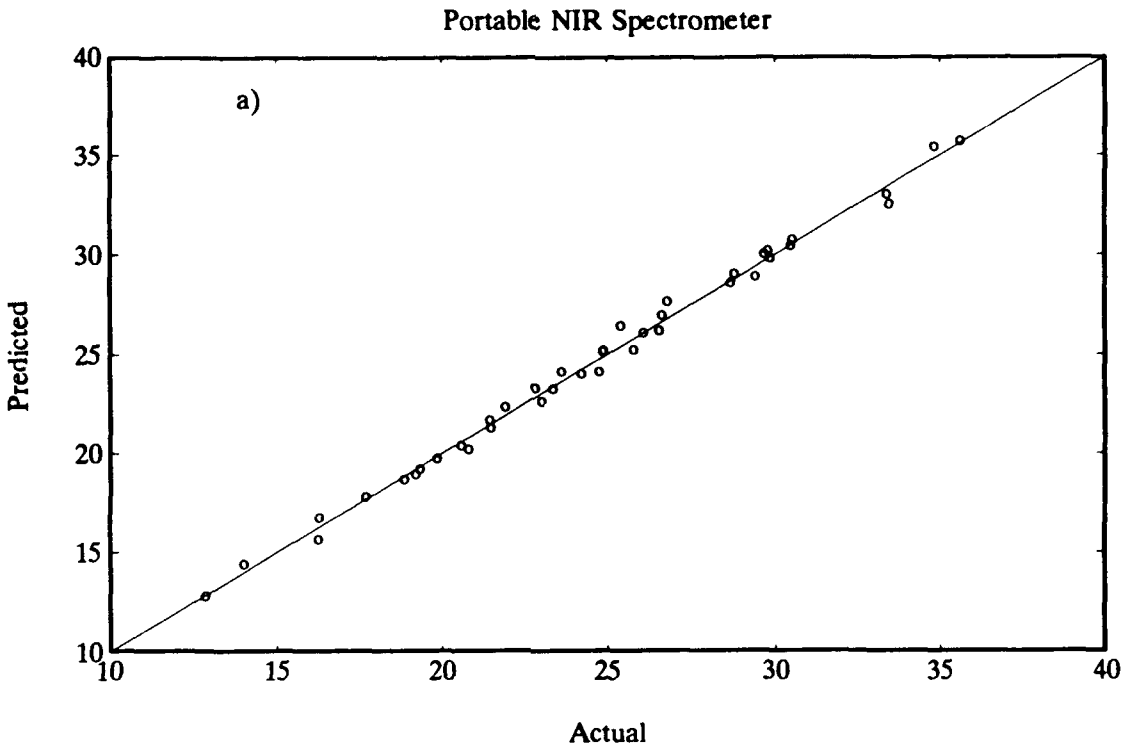
Portable NIR Spectrometer
a)
Predicted
Actual
10
15
20
25
30
35
40

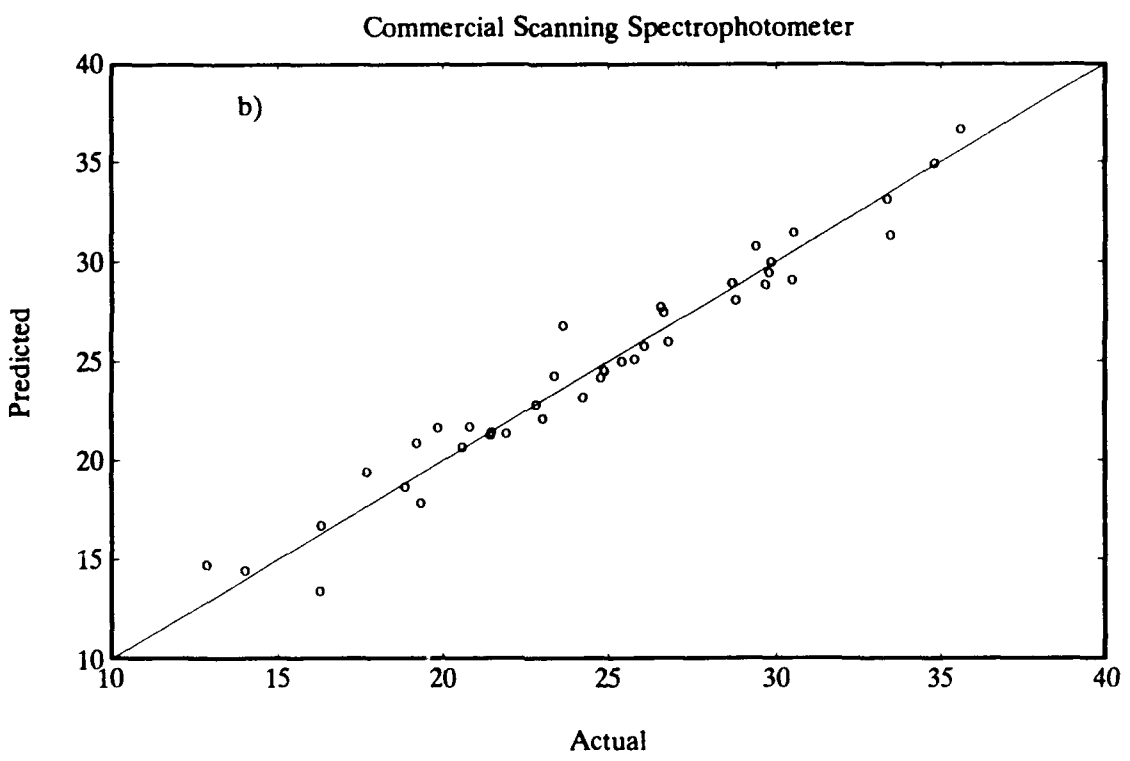
Commercial Scanning Spectrophotometer
b)
Predicted
Actual
10
15
20
25
30
35
40

Figure 5.8 PRESS plot - volume percent *ortho*-xylene.

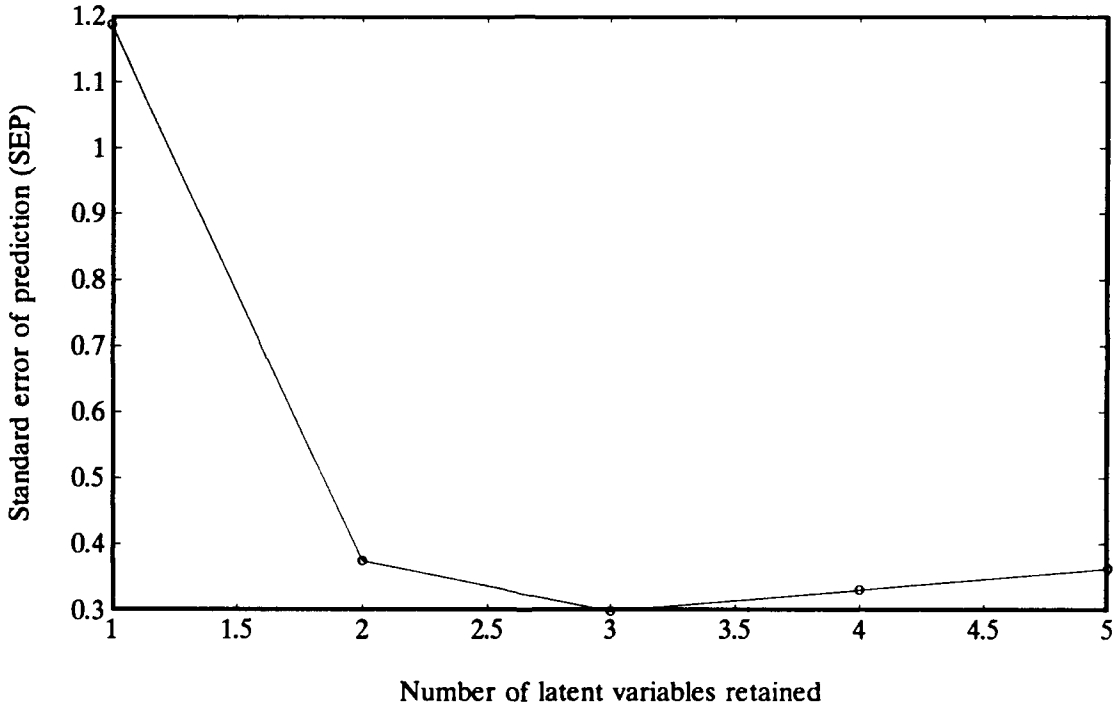
1.2
1.1
1
0.9
0.8
0.7
0.6
0.5
0.4
0.3
Standard error of prediction (SEP)
1
1.5
2
2.5
3
3.5
4
4.5
5
Number of latent variables retained

of the PLS loadings after one. two, and three latent variables are presented in Figure 5.9, Figure 5.10, and Figure 5.11 respectively. As can be seen from Figure 5.11, latent variable # 3 consists largely of noise but does have some structure. Also apparent from these figures, is the importance of the methyl C-H split in *ortho*-xylene as evidenced by the PLS loadings for latent variable # 1. Latent variable # 2, continues to correlate to the methyl and aromatic regions of the spectrum between 850 nm and 930 nm, while minimizing the importance of the rest of the spectral region. Also apparent in each of the PLS loadings is the high signal-to-noise ratio of the portable spectrometer. The results of the PLS analysis are presented in Table 5.6 for both the portable spectrometer and the scanning spectrophotometer. R^2 values were determined using three latent variables. Again, the portable spectrometer performed two to three times better than the scanning spectrophotometer in the prediction of each of the xylene isomers.

A comparison of the PLS results after two latent variables and the MLR results after three wavelengths show the two techniques perform comparably. For the portable spectrometer, where the signal-to-noise ratio is extremely good, MLR actually performs slightly better than PLS. Just the opposite is seen for the scanning spectrophotometer, where the signal-to-noise is much worse and PLS out performs MLR. When evaluating systems exhibiting low noise, linear response and no analyte-analyte interactions, stage-wise MLR appears to perform comparably with PLS.

Figure 5.9 *Ortho*-xylene -- PLS loadings for latent variable #1.

a) Portable spectrometer.

b) Scanning spectrophotometer.

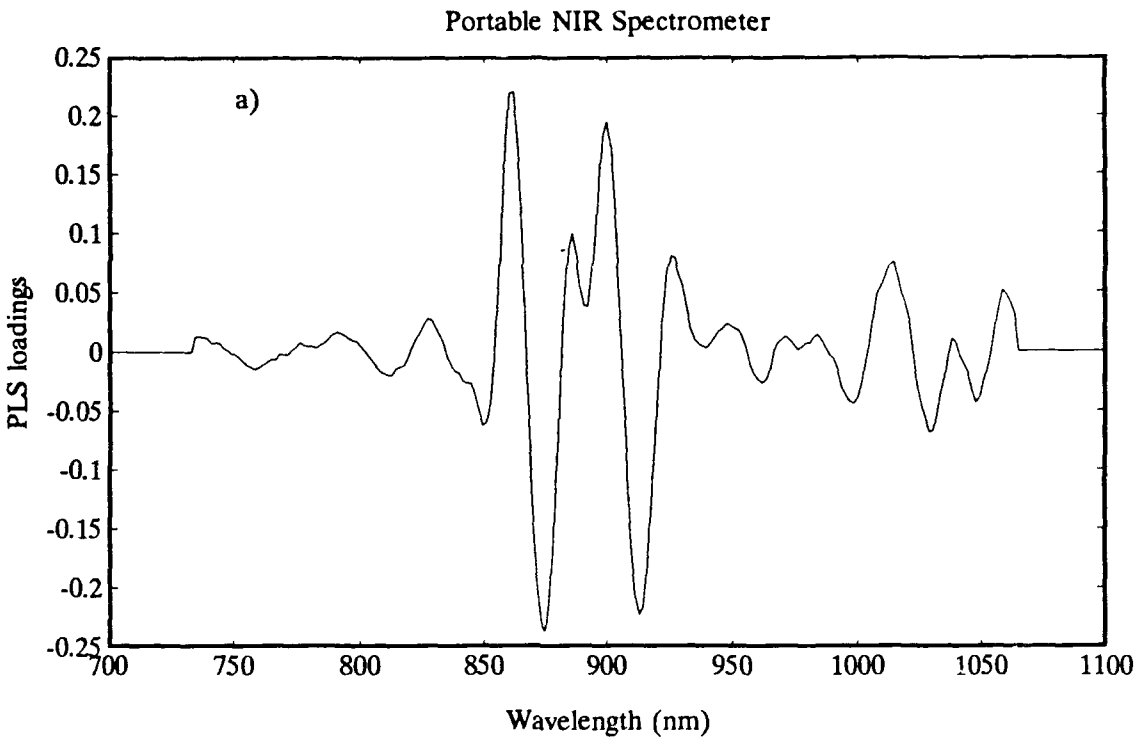
Portable NIR Spectrometer
a)
PLS loadings
0.25
0.2
0.15
0.1
0.05
0
-0.05
-0.1
-0.15
-0.2
-0.25
700
750
800
850
900
950
1000
1050
1100
Wavelength (nm)

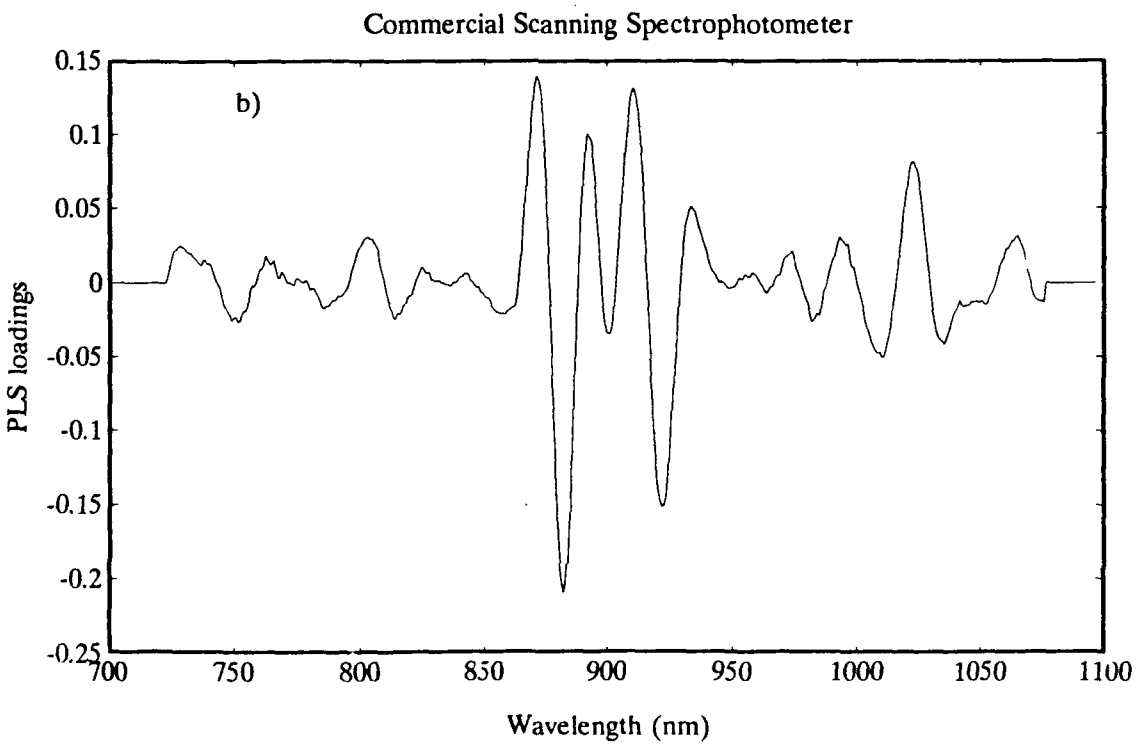
Commercial Scanning Spectrophotometer
b)
PLS loadings
0.15
0.1
0.05
0
-0.05
-0.1
-0.15
-0.2
-0.25
700
750
800
850
900
950
1000
1050
1100
Wavelength (nm)

Figure 5.10 *Ortho*-xylene -- PLS loadings for latent variable #2.

a) Portable spectrometer.

b) Scanning spectrophotometer.

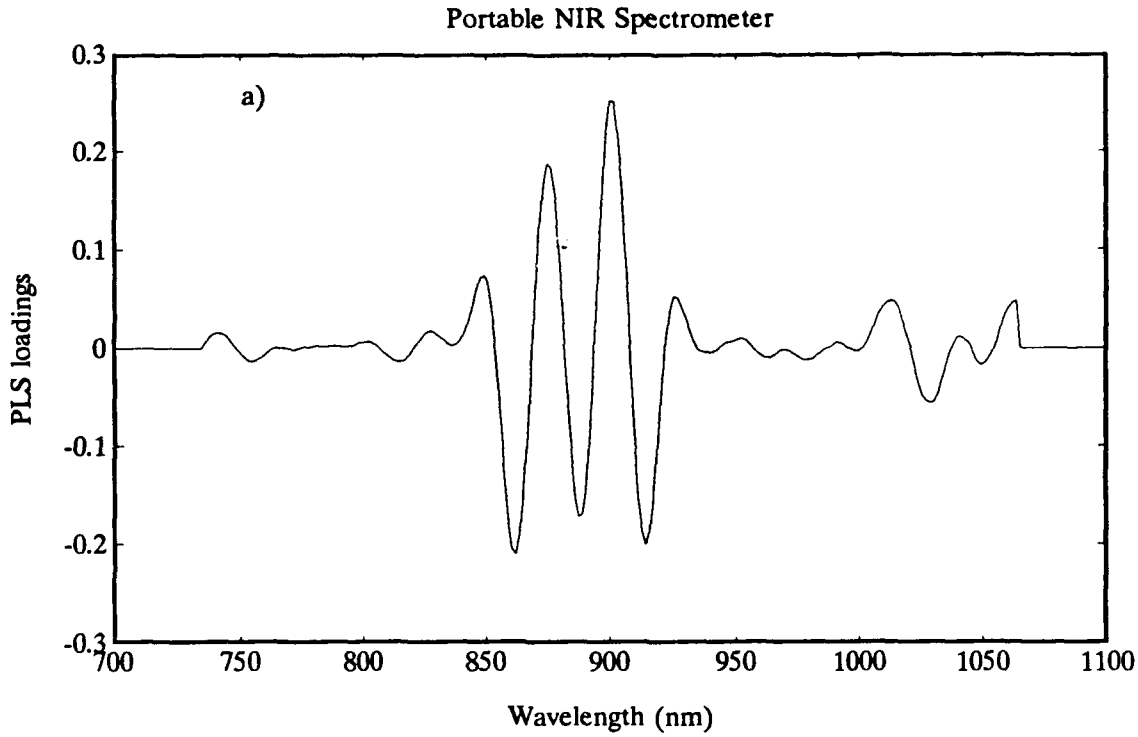
Portable NIR Spectrometer
a)
PLS loadings
0.3
0.2
0.1
0
-0.1
-0.2
-0.3
700
750
800
850
900
950
1000
1050
1100
Wavelength (nm)

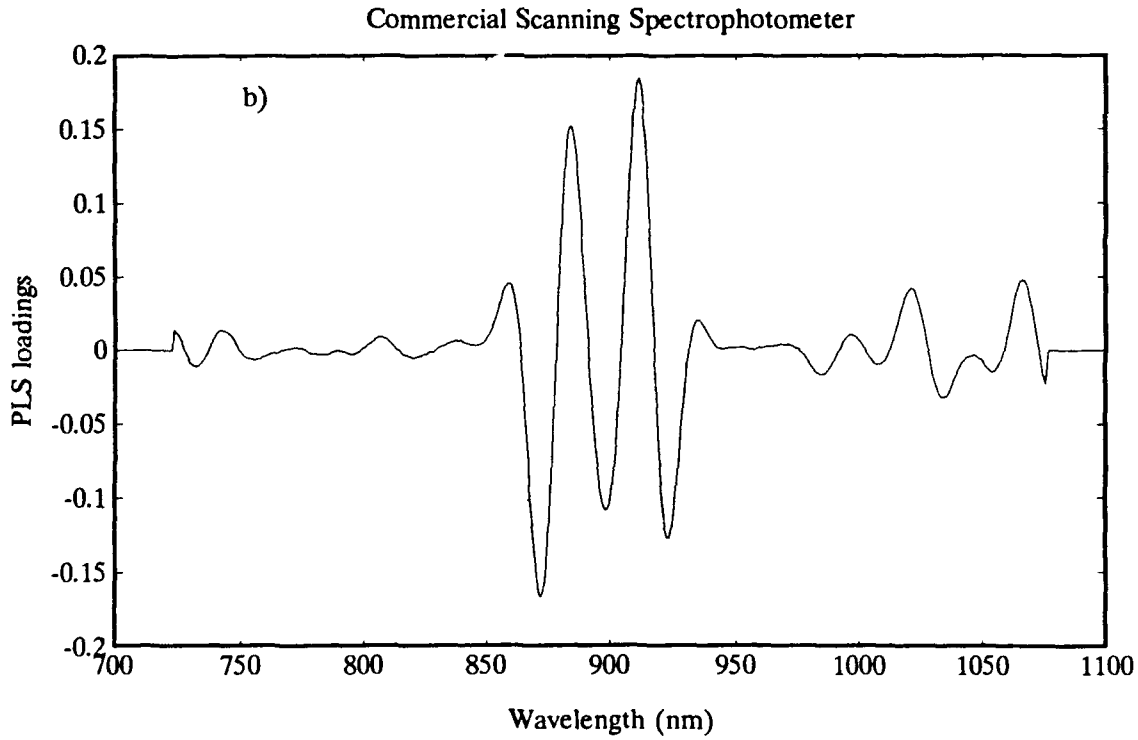
Commercial Scanning Spectrophotometer
b)
PLS loadings
0.2
0.15
0.1
0.05
0
-0.05
-0.1
-0.15
-0.2
700
750
800
850
900
950
1000
1050
1100
Wavelength (nm)

Figure 5.11 *Ortho*-xylene -- PLS loadings for latent variable #3.

a) Portable spectrometer.

b) Scanning spectrophotometer.

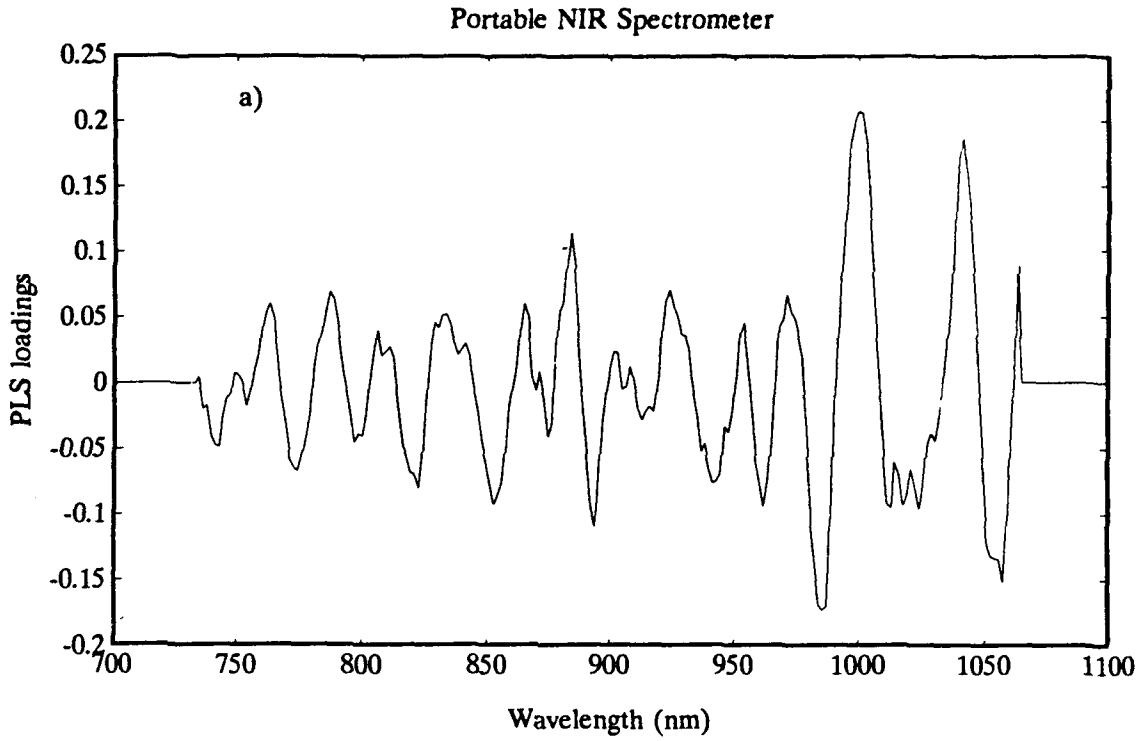
Portable NIR Spectrometer
a)
PLS loadings
0.25
0.2
0.15
0.1
0.05
0
-0.05
-0.1
-0.15
-0.2
700
750
800
850
900
950
1000
1050
1100
Wavelength (nm)

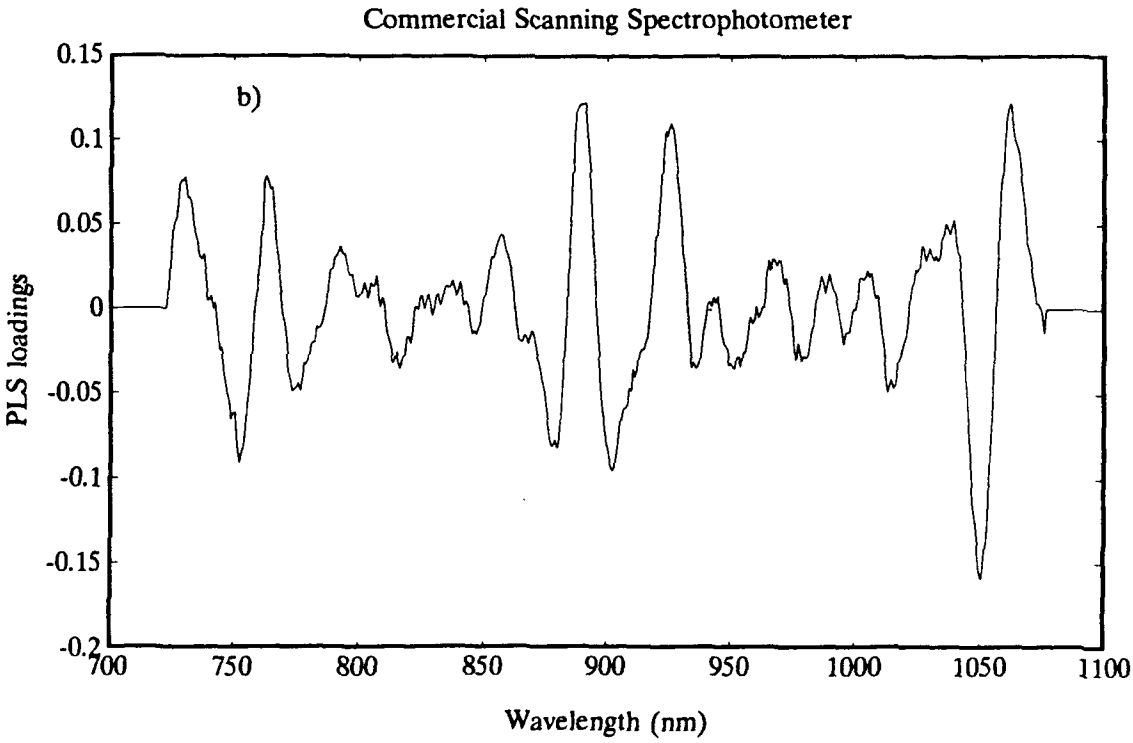
Commercial Scanning Spectrophotometer
b)
PLS loadings
0.15
0.1
0.05
0
-0.05
-0.1
-0.15
-0.2
700
750
800
850
900
950
1000
1050
1100
Wavelength (nm)

Table 5.6 PLS analysis results for the three xylene isomers.

	Portable NIR Spectrometer				
	RMSECV				R^2
	Number of Latent Variables Retained				
	1	2	3	4	
o-Xylene	1.113	0.198	0.162	0.154	0.9995
m-Xylene	4.715	0.580	0.441	0.416	0.9965
p-Xylene	3.815	0.512	0.373	0.339	0.9972
	Commercial Scanning Spectrophotometer				
	RMSECV				R^2
	Number of Latent Variables Retained				
	1	2	3	4	
o-Xylene	1.187	0.374	0.299	0.331	0.9968
m-Xylene	5.228	1.646	0.958	0.841	0.9760
p-Xylene	4.213	1.522	0.923	0.806	0.9758

5.4.3 Classical Least Squares (CLS)

To further evaluate the performance of NIR spectroscopy in the analysis of the xylenes, the direct calibration technique of classical least squares was also applied to the xylene mixtures. As with the indirect calibration methods of MLR and PLS, in CLS the response matrix (***R***) and the constituent matrix (***C***) for a calibration set of samples are known. In CLS however, the transformation matrix (***B***) relating instrumental response to constituent value, is determined by least squares methods. Given the direct calibration model:

$$\boldsymbol{R} = \boldsymbol{CB} + \boldsymbol{E}_R \tag{5.1}$$

the ***B*** matrix is determined in a least squares sense as follows:

$$\boldsymbol{B} = \boldsymbol{RC}^+ \tag{5.2}$$

where $\boldsymbol{C}^+$ is the Moore-Penrose pseudoinverse (29) of **C**. The ***B*** matrix represents the recovered pure-component spectra and can be used to provide qualitative information concerning component interaction between the sample constituents (30). Once the determination of the transformation matrix has been made, prediction of the constituent value for unknown samples is by:

$$\boldsymbol{c}_{unk} = \boldsymbol{r}_{unk}\boldsymbol{B}^+ \tag{5.3}$$

One limitation of direct calibration techniques such as CLS, is that all the components of the system must be known (31). However, because we are working with a closed system and all the components are known, this limitation does not effect the current analysis.

The results of the CLS analysis are presented in Table 5.7, for the cross-validation prediction of Data Set A. These results are nearly identical to the PLS analysis of the mean-centered data using two latent variables, further suggesting that only two latent variables need be retained in the PLS analysis. The recovered pure-component spectra for *ortho*-, *meta*-, and *para*-xylene are presented in Figure 5.12, Figure 5.13, and Figure 5.14 respectively. Superimposed on each of the recovered spectra is a plot of the corresponding pure component spectra, measured at the same time as those for Data Set A. Below the plots of the recovered spectra, are plots of the residuals between actual and recovered spectra. As with the MLR and PLS analyses, it is apparent from both the prediction results (Table 5.7) and the residual plots that the portable spectrometer performed significantly better than the scanning spectrophotometer. Examination of the residuals for the portable spectrometer, show minimal analyte-analyte interaction between the three xylene isomers. However, the residuals from the analysis on the scanning spectrophotometer, show significant structure in the third-overtone region (850 - 950 nm). This indicates non-linear behavior in the scanning spectrophotometer and explains its poorer performance in the multivariate statistical analyses.

Table 5.7 CLS analysis results for the xylenes.

	Portable NIR Spectrometer	
	Cross-Validation	
	SEP	R^2
o-Xylene	0.180	0.9995
m-Xylene	0.580	0.9952
p-Xylene	0.510	0.9959
	Commercial Scanning Spectrophotometer	
	Cross-Validation	
	SEP	R^2
o-Xylene	0.360	0.9980
m-Xylene	1.750	0.9552
p-Xylene	1.620	0.9586

Figure 5.12 Reconstructed spectra of *ortho*-xylene from CLS analysis.

Portable Spectrometer

a) Reconstructed spectra (+ + +) of *ortho*-xylene overlaid with the pure-component spectra (—).

b) Residuals between reconstructed spectra (+ + +) and pure component spectra.

Scanning Spectrophotometer

c) Reconstructed spectra (+ + +) of *ortho*-xylene overlaid with the pure-component spectra (—).

d) Residuals between reconstructed spectra and pure component spectra.

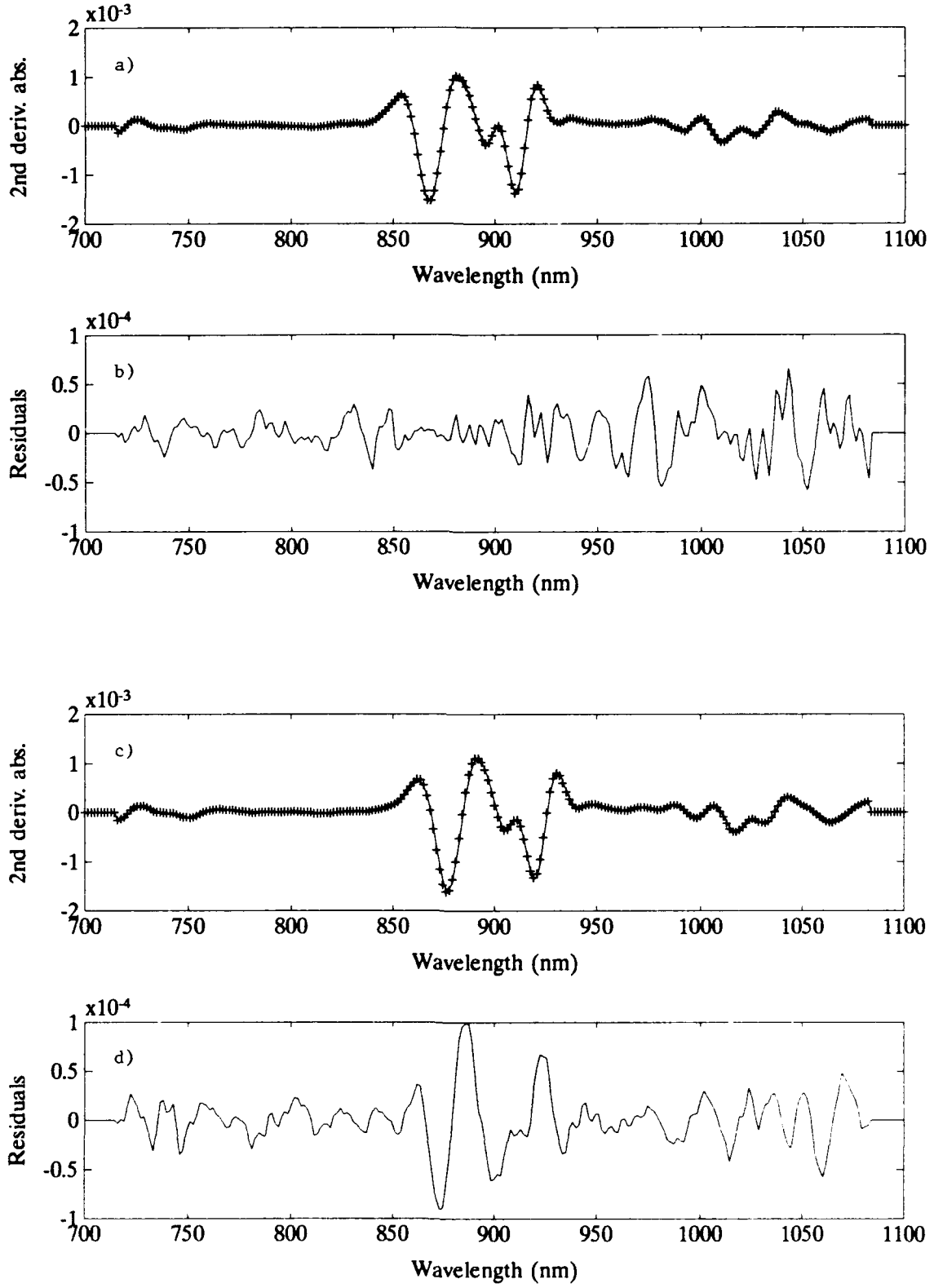
x10-3
2
1
0
-1
-2
a)
2nd deriv. abs.
700
750
800
850
900
950
1000
1050
1100
Wavelength (nm)
x10-4
1
0.5
0
-0.5
-1
b)
Residuals
Wavelength (nm)
c)
Wavelength (nm)
d)
Wavelength (nm)

Figure 5.13 Reconstructed spectra of *meta*-xylene from CLS analysis.

Portable Spectrometer

a) Reconstructed spectra (+ + +) of *meta*-xylene overlaid with the pure-component spectra (—).

b) Residuals between reconstructed spectra (+ + +) and pure component spectra.

Scanning Spectrophotometer

c) Reconstructed spectra (+ + +) of *meta*-xylene overlaid with the pure-component spectra (—).

d) Residuals between reconstructed spectra and pure component spectra.

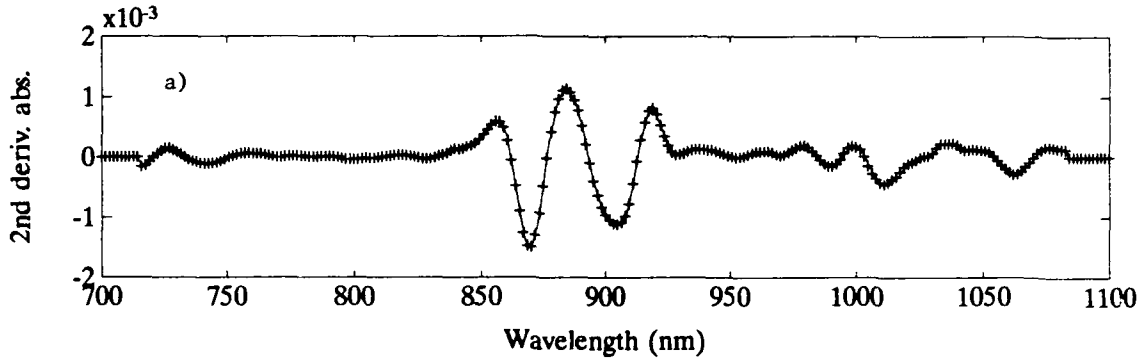
x10-3
a)
2nd deriv. abs.
2
1
0
-1
-2
700
750
800
850
900
950
1000
1050
1100
Wavelength (nm)

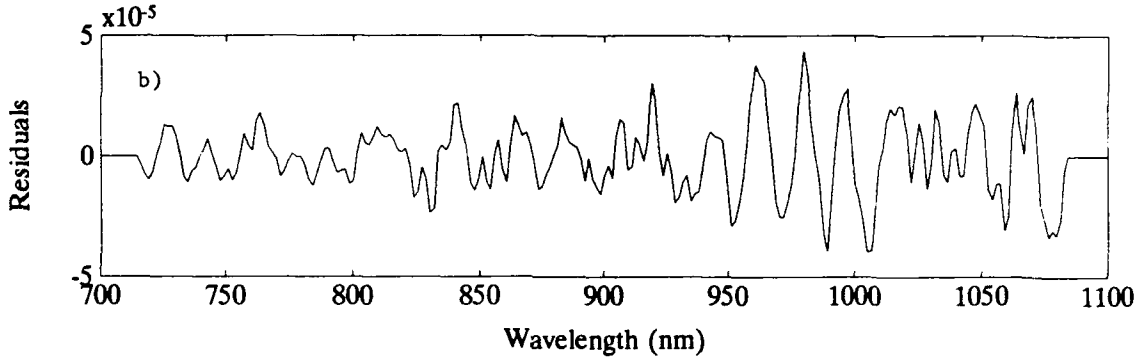
x10-5
b)
Residuals
5
0
-5
700
750
800
850
900
950
1000
1050
1100
Wavelength (nm)

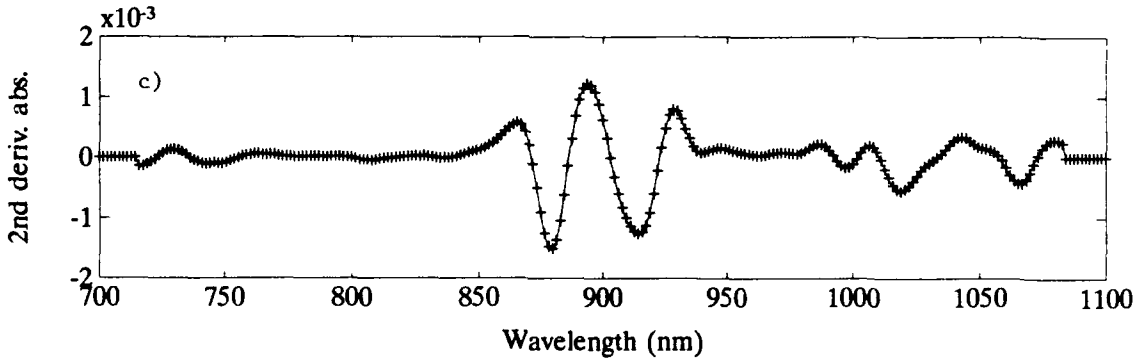
x10-3
c)
2nd deriv. abs.
2
1
0
-1
-2
700
750
800
850
900
950
1000
1050
1100
Wavelength (nm)

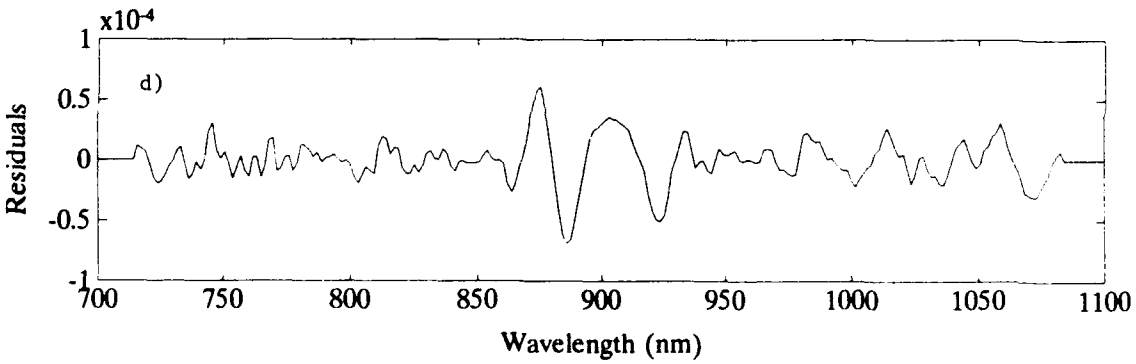
x10-4
d)
Residuals
1
0.5
0
-0.5
-1
700
750
800
850
900
950
1000
1050
1100
Wavelength (nm)

Figure 5.14 Reconstructed spectra of *para*-xylene from CLS analysis.

Portable Spectrometer

a) Reconstructed spectra (+ + +) of *para*-xylene overlaid with the pure-component spectra (—).

b) Residuals between reconstructed spectra (+ + +) and pure component spectra.

Scanning Spectrophotometer

c) Reconstructed spectra (+ + +) of *para*-xylene overlaid with the pure-component spectra (—).

d) Residuals between reconstructed spectra and pure component spectra.

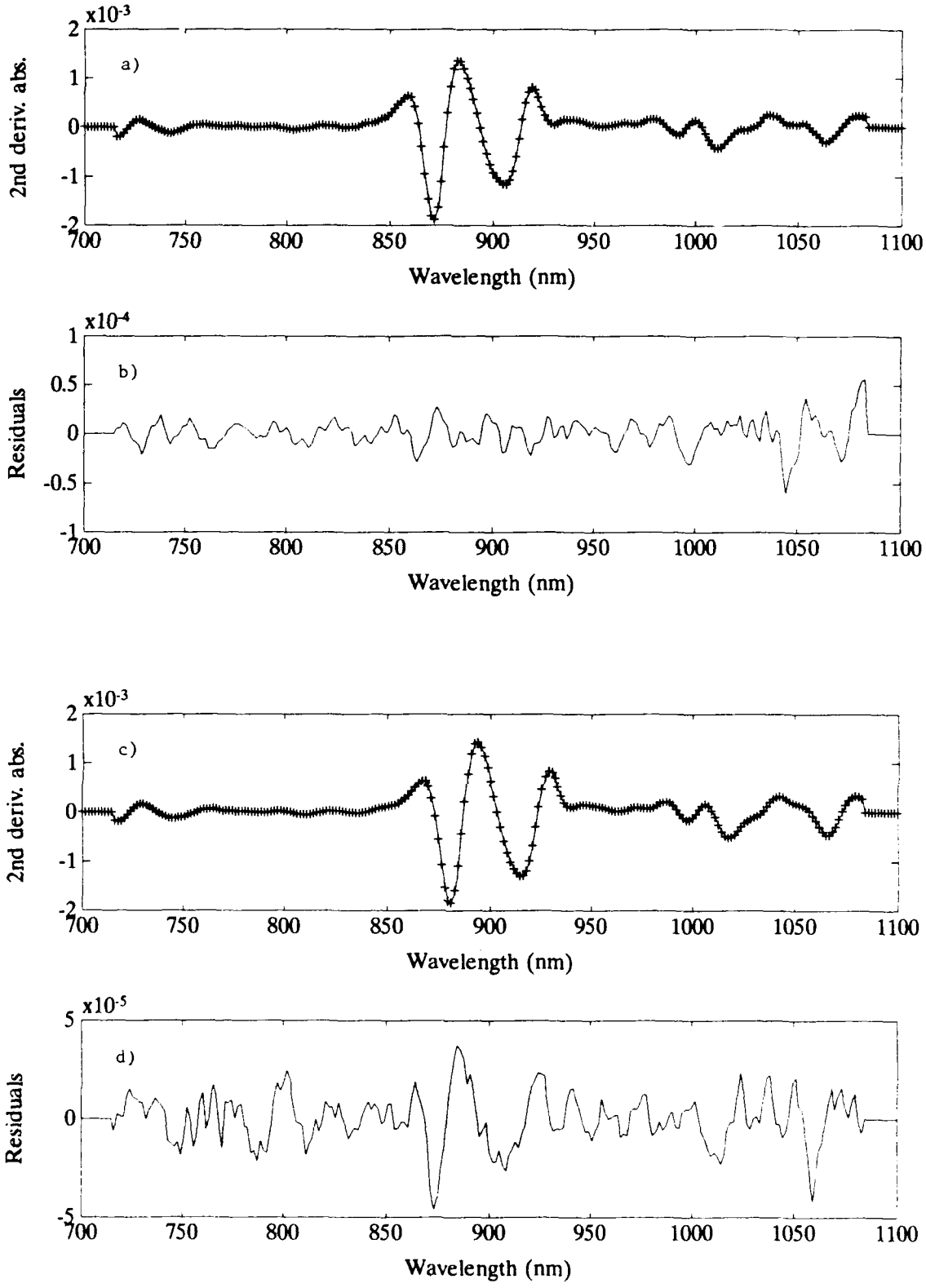
x10-3
2
1
0
-1
-2
a)
2nd deriv. abs.
700
750
800
850
900
950
1000
1050
1100
Wavelength (nm)
x10-4
1
0.5
0
-0.5
-1
b)
Residuals
700
750
800
850
900
950
1000
1050
1100
Wavelength (nm)
x10-3
2
1
0
-1
-2
c)
2nd deriv. abs.
700
750
800
850
900
950
1000
1050
1100
Wavelength (nm)
x10-5
5
0
-5
d)
Residuals
700
750
800
850
900
950
1000
1050
1100
Wavelength (nm)

5.5 Conclusions

Shortwave near-infrared spectroscopy is shown to be a feasible analysis technique for the quantitative analysis of the xylene isomers. Despite an extremely high degree of spectral overlap between the three isomers, each of the multivariate statistical methods employed were able to quantitate the individual components to less than 0.50% absolute. This represents a significant improvement over the other analytical techniques as listed in Table 5.1. Minimal sample preparation and an analysis time of a few seconds, further highlight the benefits of the NIR spectral measurement. With the importance of the xylene isomers in the petroleum industry as well as their value as chemical commodities, NIR spectroscopy should prove to be a valuable analysis technique.

A comparison of the three multivariate statistical analysis techniques of MLR, PLS and CLS indicates that each performs approximately equally, when applied to "well-behaved" NIR spectra of hydrocarbon samples. The high signal-to-noise ratios and linear instrumental response available with modern NIR instruments, coupled with minimal analyte-analyte interactions in hydrocarbon samples, puts the three analysis techniques on an equal footing.

The performance of the portable NIR spectrometer was shown to be significantly better than that of a commercially available laboratory spectrophotometer. In each of the analysis techniques employed, the portable spectrometer performed two to four times better than the commercial scanning

spectrophotometer. Apparent from these analyses, was the advantage of the increased signal-to-noise ratio and improved resolution of the portable spectrometer.

5.6 Notes to Chapter 5

1. Nasuto, R., Dabkowska, M, Kusak, R., Kwietniewski, L., *Separation Science and Technology,* **1984,** 29, 651.

2. Milewski, M., Berak, J.M., *Separation Science and Technology*, 1982, 17, 369.

3. Cahours, A., *Annales de Chimie et de la Physique*, **1859**, T76, 286.

4. Fittig, R., *Annalen*, **1869,** 153, 265.

5. Jacobsen, O., *Annalen*, **1877**, 1009.

6. Waddams, A.L., *Chemicals From Petroleum, 4th Edition*, **1978**, John Murray, London, England.

7. *Chemical Marketing Reporter - 214*, **1978,** 9, 9.

8. *Chemical Marketing Reporter - 208,* **1975,** 3, 12.

9. Hancock, E.E., *Toluene, the Xylenes and Their Industrial Derivatives,* **1982,** Elsevier Scientific Publishing Company, New York, NY.

10. Zelinski, N.D., *Ber. Deut. Chem. Ges.*, **1911,** 44, 3121.

11. Haensel, V., Sterba, M.J., *Progress in Petroleum Technology, Advance Chem. Ser.,* **1951,** 5, 60.

12. Bernstein, J., Dauber, L., *Nat. Petro. Refiners Assoc., Mid-Continental Meeting*, Wichita, Kansas, **1968**.

13. Milewski, M., Berak, J.M., *Przem. Chem.*, **1975,** 54, 698.

14. Kachlik, K., *Przem. Chem.*, **1973,** 52, 481.

15. Wiseman, P., *Petrochemicals - UMIST Series in Science and Technology*, **1986,** Ellis Horwood Limited, Chichester, England.

16. *1989 Annual Book of ASTM Standards*; American Society for Testing and Materials: Philadelphia, PA, **1989**, 06.03, 614.

17. *ASTM Special Technical Publication No. 332*, American Society for Testing and Materials, **1963**, Baltimore, MD.

18. Donahue, S.M., Brown, C.W., Obremski, R.J., *Appl. Spectrosc.*, **1988,** 42(2), 353.

19. Gough, K.M., Henry, B.R., *J. Phys. Chem.*, **1984,** 88, 1298.

20. Henry, B.R., *Accounts of Chemical Research,* **1987,** 20(12), 429.

21. Hayward, R.J., Henry, B.R., *Chemical Physics,* **1976,** 12, 387.

22. Nakagaki,R., Hanazaki, I., *Chemical Physics Letters,* **1981,** 83(3), 512.

23. Nakagaki, R., Hanazaki, I., *Chemical Physics,* **1982,** 72, 93.

24. Taylor, W.J., Wagman, D.D., Williams, M.G., Pitzer, K.S., Rossini, F.D., *J. Res. Nat. Bureau Standards,* **1946,** 37, 95.

25. Aldridge, P.K., *Doctoral Dissertation*, University of Washington, Seattle, WA, **1991**.

26. Weyer, L.G., *Appl. Spectrosc. Rev.*, **1985**, 19, 1.

27. Wheeler, O.H., *Chem. Rev.*, **1959**, 59, 629.

28. Sharaf, M.A., Illman, D.L., Kowalski, B.R., *Chemometrics*, John Wiley & Sons, NY, **1986**.

29. Strang, G., *Linear Algebra and Its Applications,* **1980**, Academic Press, FL, 137.

30. Miller, C., *Doctoral Dissertation*, University of Washington, Seattle, WA, **1989.**

31. Haaland, D.M., Thomas, E.V., *Anal. Chem.*, **1988,** 60, 1193.

BIBLIOGRAPHY

"Annex 2 - Reference Materials and Blending Accessories", in Annual Book of ASTM Standards, (ASTM Press, Philadelphia, Pennsylvania), **1988**, 5.01, 128.

"Designation: E275-83," in Annual Book of ASTM Standards, (ASTM Press, Philadelphia, Pennsylvania), **1990**, 14.01, 64.

"Designation: E387-84," in Annual Book of ASTM Standards, (ASTM Press, Philadelphia, Pennsylvania), **1990**, 14.01, 96.

1989 Annual Book of ASTM Standards; American Society for Testing and Materials: Philadelphia, PA, **1989**, 06.03, 614.

1990 Annual Book of ASTM Standards; American Society for Testing and Materials: Philadelphia, PA, **1990**, 05.02, 157.

1990 Annual Book of ASTM Standards; American Society for Testing and Materials: Philadelphia, PA, **1990**, 05.01, 509.

Abney, W., Festing, E.R., *Phil. Trans.,* **1881**, 172, 887.

Aldridge, P.K., Callis, J.B., Burns, D.H., *Manuscript in preparation.*

Aldridge, P.K., *Doctoral Dissertation*, University of Washington, Seattle, WA, **1991**.

Aldridge, P.K., Callis, J.B., Burns, D.H., *J. Liquid Chromatogr.,* **1990**, 13, 2829.

Aldridge, P.K., Burns, D.H., Kelly, J.J., Callis, J.B., *CPAC Publication # 101*, **1991**, 1, 1.

Archibald, D.D., Miller, C.E., Lin, L.T., Honigs, D.E., *Appl. Spectrosc.*, **1988**, 42, 1549.

ASTM Special Technical Publication No. 332, American Society for Testing and Materials, **1963**, Baltimore, MD.

Aviation Fuels and Their Effects on Engine Performance, Ethyl Corporation, contract No. 52-202, Department of the Navy, Bureau of Aeronautics, **1951**.

Baughman, E.H., Mayes, D.M., *Amer. Lab.*, **1989**, 10, 54.

Baughman, E.H., Vickers, G.H., Mayes, D.M., *Effect of Wavelength on Prediction Errors in the NIR*, **1990** Pittsburgh Conference, NY, Paper # 526.

Beebe, K.R., Kowalski, B.R., *Anal. Chem.*, **1987**, 59, 1007A.

Bernstein, J., Dauber, L., *Nat. Petro. Refiners Assoc., Mid-Continental Meeting*, Wichita, Kansas, **1968**.

Biggs, D.A., *Assoc. Off. Anal. Chem.,* **1983**.

Bilhorn, R. B., Epperson, P. M., Sweedler, J. V., Denton, M. D., *Appl. Spectrosc.*, **1987**, 41(7), 1125.

Birth, G.S., Hecht, H.G., in *Near Infrared Analysis in the Agricultural and Food Industries, Chapter 1*, **1987**, P.W.Williams and K. Norris, Eds.; American Association of Cereal Chemists: St. Paul, MN.

Brackett, F.S., *Proc. Natl. Acad. Sci. (U.S.)*, **1928**, 14, 857.

Brown, C.W., Lynch, P.F., Obremski, R.J., Lavery, D.S., *Anal. Chem.*, **1982**, 54, 1472.

Brown, C.W., Obremski, R.J., *Appl. Spectrosc. Rev.*, **1984**, 20, 373.

Brown, G.K., *Coatweight and Film Thickness Measurement Using Near Infrared Techniques*, 1987 Air Knife Coating Seminar, **1987**, TAPPI Seminar Notes, 87.

Buchanan, B.R., *Doctoral Dissertation*, University of Washington, Seattle, WA, **1987**.

Cahours, A., *Annales de Chimie et de la Physique*, **1859**, T76, 286.

Callis, J.B., Illman, D.L., Kowalski, B.R., *Anal. Chem.*, **1987**, 59, 624A.

Campbell, R.M., Djordjevic, N.M., Markides, K.E., Lee, M.L., *Anal. Chem.,* **1988**, 60, 356.

Caswell, K.A., Glass, T.E., Swann, M., Dorn, H.C., *Anal. Chem.,* **1989**, 61, 206.

Cavinato, A.G., Mayes, D.M., Ge, Z., Callis, J.B., *Anal. Chem.*, **1990**, 62, 1977.

Chemical Marketing Reporter - 208, **1975,** 3, 12.

Chemical Marketing Reporter - 214, **1978,** 9, 9.

Clevett, K.J., *Process Analyzer Technology*, John Wiley: New York, 1986.

Coblentz, W.W., Natl. Bur. Standards (U.S.), *Special Publication No. 418*, **1921**.

Coblentz, W.W., *Investigation of Infrared Spectra, Part 1*, Carnegie Institution, Washington, D.C., **1905**.

Colthup, N.B., Daly, L.H., Wiberly, S.E., *Introduction to Infrared and Raman Spectroscopy, 2nd edition*, **1975**, Academic: NY.

Dannenberg, H., *SPE Transactions,* **1963,** 1, 78.

Donahue, S.M., Brown, C.W., Obremski, R.J., *Appl. Spectrosc.*, **1988,** 42(2), 353.

Donath, B., *Ann. Physik,* **1896**, 58, 609.

Draper, N., Smith, H., *Applied Regression Analysis 2nd Edition*, John Wiley and sons, NY, **1981**.

Durand, J.P., Boscher, Y., Petroff, N., Berthelin, M., *Journal of Chromatography,* **1987**, 395, 229.

EG&G Reticon Data Book, Image Sensing Products, **1989**, 39.

Epperson, P.M., Sweedler, J.V., Bilhorn, R.B., Sims, G.R., Denton, M.B., *Anal. Chem.*, **1988**, 60, 327A.

Fittig, R., *Annalen*, **1869,** 153, 265.

Fox, J.J., Martin, A.E , *Proc. R. Soc. London*, **1938**, A175, 208.

Fox, J.J., Martin, A.E., *Proc. R. Soc. London*, **1938**, A167, 257.

Geladi, P., Kowalski, B.R., *Anal. Chim. Acta*, **1986**, 185, 1.

Ghosh, S., Rodgers, J.E., *Textile Res. J.*, **1985**, 9, 556.

Goddu, R.F., *Advan. Anal. Chem. Instr.*, **1960,** 1, 347.

Gough, K.M., Henry, B.R., *J. Phys. Chem.*, **1984,** 88, 1298.

Haaland, D.M., Easterling, R.G., *Appl. Spectrosc.*, **1980**, 34, 539.

Haaland, D.M., Thomas, E.V., *Anal. Chem.*, **1988**, 60, 1202.

Haaland, D.M., Thomas, E.V., *Anal. Chem.*, **1988,** 60, 1193.

Haensel, V., Sterba, M.J., *Progress in Petroleum Technology, Advance Chem. Ser.,* **1951,** 5, 60.

Hamamatsu Technical Data Sheet No. S-501-02, **1987**, 2.

Hancock, E.E., *Toluene, the Xylenes and Their Industrial Derivatives,* **1982,** Elsevier Scientific Publishing Company, New York, NY.

Hayes, P.C., Jr., Anderson, S.D., *Anal. Chem.,* **1985**, 58, 2384.

Hayes, P.C., Jr., Anderson, S.D., *Anal. Chem.*, **1985**, 57, 2094.

Hayward, R.J., Henry, B.R., *Chemical Physics,* **1976,** 12, 387.

Henry, B.R., *Accounts of Chemical Research,* **1987,** 20(12), 429.

Herschel, W., *Philos. Trans.*, **1800**, 90, 225.

Herzberg, G., *Infrared and Raman Spectra*, **1945**, Van Nostrand Reinhold Co., NY, NY, 239.

Hindle, P.H., Roberts, D.L., *An Introduction to Infrared Absorption Gauging*, **1987**, September, Tobacco Reporter.

Honigs, E.E., Hirschfeld, T.B., Hieftje, G.M., *Anal. Chem.*, **1985**, 57, 443.

Hruscha, W.R. in *Near Infrared Analysis in the Agricultural and Food Industries,* **1985**, P.W. Williams and K. Norris, Eds.; American Association of Cereal Chemists: St. Paul, MN, 35.

Jacobsen, O., *Annalen*, **1877**, 1009.

James, J.F., Sternberg, R.S., *The Design of Optical Spectrometers*, **1969,** Chapman and Hall Ltd. London, England.

Janesick, J.R., Elliott, T., Collins, S., Blouke, M.M., Freeman, J., *Optical Engineering*, **1987**, 26, 692.

Jobsis, F.F., *Science*, **1977**, 198, 1264.

Jones, D. G. *Anal. Chem.* **1985**, 57, 1057A.

Jones, D.G., *Anal. Chem.*, **1985**, 57, 1207A.

Kachlik, K., *Przem. Chem.*, **1973,** 52, 481.

Kaye, W., *Anal. Chem.*, **1981**, 53, 2201.

Kaye, W.I., *Spectrochim. Acta.*, **1954**, 6, 257.

Kaye, W.I., *The Encyclopedia of Spectroscopy,* **1960**, Clark, G.L., Ed., Reinhold, NY, 494.

Kaye, W.I., *Spectrochim. Acta.*, **1955**, 7, 181.

Kelly, J.J., Callis, J.B., *Anal. Chem.*, **1990**, 62, 1444.

Kelly, J.J., Barlow, C.H., Jinguji, T.M., Callis, J.B., *Anal. Chem.*, **1989**, 61, 313.

Kisner, H.J., Brown, C.W., Kavarnos, G.J., *Anal. Chem.*, **1983**, 55, 1694.

Kortum, G., *Reflectance Spectroscopy: Principles, Methods, Applications*, Springer-Verlag, NY, **1969**.

Kowalski, K.G., *Chemometrics and Intelligent Laboratory Systems*, **1990**, 9, 177.

Kubelka, P., Munk, F., *Z. Tech. Phys.*, **1931**, 12, 593.

Landa, I., *Rev. Sci. Instrum.*, **1979**, 50(1), 34.

Lauer, J.L., Rosenbaum, E.J., *Appl Spectrosc.*, **1952,** 6, 29.

Lysaght, M.J., van Zee, J.A., Callis, J.B., *Rev. Sci. Inst.*, **1991**, 2, 507.

Lysaght, M.J., Kelly, J.J., Callis, J.B., *CPAC Publication Announcement # 102*, **1991**, 1, 1.

Lysaght, M.J., Danielson, J.D.S., Callis, J.B., *CPAC Publication Announcement # 106*, **1991,** 2, 1.

Maris, M.A., Brown, C.W., Lavery, D.S., *Anal. Chem.*, **1983**, 55, 1694.

Martel, C.R., *Military Jet Fuels, 1944-1987: Report # AFWAL-TR-87-2062*, Aero Propulsion Lab, AFWAL/POSF, Wright-Patterson Air Force Base, OH **1987**.

Martens, H., Naes, T., *Trends Anal. Chem.*, **1984**, 3, 204.

Mathews, J.H., *Numerical Methods*, Prentice-Hall, NJ, **1987**, 279.

Mayes, D.M., Callis, J.B., *Appl. Spectrosc.*, **1989**, 43, 27.

McClure, W.F., in *Near-Infrared Technology in the Agricultural and Food Industries*, P. Williams, and K. Norris, Eds., American Association of Cereal Chemists, Inc., St. Paul, Minnesota, **1987**.

Milewski, M., Berak, J.M., *Przem. Chem.*, **1975,** 54, 698.

Milewski, M., Berak, J.M., *Separation Science and Technology*, 1982, 17, 369.

Miller, C., *Doctoral Dissertation*, University of Washington, Seattle, WA, **1989.**

Miller, C.E., Edelman, P.G., Ratner, B.D., Eichinger, B.E., *Appl. Spectrosc.*, **1990**, 4, 581.

Miller, R.L., Ettre, L.S., Johansen, N.G., *J. Chromatogr.*, **1983**, 264, 19.

Moessner, R.C., Russell, D.A., *ISA Proceedings Report #90-486*, **Oct 1990**, 691.

Morrison, R.T., Boyd, R.N, *Organic Chemistry, Third Edition,* **1974**, Allyn and Bacon, Inc., Boston, 85.

Nakagaki, R., Hanazaki, I., *Chemical Physics,* **1982,** 72, 93.

Nakagaki,R., Hanazaki, I., *Chemical Physics Letters,* **1981,** 83(3), 512.

Nasuto, R., Dabkowska, M, Kusak, R., Kwietniewski, L., *Separation Science and Technology,* **1984,** 29, 651.

NIR Spectral Analysis Software, Ver. 3.07, NIRSystems, Silver Spring Maryland, **1989**.

Norris, A.T., Rawdon, M.G., *Anal. Chem.,* **1984**, 56, 1767.

Norris, K.H., *NATO Adv. Study Inst. Sec. A,* **1983**, 46, 471.

Ozubko, R.S., Clungston, D.M., Furimsky, E., *Anal. Chem.,* **1981**, 53, 183.

PC-MATLAB for 80386-based MS-DOS Personal Computers, Version 3.5e, The Math Works Inc., **1989**.

Pell, R.J., *Doctoral Dissertation*, University of Washington, Seattle, WA, **1990**.

Petrakis, L., Allen, D.T., Gavalas, G.R., Gates, B.C., *Anal. Chem.,* **1983**, 55, 1557.

Peuchant, E., Salles, C., Jensen, R., *Anal. Chem.*, **1987**, 59, 816.

Phelan, M.K., Barlow, C.H., Kelly, J.J., Jinguji, T.M., Callis, J.B., *Anal. Chem.*, **1989**, 61, 1419.

Phelan, M.K., *Doctoral Dissertation*, University of Washington, Seattle, WA, **1990**.

Puccianti, L., *Physik. Z.*, **1899-1900**, 49, 494.

Puccianti, L., *Nuovo Cimento*, **1900**, 11, 141.

Riebe, M.T., Eustace, D.J., *Anal. Chem.,* **1990**, 62, 65A.

Robert, P., Bertrand, D., Devaux, M.F., *Anal. Chem.*, **1987**, 59, 2187.

Savitsky, A., Golay, M., *Anal. Chem.*, **1964**, 36, 1627.

Sedlmair, J., Ballard, S.G., Mauzerall, D.C., *Rev. Sci. Instrum.*, **1986**, 57, 2995.

Sharaf, M.A., Illman, D.L., Kowalski, B.R., *Chemometrics*, John Wiley & Sons, NY, **1986**.

Stark, E., Luchter, K., Margoshes, M., *Appl. Spectrosc. Rev.*, **1986**, 22, 335.

Stone, M., *J. R. Statistical Soc., B*, **1974**, 36, 111.

Strang, G., *Linear Algebra and Its Applications,* **1980**, Academic Press, FL, 137.

Sverdlov, L.M., Kovner, M.A., Krainov, E.P., *Vibrational Spectra of Polyatomic Molecules*, **1974**, John Wiley and Sons, NY.

Sweedler, J.V., Jalkian, R.D., Denton, M.B., *Appl. Spectrosc.*, **1989**, 43, 953.

Szakasits, J.J., Robinson, R.E., *Anal. Chem.*, **1991**, 63, 114.

Talmi, Y., *Appl. Spectrosc.*, **1982**, 36(1), 1.

Taylor, W.J., Wagman, D.D., Williams, M.G., Pitzer, K.S., Rossini, F.D., *J. Res. Nat. Bureau Standards,* **1946,** 37, 95.

Tong, L., Lysaght, M.J., Kelly, J.J., Callis, J.B., *HP Application Note, Performance Evaluation of the HP8452A with NIR Modification*, to be published.

Veltkamp, D., Gentry, D., *PLS 2-Block Modeling: User's Manual Version 3.1,* **1988**, Center for Process Analytical Chemistry, University of Washington, Seattle, WA.

Waddams, A.L., *Chemicals From Petroleum, 4th Edition*, **1978**, John Murray, London, England.

Watson, C.A., *Anal. Chem.*, **1977**, 49, 837A.

Watson, E. Jr., Baughman, E.H., *Spectroscopy,* **1987**, 2, 44.

Wendlandt, W.W., Hecht, H.G., *Reflectance Spectroscopy*, Elving, P.J.,

Kolthoff, I.M., Eds., Interscience Publishers, NY, **1966**.

Wetzel, D.L., *Anal. Chem.*, **1983**, 55(12), 1165A.

Weyer, L.G., *Appl. Spectrosc. Rev.*, **1985**, 19, 1.

Wheeler, O.H., *Chem. Rev.,* **1959**, 59, 629.

Whetsel, K.B., *Encyclopedia of Industrial Chemical Analysis, Vol. 2*, **1966,** Snell, F.D., Ed., Wiley-Interscience, NY, 648.

Wilks, P.A., *Infrared in the Real World: FT-IR Versus IR in Process Monitoring*, Spectroscopy, 1(4), 42.

Williams, P.C., and Norris, K.H., *Near-Infrared Technology in the Agricultural and Food Industries*, American Association of Cereal Chemists, Inc., St. Paul, Minnesota **1987**.

Wilson, E.B., Decius, J.C., Cross, P.C., *Molecular Vibrations*, **1955**, McGraw-Hill, NY.

Winson, R.J., *Coating Measurement and Control*, Advances in Pressure Sensitive Tape Technology, Technical Seminar Proceedings, **1987**.

Wiseman, P., *Petrochemicals - UMIST Series in Science and Technology*, **1986,** Ellis Horwood Limited, Chichester, England.

Zelinski, N.D., *Ber. Deut. Chem. Ges.*, **1911,** 44, 3121.

Appendix A

Portable NIR Schematics

Component layout diagrams and schematics for the two portable near-infrared spectrometers are presented here. The design and construction of the various components was accomplished by the University of Washington Chemistry Electronics Shop. Mr. Roy Olund designed the components used in the prototype instrument, while Mr. Lon Buck and Mr. J.D.S. Danielson designed the components used in the second-generation instrument.

Figure A.1 Prototype NIR spectrometer - component layout.

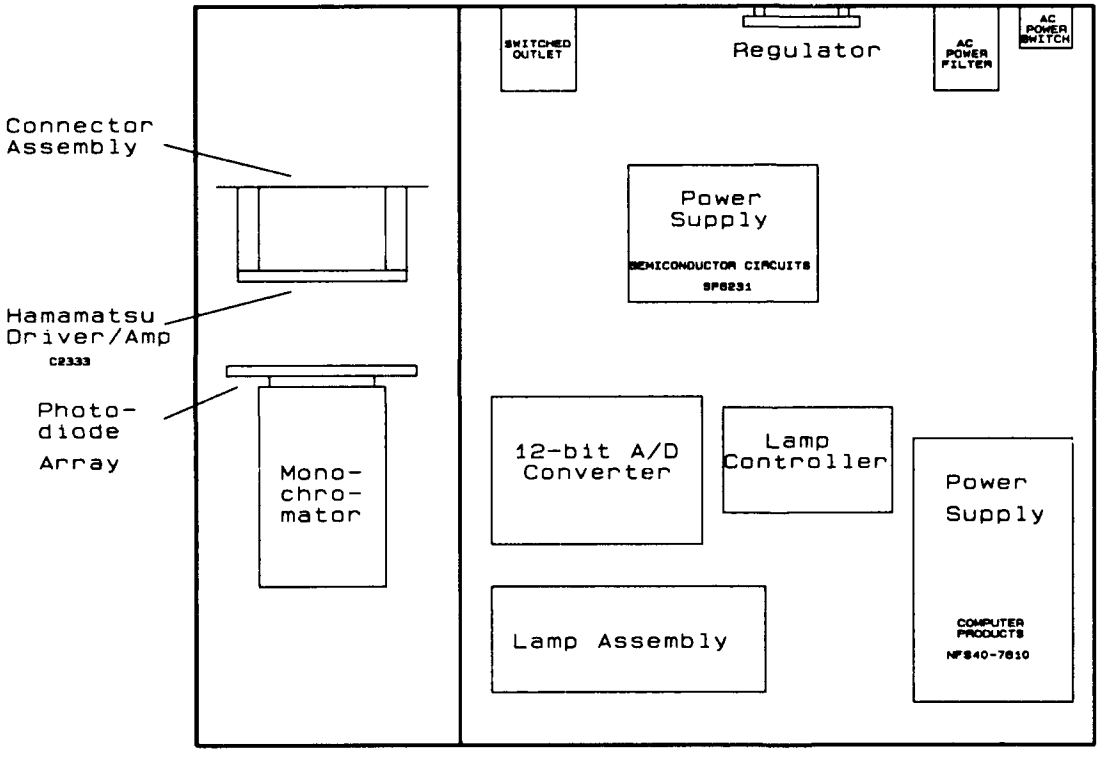

Center for Process Analytical Chemistry
University of Washington
Seattle, Washington 98195

Title
Hamamatsu NIRS Physical Layout

Size	Document Number	REV
B	HAM-NIRS.SCH	

Date: February 14, 1991 Sheet of

Figure A.2 Schematic of light source control circuitry.

Prototype spectrometer.

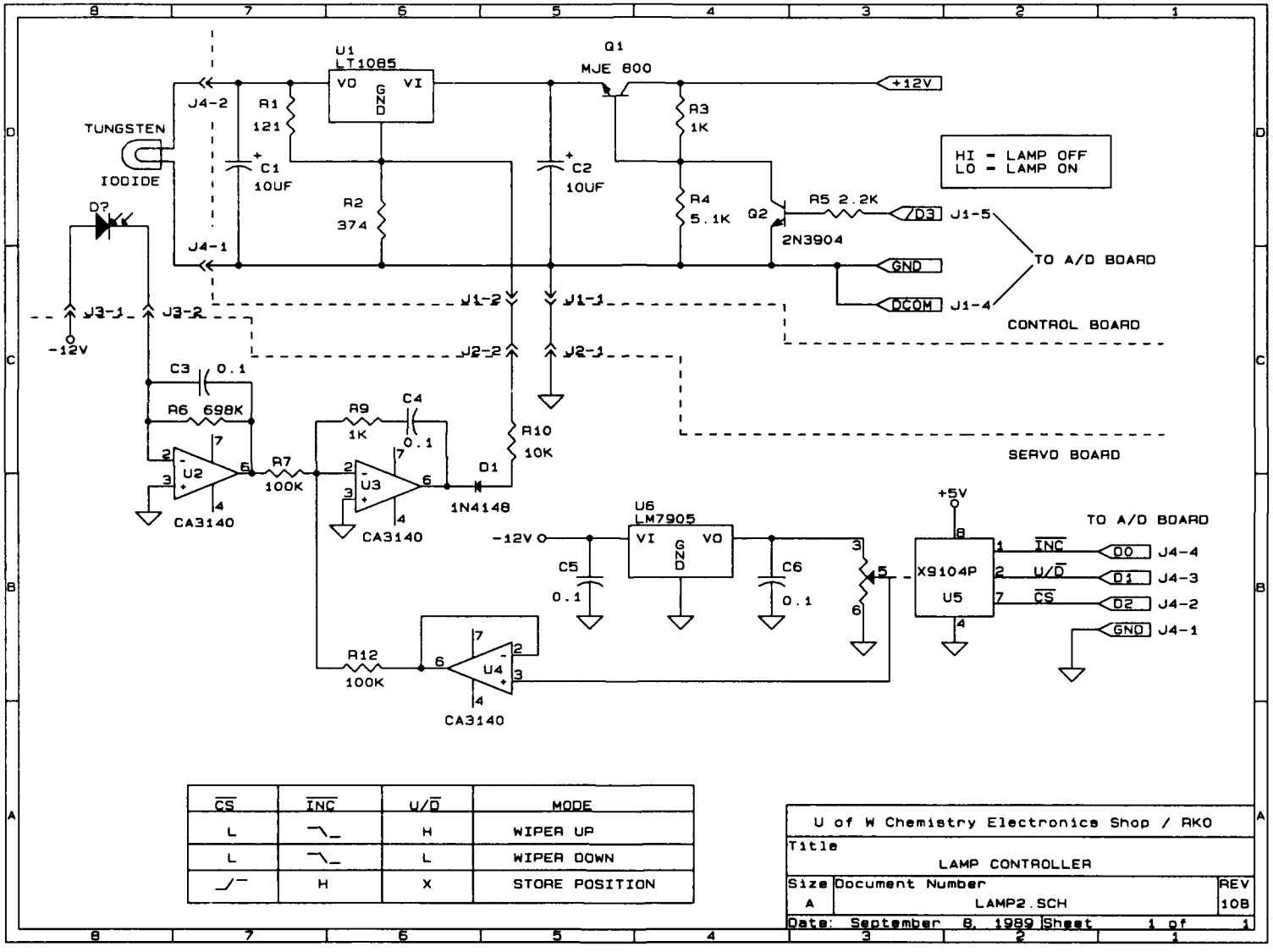

$\overline{CS}$	$\overline{INC}$	U/$\overline{D}$	MODE
L	¬_	H	WIPER UP
L	¬_	L	WIPER DOWN
_/¬	H	X	STORE POSITION

U of W Chemistry Electronics Shop / RKO

Title: LAMP CONTROLLER

Size: A | Document Number: LAMP2.SCH | REV: 10B

Date: September 8, 1989 | Sheet 1 of 1

Figure A.3 Schematic diagram of data acquisition and transfer circuitry. Prototype spectrometer.

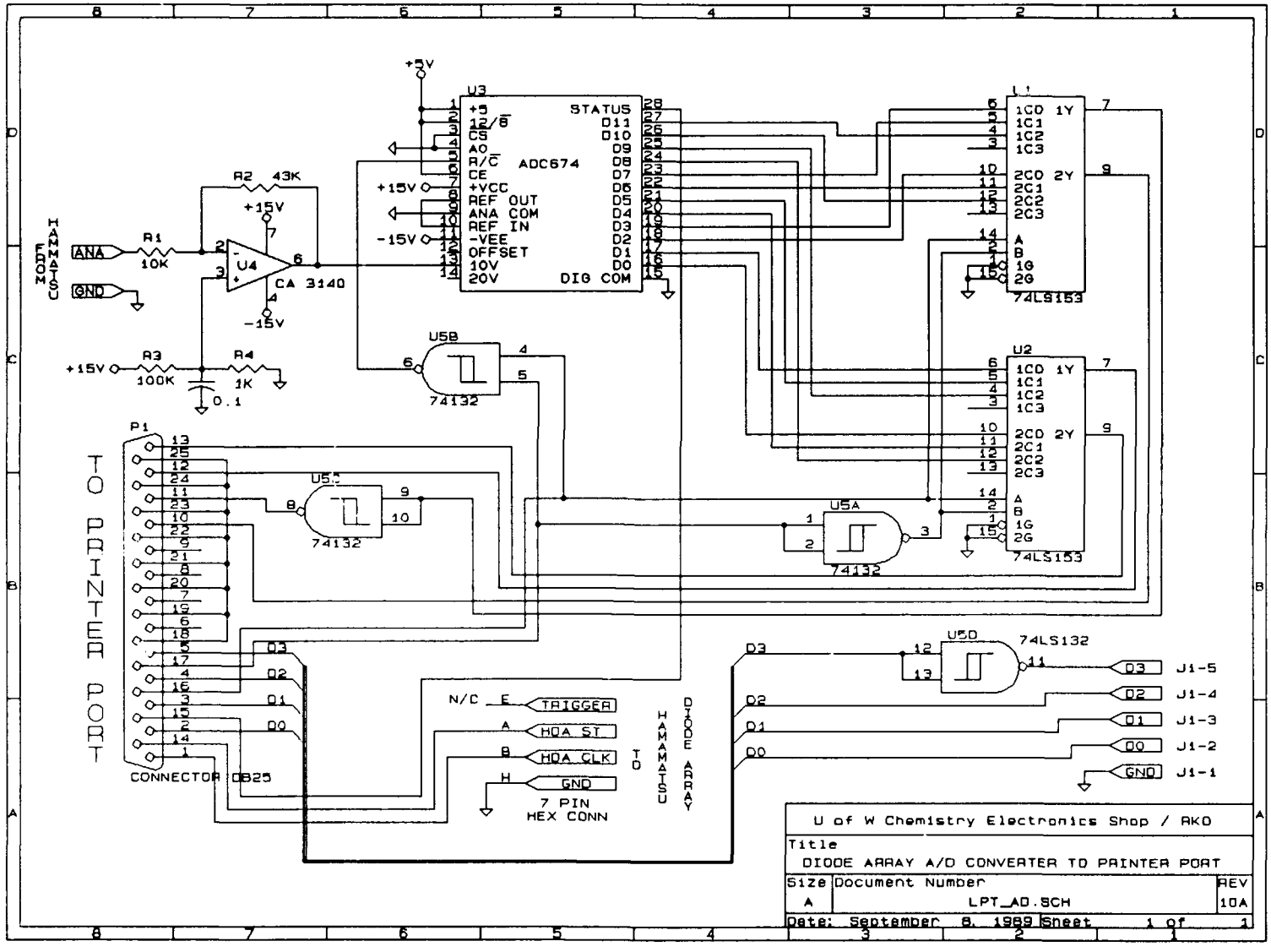
U3
ADC674
STATUS
D11
D10
D9
D8
D7
D6
D5
D4
D3
D2
D1
D0
DIG COM
+5
12/8
CS
A0
R/C
CE
+VCC
REF OUT
ANA COM
REF IN
-VEE
OFFSET
10V
20V
+5V
+15V
-15V
R2 43K
R1 10K
R3 100K
R4 1K
0.1
U4
CA 3140
HAMMATSU
ANA
GND
U5B
74132
U5C
74132
U5A
74132
U5D
74LS132
U1
U2
74LS153
1C0 1Y
1C1
1C2
1C3
2C0 2Y
2C1
2C2
2C3
A
B
1G
2G
P1
TO PRINTER PORT
CONNECTOR DB25
D3
D2
D1
D0
N/C
E
A
B
H
TRIGGER
HDA ST
HDA CLK
GND
7 PIN
HEX CONN
TO HAMMATSU DIODE ARRAY
J1-5
J1-4
J1-3
J1-2
J1-1
U of W Chemistry Electronics Shop / RKD
Title
DIODE ARRAY A/D CONVERTER TO PRINTER PORT
Size
A
Document Number
LPT_AD.SCH
REV
10A
Date: September 8, 1989
Sheet 1 of 1

Figure A.4 NIR spectrometer component layout.

Second generation spectrometer.

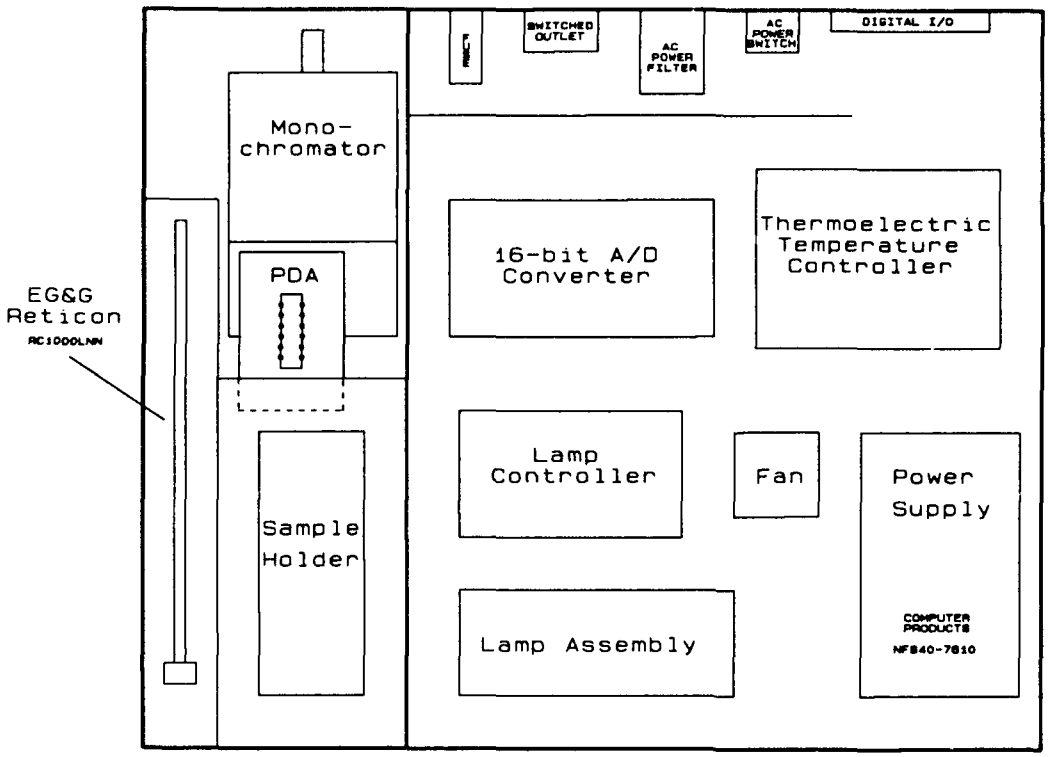

Center for Process Analytical Chemistry
University of Washington
Seattle, Washington 98195

Title
NIRS Physical Layout

Size B | Document Number NIRS.SCH | REV

Date: February 6, 1991 Sheet of

Figure A.5 Portable NIR spectrometer electrical interconnections.

Second generation spectrometer.

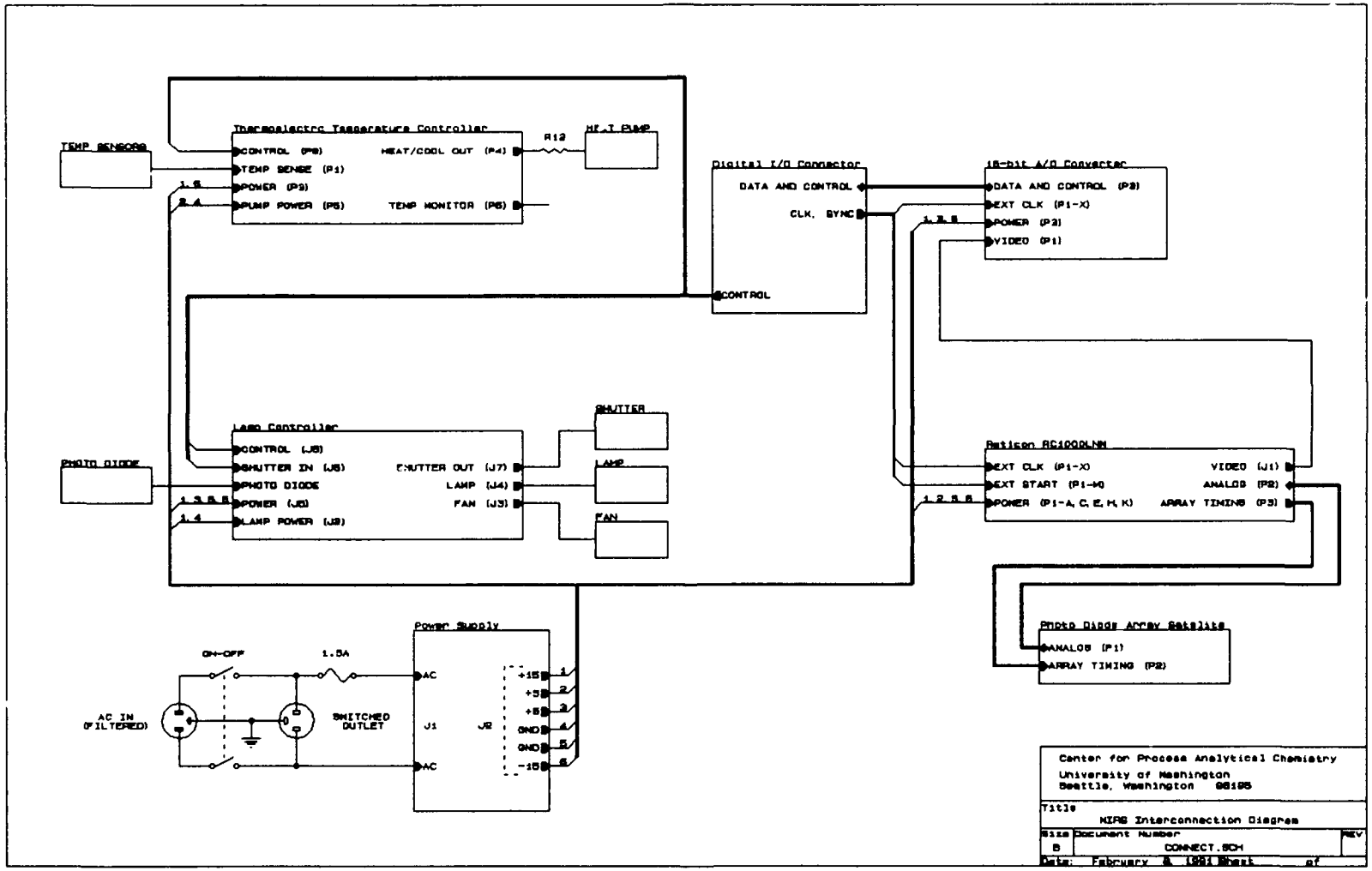
TEMP SENSORS
Thermoelectric Temperature Controller
CONTROL (P8)
TEMP SENSE (P1)
POWER (P9)
PUMP POWER (P5)
HEAT/COOL OUT (P4)
TEMP MONITOR (P6)
R12
HF-T PUMP
Digital I/O Connector
DATA AND CONTROL
CLK, SYNC
CONTROL
18-bit A/D Converter
DATA AND CONTROL (P2)
EXT CLK (P1-X)
POWER (P2)
VIDEO (P1)
PHOTO DIODE
Lamp Controller
CONTROL (J8)
SHUTTER IN (J6)
PHOTO DIODE
POWER (J5)
LAMP POWER (J3)
SHUTTER OUT (J7)
LAMP (J4)
FAN (J3)
SHUTTER
LAMP
FAN
Reticon RC1000LNN
EXT CLK (P1-X)
EXT START (P1-W)
POWER (P1-A, C, E, H, K)
VIDEO (J1)
ANALOG (P2)
ARRAY TIMING (P3)
Photo Diode Array Satellite
ANALOG (P1)
ARRAY TIMING (P2)
Power Supply
ON-OFF
1.5A
AC IN (FILTERED)
SWITCHED OUTLET
AC
AC
J1
J2
+15
+5
+5
GND
GND
-15
Center for Process Analytical Chemistry
University of Washington
Seattle, Washington 98195
Title
MIRS Interconnection Diagram
Size
B
Document Number
CONNECT.SCH
REV
Date: February 8, 1991 Sheet of

Figure A.6 Thermoelectric temperature controller board.

Second generation spectrometer.

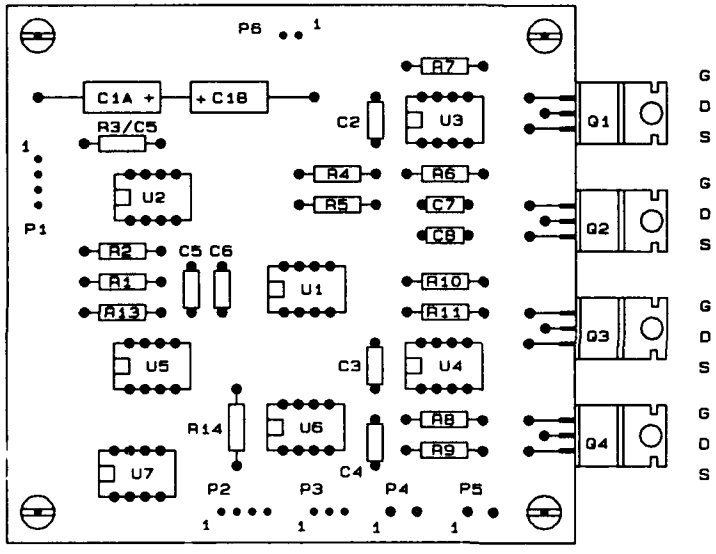

Center for Process Analytcal Chemistry
University of Washington
Seattle, Washington 98195

Title	Thermoelectric Temperature Controller Board	
Size A	Document Number COOL.SCH	REV
Date: February 13, 1991	Sheet of	

Figure A.7 Schematic of PDA thermoelectric temperature controller.

Second generation spectrometer.

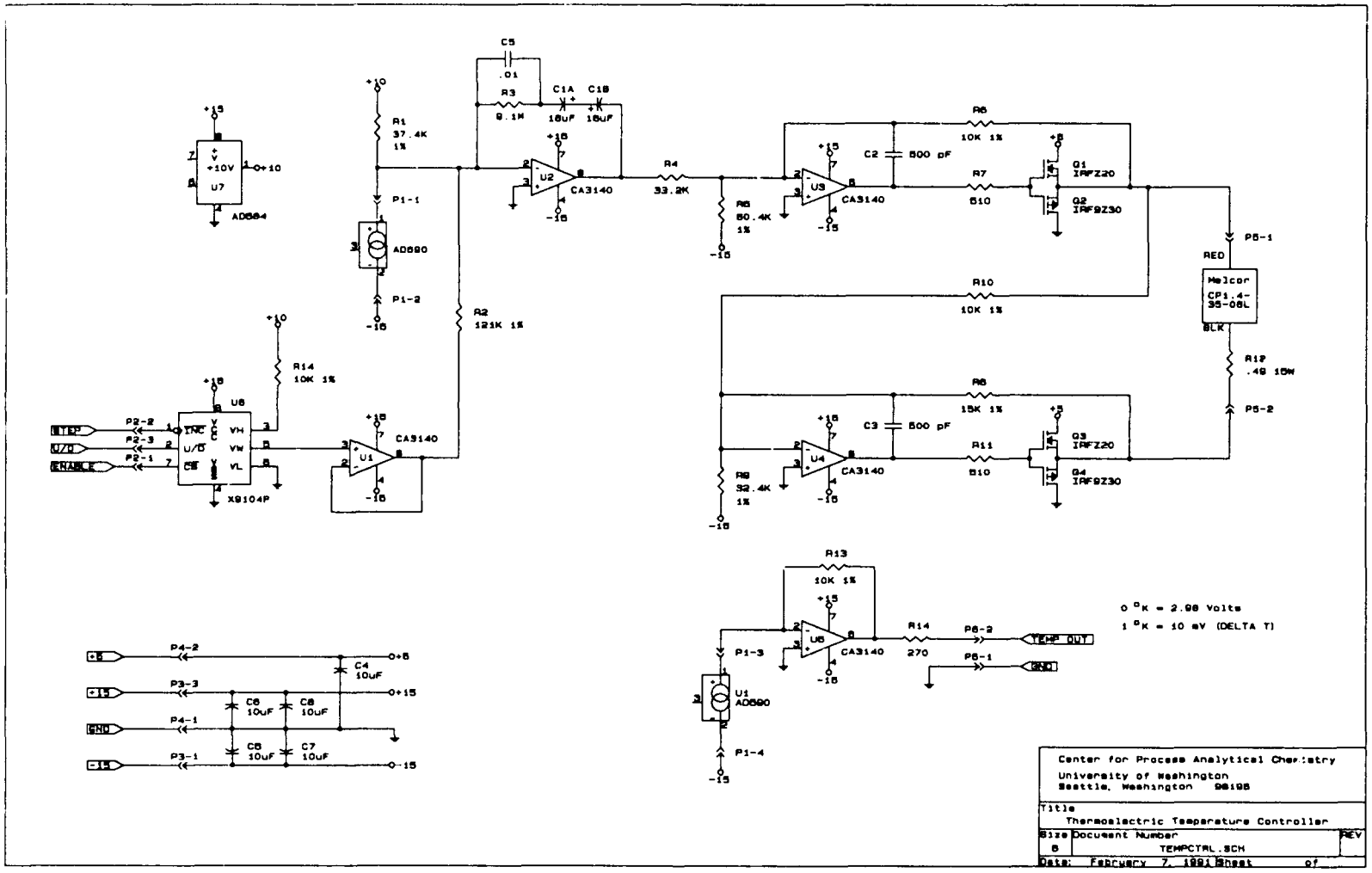
C5
.01
R3
9.1M
C1A
18uF
C1B
18uF
R1
37.4K
1%
P1-1
AD590
P1-2
R2
121K 1%
U2
CA3140
R4
33.2K
R5
80.4K
1%
U3
CA3140
C2
500 pF
R6
10K 1%
R7
510
Q1
IRFZ20
Q2
IRF9Z30
R10
10K 1%
U4
CA3140
C3
500 pF
R8
15K 1%
R11
510
Q3
IRFZ20
Q4
IRF9Z30
R9
32.4K
1%
P5-1
RED
Melcor
CP1.4-
35-06L
BLK
R12
.49 10W
P5-2
U7
+10V
AD584
R14
10K 1%
U8
X9104P
INC
U/D
CS
VH
VW
VL
INTP
U/D
ENABLE
P2-2
P2-3
P2-1
U1
CA3140
R13
10K 1%
U6
CA3140
R14
270
P6-2
TEMP OUT
P6-1
GND
U1
AD590
P1-3
P1-4
0 °K = 2.98 Volts
1 °K = 10 mV (DELTA T)
P4-2
P3-3
P4-1
P3-1
C4
10uF
C6
10uF
C8
10uF
C5
10uF
C7
10uF
Center for Process Analytical Chemistry
University of Washington
Seattle, Washington 98195
Title
Thermoelectric Temperature Controller
Size
B
Document Number
TEMPCTRL.SCH
REV
Date: February 7, 1991
Sheet of

Figure A.8 Light source/shutter controller component layout.

Second generation spectrometer.

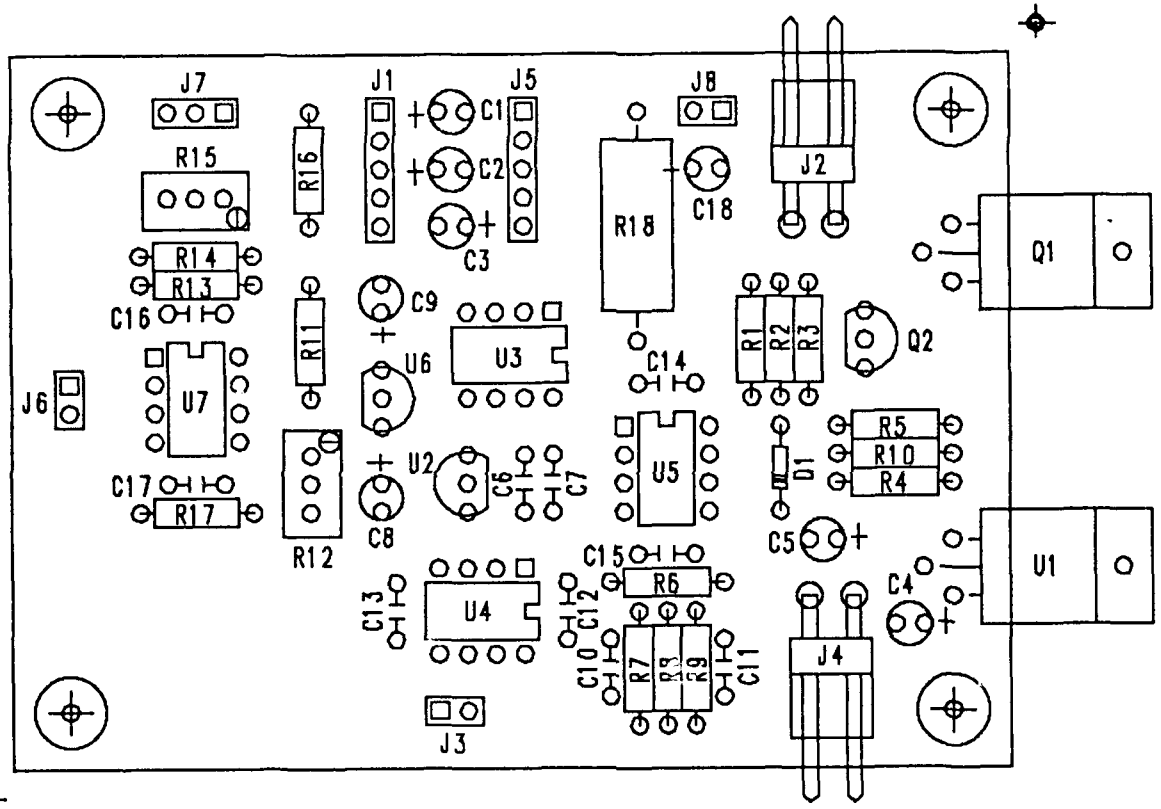

Center for Process Analytical Chemistry
University of Washington
Seattle, Washington 98195

Title	NIRS - Lamp Controller Board Layout	
Size A	Document Number LAMPBRD.SCH	REV
Date: February 14, 1991	Sheet of	

Figure A.9 Schematic diagram of light source/shutter control circuitry.

Second generation spectrometer.

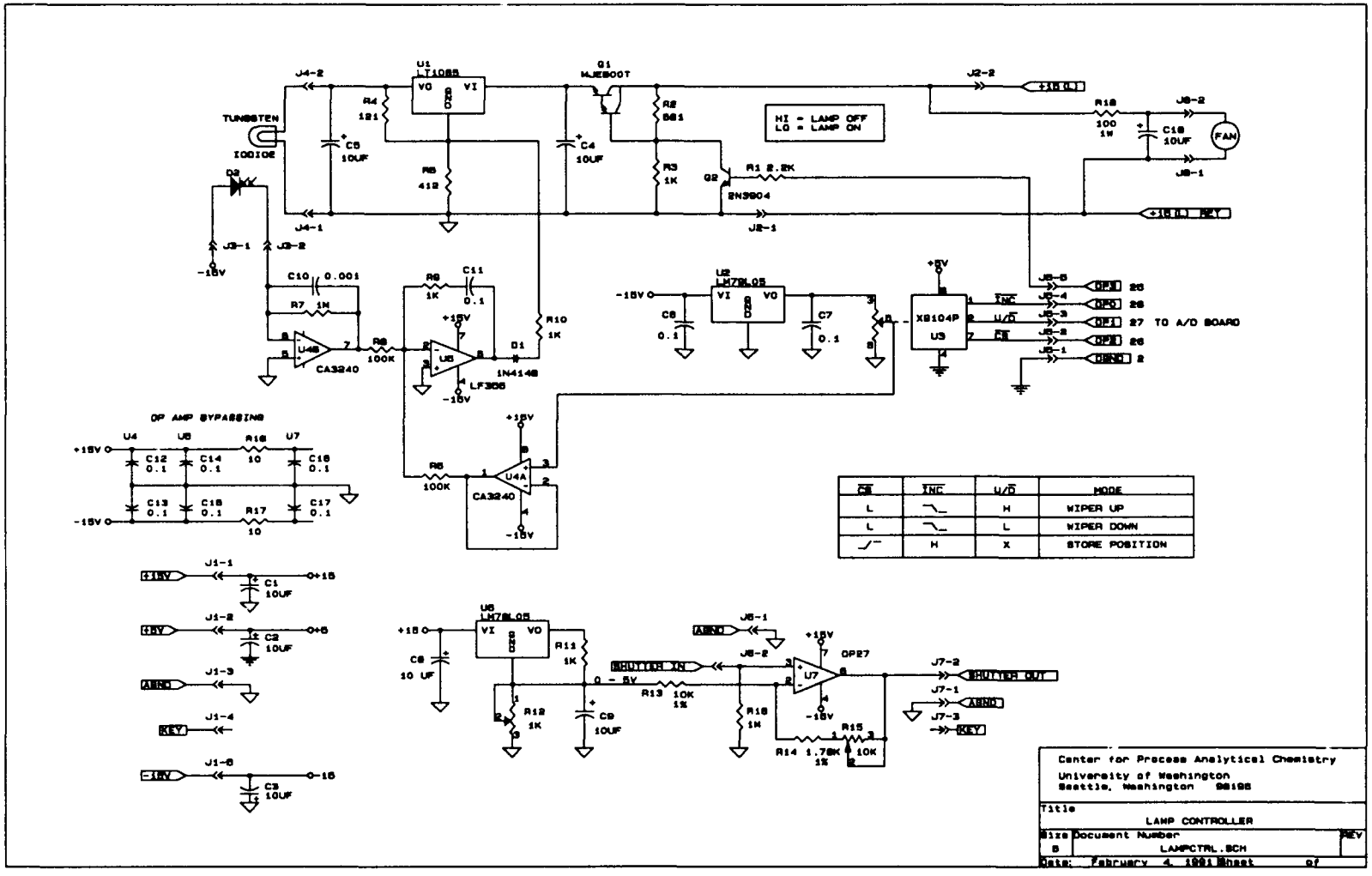

$\overline{CS}$	$\overline{INC}$	U/$\overline{D}$	MODE
L	↓	H	WIPER UP
L	↓	L	WIPER DOWN
↑	H	X	STORE POSITION

Figure A.10 Analog-to-Digital converter component layout diagram.

Second generation spectrometer.

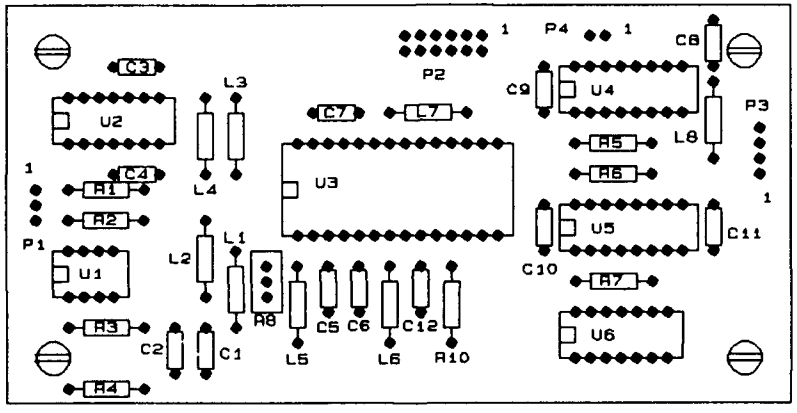

C8 and A9 are below the board

Center for Process Analytical Chemistry

University of Washington
Seattle, Wasington 98195

Title	16-bit A/D Converter - Board Layout	
Size A	Document Number ATOD.SCH	REV
Date: February 13, 1991	Sheet of	

Figure A.11 Schematic diagram of data acquisition control circuitry.

Second generation spectrometer.

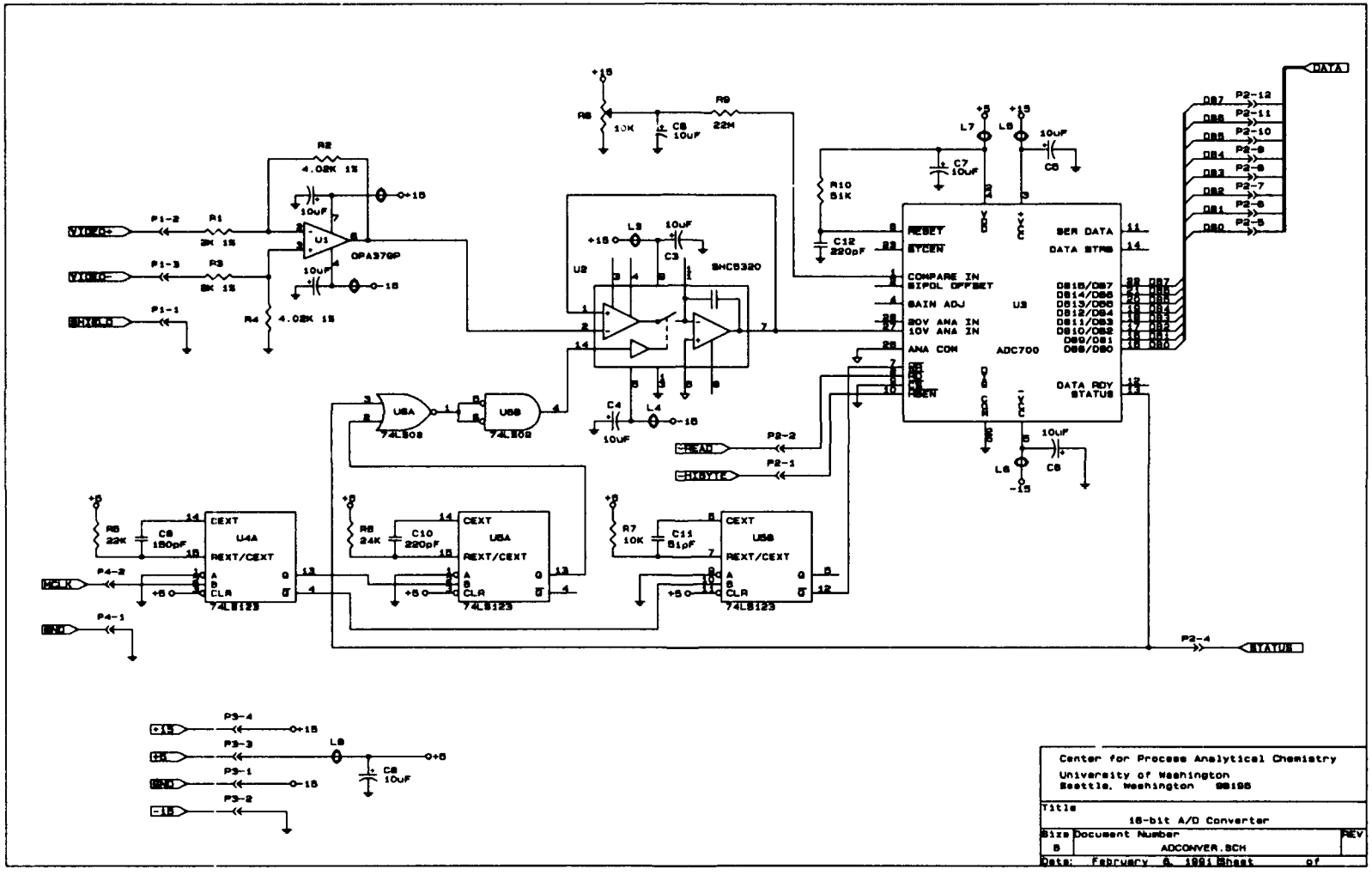
VIDEO+
VIDEO-
SHIELD
P1-2
P1-3
P1-1
R1
2K 1%
R3
2K 1%
R2
4.02K 1%
R4
4.02K 1%
U1
OPA37GP
10uF
+15
-15
R5
10K
C8
10uF
R9
22K
L3
C3
U2
SHC5320
C4
L4
U6A
74LS02
U6B
74LS02
R10
51K
C12
220pF
C7
L7
L9
C5
RESET
BYCEN
COMPARE IN
BIPOL OFFSET
GAIN ADJ
20V ANA IN
10V ANA IN
ANA COM
U3
ADC700
SER DATA
DATA STRB
DB15/DB7
DB14/DB6
DB13/DB5
DB12/DB4
DB11/DB3
DB10/DB2
DB9/DB1
DB8/DB0
DATA RDY
STATUS
L6
C6
DATA
DB7
DB6
DB5
DB4
DB3
DB2
DB1
DB0
P2-12
P2-11
P2-10
P2-9
P2-8
P2-7
P2-6
P2-5
-READ
-HIBYTE
P2-2
P2-1
P2-4
STATUS
+5
R6
22K
C9
150pF
U4A
CEXT
REXT/CEXT
CLR
74LS123
R8
24K
C10
220pF
U5A
R7
10K
C11
51pF
U5B
MCLK
P4-2
GND
P4-1
P3-4
P3-3
P3-1
P3-2
L8
C9
10uF
Center for Process Analytical Chemistry
University of Washington
Seattle, Washington 98195
Title
16-bit A/D Converter
Size
B
Document Number
ADCONVER.SCH
REV
Date: February 6, 1991
Sheet of

Appendix B

Hamamatsu Photodiode Array - Data Acquisition Program

The assembly language program used to acquire the data from the Hamamatsu photodiode array is listed below. Analog to digital (A/D) conversion was accomplished using a Burr-Brown ADC-674 12-bit successive approximation A/D converter. This 12-bit data was then split into three 4-bit nibbles using two Texas Instruments 74LS153 multiplexers for input into the computer through the parallel port (LPT 1) of the laptop computer. The three 4-bit data values are then recombined by software. This data acquisition program was written by the author and Dr. James A. van Zee using Microsoft Assembler. *Timing is controlled via* software timing loops.

```
page 84,132;
title HDA: Hamamatsu Diode Array function for MS BASIC
.286

;   This function provides the timing signals to drive the Diode Array
;   and the A/D converter, returning the value of all 35 elements.
;   The hardware consists of a Burr-Brown ADC-674 12-bit A/D converter
;   connected to the port for LPT1 on any machine.  Due to the limited
;   number of input data lines available (5), the data is multiplexed
;   in three 4-bit nibbles.  The A/D is triggered by selecting the 4th
;   nibble; the data on pins 11 (80H) and 17 (08H) is inverted.
;       The call from the Microsoft QuickBasic program is:  CALLS HDA(iarray(1))
;   where 'iarray' is declared by DIM IARRAY(35) AS INTEGER

    a1=     08                      ; Bit assignments for port 37A
    a0=     04                      ; (output signals)
    start=  02                      ;       (msb)       (lsb)
    clk=    01                      ; DB25 pins [17],[16],[14],[1]
    data=   Fx-0x                   ; Bit assignments for port 379:
    status= 08                      ; Pins [11],[10],[12],[13],[15]

cseg segment    public para 'codes'
     assume     cs:cseg,ds:nothing

hda  proc       far                 ; hence must use CALLS
     public     hda
     push       bp                  ; save vital registers
     push       ds
     mov        bp,sp
     les        di,[bp+8]           ; address of 'iarray'
     xor        ax,ax
     mov        ds,ax               ; DS = BIOS data area
     mov        dx,ds:[408h]        ; DOS address of LPT1
     pop        ds
     inc        dx
     inc        dx
     mov        cl,35               ; # elements to read

mainlp:
     mov        al,start+clk
     out        dx,al               ; lower start, clk
     mov        ch, 4
```

```
clk_lp:
        dec     ax
        out     dx,al           ; clk goes high
        inc     ax
        jmp     $+2             ; time delay
        mov     ah,al
        out     dx,al           ; clk goes low
        dec     ch
        jnz     clk_lp          ; four cycles

        or      al,a1+a0
        out     dx,al           ; start the A/D
        xor     al,a1
        out     dx,al           ; select mid nibble
        dec     dx

w8t_lp:
        in      al,dx           ; check status line
        test    al,status
        jnz     w8t_lp

        and     al,0F0h         ; save mid nibble
        mov     bl,al
        or      al,a1+start+clk ; add control bits
        inc     dx
        out     dx,al           ; select hi nibble
        jmp     $+2             ; time delay
        dec     dx
        in      al,dx           ; get high nibble
        xchg    al,ah
        inc     dx
        out     dx,al           ; select low nibble
        jmp     $+2             ; time delay
        dec     dx
        in      al,dx           ; read low nibble
        shr     ax, 4
        and     al,0Fh
        or      al,bl
        stosw                   ; store data away
        inc     dx
        loop    mainlp          ; repeat 35 times
```

```
mov     al, 0
out     dx,al           ; reset start, clk

pop     ds              ; restore ds, bp
pop     bp
ret     1*4             ; dump argument list

hda     endp
cseg    ends
        end
```

Appendix C

Reticon Photodiode Array - Data Acquisition Program

The assembly language program used to acquire the data from the EG&G Reticon photodiode array is listed below. Analog-to-digital (A/D) conversion was accomplished with a Burr Brown ADC700JH 16-bit successive approximation A/D converter. Timing and digital input-output (I/O) is provided by a Real Time Devices TC24 timer/counter and digital I/O board. This data acquisition program was written by the author and J.D.S Danielson using Microsoft Assembler.

```
page        66,132                  ;PAGE: [LENGTH=nn],[COLUMNS=nnn]
title     AD16BIT.ASM: Data acquisition (Laptop NIR) using the 16-bit ADC.

; Format for the QuickBasic CALLS statement is as follows:
;             CALLS(number of scans, number of pixels, local storage array name)
;     i.e.    CALLS(scans%, npts%, array&(1))
; The number of scans for signal averaging, the number of pixels to read and
; the address of the first point of the storage array are passed to this
; assembly program. The specified number of scans are summed into memory
; and the cumulative value for npts% data points are returned to the QuickBasic
; array ARRAY&. Binning and normalization will have to be done in QuickBasic if
; desired.

STAK            STRUC                   ; Structure representing the
                                        ; arrangement of elements on the
                                        ; stack at entry plus added items.
   FRAMES       DW    ?                 ; Copy of number of adds
   SAVEDI       DW    ?
   SAVESI       DW    ?
   SAVEDS       DW    ?                 ; Saved copy of DS reg.
   SAVEBP       DW    ?                 ; Saved copy of BP reg.

   RETADDR      DD    ?                 ; Return addr placed by caller. (DW)
   ARRAY        DD    ?                 ; 4 byte addr of ARG3.
   NPTS         DD    ?                 ; 4 byte addr of ARG2.
   NFRAMES      DD    ?                 ; Addr of number of frames.
STAK            ENDS
CODES
   SEGMENT      PARA PUBLIC 'CODE'
   ASSUME       CS:CODES,DS:CODES
   PUBLIC       AD16BIT                 ; Establishes entry as global
                                        ; (PUBLIC) & callable.
AD16BIT    PROC     FAR                 ; Basic 'Calls' are called as "FAR".
   PUSH             BP                  ; Save BP on stack.
   PUSH             DS                  ; Save DS on stack.
   PUSH             SI
   PUSH             DI
   PUSH             DX                  ; Phony - then get SP for based.
   MOV              BP,SP               ; Addressing of entire stack.
   POP              DX                  ; Remove phony.
   LDS              SI,[BP].NFRAMES     ; Get addr of number of frames.
   MOV              DX,[SI]             ; Get number of frames.
   PUSH             DX                  ; Put on stack.
```

```
portA   EQU     240h            ; Set portA equal to 240h.
portC   EQU     242h            ; Set portC equal to 242h.

        LES     DI,[BP].ARRAY   ; Get array address into ES:DI.
        LDS     SI,[BP].NPTS    ; Get address of npts into SI.
        MOV     CX,[SI]         ; Load counter with npts.
        XOR     AX,AX           ; Zero AX register.

INIT:
        STOSW                   ; Fill array memory with zeros.
        STOSW                   ; in preparation for data storage.
        LOOP    INIT

        IN      AL,21h          ; TOD interrupt.
        OR      AL,1
        OUT     21h,AL

FRAME:
        MOV     DX,portC        ; Port C input.
        LDS     SI,[BP].NPTS    ; Set address of number of points.
        MOV     CX,[SI]         ; Put in CX for counter.
        LDS     SI,[BP].ARRAY   ; Array addr into DS:SI for LODSW.
        LES     DI,[BP].ARRAY   ; Ditto, for STOSW.

WAIT_LO:
        IN      AL,DX           ; Monitor bit 5 and wait
        TEST    AL,20h          ; for frame clock to
        JZ      WAIT_LO         ; go high.

WAIT_HI:                        ; Monitor bit 5 and wait
        IN      AL,DX           ; for frame clock to go
        TEST    AL,20h          ; low indicating start of
        JNZ     WAIT_HI         ; new frame.

PIXEL:
        MOV     DX,portC        ; Get an array LO WORD.
        MOV     AL,7h           ; Assert bit-3 LO-BYTE (HI).
        OUT     DX,AL

AD_HI:
        IN      AL,DX           ; Monitor bit 8 and wait
        TEST    AL,80h          ; for 'hi' indicating
        JZ      AD_HI           ; A/D busy.
```

```
AD_LO:
    IN          AL,DX           ; Monitor bit 8 and wait
    TEST        AL,80h          ; for 'lo' indicating
    JNZ         AD_LO           ; A/D conversion complete.

    MOV         DX,portA        ; Port A input.
    IN          AL,DX           ; Get low byte.
    MOV         BL,AL           ; Save low byte in AH.
    MOV         DX,portC        ; Port C input.
    MOV         AL,3h           ; Assert bit-3 HI-BYTE (LO).
    OUT         DX,AL

    MOV         DX,portA        ; Port A input.
    IN          AL,DX           ; Get high byte.
    MOV         BH,AL           ; Put bytes in proper order.
    LODSW

    ADD         AX,BX           ; Sum value with previous sum
    STOSW                       ; and store it in AX.

    LODSW                       ; Get HI order word.
    ADC         AX,0            ; Add carry to it.
    STOSW                       ; Store HI word in AX.
    LOOP        PIXEL           ; Keep it up until CX => 0.

    SUB         [BP].FRAMES,1   ; Decrement loops counter.
    JNZ         FRAME           ; Do loop over if not zero.

    IN          AL,21h          ; Reset TOD interrupt.
    AND         AL,0feh
    OUT         21h,AL

    POP         DX              ; Get rid of temp stores on stack
    POP         DI              ; and pop the saved registers.
    POP         SI
    POP         DS              ; Restore DS from stack.
    POP         BP              ; Restore BP from stack.

    RET         4*3             ; Skip <n> things that had been
                                ; passed on stack : n = 4 * <#
                                ; ARGS> .
```

```
AD16BIT     ENDP        ; End PUBLIC user process .

CODES       ENDS        ; Marks end of user area
                        ; (SEGMENT).
            END         ; Marks end of assembly, end of file.
```

Appendix D

Instrument Control Software

The QuickBasic program used to control the instrument described in Chapter 3 is listed below. The program calls the assembly language program "AD16BIT.ASM" listed in Appendix C for data acquisition using the EG&G Reticon RL1024S photodiode array. All timing and instrument settings are software defined and interfaced to the instrument through the Real Time Devices TC24 digital I/O board. Base address of the RTD board is &H240. All software code dealing with graphical display has been omitted from the program listed below for sake of conciseness and ease of readability. Portions of the following program were written by J. D. S. Danielson.

```
' ********************** PROGRAM SHELL ***************************

DEFINT A-Z
DECLARE SUB ARRAYSTDEV ( )
DECLARE SUB AUTOLAMPINTENSITY (threshold&)
DECLARE SUB CALIBRATE (C1POS%, C1NEG%, C2%, integrationtime%)
DECLARE SUB CLOCK (C1POS%, C1NEG%, C2%)
DECLARE SUB DARK ( )
DECLARE SUB DEMO ( )
DECLARE SUB DISPLAYSHELL ( )
DECLARE SUB DISPLAYSHELL1 ( )
DECLARE SUB GETDATA ( )
DECLARE SUB LAMP (onoff$, updown$, steps%)
DECLARE SUB LAMPADJUST (lampmax&)
DECLARE SUB NOISE (integrationtime%)
DECLARE SUB PRINTDATA ()
DECLARE SUB REFERENCE ( )
DECLARE SUB SAMPLE (samplenum%, filename$)
DECLARE SUB SHUTTER (condition$)
DECLARE SUB TEMP (updown$, steps%)
DECLARE SUB XAXIS (XMIN%, XMAX%)
DECLARE SUB YAXISINTENSITY ( )
DECLARE SUB YAXISABSORBANCE ( )

'                    Global Variables

COMMON SHARED B%, pixels%, frames%, addrpA%, addrpB%, addrpC%
COMMON SHARED PortBdata%, PortCdata%, bin%, strt%, fin%, pixeltime%
COMMON SHARED samplenum%, filename$, lampmax&, npts%, scans%
CONST low& = 0, high& = 65536, version$ = "Version 1.0"

CLEAR , , 5000: SCREEN 2: CLS


'                    Initial Set-up Conditions

pixels% = 1024: frames% = 1: bin% = 1: integrationtime% = 50: scans% = 64
lampthreshold& = 95: npts% = 1012 / bin%: samplenum% = 0
strt% = 7: filename$ = "test": detectortemp% = 10
fin% = 1018: threshold& = lampthreshold& * 655.36

DIM SHARED array&(pixels%): DIM SHARED refer(1 TO npts%) AS SINGLE
```

```
'                    Board Addresses

B% = &H240: addrpA% = B% + 0: addrpB% = B% + 1: addrpC% = B% + 2

'      8255 PPI mode (ports A & Chi: IN; ports B & Clo: out  = &H98)

PPI.MODE% = &H98
OUT B% + 3, PPI.MODE%                    'Set 8255 PPI mode RIGHT NOW!
OUT addrpC%, &HF                         'UN-assert READ(L) and LOBYTE(L)
PortBdata% = &HFE
OUT addrpB%, PortBdata%          'Deselect lamp and temp pots, close shutter

'              Start timer for 25 uS pixels and 50 mS frames

C1POS% = 50: C1NEG% = 75:C2% = 2000
CALL CLOCK(C1POS%, C1NEG%, C2%)

CALL LAMP("ON", "UP", 30)
CALL TEMP("DOWN", 100)
CALL TEMP("UP", detectortemp% * 2.1256 + 11.786)

'********************** MAIN MENU SCREEN ************************

mainmenu:

   CLS 0                                                        'Activate
   FOR n = 1 TO 5: KEY(n) ON: NEXT: KEY(10) ON                  'function keys
     ON KEY(1) GOSUB CALIBRATIONROUTINE
     ON KEY(2) GOSUB DEMOROUTINE
     ON KEY(3) GOSUB DIAGNOSTICROUTINES
     ON KEY(4) GOSUB DATAACQUISITION
     ON KEY(5) GOSUB DOSSHELL
     ON KEY(10) GOSUB PROGRAMEND
   WHILE INKEY$ = "": WEND                          'Waiting for user selection
   GOTO DATAACQUISITION

CALIBRATIONROUTINE:

   FOR n = 1 TO 10: KEY(n) OFF: NEXT
   CALL CALIBRATE(C1POS%, C1NEG%, C2%, integrationtime%)
   RETURN mainmenu                                  'Pass program execution to
                                                                 'calibration routine
```

```
DEMOROUTINE:

   FOR n = 1 TO 10: KEY(n) OFF: NEXT
   CALL DEMO                                    'Pass program execution
   RETURN mainmenu                                  'to demo sub-routine

DIAGNOSTICROUTINES:

diagnosticsmenu:

   CLS 0
   FOR n = 1 TO 10: KEY(n) ON: NEXT
     ON KEY(1) GOSUB setcounters
     ON KEY(2) GOSUB setlamp
     ON KEY(3) GOSUB dataget
     ON KEY(4) GOSUB setshutter
     ON KEY(5) GOSUB settemperature
     ON KEY(6) GOSUB inttoport
     ON KEY(7) GOSUB dataprint
     ON KEY(8) GOSUB arraystandarddeviation
     ON KEY(9) GOSUB test
     ON KEY(10) GOSUB pulseppi
   WHILE INKEY$ = "": WEND
   GOTO mainmenu

setcounters:

   FOR n = 1 TO 10: KEY(n) OFF: NEXT          'get parameters for timer chip

   PRINT USING "Counter 1 pos count [####]: "; C1POS%;
   INPUT "", rply%
     IF rply% < > 0 THEN C1POS% = rply%
   PRINT USING "Counter 1 neg count [####]: "; C1NEG%;
     INPUT "", rply%
     IF rply% < > 0 THEN C1NEG% = rply%
   PRINT USING "Counter 2 count [####]: "; C2%;
     INPUT "", rply%
     IF rply% < > 0 THEN C2% = rply%
   CALL CLOCK(C1POS%, C1NEG%, C2%)
   RETURN diagnosticsmenu

setlamp:

   FOR n = 1 TO 10: KEY(n) OFF: NEXT
```

```
    LOCATE 24, 1: PRINT USING "Lampset percent [###]: "; lampinten%;
    INPUT "", rply$
      IF rply$ < > "" THEN lampinten% = VAL(rply$)
      IF lampinten% = 0 THEN
        CALL LAMP("OFF", "DOWN", 100)
      ELSE
        CALL LAMP("ON", "DOWN", 100)
        CALL LAMP("ON", "UP", lampinten%)
      END IF
    RETURN diagnosticsmenu

dataget:

    FOR n = 1 TO 10: KEY(n) OFF: NEXT
    CALL GETDATA
    RETURN diagnosticsmenu

setshutter:

    FOR n = 1 TO 10: KEY(n) OFF: NEXT
    LOCATE 24, 1: INPUT "Shutter open (O) or closed (C): ", rply$
    rply$ = UCASE$(rply$)

    IF rply$ = "" THEN
    ELSEIF rply$ = "O" THEN
      CALL SHUTTER("OPEN")
    ELSEIF rply$ = "C" THEN
      CALL SHUTTER("CLOSE")
    END IF
    RETURN diagnosticsmenu

settemperature:

    FOR n = 1 TO 10: KEY(n) OFF: NEXT
    LOCATE 23, 1: PRINT USING "Temperture (10 to 40) [###.#]: "; tempr!;
    INPUT "", rply$
    IF rply$ < > "" THEN tempr! = VAL(rply$)
      steps% = tempr! * 2.1256 + 11.786
    LOCATE 24, 1: PRINT "temp = "; tempr!, "steps = "; steps%
      FOR i = 1 TO 15000: a! = SQR(29): NEXT                '2 sec delay loop

    CALL TEMP("DOWN", 100): CALL TEMP("UP", steps%)
    RETURN diagnosticsmenu
```

```
inttoport:

    FOR n = 1 TO 10: KEY(n) OFF: NEXT
    LOCATE 24, 45: PRINT "(Enter >255 to Exit)"
    DO
      PortBdataRead% = INP(addrpB%)
      LOCATE 24, 6: PRINT "    "
      LOCATE 23, 1: PRINT "Port B: ", PortBdataRead%, PortBdata%
      INPUT "Int: ", intgr%
      IF intgr% > 255 THEN GOTO exittt
      PortBdata% = intgr%
      OUT addrpB%, PortBdata%
    LOOP
exittt:
    RETURN diagnosticsmenu

dataprint:

    FOR n = 1 TO 10: KEY(n) OFF: NEXT
    CALL PRINTDATA
    RETURN diagnosticsmenu

arraystandarddeviation:

    FOR n = 1 TO 10: KEY(n) OFF: NEXT
    CALL ARRAYSTDEV
    RETURN diagnosticsmenu

test:

    FOR n = 1 TO 10: KEY(n) OFF: NEXT
    LOCATE 24, 48: PRINT USING "Port B Address - ####"; addrpB%
    LOCATE 24, 12: PRINT USING "Port B Data - ####"; PortBdata%
    OUT addrpB%, PortBdata%
      FOR i = 1 TO 15000: a! = SQR(29): NEXT                '2 sec delay loop
    RETURN diagnosticsmenu

pulseppi:

    FOR n = 1 TO 10: KEY(n) OFF: NEXT
    LOCATE 24, 1: PRINT "Pulsing.  Strike any key to continue..."
    DO
      IF INKEY$ <> "" THEN GOTO endloop
      OUT B% + 1, intgr%
```

```
      intgr% = intgr% + 1
      intgr% = intgr% AND &HFF
    LOOP
endloop:
    RETURN diagnosticsmenu
    GOTO mainmenu


DATAACQUISITION:

    CALL SHUTTER("close")
    FOR n = 1 TO 10: KEY(n) OFF: NEXT
    CLS 0

    FOR n = 2 TO 7: KEY(n) ON: NEXT
      ON KEY(2) GOSUB CHANGEPARAMETERS
      ON KEY(3) GOSUB AUTOSAMPLE
      ON KEY(4) GOSUB CHANGELAMPINTENSITY
      ON KEY(5) GOSUB ACQUIREDARK
      ON KEY(6) GOSUB ACQUIREREFERENCE
      ON KEY(7) GOSUB ACQUIRESAMPLE
    WHILE INKEY$ = "": WEND
    FOR n = 1 TO 10: KEY(n) OFF: NEXT
    GOTO mainmenu

CHANGEPARAMETERS:

    CLS 0
    FOR n = 2 TO 7: KEY(n) ON: NEXT
      ON KEY(2) GOSUB changescans
      ON KEY(3) GOSUB changeintegrationtime
      ON KEY(4) GOSUB changelampthreshold
      ON KEY(5) GOSUB changefilename
      ON KEY(6) GOSUB changebin
      ON KEY(7) GOSUB changedetectortemperature
    WHILE INKEY$ = "": WEND
    RETURN DATAACQUISITION

changescans:

    FOR n = 1 TO 6: KEY(n) OFF: NEXT: KEY(10) OFF
    LOCATE 23, 3:  INPUT " Desired Number of Scans: ", scans%
    RETURN CHANGEPARAMETERS
```

```
changeintegrationtime:

    FOR n = 1 TO 6: KEY(n) OFF: NEXT: KEY(10) OFF
    LOCATE 22, 3:  INPUT "Desired Integration Time: ", integrationtime%
        IF integrationtime% < 47 THEN
        BEEP: GOTO changeintegrationtime
      ELSEIF integrationtime% > 819 THEN
        BEEP: GOTO changeintegrationtime
      END IF
    C2% = integrationtime% / (((C1POS% + C1NEG%) / 5) / 1000)
    CALL CLOCK(C1POS%, C1NEG%, C2%)
    RETURN CHANGEPARAMETERS

changelampthreshold:

    FOR n = 1 TO 6: KEY(n) OFF: NEXT: KEY(10) OFF
    LOCATE 22, 4:  INPUT "Desired Lamp Threshold: ", lampthreshold&
      IF lampthreshold& < 1 THEN
        BEEP: GOTO changelampthreshold
      ELSEIF lampthreshold& > 100 THEN
        BEEP: GOTO changelampthreshold
      END IF
    threshold& = lampthreshold& * 655.36
    RETURN CHANGEPARAMETERS

changefilename:

    FOR n = 1 TO 6: KEY(n) OFF: NEXT
    LOCATE 21, 4: INPUT "Desired Filename: ", filename$

    OPEN "c:\laptop\data\" + filename$ + ".DAT" FOR OUTPUT AS #1
      PRINT #1, 50, npts%, 0
    CLOSE #1

    samplenum% = 0
    RETURN CHANGEPARAMETERS

changebin:

    FOR n = 1 TO 6: KEY(n) OFF: NEXT
    LOCATE 23, 3:  INPUT " Desired Binning Number: ", bin%
      npts% = 1012 / bin%
      REDIM c(1 TO npts%) AS SINGLE
      REDIM d(1 TO npts%) AS SINGLE
```

```
    REDIM refer(1 TO npts%) AS SINGLE
  RETURN CHANGEPARAMETERS

changedetectortemperature:

  FOR n = 1 TO 6: KEY(n) OFF: NEXT
  LOCATE 22, 2:  INPUT "Desired Detector Temperature: ", detectortemp%
    steps% = detectortemperature% * 2.1256 + 11.786
    CALL TEMP("DOWN", 100)
    CALL TEMP("UP", steps%)
  RETURN CHANGEPARAMETERS

AUTOSAMPLE:

  CLS 0
  CALL AUTOLAMPINTENSITY(threshold&)
  CALL REFERENCE
  WINDOW: VIEW
  CALL SAMPLE(samplenum%, filename$)
  GOTO sampleend

ACQUIREDARK:

  CALL DARK                                    'Acquire dark measurement
darkend:
  WINDOW: VIEW
  KEY(1) OFF
  RETURN DATAACQUISITION

ACQUIREREFERENCE:

  CALL REFERENCE                             'Acquire reference measurement
refend:
  WINDOW: VIEW
  KEY(1) OFF
  RETURN DATAACQUISITION

ACQUIRESAMPLE:

  CALL SAMPLE(samplenum%, filename$)          'Acquire sample spectrum
  GOTO sampleend
sampleend:
```

```
    VIEW: WINDOW
    samplenum% = samplenum% - 1        'Resets samplenum to previous value
    FOR i = 1 TO 6: KEY(i) OFF: NEXT
    RETURN DATAACQUISITION

CHANGELAMPINTENSITY:

    FOR n = 1 TO 6: KEY(n) OFF: NEXT
    KEY(1) ON: ON KEY(1) GOSUB DATAACQUISITION
    CLS 0
    WHILE INKEY$ = "": WEND
    KEY(1) OFF
    CALL AUTOLAMPINTENSITY(threshold&)
    WHILE INKEY$ = "": WEND
    RETURN DATAACQUISITION

DOSSHELL:

    CLS 0
    SHELL
    RETURN mainmenu

PROGRAMEND:

    SCREEN 0
    CLS
    CALL LAMP("OFF", "DOWN", 0)
    CALL TEMP("DOWN", 100)
    CALL TEMP("UP", 25 * 2.1256 + 11.786)

END


'       ************ Array Standard Deviation Sub-routine ************

DEFSNG A-Z
SUB ARRAYSTDEV
REDIM array&(1 TO pixels%): REDIM array1&(1 TO pixels%)

CLS 0
acquire2:

    CALLS ad16bit(1, pixels%, array&(1))
    CALLS ad16bit(1, pixels%, array1&(1))
```

```
    nmin& = high&: nmax& = low&
    sum = 0: sumsqdev = 0

    FOR i% = strt% TO fin%
      array&(i%) = array&(i%) - array1&(i%)          'subtract the second array
      sum = sum + array&(i%)
      IF array&(i%) < nmin& THEN
        nmin& = array&(i%)
      END IF
      IF array&(i%) > nmax& THEN
        nmax& = array&(i%)
      END IF
    NEXT i%

    IF nmin& = nmax& THEN nmax& = nmin& + 1
    mean = sum / (fin% - strt% + 1)

    FOR i% = strt% TO fin%
      sumsqdev = sumsqdev + (mean - array&(i%)) ^ 2
    NEXT i%
    stdev = SQR(sumsqdev / (fin% - strt%))

    CLS 0
    LOCATE 25, 1: PRINT "[H] TO HOLD SPECTRA ON SCREEN  [X] TO EXIT"
    WINDOW (strt%, nmin&)-(fin%, nmax&)
    PSET (strt%, array&(strt%))
    FOR i% = strt% + 1 TO fin%: LINE -(i%, array&(i%)): NEXT
    rply$ = UCASE$(INKEY$)
      IF rply$ = "H" THEN
        rply$ = INPUT$(1): GOTO acquire2
      ELSEIF rply$ <> "X" THEN
        GOTO acquire2
      END IF
    WINDOW: VIEW

END SUB


'****************** AUTOLAMPINTENSITY SUB-ROUTINE ******************

SUB AUTOLAMPINTENSITY (threshold&)
CALL LAMP("ON", "UP", 1)
CALL SHUTTER("OPEN")
```

```
lampsetting = 0                          'Initializes counter for lamp adjustment

CLS 0
   CALL LAMPADJUST(lampmax&)
   IF lampmax& > threshold& THEN GOTO decrease

increase:
   IF lampmax& < threshold& THEN
     CALL LAMP("ON", "UP", 1)
     CALL LAMPADJUST(lampmax&)
     lampsetting = lampsetting + 1
     IF lampsetting = 100 THEN GOTO continue
     GOTO increase
   ELSEIF lampmax& > threshold& THEN
     GOTO decrease
   END IF

decrease:
   IF lampmax& > threshold& THEN
     CALL LAMP("ON", "DOWN", 1)
     CALL LAMPADJUST(lampmax&)
     lampsetting = lampsetting + 1
   IF lampsetting = 100 THEN GOTO continue
   GOTO decrease
   END IF
   GOTO continue

continue:
   BEEP: CALL SHUTTER("CLOSE")

END SUB


'********************** CALIBRATION SUB-ROUTINE *********************

SUB CALIBRATE (C1POS%, C1NEG%, C2%, integrationtime%)

CALL LAMP("ON", "DOWN", 100)
CLS 0
   LOCATE 9, 10: PRINT "Light Source Intensity";
   LOCATE 11, 15: PRINT "(1 - 100 %)";
   LOCATE 17, 9: INPUT "Enter Selection Now: ", light%
   CALL LAMP("ON", "UP", light%)                    'Set lamp intensity
```

```
calib:
   LOCATE 9, 48: PRINT "Desired Integration Time";
   LOCATE 11, 55: PRINT "47 mSec MIN";
   LOCATE 12, 54: PRINT "819 mSec MAX";
   LOCATE 17, 50: INPUT "Enter Selection Now: ", integrationtime%

   IF integrationtime% = 0 THEN                          'Return to main menu
     GOTO endcalib
   ELSEIF integrationtime% < 47 THEN                   'Prevent below minimum
     BEEP: LOCATE 17, 71: PRINT "   "                          'integration time
     GOTO calib
   ELSEIF integrationtime% > 819 THEN                  'Prevent above maximum
     BEEP: LOCATE 17, 71: PRINT "   "                          'integration time
     GOTO calib
   ELSE
   END IF

   C2% = integrationtime% / (((C1POS% + C1NEG%) / 5) / 1000)
   CALL CLOCK(C1POS%, C1NEG%, C2%)              'Set new integration time

   LOCATE 22, 23: INPUT "Enter Starting Diode"; XMIN%
   IF XMIN% = 0 THEN XMIN% = 1
   LOCATE 22, 22:
   PRINT USING "Enter Ending Diode ( <#### )"; 1012 / bin%
   LOCATE 22, 50: INPUT ""; XMAX%
     IF XMAX% = 0 THEN XMAX% = 1012 / bin%

   CALL SHUTTER("OPEN")
   Q = 2
   WHILE Q >= 1
   LOCATE 22, 22
   PRINT "Do you want to signal average? (Y/N)   ",
350  Q$ = INPUT$(1): Q = INSTR("YNyn", Q$)
   IF Q = 0 GOTO 350
   ON Q GOSUB 352, 351, 352, 351
   WEND
351  numscans% = 1
   GOTO start
352  LOCATE 22, 22
   INPUT " How many scans to signal average?  ", numscans%

start:
   CLS 0
   VIEW (180, 28)-(626, 122), , 1
```

```
DO                                                    'Calibration display loop
   REDIM c(1 TO npts%) AS SINGLE: REDIM array&(1 TO pixels%)
   CALLS ad16bit(numscans%, pixels%, array&(1))
   FOR i = 1 TO (1012 - bin% + 1) STEP bin%
     FOR x = 1 TO bin%
       c((npts% + 1) - ((i + bin% - 1) / bin%)) = c((npts% + 1) -
              ((i + bin% - 1) / bin%)) + array&(i + x + 5)
     NEXT x
   NEXT i

   FOR i = 1 TO npts%                                 'Normalize spectrum
     c(i) = c(i) / (bin% * numscans%)                      'to binning size
   NEXT

   dmin! = high&: dmax! = low&: maxi% = 0
   FOR i = XMIN% TO XMAX%
     IF c(i) < dmin! THEN dmin! = c(i)
     IF c(i) > dmax! THEN dmax! = c(i)
     IF c(i) = dmax! THEN maxi% = i
   NEXT
   WINDOW (XMIN%, low&)-(XMAX%, high&)
    CLS 1

   PSET (1, c(XMIN%))                                        'Plot spectrum
   FOR i = XMIN% + 1 TO XMAX%: LINE -(i, c(i)): NEXT

   LOOP UNTIL INKEY$ < > ""
   CALL SHUTTER("CLOSE")
   WINDOW

endcalib:

END SUB


'***************** A/D TIMER SETTINGS SUB-ROUTINE *****************
'
SUB CLOCK (C1POS%, C1NEG%, C2%)

'set up counter/timer AMD Am9513  --  counter/timer master mode = &H0000
   MM.LO% = &H0: MM.HI% = &H0

'define counter mode bytes
```

```
    C1M.LO% = &H62: C1M.HI% = &HB
    C2M.LO% = &H21: C2M.HI% = &H1

'isolate high and low bytes of counter presets
    C1POS.LO% = C1POS% AND &HFF: C1POS.HI% = C1POS% \ 256
    C1NEG.LO% = C1NEG% AND &HFF: C1NEG.HI% = C1NEG% \ 256
    C2.LO% = C2% AND &HFF: C2.HI% = C2% \ 256

'initialize counter/timer
    OUT B% + 5, &HFF                                    'reset
    OUT B% + 5, &H5F                                    'zero all counters
    OUT B% + 5, &H17                                    'point to master mode register
    OUT B% + 4, MM.LO%                                  'master control low byte
    OUT B% + 4, MM.HI%                                  'master control hy byte
    OUT B% + 5, &H1                                     'point to counter #1 mode
    OUT B% + 4, C1M.LO%                                 'counter #1 mode lo
    OUT B% + 4, C1M.HI%                                 'counter #1 mode hi
    OUT B% + 5, &H2                                     'point to counter #2 mode
    OUT B% + 4, C2M.LO%                                 'counter #2 mode lo
    OUT B% + 4, C2M.HI%                                 'counter #2 mode hi

'set counter load and hold registers
    OUT B% + 5, &H9                                     'point to counter #1 load
    OUT B% + 4, C1NEG.LO%                               'other half cycle count lo
    OUT B% + 4, C1NEG.HI%                               'other half cycle count hi
    OUT B% + 5, &H11                                    'point to counter #1 hold
    OUT B% + 4, C1POS.LO%                               'half cycle count lo
    OUT B% + 4, C1POS.HI%                               'half cycle count hi
    OUT B% + 5, &HA                                     'point to counter #2 load
    OUT B% + 4, C2.LO%                                  'counter #2 load lo
    OUT B% + 4, C2.HI%                                  'counter #2 load hi
    OUT B% + 5, &H3F                                    'arm counters #1 and #2 and go

END SUB


'***************** DARK MEASUREMENT SUBROUTINE *****************

SUB DARK
REDIM array&(1 TO pixels%): REDIM d!(1 TO npts%)
    FOR n = 1 TO 7: KEY(n) OFF: NEXT: KEY(10) OFF

CLS 0
```

```
    CALL SHUTTER("CLOSE")
    CALLS ad16bit(scans%, pixels%, array&(1)): BEEP

    FOR i = 1 TO (1012 - bin% + 1) STEP bin%
      FOR x = 1 TO bin%
        d!((npts% + 1) - ((i + bin% - 1) / bin%)) = d!((npts% + 1) -
              ((i + bin% - 1) / bin%)) + array&(i + x + 5)
      NEXT x
    NEXT i

    sumd! = 0: dmin! = high&: dmax! = low&
    FOR i = 1 TO npts%
      d!(i) = d!(i) / (bin% * scans%)                    'Normalize spectrum
      sumd! = d!(i) + sumd!                                    'Sum all points
      IF d!(i) < dmin! THEN dmin! = d!(i)                     'Calculate min
      IF d!(i) > dmax! THEN dmax! = d!(i)                   'and max values
    NEXT
    avgd! = sumd! / (npts%)

    CLS 0
    VIEW (180, 28)-(626, 122), , 1

    WINDOW (1, dmin!)-(npts%, dmax!)
    CLS 1
    PSET (1, d!(1))
    FOR i = 2 TO npts%: LINE -(i, d!(i)): NEXT

    OPEN "c:\laptop\data\dark.dat" FOR OUTPUT AS #1
      PRINT #1, 1, npts%, 0                     'Saves data in ASCII format
      FOR i = 1 TO npts%
        WRITE #1, d!(i)
      NEXT
    CLOSE #1

    WHILE INKEY$ = "": WEND
enddark:

END SUB


'************************ DEMO SUB-ROUTINE ************************

SUB DEMO
```

```
newnpts% = 35
CLS 0
   LOCATE 3, 29: PRINT "SAMPLE ABSORPTION SPECTRA"
   LOCATE 7, 17: PRINT "n-Heptane"
   VIEW (30, 58)-(300, 108), , 1
   DIM H(1 TO newnpts%) AS SINGLE

   OPEN "c:\laptop\demo\" + "HEPTANE.DAT" FOR INPUT AS #1
     FOR i = 1 TO newnpts%: INPUT #1, H(i): NEXT
   CLOSE #1

   dmin! = 4095: dmax! = -4095                          'Scaling routine to
   FOR i = 1 TO newnpts%                                'fit spectrum to view
     IF H(i) < dmin! THEN dmin! = H(i)                                 'window
   IF H(i) > dmax! THEN dmax! = H(i)
   NEXT

   WINDOW (1, dmin!)-(newnpts%, dmax!)                  'Plot the spectrum
   PSET (1, H(1)): FOR i = 2 TO newnpts%: LINE -(i, H(i)): NEXT

   VIEW (330, 58)-(600, 108), , 1
   DIM c6h6(1 TO newnpts%) AS SINGLE
   LOCATE 7, 17: PRINT "n-Heptane                       Benzene  "

   OPEN "c:\laptop\demo\" + "BENZENE.DAT" FOR INPUT AS #1
     FOR i = 1 TO newnpts%: INPUT #1, c6h6(i): NEXT
   CLOSE #1

   min! = 4095: dmax! = -4095                           'Scaline routine to
   FOR i = 1 TO newnpts%                                'fit spectrum to view
     IF c6h6(i) < dmin! THEN dmin! = c6h6(i)                           'window
     IF c6h6(i) > dmax! THEN dmax! = c6h6(i)
   NEXT i

   WINDOW (1, dmin!)-(newnpts%, dmax!)                  'Plot the spectrum
   PSET (1, c6h6(1)): FOR i = 2 TO newnpts%: LINE -(i, c6h6(i)): NEXT
   VIEW (30, 130)-(300, 180), , 1
   DIM T(1 TO newnpts%) AS SINGLE
   LOCATE 16, 17: PRINT "Isooctane"

   OPEN "c:\laptop\demo\" + "ISOOCT.DAT" FOR INPUT AS #1
     FOR i = 1 TO newnpts%: INPUT #1, T(i): NEXT
   CLOSE #1
```

```
    dmin! = 4095: dmax! = -4095                          'Scaling routine to
    FOR i = 2 TO newnpts%                                'fit spectrum to view
      IF T(i) < dmin! THEN dmin! = T(i)                  'window
      IF T(i) > dmax! THEN dmax! = T(i)
    NEXT i

    WINDOW (1, dmin!)-(newnpts% , dmax!)                 'Plot the spectrum
    PSET (1, T(1)): FOR i = 2 TO newnpts%: LINE -(i, T(i)): NEXT

    VIEW (330, 130)-(600, 180), , 1
    DIM u(1 TO newnpts%) AS SINGLE
    LOCATE 16, 17: PRINT "Isooctane                    Unleaded Gasoline"

    OPEN "c:\laptop\demo\" + "UNLEADED.DAT" FOR INPUT AS #1
      FOR i = 1 TO newnpts%: INPUT #1, u(i): NEXT
    CLOSE #1

    dmin! = 4095: dmax! = -4095                          'Scaling routine to
    FOR x = 1 TO newnpts%                                'fit spectrum to view
      IF u(x) < dmin! THEN dmin! = u(x)                  'window
      IF u(x) > dmax! THEN dmax! = u(x)
    NEXT x

    WINDOW (1, dmin!)-(newnpts%, dmax!): PSET (1, u(1))
    FOR x = 2 TO newnpts%: LINE -(x, u(x)): NEXT x

    WHILE INKEY$ = "": WEND
    WINDOW

END SUB


'********************** GET DATA SUB-ROUTINE **********************

SUB GETDATA

    PRINT USING "Number of data points [####]: "; pixels%;
    INPUT "", rply%
    IF rply% > 0 THEN pixels% = rply% + 6
    REDIM array&(1 TO pixels%)

CLS 0
acquire:
```

```
    CALLS ad16bit(1, pixels%, array&(1))
    nmin& = 65535: nmax& = 0: sum& = 0: mean! = 0: sumsqdev! = 0
    FOR i% = 7 TO pixels% - 6
      sum& = sum& + array&(i%)
      IF array&(i%) < nmin& THEN
        nmin& = array&(i%)
      END IF
      IF array&(i%) > nmax& THEN
        nmax& = array&(i%)
      END IF
    NEXT
    mean! = sum& / (pixels% - 12)

    FOR i% = 7 TO pixels% - 6
      sumsqdev! = sumsqdev! + (mean! - array&(i%)) ^ 2
    NEXT
    stdev! = SQR(sumsqdev! / (pixels% - 13))

    IF nmin& = nmax& THEN nmax& = nmin& + 1
    WINDOW (1, nmin&)-(pixels%, nmax&)

    CLS 0
    LOCATE 25, 1: PRINT "[H] TO HOLD SPECTRA ON SCREEN  [X] TO EXIT"
    PSET (1, array&(7))
    FOR i% = 8 TO pixels% - 6
      LINE -(i%, array&(i%))
    NEXT

    rply$ = UCASE$(INKEY$)
    IF rply$ = "H" THEN
      rply$ = INPUT$(1)
      GOTO acquire
    ELSEIF rply$ < > "X" THEN
      GOTO acquire
    END IF

    CLS
    WINDOW: VIEW
    pixels% = 1024

END SUB
```

```
'************************* LAMP SUB-ROUTINE *************************

SUB LAMP (onoff$, updown$, steps%)

'Function names are integers with a 1 in the relevent bit position.
'The state (always 0 for pot adjust functions) following the function name
'shows the bit state that accomplishes the task suggested by the name.
'To set a bit to 1, use < PortBdata% OR FunctionName0% >
'To set a bit to zero, use < PortBdata% AND NOT FunctionName0% >

    LampDown0% = &H40: LampSel0% = &H80
    LampStep0% = &H20: LampOn0% = &H10

    PortBdata% = PortBdata% AND NOT LampSel0%
    OUT addrpB%, PortBdata%

    IF onoff$ = "ON" THEN
      PortBdata% = PortBdata% AND NOT LampOn0%          'turn lamp on
    ELSE
      PortBdata% = PortBdata% OR LampOn0%               'turn lamp off
    END IF

    IF updown$ = "UP" THEN
      PortBdata% = PortBdata% OR LampDown0%               'set 1 = up
    ELSEIF updown$ = "DOWN" THEN
      PortBdata% = PortBdata% AND NOT LampDown0%        'set 0 = down
    END IF
    OUT addrpB%, PortBdata%

    FOR i% = 1 TO steps%
      PortBdata% = PortBdata% AND NOT LampStep0%        'lower step bit
      OUT addrpB%, PortBdata%
      PortBdata% = PortBdata% OR LampStep0%             'raise step bit
      OUT addrpB%, PortBdata%
    NEXT
    PortBdata% = PortBdata% OR LampSel0%
    OUT addrpB%, PortBdata%

END SUB

'******************** LAMPADJUST SUB-ROUTINE ********************
```

```
SUB LAMPADJUST (lampmax&)

    REDIM array&(1 TO pixels%)
    CALLS ad16bit(1, pixels%, array&(1))

    lampmax& = 0
    FOR i = 1 TO pixels%
      IF array&(i) > lampmax& THEN lampmax& = array&(i)
    NEXT

END SUB


'********************** PRINTDATA SUB-ROUTINE **********************

SUB PRINTDATA

    CLS 0
    LOCATE 1, 1: PRINT USING "Number of data points [####]:"; pixels%;
      INPUT "", rply%
      IF rply% > 0 THEN pixels% = rply%

acquire1:

    CALLS ad16bit(1, pixels%, array&(1))
    nmin& = 65536: nmax% = 0: sum& = 0: sumsqdev& = 0

    FOR i% = 7 TO pixels% - 6
      sum& = sum& + array&(i%)
      IF array&(i%) < nmin& THEN nmin& = array&(i%)
      IF array&(i%) > nmax& THEN nmax& = array&(i%)
    NEXT
    mean = sum& / (pixels% - 12)

    FOR i% = 7 TO pixels% - 6
      sumsqdev& = sumsqdev& + (mean - array&(i%)) ^ 2
    NEXT
    stdev = SQR(sumsqdev& / (pixels% - 13))

END SUB
```

```
'************* REFERENCE MEASUREMENT SUBROUTINE *************
'
SUB REFERENCE

    REDIM arrayd&(1 TO pixels%): REDIM array&(1 TO pixels%)
    DIM drk!(1 TO npts%): DIM ref!(1 TO npts%)
    REDIM refer!(1 TO npts%)

    FOR n = 1 TO 6: KEY(n) OFF: NEXT: KEY(10) OFF
    CALL SHUTTER("CLOSE")
    CLS 0

    CALLS ad16bit(scans%, pixels%, arrayd&(1))              'take dark reading
    CALL SHUTTER("OPEN")

    FOR i = 1 TO 15000: a! = SQR(29): NEXT                  '2 sec delay loop
    CALLS ad16bit(scans%, pixels%, array&(1))             'take ref. measurement
    BEEP
    CALL SHUTTER("CLOSE")

    FOR i = 1 TO (1012 - bin% + 1) STEP bin%
      FOR x = 1 TO bin%
        drk!((npts% + 1) - ((i + bin% - 1) / bin%)) = drk!((npts% + 1) -
              ((i + bin% - 1) / bin%)) + arrayd&(i + x + 5)
        ref!((npts% + 1) - ((i + bin% - 1) / bin%)) = ref!((npts% + 1) -
              ((i + bin% - 1) / bin%)) + array&(i + x + 5)
      NEXT x
    NEXT i

    dmin! = 4095: dmax! = -4095: maxi% = 0
    FOR i = 1 TO npts%
      drk!(i) = drk!(i) / (bin% * scans%)                 'Normalize spectrum
      ref!(i) = ref!(i) / (bin% * scans%)                 'Normalize spectrum
      IF ref!(i) < dmin! THEN dmin! = ref!(i)                     'Calculate min
      IF ref!(i) > dmax! THEN dmax! = ref!(i)                   'and max values
      IF ref!(i) = dmax! THEN maxi% = (i)
    NEXT

    CLS 0
    VIEW (180, 28)-(626, 122), , 1
    WINDOW (1, dmin!)-(npts%, dmax!)
    CLS 1
    PSET (1, ref!(1))
```

```
    FOR i = 2 TO npts%: LINE -(i, ref!(i)): NEXT
    FOR i = 1 TO npts%
      refer!(i) = ref!(i) - drk!(i)                          'Reference - dark
      IF refer!(i) < 1 THEN refer!(i) = 1
    NEXT

    OPEN "c:\laptop\data\refer.dat" FOR OUTPUT AS #1
      PRINT #1, 1, npts, 0
      FOR i = 1 TO npts%
        WRITE #1, ref!(i)
      NEXT
    CLOSE #1

    WHILE INKEY$ = "": WEND
endref:

END SUB


'**************** SAMPLE MEASUREMENT SUBROUTINE ****************

SUB SAMPLE (samplenum%, filename$)

    REDIM arrayd&(1 TO pixels%): REDIM array&(1 TO pixels%)
    REDIM drk!(1 TO npts%): REDIM sam!(1 TO npts%)
    REDIM samp!(1 TO npts%): REDIM a!(1 TO npts%)

    CLS 0
    FOR n = 1 TO 7: KEY(n) OFF: NEXT: KEY(10) OFF

    CALL SHUTTER("CLOSE")
    LOCATE 16, 11: INPUT "(0 TO QUIT):", samplenum%
    IF samplenum% = 0 THEN
      samplenum% = samplenum% + 1
      GOTO endsample
    END IF
    samplenum$ = STR$(samplenum%): samplenum$ = LTRIM$(samplenum$)

    CLS 0
    CALLS ad16bit(scans%, pixels%, arrayd&(1))              'take dark reading
      CALL SHUTTER("OPEN")
    FOR i = 1 TO 15000: a! = SQR(29): NEXT                  '2 sec delay loop
    CALLS ad16bit(scans%, pixels%, array&(1))               'take samp. reading
```

```
BEEP
CALL SHUTTER("CLOSE")

FOR i = 1 TO (1012 - bin% + 1) STEP bin%
  FOR x = 1 TO bin%
    drk!((npts% + 1) - ((i + bin% - 1) / bin%)) = drk!((npts% + 1) -
          ((i + bin% - 1) / bin%)) + arrayd&(i + x + 5)
    sam!((npts% + 1) - ((i + bin% - 1) / bin%)) = sam!((npts% + 1) -
          ((i + bin% - 1) / bin%)) + array&(i + x + 5)
  NEXT x
NEXT i

dmin! = 4095: dmax! = -4095
FOR i = 1 TO npts%
  drk!(i) = drk!(i) / (bin% * scans%)                'Normalize dark spectrum
  sam!(i) = sam!(i) / (bin% * scans%)                 'Normalize ref spectrum
  IF sam!(i) < dmin! THEN dmin! = sam!(i)
  IF sam!(i) > dmax! THEN dmax! = sam!(i)
NEXT

CLS 0
VIEW (180, 28)-(626, 122), , 1
WINDOW (1, dmin!)-(npts, dmax!)
CLS 1
PSET (1, sam!(1))
FOR i = 2 TO npts%: LINE -(i, sam!(i)): NEXT

FOR i = 1 TO npts%
  samp!(i) = sam!(i) - drk!(i)                                  'Sample - dark
  IF samp!(i) < 1 THEN samp!(i) = 1
  a!(i) = (LOG(refer!(i) / samp!(i))) / 2.302585093#          'Abs. calculation
NEXT
FOR i = 1 TO 15000: a! = SQR(29): NEXT                        '2 sec delay loop
WHILE INKEY$ = "": WEND

dmin! = 4095: dmax! = -4095
FOR i = 1 TO npts%
  IF a!(i) < dmin! THEN dmin! = a!(i)
  IF a!(i) > dmax! THEN dmax! = a!(i)
NEXT

CLS 0
WINDOW: VIEW
VIEW (180, 28)-(626, 122), , 1
```

```
    WINDOW (1, dmin!)-(npts%, dmax!)
    CLS 1
    PSET (1, a!(1))
    FOR i = 2 + 1 TO npts%: LINE -(i, a!(i)): NEXT

    OPEN "A", #1, "c:\laptop\data\" + filename$ + ".DAT"
      FOR i = 1 TO npts%
        WRITE #1, a(i)
      NEXT
    CLOSE #1

    samplenum% = samplenum% + 1
    GOTO endsample

endsample:

END SUB


'********************** SHUTTER SUB-ROUTINE **********************

SUB SHUTTER (condition$)

'Function names are integers with a 1 in the relevent bit position.
'The state following the function name shows the bit state that accomplishes
'the task suggested by the name.
'To set a bit to 1, use < PortBdata% OR FunctionName0% >
'To set a bit to zero, use < PortBdata% AND NOT FunctionName0% >

    ShutterOpen!% = &H1
    IF condition$ = "OPEN" THEN
      PortBdata% = PortBdata% OR ShutterOpen1%
    ELSE
      PortBdata% = PortBdata% AND NOT ShutterOpen1%
    END IF
    OUT addrpB%, PortBdata%

END SUB


'************************ TEMP SUB-ROUTINE ************************

SUB TEMP (updown$, steps%)
```

```
'Function names are integers with a 1 in the relevent bit position.
'The state (always 0 for pot adjust functions) following the function name
'shows the bit state that accomplishes the task suggested by the name.
'To set a bit to 1, use < PortBdata% OR FunctionName0% >
'To set a bit to zero, use < PortBdata% AND NOT FunctionName0% >

    TempSel0% = &H2: TempStep0% = &H4: TempDown0% = &H8
    IF updown$ = "UP" THEN
      PortBdata% = PortBdata% OR TempDown0%
    ELSEIF updown$ = "DOWN" THEN
      PortBdata% = PortBdata% AND NOT TempDown0%
    END IF

    PortBdata% = PortBdata% AND NOT TempSel0%          'select temp pot
    OUT addrpB%, PortBdata%                                 'send to PPI

    FOR i% = 1 TO steps%
      PortBdata% = PortBdata% AND NOT TempStep0%
      OUT addrpB%, PortBdata%                          'lower the step bit
      PortBdata% = PortBdata% OR TempStep0%
      OUT addrpB%, PortBdata%                           'raise the step bit
    NEXT i%

    PortBdata% = PortBdata% OR TempDown%             'reset direction to UP
    PortBdata% = PortBdata% OR TempSel0%             'deselect and write to
    OUT addrpB%, PortBdata%                                 'pot memory

END SUB
```